Neuromechanics of running

Contribution to the comprehension of the relationship between bouncing mechanics, kinematics and muscular coordination

Raphael Da Rosa Macedo Mesquita

Mars 2025

Thèse présentée en vue de l'obtention du
Doctorat en Sciences de la Motricité

Secteur des Sciences de la Santé
Institute of NeuroScience

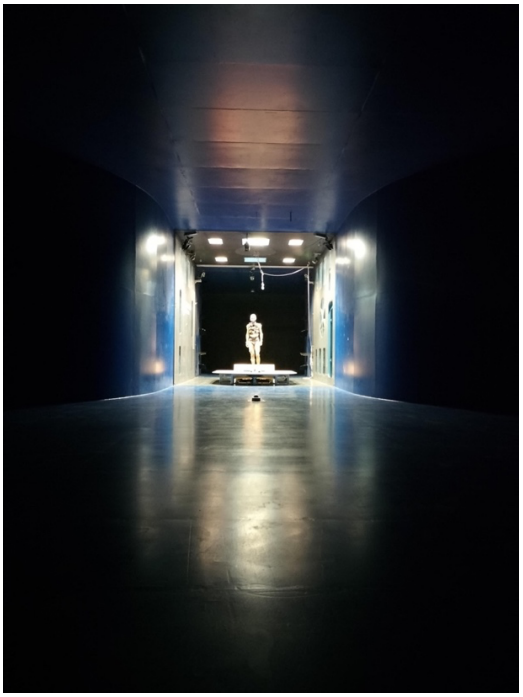

Acknowledgements

This section marks the final sentences of the work I conducted in the LOCO lab over the last seven years. None of it would have been possible without the support of countless individuals, each of whom, in their own way, helped me grow into the person I am today. I began this thesis with over 25,000 km covered on foot, yet I leave it with the firm belief that I understand less about running than I once thought I did.

I would firstly like to thank the Rector, Vincent Blondel, for accepting my candidature and giving me the reins to discover the world of academia, allowing me to teach and do research jointly.

I am deeply grateful to my advisors, Professors Arthur Dewolf and Patrick Willems, for their unwavering support and dedication. They not only mentored me throughout these years, but also challenged me every step of the way. They pushed me daily to become better, more attentive and precise in my actions. In our time spent together and moments shared both in the lab and abroad, I consider both to have become friends. Thank you to Professor Willems for bringing me into the lab and for his meticulousness, which fostered a need for comprehension and attention to detail in me that I never had before. A special thanks to Professor Dewolf, who coming into a new position and the challenges that it brings, on top of having two small children, never once told me he didn't have time. His trust, sound advice at the right moments and balance between oversight and space pushed me over our years together.

I would like to acknowledge the members of my steering committee, Professors Robert Hardwick as president, Julie Duque and Guillaume Bastien for their help and guidance over our different committee meetings. Also, my gratitude is extended to Professor Benedicte Vanwanseele (KU Leuven) and Dr. Alessandro Santuz (Max Delbrück Center) for accepting to take part in the jury. Their sound questions, remarks and ideas have helped improve this work and given ideas for future research which has been invaluable.

These years have sped by, largely thanks to the great environment that we had at our lab. In light of this, I extend my gratitude to: Professors Bénédicte Schepens, Dominique De Jaeger and Massimo Penta. I would also like to thank both the Arsalis team members, post-doctoral researchers, doctoral and master's students, and our technicians which I have had the pleasure of working with every day: Fifamè, Giovanna, Guillaume M., Pegdwendé, Sènan, Romain, Mario, Van, Minh, Marine, Arnaud, Thierry, Tristan, Marjorie, Michael, Didi, Vadim and especially Maxime.

Naturally, special recognition goes to our executive event architect, poet-musician badge holder — Professor Guillaume Bastien — for ensuring that not a single day passed without a warm greeting, and for always being available and willing to share his love of programming. A second special thanks goes out to my office buddy, Thibaut Toussaint, for the last six years spent 3 m to my left. Our discussions, jokes, frustrations and 2PM Cokes will probably be the best memory of this thesis.

Finally I would like to thank my families (*Brasileira, Nederlandse,* and *Réyoné*) for always being there to lend a hand, babysit a sick child, and have my back. Their help has always been present, no matter the project, idea or adventure undertaken. They have all, in some form or other, been part of one of my all my projects and their contribution is not taken lightly. Which of course brings me to thanking my figurative *centre of mass*: my two children, Cassie and Archie, for their innocence and reminder that life should balance spending time making animal sounds and wondering why they move the way they do. Lastly, I would like to thank my wife, Maelle, for her *almost* unfaltering patience and comprehension for the importance I give to my work. This thesis would have strictly not been possible without her involvement, therefore its result is as much mine as it is hers.

Table of Contents

Introduction 7

The bouncing mechanism of running – kinetic modulation 10

Kinematic and muscular activity modulation 11

Structure of the present thesis 13

Chapter 1. General methods 15

Experimental set-ups 15

Data processing 18

Bouncing mechanism 22

Intersegmental coordination – Kinematic modulation 23

Chapter 2. Gait modifications with non-environmental perturbations 25

2.1 Kinematics and mechanical changes with step frequency at different running speeds 29

Introduction 31

Materials & Methods 33

Results 42

Discussion 47

Limitations 53

Conclusion 53

2.2 Kinetics and mechanical work done to move the body centre of mass along a curve 57

Introduction 60

Materials & Methods 63

Results 73

Discussion 79

Limitations 82

Conclusion and Perspectives 83

2.3 Kinematic and motor coordination of the inner and outer limb in running while turning 89
Introduction 90
Materials & Methods 93
Results 101
Discussion 110
Conclusion 116

Chapter 3. Gait modifications with environmental perturbations 121
3.1 The bouncing mechanism of running against hindering, or with aiding traction forces - A comparison with running on a slope 125
Introduction 129
Materials & Methods 132
Results 138
Discussion 146
3.2 Biomechanics of Human Locomotion in the Wind 151
Introduction 152
Materials & Methods 154
Results 164
Discussion 169
Limitations 175
Conclusion 176

Chapter 4. General discussion 191
Mechanical work 192
Kinematic coordination of gait 201
Shortcomings 204
Future perspectives - Understanding performance 206

Conclusion 209

References 211

Introduction

In humans, as in other animals, locomotion arises from a closed-loop interaction between the neural command, the physical dynamics of the body system (morphology, inertia, muscle-tendon dynamics, *etc.*) and the ability to adjust motion to the external environment (Taga 1995; Hatsopoulos 1996; Aoi and Tsuchiya 2006). Understanding movement in general and in locomotion in particular, requires examining the organisational integration across joints, limb segments, whole-body dynamics, and muscles, forming a relatively new branch of science known as neuromechanics (Nishikawa et al. 2007). In other words, analysing gait requires more than a single biomechanical perspective, solely focused on the locomotor system; it benefits from a multidisciplinary approach such as that of neuromechanics to understand how the nervous system interacts with the locomotor system to control movement.

Historically, the extensive and valuable work of 20th-century physiologists such as Nobel laureate Archibald Hill, Herbert Elftman, Wallace Fenn, Griffith Pugh, etc. established a foundation and inspired truly great research focused on understanding muscle mechanics, metabolic and mechanical cost of locomotion, and also how the body moves its segments and interacts with the environment (Hill 1913; Fenn 1930; Elftman 1934; Pugh 1970). Through the initial conception of the force platform by Marey, Carlet, Demey, and Fenn, then followed with the work of Cavagna (1975), we are able to understand how the body, simplified to one central point – its centre of mass (CoM) – interacts with its environment (Sutherland 2005). It is striking to note that the signal produced by Carlet and Marey in 1872 (Fig. 0.1), through a system of air reservoirs placed in the shoe, had a similar M-shape during walking that the vertical ground reaction force (Fv) has today (Carlet 1872; Sutherland 2005). From the study of the ground reaction forces, we are able to understand how muscles store and release energy over a step (Margaria 1968) and how the body adapts to moving through various environments (e.g. Davies 1980; Cananga et al. 1998; Lejeune et al. 1998).

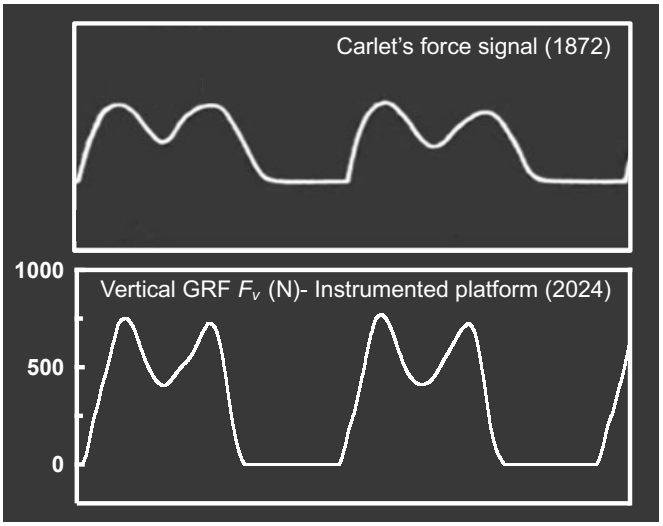

Fig. 0.1 *Top: Carlet's "M-shaped" curve during walking produced by a system of air reservoirs in one shoe which closely resembles the motion of the vertical ground reaction force under one foot today (1872). Adapted from Sutherland 2005. Below: vertical ground reaction force signal over a stride, decomposed by foot, when walking at 1.5 m* s^{-1} *on an instrumented treadmill. The force under the right foot is decomposed from a single platform based on the algorithm of Meurisse and Bastien 2014.*

The analysis of force data has long been associated with both the kinematic assessment of body segment positions and electromyographic (EMG) evaluation of muscular activity during locomotion. The former can be traced back to Etienne Marey (1873) and Eadweard Muybridge's (1887) work on photographing motion respectively from a physiologist's and artist's perspective. Similarly, Braun and Fisher, two German military doctors (1889), were the first to photograph joint angle displacement with a "modern" scientific approach by using Geissler tubes attached to body segments. Since those early days, technology has made remarkable progress. Today's locomotion laboratories are typically equipped with multi-camera systems. For example, most studies in this thesis used a Qualisys (Gothenburg, Sweden) kinematic recording system of 12 cameras capable of recording motion up to 480 frames per second. Subjects are no longer equipped with gas lamps and rubber suits to avoid electrocution, but passive retro-reflective markers which capture the movements of the body segments with an acceptable error of less than 5 mm across 5 m (Fig. 0.2) (Qualisys Track Manager, 2024).

In terms of EMG analysis, the 1940s marked a turning point with the work of Inman and colleagues (Inman et al. 1981), who introduced the use of indwelling wire electrodes to record muscle activity during gait. Prior to this, EMG was largely

limited to seated measurements, primarily for detecting abnormal nerve conduction velocities (Sutherland 2001; Abu-Faraj et al. 2015).

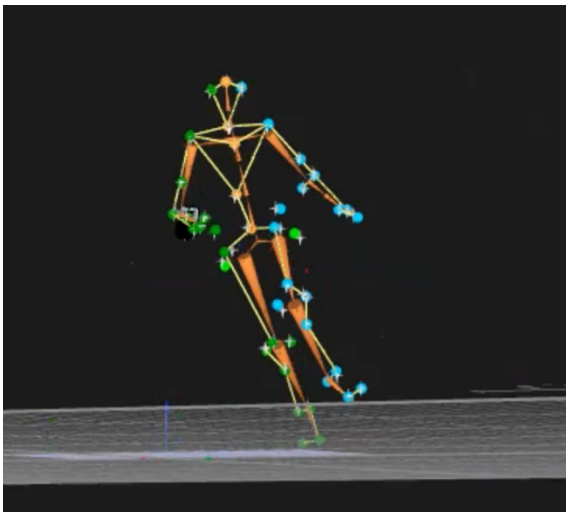

Fig. 0.2 Representation of a kinematic recording of a subject running on a curve *(see Chapter 2.2 & 2.3) equipped with the retro-reflective markers, corresponding to each point of the image.*

Using, but not limited to, these different instruments, the documented analysis of gait has taken enormous leaps since its beginnings. Today, the challenges faced are different from those of our predecessors, by having *carte blanche* in the amount of data available, researchers need to handle extensive and complex datasets. However, the fundamental goal remains unchanged: to understand how the control of a highly complex and redundant motor system is simplified by the central nervous system (CNS). Researchers have often turned to models to make sense of these data, offering a structured framework that provides meaning to motion and breaks down the complexity of gait into simplified and manageable components.

Indeed, as claimed by the Hungarian-American mathematician, John Von Neumann, a model is "[..] a mathematical construct which, with the addition of certain verbal interpretations, describes observed phenomena. The justification of such a mathematical construct is solely and precisely that it is expected to work – that is, correctly to describe phenomena from a reasonably wide area" (cited by Brody and Vámos 1995). To build on a reference introduced by my advisor, consider Italo Svevo's famous character, Zeno Cosini: who upon discovering the "terrifically complicated" fact that walking involves 54 muscles working simultaneously as part of an "infernal machine", becomes paralysed by this awareness and can no longer walk without a limp (Meyer 1972). This illustration should be taken as an example

of why biomechanists often rely on mechanical models to break apart, simplify and explain motion. In locomotion, examples of these models are the pendular mechanics for walking (Cavagna et al. 1963) and bouncing mechanics for running (Fenn 1930; Cavagna et al. 1964; Blickhan 1989).

"All models are wrong, but some are useful" – George E.P. Box

Even more daunting, is imagining the role of the CNS in such a locomotor task, as it must regulate and coordinate the movements of both upper and lower limb segments and the contraction of numerous muscles. For each muscle, the force generated must be regulated through the activation of motor units and combined across all muscles to produce a correct amount of torque at each joint (Torricelli et al. 2016). A long-standing theory is that the CNS contains specific neural pathways which facilitate and regulate motion and muscular activity (Hatsopoulos 1996). Like a conductor in an orchestra, if a symphony is the combined result of each instrument playing its complex part, the conductor (the CNS) regulates groups of musicians instead of directing to each one individually (Torricelli et al. 2016). For example, from a kinematic point of view, the planar covariance law shows that rather than controlling the positioning of each lower limb segment (the thigh, shank and foot), the CNS controls the positioning and retraction of the lower limb (Borghese et al. 1996; Poppele et al. 2002; Ivanenko et al. 2008). The organisation of kinetic, kinematic and muscular activity variables in the CNS has common factors: they reduce the controllable degrees of freedom of a system and regulate the temporal and spatial organisation of a task (Ivanenko et al. 2008; Torricelli et al. 2016). This thesis uses many of these techniques to explain running gait neuromechanics when it is confronted to specific situations. These techniques are briefly described in the following paragraphs and examined in detail throughout the following chapters.

The bouncing mechanism of running – kinetic modulation

Running is a succession of stance and aerial phases, comparable to a ball bouncing on the floor. When running on level ground at a constant average speed, the mechanical energy of the CoM returns to its initial level at the end of each step. However, throughout the step, the CoM energy fluctuates (Cavagna et al. 1976). During the first part of stance, both the mechanical energy due to the CoM's forward motion, E_f, and the mechanical energy due to the vertical movements, E_v, decrease in-phase and muscles contract eccentrically to slow and to lower the CoM, absorbing

elastic energy in the muscle-tendon units (MTU). In the second part of stance, part of the energy which was absorbed during the eccentric phase is restored and the MTU must contract concentrically to increase both E_f and E_v, returning levels back to their initial values and beginning the flight phase (Cavagna et al. 1976).

By observing the exchanges between energy forms of the CoM and their fluctuations, the trajectory of the CoM in running has been modelled by a spring-mass system: a mass mounted on a massless-spring, oscillating over a step cycle (Cavagna et al. 1976; Blickhan 1989). Quantifying the changes in energy forms of the CoM, and the spring characteristics of the lower limb and its joints has led to several decades of research to understand how intrinsic and extrinsic factors modify the bouncing mechanism of running (*e.g.* Pugh 1971; Lejeune et al. 1998; Schepens et al. 1998, 2004; Cavagna 2005; Dewolf et al. 2016).

While the bouncing mechanics of the spring-mass model has proven useful in steady-state, constant-speed locomotion, it doesn't directly apply in all situations, such as when running on slopes (Dewolf et al. 2016). In up/downhill running, potential energy must be added or removed from the system with each step to account for climbing or descending. As a result, linear spring mechanics alone cannot fully model the CoM motion, and an actuator functioning as a motor or damper must be incorporated to account for these energy changes (Dewolf et al. 2016). The addition of a damper is similarly required in situations like landing from a jump, where the body must dissipate energy and come to a stop after touchdown (Gambelli et al. 2016; Toussaint and Schepens 2024).

Moreover, modelling lower limb joint mechanics has also benefited from including motors or struts, rather than solely relying on torsional spring behaviour to better explain their movement (Qiao et al. 2017). In essence, mechanical models provide valuable insights into how locomotion adapts to different conditions. However, relying on different mechanical models for each specific situation makes it challenging to propose a unified central programming model for locomotion.

The first goal of the present thesis is to challenge the locomotor system to better understand the modifications of the CoM mechanical model.

Kinematic and muscular activity modulation

It has been suggested that the trajectory of the CoM serves as a target for the motor control of legged locomotion (Alexander 1984; Lee and Farley 1998; Ivanenko et al. 2008). The CoM displacement mainly depends on the combined movements of the lower-limb segments (Saunders et al. 1953; Ivanenko et al. 2002) which contribute

in maintaining a stable and economic locomotor gait pattern (Lacquaniti et al. 1999; Ivanenko 2004). Given that the motor coordination of the limb segments arises from the interaction between neural oscillators and physical oscillators of the musculoskeletal system (Hatsopoulos 1996), one way to understand CNS programming is by analysing motor function. Thus, in addition to analysing the CoM and joint mechanics, in the frame of the present work, we also analysed the inter-segmental coordination of the lower-limb segments (Borghese et al. 1996; Ivanenko et al. 2007), and EMG activity of the lower-limb muscles.

The lower limb segmental motion and coordination can be analysed using the planar covariation method (Borghese et al. 1996; Bianchi et al. 1998; Ivanenko et al. 2008). In running, the elevation angles of the foot, shank, and thigh follow a coordinated pattern, forming a closed-loop trajectory over a stride when plotted one versus the others. These three angular movements covary along a plane, effectively reducing the degrees of freedom of the locomotor system to two principal components: limb length and limb orientation. (Poppele et al. 2002; Ivanenko et al. 2008). The orientation of the covariation plane, along with the characteristics of the loop, defines a general kinematic pattern of locomotion. This pattern adapts to different locomotor conditions (Catavitello et al. 2015; Dewolf et al. 2018), adjusts with changes in speed (Ivanenko et al. 2007; Mesquita et al. 2024a) and mechanical demands (Dewolf et al. 2018).

The coordination of lower limb muscular activity depends on both the spatial and temporal organisation of muscle activation (Yakovenko et al. 2002; Ivanenko et al. 2006; Martino et al. 2014). Thus, to assess the coordination, muscular demands of the limbs, and left vs. right organisational differences in an asymmetrical task we analysed the bilateral activity of the lower limb muscles.

Understanding running gait requires bridging a gap between biomechanics and motor control, as coordinated movement emerges from the interaction between the mechanical execution and neural control (Nishikawa et al. 2007). This work tries to look inwards from the periphery focusing on CoM mechanics, joint dynamics, inter-segmental coordination and muscular activity to understand how movement is regulated centrally. Ultimately, this approach provides insight into the interaction between motor execution and control, providing a broader view of the running locomotor system.

Consequently, the second aim of this work is to examine the interaction between the neural commands and the biomechanics of running when the system is challenged.

Structure of the present thesis

The present thesis studies the combined kinetic, kinematic and, in one case, muscular variations of the patterned control of running. To achieve this, we present different situations where the locomotor system (including its control) is challenged, out of many possible topics, and divide this thesis into four separate chapters. First, we provide a general methodology of our work, explaining some of the different analyses used in different sections **(chapter 1)**. Second, we present situations where the gait was challenged without work being done against the environment, *i.e. non-environmental perturbations*, such as the adaptions of the bouncing mechanism and the corresponding kinematic changes (1) when running at a given speed with a change in step frequency (**chapter 2.1,** published in the *European Journal of Applied Physiology*) and (2) when running while following a curved trajectory (**chapter 2.2,** published in *Plos ONE* & **chapter 2.3,** submitted to *Medicine & Science in Sport & Exercise*). Next, we compare two situations where work had to be done against the environment, *i.e. environmental perturbations*: running against tractive forces which aided or hindered the CoM (**chapter 3.1,** published in the *European Journal of Applied Physiology)*, and locomotion against the wind (**chapter 3.2** published in the *Journal of Applied Physiology)*. This is followed by a general discussion linking these different themes **(chapter 4)**.

Fig. 0.3 – Observing the different styles when running at low frequencies. *Photos captured from the video recording (60 Hz) of three instants 1) the image prior foot took off, 2) at the highest point of the aerial phase, and 3) the instant of foot touchdown, for all eight subjects who participated in a pilot study (Mesquita et al. 2021) prior to the conceiving the protocol for running with a change in step frequency. All subjects are running at 17 km h^{-1} and at 70% of their preferred step frequency (approximately 1.96 Hz). The pilot study used a percentage of the preferred step frequency instead of a fixed step frequency, as used in the future papers.*

Chapter 1. General methods

The goal of this section is not to explain in detail each method used, but rather to give an overview of methods employed in the thesis. Considering this, we chose to focus on methods used in multiple papers.

Experimental set-ups

Three types of data were collected throughout our studies: 1) ground reaction force data (GRF), 2) 3D–kinematic data of the body segment motion, and 3) electromyographic (EMG) data of muscular activity. First, we detail the instrumentation and then outline some analyses performed.

Ground reaction force measurements

Ground reaction force data was primarily measured on a commercial treadmill (h/p/Cosmos, Germany) with a belt surface of 1.6 x 0.65 m. The entire treadmill, including the motor was mounted onto four strain-gauge force transducers (Arsalis, Belgium) (Willems and Gosseye 2013). Each transducer's analogue signals were amplified, low-pass filtered (4-pole Bessel filter with a -3dB cut-off frequency at 200 Hz) to avoid aliasing during digitisation. Signals were recorded with a sampling rate of 1 kHz and digitized by a 16-bit analogue-to-digital converter (National Instrument, PCI-MIO-16E-4). The electrical motor of the treadmill was instrumented with an optical angle encoder to measure the speed of the belt (v_{belt}). The average speed of the belt over a stride (V_{belt}) differed by less than 3% in all experiments from the given speed and the instantaneous v_{belt} did not change by more than 6% of V_{belt}.

When investigating running while turning (chapter 2.2 & 2.3), the ground reaction force data was measured on 16 custom built force plates of 1 m x 1 m each, placed side by side. Each plate measured the three components of the GRF by means of four force transducers placed under each corner of an individual plate surface. Each plate possessed its own data acquisition system comprising amplifiers, similar anti-aliasing low-pass filters (4-pole Bessel filter with a -3 dB cut-off frequency of 200 Hz), a 16-bit analogue-to-digital converter sampling at 1 kHz and a micro-controller (Rabbit Semiconductor, Davis, CA, USA). The 16 plates were connected to a central PC *via* ethernet using the TCP/IP protocol (Genin et al. 2010).

Kinematic data measurement

Second, the kinematic movements of the upper and lower limb segments were recorded in three of the four situations (Chapters 2.1, 2.2 & 2.3, and 3.2). In chapter 2, bilateral, full-body 3D- kinematics were recorded using a Qualisys system (Gothenburg, Sweden) equipped with 12 Mocap OQUS 6+ cameras placed around the running track and/or treadmill, plus one video Miqus M1 camera. For chapter 3.2, data were recorded by means of a VICON system (Oxford, United Kingdom) with 8 cameras (6 MX-13 and 2 T20-S) placed around the treadmill. Participants were equipped with passive retro-reflective markers glued onto the skin. Marker placement varied between chapters depending on the study objectives. When data were linear, and thus primarily explained by sagittal plane motion, a relatively simple marker set was used (±18 markers). In curved running, as the movements in the frontal plane explain a considerable portion of movement, a more consequent marker set containing 43 markers was chosen.

The recording frequency was between 100-250Hz for all studies and oversampled during post-processing to match the ground reaction force data. An oversampling of the kinematic data rather than downsampling kinetic data, was generally preferred to ensure that no information was lost when recording the force signals. For example, consider a situation where one is running at fast speeds with a relatively low step frequency (below 2.5 steps s^{-1}), a fast-Fourier transform (*fft*) frequency analysis of the GRF reveals that frequencies up to 200 Hz are kinetically relevant. Thus, to appropriately consider simple variables such as the timing of the maximal vertical force index, approximately 30 ms after touch down, if the force signal was downsampled to match the kinematic data frequency of 200 Hz, only 6 points would describe the force signal rather than the 30 points initially recorded. This choice becomes more apparent when trying to quantify the difference between touchdown (generally decided by a signal-to-noise ratio analysis and set in our studies between 30 - 80 N) and this first instant that F_v passes over *BW*. At similar low frequency and fast speed conditions, the difference between both is about 10 ms (10 points at 1000Hz, 2 points at 200Hz). Whereas an oversampling of the kinematic data 'does no harm' to the behaviour of a signal, or so, if the signal was linear between two points, it will continue to be linear throughout 10 points. The opposite limits the information of the force data.

Note the instant of touchdown became more systematic and less time consuming during the data analysis throughout the different experiments. In the first study, running with tractive forces, touchdown was defined at 10 N (~2% of *BW*) — requiring visual inspection of each foot contact to avoid false detections — an

extremely tedious process for over 6000 steps. To reduce manual inspection, the threshold was increased to 10% of *BW* (~70 N) in the next paper (running with a change in step frequency).

Although this second method was more robust efficient, as mentioned above this threshold should ideally depend on the signal-to-noise ratio rather than a fixed percentage of *BW* which varies between subjects. This ratio therefore depends on factors such as force plate positioning, the natural frequency of the plate and of the ground at which the plate is fixed on, and on the properties of the electronic signal conditioner. In the final three studies (running while turning and running in the wind), we refined the method further, setting the threshold at 30°N (~4% of *BW*) based on the signal noise of the vertical ground reaction force during the aerial phase. While slightly higher than the initial method, this approach balanced accuracy and efficiency, eliminating the need for in-depth visual inspection while not losing in precision. Mostly, the difference in timing between the first and last method was in the order of 2-3 ms.

Measurement of EMG data

The EMG activity was recorded during curved running (Chapter 2.3) and in wind running. However, due to time constraints, only data from curved running muscular activity are presented in this thesis. The lower limb muscles were recorded at 2.15 kHz with a Delsys Trigno surface electrode system (Natick, MA, USA). After preparing the shaved skin with alcohol, EMG electrodes were placed following the SENIAM protocol (seniam.org), a European project on surface EMG. To this end, we located the muscle bellies by means of palpation and oriented the electrodes along the main direction of the fibres (Kendall et al. 2005; Winter 2009). In wind running, the muscular activity of 16 muscles of the right limb were recorded. Whereas due to the asymmetrical nature of limb movements between the inner and outer limb in curved running, the bilateral muscular activity of 24 muscles was recorded (Fig. 1.1). The raw EMG signals were downsampled to 1 kHz during post processing to match the other types of data.

Fig. 1.1 *Subject equipped with 43 retro-reflective markers and 24 EMGs about to start their running while turning session.*

Data processing

As each chapter presents a peculiar modification to the gait, some analyses required adaptation for appropriate use. In this section, we explain the calculated variables for a hypothetical subject running at a constant speed on a treadmill with no inclination. Air resistance is considered negligible, and it is assumed that the foot does not skid on the ground (Cavagna et al. 1976).

Computation of Acceleration, Velocity and Vertical Displacement of the CoM

In the situation presented above, the human body is submitted to two external forces: (1) the gravitational force (mg) and (2) the GRF. The components of the GRF are the lateral (F_l), fore-aft (F_f) and vertical (F_v) forces and their accelerations are respectively a_l, a_f, and a_v and are obtained by:

$$a_{\mathrm{l}} = \frac{F_{\mathrm{l}}}{m},$$

$$a_{\mathrm{f}} = \frac{F_{\mathrm{f}}}{m},$$

$$a_{\mathrm{v}} = \frac{F_{\mathrm{v}} - \bar{F}_{\mathrm{v}}}{m},$$

where m is the body mass, and $\bar{F}_{\mathrm{v}} \approx BW$.

Accelerations are time-integrated to determine the variations of vertical (v_{v}), fore-aft (v_{f}) and lateral (v_{l}) velocities of the CoM plus an integration constant. In the fore-aft direction, since the subject runs at an constant average speed, the integration constant is equal to V_{belt}, the average speed of the treadmill belt. In the lateral and vertical direction, the integration constants of v_{l} and v_{v} are equal to zero, on the assumption that the CoM returns to its initial lateral position and height at the end of each stride.

The forward (s_{f}), lateral (s_{l}) and vertical (s_{v}) displacements of the *COM* relative to the treadmill are then computed by numerical integration of v_{f}, v_{l} and v_{v}, respectively. This procedure assumes that, at the beginning and at the end of the steps analysed, the subject is in the same position on the treadmill (Cavagna et al. 1964; Willems et al. 1995).

Computation of the external mechanical work (W_{ext}) and power ($\dot{W}_{ext}$)

In the hypothetical situation described in the beginning of the chapter, the positive mechanical work done/or negative mechanical work absorbed by the MTU, respectively W_{ext}^{+} / W_{ext}^{-}, can be assessed through different methods. Firstly, the positive and negative increments of mechanical work can be computed from the time-integrals of external mechanical power ($\dot{W}_{\mathrm{ext}}$) (Donelan et al. 2001).

The external mechanical power, $\dot{W}_{\mathrm{ext}}$, is the sum of the power developed by the GRF ($\dot{W}_{\mathrm{com}}$), plus the power developed to move against the environment ($\dot{W}_{\mathrm{env}}$), $\dot{W}_{\mathrm{ext}} = \dot{W}_{\mathrm{com}} + \dot{W}_{\mathrm{env}}$. Here, since we consider air resistance and foot friction forces to be negligible, $\dot{W}_{\mathrm{env}} = 0$. Thus, in the present situation the external mechanical power developed is only due to the GRF ($\dot{W}_{\mathrm{ext}} = \dot{W}_{\mathrm{com}}$). $\dot{W}_{\mathrm{com}}$ is computed as the dot product of the GRF and velocity vector of the CoM relative to its surroundings:

$$\dot{W}_{com} = \overrightarrow{GRF} \cdot \vec{V} = (F_{\mathrm{v}} \cdot v_{\mathrm{v}}) + (F_{\mathrm{f}} \cdot v_{\mathrm{f}}) + (F_{\mathrm{l}} \cdot v_{\mathrm{l}}).$$

The time-integral $\dot{W}_{\mathrm{com}}$ gives the mechanical energy due to the movements of the CoM (E_{com}):

$$E_{com} = \int \dot{W}_{com}\ dt.$$

Secondly, E_{com} can also be written as the sum of the kinetic and potential energy sources done to sustain the movements of the CoM in the three directions (Cavagna et al. 1976),

$$E_{com} = E_v + E_f + E_l,$$

where E_v, is the energy due to the vertical movements of the CoM, equal to the sum of the potential, E_p, and kinetic, E_{kv} energy done,

$$E_v = E_p + E_{kv} = m\,g\,S_v + \frac{1}{2}mv_v^2.$$

E_f and E_l are the kinetic energies done to sustain the fore-aft and lateral movements of the CoM (respectively, $\frac{1}{2}m\,v_f^2$ and $\frac{1}{2}m\,v_l^2$). The positive and negative increments of E_v, E_f, E_l and E_{com} give, respectively, W_v^+, W_f^+, W_l^+, W_{com}^+ and W_v^-, W_f^-, W_l^-, W_{com}^-, the mechanical work done to sustain the movements in each direction of the CoM and the resultant CoM work. Note, sometimes in the literature W_{com} and W_{ext} are used interchangeably (*e.g.* Cavagna et al. 1991). In fact, this distinction is not important when the work done against the environment is nil and thus $W_{ext} = W_{com}$. In the present thesis, this will not always be the case. As the runner maintains a constant average speed, in the present situation there is as much positive as negative work done by the MTUs (Fig. 1.2) (Cavagna et al. 1976). How the energy and CoM mechanics adapt to specific gait modifications can be found in the following sections of this thesis: 2.1, 2.2, 3.1, 3.2.

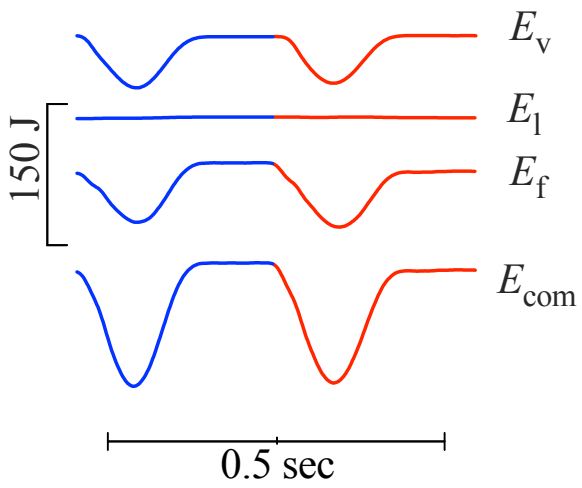

Fig. 1.2 *Typical stride of the CoM energy curves of a subject (1.8 m and 81 kg) running on a treadmill at the constant average speed of 14 km h^{-1}, when the air resistance is negligible. The blue portion represents the step following a left foot contact and red, the step following the right foot. Note, the energy due to the lateral movements of the CoM, when maintaining a linear trajectory, is negligible (Cavagna et al. 1963) and is usually not considered when accounting for W_{com}.*

Statistical Power Computation and sample size

Sample sizes were computed using two different programs: G*Power (Faul et al. 2007) and GLIMMPSE 3.1.2 (Kreidler et al. 2013) on key variables used in specific studies (see table 1.1 below). In two cases — running against tractive forces and running with a change in step frequency — sample sizes were determined from pilot study data (Mesquita et al. 2019, 2021). In running while turning, the power analysis was done to confirm the sample size required for each key variable was greater or equal to the experimental sample size (9 subjects for the mechanical data and 10 for the mechanical, kinematic and EMG analysis). Finally, in wind running, sample size calculations were based on data from running against tractive forces as we expected similar results in both studies.

Study + Year of conducted experiments	Program	Statistical test used	Variable used	N° Subjects for Power 1-β ≥ 0.8	Experimental Sample size
Running Frequency (2021)	G*Power	Linear mixed effect model	k_{vert}, W_{ext}, u_3t	8	8
Running while Turning Mechanics (2022)	GLIMMPSE	Linear mixed effect model	W_{com}	9	11
Running while Turning : Kinematics and EMG (2022)	GLIMMPSE	Linear mixed effect model	W_{ext} , u_3t, FWMH	10	11
Running with tractive forces (2018)	G*Power	Two-Way ANOVA	W_{ext}	8	8
Running with the wind (2022)	G*Power	Linear mixed effect model	W_{ext}	8	8

Table 1.1 *Power analysis details for the different studies.*

All studies included enough number of participants to avoid type II error, with a statistical power of 1-ß ≥ 0.8. However, most sample sizes remained relatively small. To reduce variability in these small sample sizes, we prioritised homogeneity in our subjects: all subjects were male and had similar height and weight. This introduces bias when extrapolating these findings to a broader population, a limitation further discussed in the general shortcomings of the thesis.

Bouncing mechanism

The trajectory of the CoM during running has often been modelled as a spring-mass system, with the CoM represented as a mass atop a massless spring that oscillates throughout each step cycle (Cavagna et al. 1988; Blickhan 1989). During this cycle, the vertical ground reaction force, F_v, oscillates about a point of equilibrium proportional to the *BW* of the subject (where $a_v = 0$). This oscillation can be split into two periods around the *BW*: First, an effective contact period (t_{ce}), occurring during the contact phase, representing the lower part of the oscillation, where $F_v > BW$ ($a_v > 0$). The second part, the effective aerial time (t_{ae}), occurring during both the contact and aerial phases, is when $F_v < BW$ ($a_v < 0$) (Cavagna et al. 1988; Cavagna 2009).

During t_{ce}, the MTUs of the lower-limb act like a single linear spring bouncing vertically on the ground. The stiffness, k_{vert}, of this spring can be computed as the slope of the *quasi*-linear relationship between F_v and S_v during t_{ce} (Fig. 1.3).

$$k_{\mathrm{vert}} = \frac{F_{\mathrm{v}}}{S_{\mathrm{v}}}.$$

t_{ce} always corresponds to half the period of oscillation of the elastic rebound of the body over a step cycle.

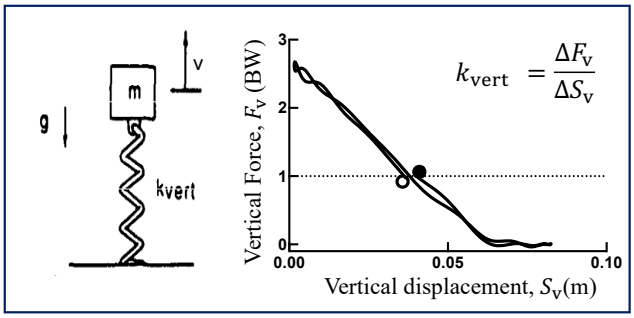

Fig. 1.3 *Image adapted from (McMahon and Cheng 1990) and typical trace of the F_v - S_v relationship when running at 14 km h $^{-1}$. When F_v is greater than 1 BW, one observes a quasi-linear relationship between both. The slope of this curve corresponds to the lower-limb stiffness, k_{vert}. The trace begins at the open circle, when $F_v > BW$, and increases as the ground exerts a vertical force on the lower limb. When the trace reaches 0, the subject takes-off and maintains an aerial phase until the force begins to rise again, at the following foot contact. The closed circle corresponds to the end the stride. t_{ce}, corresponds to when $F_v > BW$ and t_{ae}, when $F_v < BW$. The subject is the same as in Fig. 1.2.*

When running at an average speed, v_f, the step length L covered over the step period, T, can be computed as:

$$L = v_{\mathrm{f}} \times T = L_{\mathrm{ce}} + L_{\mathrm{ae}} = t_{\mathrm{ce}} v_{\mathrm{f}} + t_{\mathrm{ae}} v_{\mathrm{f}},$$

where L_{ce} is the length covered during the period t_{ce} and L_{ae} is the length covered during the period t_{ae}.

At a constant average speed on a flat firm ground, the momentum lost and gained during t_{ce} should be equal to that of t_{ae} (Cavagna et al. 1988; Cavagna 2009). At low speeds, $t_{ce} \approx t_{ae}$ and $L_{ce} \approx L_{ae}$. In this case the bounce is considered symmetric. When speed increases up to ~3.1 m s^{-1}, both distances will increase approximately symmetrically and timings do not change, which implies that k_{vert} remains about the same (Cavagna et al. 1988).

When speeds increase beyond this point (above 3.1 m s^{-1}), $t_{ae} > t_{ce}$ and the bounce is considered asymmetric. Indeed, to be able to cover the step length L, two phenomena occur. First, L_{ce} cannot increase indefinitely; when the foot is on the ground L_{ce} is constrained by anatomical limitations such as hip flexor and coxo-femoral joint capsule tautness and reaches a limit (~1 m) (Cavagna et al. 1988; Van Wingerden et al. 1993; Franz et al. 2009). Thus, to increase velocity when L_{ce} is at its maximum t_{ce} must decrease. This is done by increasing the spring stiffness with a greater average vertical force. To maintain similar phase momentums during t_{ce} and t_{ae}, the runner could either increase their vertical force during t_{ae}, which is not possible given that this phase occurs mostly in the air, or they could increase t_{ae} (and by consequence L_{ae}). An asymmetry arises where t_{ae} becomes greater than t_{ce}, a necessary result to compensate for the lessened force.

Cavagna et al. (1988) claim that "at a given speed, the asymmetric bounce requires a greater power to maintain the motion of the CoM ($\dot{W}_{\mathrm{ext}}$) than the symmetric bounce. A reduction of the push during t_{ce} would decrease $\dot{W}_{\mathrm{ext}}$ but the resulting greater step frequency would increase the power required to accelerate the limbs relative to the CoM ($\dot{W}_{\mathrm{int}}$)." It was concluded by Cavagna et al. (1988) and by Cavagna et al. (1991) that "the asymmetric rebound is adopted to minimise the total power ($\dot{W}_{\mathrm{ext}} + \dot{W}_{\mathrm{int}}$)". The analysis of the bouncing mechanism can be found in chapters 2.1 and 3.1.

Intersegmental coordination – Kinematic modulation

The elevation angle of a limb segment (θ) in the sagittal plane (*i.e.* the orientation of the segment in the sagittal plane relative to vertical) can be computed as: $\theta = \arctan\left(\frac{y_p - y_d}{z_p - z_d}\right)$, where ($y_p$, z_p) and (y_d, z_d) are, respectively, the fore-aft (y) and vertical (z) coordinates of the proximal (subscript p) and distal (subscript d) markers of the segment. For each trial, the time-curves of the thigh, shank and foot elevation angles are time-interpolated over individual strides to fit a normalised fixed-point

time-base. When observing both limbs in a symmetrical movement, the movements of one limb should be time shifted by 50% of the stride period, for both limbs to match. Note, this should not be the case when limbs are working asymmetrically, *i.e.* running while turning.

Intersegmental coordination of the lower limbs was then assessed using principal component analysis (PCA). The centred thigh, shank, and foot elevation angles once plotted in a three-dimensional space form a loop which lies close to a plane (Fig. 1.4). The best fitting plane is the one generated by the first two components extracted from a PCA performed on the covariance matrix of the three elevation angles waveforms. The PCA returns a matrix of eigenvectors *U* with their associated eigenvalues (λ_1, λ_2, λ_3) rank-ordered from the highest to the lowest. The eigenvectors u_1 and u_2 generate the best fitting plane and the third eigenvector, u_3, orthogonal to the first two, defines the orientation of the plane. The components of the u_3 vector: u_{3t}, u_{3s}, and u_{3f} correspond to the direction cosines with the positive semi-axis of the thigh, shank and foot angular coordinates, respectively. The percentage of variance associated to vectors u_1, u_2, u_3 are respectively PV1, PV2 and PV3 and is computed as the ratio of each eigenvalue to the total eigenvalue sum (*e.g.* PV3 = λ3/ (λ1 + λ2 + λ3)). PV3 is used as an index of planarity, with PV3 = 0% indicating maximum planarity. These methods have been thoroughly explained in the following sources (*e.g.* (Borghese et al. 1996; Daffertshofer et al. 2004; Dewolf et al. 2018; Catavitello et al. 2018) and were used in chapters 2.1 & 2 .3.

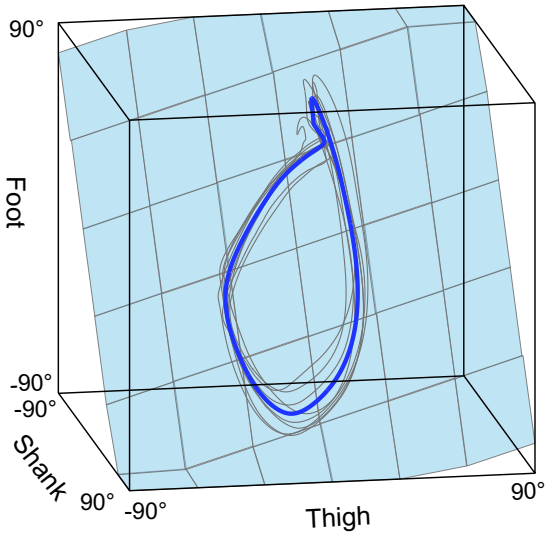

Fig. 1.4 *3D plots of the centred and time-normalised thigh, shank, and foot elevation angles, along with the best-fitting plane for the same subject as Fig. 1.2, running on a treadmill at 14 km h^{-1}. Grey lines correspond to individual strides and the dark blue is the average stride.*

Chapter 2. Gait modifications with non-environmental perturbations

Running with a change in step frequency

The modification of step frequency in running has already been extensively studied (Cavagna et al. 1988, 1991; McMahon and Cheng 1990; Farley and González 1996; Lieberman et al. 2015), however, the relationship between the bouncing mechanism and the kinematic coordination pattern of the lower limb when modifying step frequency (SF) still raised several interesting unanswered questions.

For example, the kinematic synergy of the lower limb segments had been shown to adapt with speed (Ivanenko et al. 2007) however, a change in SF at the same speed changes the range of motion of the lower limbs and could thus affect the coordination between segments. The aim of this first section was to shed light on how the changes in step frequency at a fixed speed affected the kinematic movement patterns. Furthermore, we wanted to better understand how the CoM adapted to such changes in leg configuration, and by extension adapted its spring stiffness, to perform these more complex movements.

In this study, we compared the running mechanics and kinematics at different speeds from 8 - 17 km h^{-1} with different imposed step frequencies (from 2 to 3.6 step s^{-1}) to understand the relationship between kinematic and kinetic parameters. Eight recreational male runners ran on a treadmill at 5 different speeds and 5 different step frequencies. The motion of the lower and upper limbs and the ground reaction forces were recorded. Mechanical work and power, general gait parameters, lower-limb movements and coordination were investigated.

At low step frequencies, to limit the magnitude of the ground reaction force, the vertical stiffness was reduced and runners deviated from a stereotypical elastic rebound. At high step frequencies, the stiffness was increased, and the elastic rebound was optimised in its ability to absorb and restore energy during the stance phase. We studied the consequences of a change in step frequency on the bouncing mechanics of running. We showed that the lower limb stiffness and the intersegmental coordination of the lower-limb segments were affected by running frequency rather than speed. The runner adapted their lower limb stiffness to match a step frequency for a given speed rather than the opposite. This first section was published in the *European Journal of Applied Physiology* (Fig. 2.0.1).

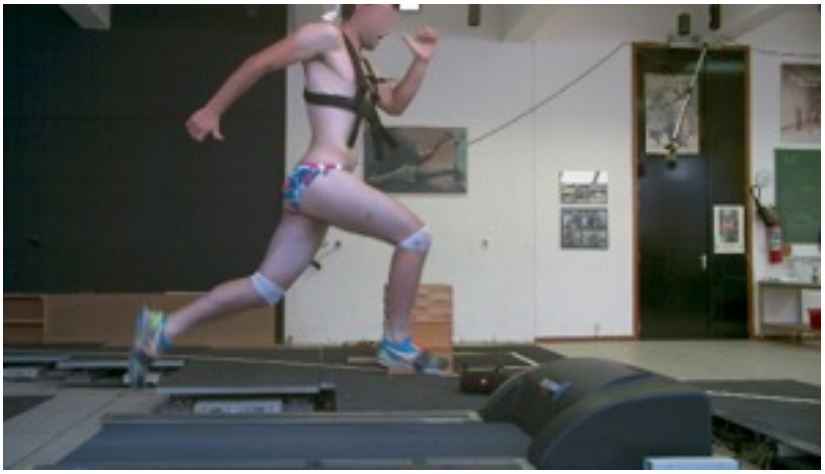

Fig. 2.0.1 *Subject running on a treadmill at 17 km h^{-1} and at 2.0 steps s^{-1}*

Running while turning

In laboratory conditions, human locomotion is typically analysed at a constant average speed while maintaining linear motion (Cavagna et al. 1991; Willems et al. 1995). However, in nature (Usherwood and Wilson 2006; Wilson et al. 2013b, a), in daily life or during sport activities (Gabbett et al. 2008; Minetti et al. 2011; Taylor et al. 2017), movement rarely occurs in a single direction. Humans and other legged animals must constantly change directions as they navigate over their surroundings. Although some principles and specific hypotheses had been studied in relation to human running while turning (Greene 1985, 1987; Hamill et al. 1987; Hase and Stein 1999; Chang and Kram 2007; Segal et al. 2008; Qiao et al. 2014; Churchill et al. 2016; Dos'Santos et al. 2019) the strategy employed by the CoM and the mechanical work done to maintain a running curve had never been explored.

The goal of section 2.2 was to understand how the trajectory of the CoM and the work done to maintain its movements relative to the surroundings (W_{com}) were modified as a function of running speed and radius of curvature. Eleven participants ran at different speeds on a straight line and on circular curves with a 6 m and 18 m radius (Fig. 2.0.2). The trajectory of the CoM and the work W_{com} were calculated using force-platforms measuring the ground reaction forces and high - speed infrared cameras recording the movements of the pelvis.

To follow a circular path, runners overcompensated the rotation of their trajectory during contact phases. The deviation from the circular path increased when the radius of curvature decreased and speed increased. The method to evaluate W_{com} on a straight-line was adapted using a referential that rotates at heel strike and remains fixed during the whole step cycle. In an 18 m radius curve and at low speeds on a 6 m radius, W_{com} changed little compared to a straight-line run. Whereas at 6 m s^{-1} on a 6 m radius, W_{com} increased by ~25%, due to an augmentation in the work to move the CoM laterally. Understanding these adaptations provides valuable insight for sports sciences, aiding in optimising training and performance in sports with multidirectional movements. This section was published in *Plos ONE.*

Additionally, this initial study confirmed previous observations which showed that the inner and outer limbs display distinct roles during curved running (Chang and Kram 2007; Churchill et al. 2011; Alt et al. 2015; Viellehner et al. 2016). Turning presents unique mechanical demands on the musculoskeletal system and relies on a multi-level coordination of the lower limb to regulate efficient and precise movements. Section 2.3 further analysed the kinematic, kinetic, and muscular adjustments of the inner and outer limbs on curves and compares these to straight-line running.

We hypothesised that the inner and outer limbs would adopt distinct functional roles to accommodate lateral forces. We recorded the ground reaction force, kinematic motion and muscular activity of the same eleven runners on two different radii of curvature (6 and 18 m) at speeds ranging from 7-19 km h^{-1}. The joint coordination in the frontal and sagittal planes, intersegmental coordination and muscular activity were analysed. Based on the distinct role that each lower limb had in curved running; we showed that coordination is limb specific and identified key traits which separated either limb. The inner limb primarily manages lateral redirection of the body, relying on increased joint compliance and enhanced muscular activation in the hip abductors to accommodate the greater lateral forces. In contrast, the outer limb contributes more to propulsion and stabilisation to drive forward motion. This section provides insight into how humans modulate limb mechanics and coordination to maintain stability and performance in curved trajectories, with potential applications in sports and rehabilitation. This section has been submitted to *Medicine & Science in Sport & Exercise* (Fig. 2.0.2).

Fig. 2.0.2 *Subject running on force platforms disposed in a manner which allowed an 18 m curved radius to be drawn. The subject was instructed to keep to their 50 cm lane and was equipped with retro-reflective markers which are shining against the flash of the camera. See sections 2.2 & 2.3.*

2.1 Kinematics and mechanical changes with step frequency at different running speeds

Raphael M. Mesquita, Patrick A. Willems, Giovanna Catavitello &
Arthur H. Dewolf

European Journal of Applied Physiology (2024) 124(2), 607–622.

Keywords: Bouncing mechanism; Intersegmental coordination; Stiffness; Neuromechanics

List of Abbreviations

BW:	Body weight.
CoM:	Body centre of mass.
GRF:	Ground reaction force.
F_x, F_y, F_z:	Lateral, fore-aft and vertical components of the GRF.
a_f, a_v and v_f, v_v:	Fore-aft (f) and vertical (v) accelerations and velocities of the CoM.
E_{com}, E_{kf}, E_v:	Energy of the CoM, kinetic energy about the fore-aft direction, vertical energy.
E_{int}^{i}:	Internal energy of each segment (i) in relation to the CoM.
k_{vert}:	Vertical stiffness of the CoM spring.
PV:	Percentage of variance.
ROM:	Range of motion.
$S_{c,down}$ and $S_{c,up}$:	S_v during the contact phases divided into its down and upwards increment.
SF, SFs and PSF:	Step frequency, step frequencies and preferred step frequency.
SL, L_{ce} , L_{ae}:	Step length, effective contact and effective aerial lengths.
S_v:	Vertical displacement of the CoM.
T, t_c and t_a:	Step, contact and aerial times.
t_{brake} and t_{push}:	Time spent braking and spent re-accelerating the CoM during t_c.
t_{ce} and t_{ae}:	Effective contact time and effective aerial time.
u_{3t}, u_{3s}, u_{3f}:	Direction cosines of the thigh, shank and foot of the normal covariation plane.
v_{belt} and V_{avg}:	Speed of the treadmill belt and average of v_{belt} over one stride.
W_{ext}^{+}:	positive external work of the CoM.
$\dot{W}_{ext}^{+}$ and $\dot{W}_{ext,push}^{+}$:	positive external power of the CoM over a step and over t_{push}.
W_{int}^{+} and $\dot{W}_{int}^{+}$:	positive internal work and power of the segments as compared to the CoM

Introduction

Running is a cyclic movement that alternates between unipodal contact and aerial phases. During these phases, the centre of mass (CoM) of the body exhibits a motion comparable to a mass m (equivalent to the body mass) attached to a weightless spring, rebounding off the ground (Blickhan 1989) and oscillating around an equilibrium point where the vertical force equals the body weight (BW). Consequently, the vertical oscillation of the CoM is divided into two parts (Cavagna et al. 1988). First, an effective contact period (t_{ce}), occurring during the contact phase, and representing the lower part of the oscillation during which the vertical ground reaction force (GRF) is greater than body weight. Second, an effective aerial period (t_{ae}), taking place both during the contact and aerial phases, representing the upper part of the oscillation during which the GRF is smaller than body weight.

In this model, the supporting leg behaves like a spring with a 'dual action' stance phase: throughout the first part of contact, the spring-mass system is compressed and potential elastic energy is stored into the muscle-tendon units of the lower limb to be further released during the second part of contact when the spring expands. During t_{ce}, the half period of the elastic oscillation, a linear relationship between the vertical component of GRF (F_z) and the vertical displacement (S_v) of the CoM exists. Therefore, the stiffness (k_{vert}) of the spring-mass model, reflecting the overall limb behaviour, can be approximated by the slope of the F_z-S_v relation. When humans increase their step frequency at a given running speed, the most important adjustment to the body's spring system is that the spring becomes stiffer (Farley and González 1996; Dewolf et al. 2022).

Running at a given speed can be achieved by taking large steps at a low frequency or on the contrary by taking small steps at a high frequency. The choice of the preferred step frequency (PSF) has been carefully documented by Cavagna et al. (1988, 1991). However, what are the consequences of a change in step frequency, and in turn of spring stiffness, on the running kinematic and kinetic parameters?

First, from a mechanical point of view, because the spring-mass system oscillates around a point of equilibrium at which $F_z = BW$, the vertical momentum lost and gained during t_{ce} must equal the vertical momentum lost and gained during t_{ae}. When running at speeds up to ~3.1 m s^{-1}, t_{ce} approximates t_{ae} (symmetric step). As speed increases above 3.1 m s^{-1}, t_{ae} is greater than t_{ce} and the step becomes asymmetric (Cavagna et al. 1988; Schepens et al. 1998; Dewolf et al. 2016). Decreasing the step frequency (SF) below the PSF requires an increase in step length (L) to maintain the same constant speed. Indeed, an 'unusually' long step at a low

frequency requires a decreased vertical stiffness (Farley and González 1996). During the contact phase, the distance travelled by the CoM is limited due to anatomical restrictions (Cavagna et al. 1988), thus an asymmetric rebound would be observed at lower step frequencies. In addition, a longer aerial phase demands greater external power generated during the contact phase to accelerate and lift the CoM appropriately. Thus, one could expect to observe adjustments to the bouncing mechanism similar to those observed when running on a slope (Dewolf et al. 2016) or against a hindering traction force (Mesquita et al. 2020) in order to limit the increase in muscular power. At frequencies higher than PSF, the vertical stiffness increases (Farley and González 1996), which potentially implies that the bounce remains symmetric as speeds increase, in this way the muscular power done to move the CoM should no longer be a limiting factor.

Second, from a kinematic point of view, the lower limb intersegmental coordination during stance is expected to contribute to the modification of stiffness. Indeed, the body is a dynamical system where the position in space of the CoM depends among others on the overall configuration of the lower limb segments. In particular, the vertical displacement of the CoM and the stiffness of the lower limb depends on the configuration of the lower limb segments, the thigh, shank, and foot, during the stance phase.

Movements of the lower-limb segments and their coordination can be investigated using the planar covariation method (Borghese et al. 1996; Bianchi et al. 1998). These studies have shown that the changes of the angular motion of the lower-limb segments covary along a plane indicating a reduction in the degrees of freedom of the system from three to two. The planar covariation law shows that a general kinematic coordination pattern is maintained in various animal species (Courtine et al. 2005; Ogihara et al. 2014; Catavitello et al. 2018), in different locomotor conditions (Borghese et al. 1996; Catavitello et al. 2015; Dewolf et al. 2018; Grasso et al. 2000), and is adapted with the speed of progression (Ivanenko et al. 2007). However, to the best of our knowledge, the relationship between stiffness and the intersegmental coordination has never been explored.

Although the modification of step frequency and running has been extensively studied (Cavagna et al. 1988, 1991; McMahon and Cheng 1990; Farley and González 1996; Lieberman et al. 2015; van Oeveren et al. 2021), the relationship between the bouncing mechanism and the kinematic coordination of the lower limb segments when modifying step frequency still raises many interesting unanswered questions. The aim of this paper is to shed light on the consequences of a change in step frequency on the running mechanics. Five different imposed step frequencies and the

preferred step frequency (PSF) were analysed at four different running speeds to try to answer this question. When running at higher SFs, we expect the bouncing mechanics to remain symmetrical, whereas the more the runner decreases their SF below the PSF the more their bouncing mechanics becomes asymmetrical for a similar speed. The kinematic synergy of the lower limb segments has been shown to adapt with speed (Ivanenko et al. 2007) however, a change in SF either increases/decreases the range of motion of the lower limbs and thus of their segments. Consequentially, this could change the relationship between them and, as seen in (Barliya et al. 2009), change the coordination patterns. The aim of this study was to investigate how changes in step frequency affect movement patterns and to better understand how the body's dynamic system adapts its leg configuration, and therefore its spring stiffness, to perform these more complex movements.

Materials & Methods

Participants and experimental procedure

Eight recreational healthy male runners with no injuries in the last 6 months participated in the study. The number of subjects chosen was based on an *a priori* statistical power analysis from results of a pilot study (Mesquita et al. 2021). The anthropometric and running characteristics of the subjects are presented in Table 2.1.1. Informed written consent was obtained and the study followed the guidelines of the Declaration of Helsinki. All procedures were accepted by the UCLouvain ethical committee (B403201838331).

	Subject information				**Preferred Step Frequency (steps s^{-1})**			
Subject	Height (m)	Mass (kg)	Leg Length (m)	Age (years)	08 km h^{-1}	11 km h^{-1}	14 km h^{-1}	17 km h^{-1}
1	1.88	74.1	0.98	21	2.44	2.44	2.62	2.74
2	1.83	68.7	0.96	21	2.75	2.70	2.74	2.84
3	1.83	70.4	0.95	22	2.40	2.58	2.53	2.66
4	1.82	68.0	0.92	22	2.76	2.90	2.92	2.95
5	1.89	83.9	0.99	23	2.76	2.85	3.01	3.10
6	1.79	69.4	0.91	24	2.77	2.89	2.93	3.00
7	1.87	77.2	1.00	22	2.56	2.61	2.68	2.74
8	1.80	78.2	0.97	23	2.65	2.79	3.01	3.15
Mean SD	**1.84** 0.03	**73.7** 5.65	**0.96** 0.03	**22.2** 1.03	**2.66** 0.14	**2.72** 0.17	**2.81** 0.18	**2.90** 0.18

Table 2.1.1 *Participants' anthropometric information and each subject's PSF at the different speeds along with the averages and standard deviations for each class.*

Participants ran on a treadmill at four different constant speeds: 8, 11, 14 and 17 km h^{-1} (corresponding to 2.22, 3.06, 3.89 and 4.72 m s^{-1}, respectively). At each speed, subjects were asked to run at 6 different step frequencies: their preferred step frequency (PSF), and 2.0, 2.4, 2.8, 3.2, 3.6 step s^{-1} conveyed *via* an electronic metronome and amplified on loudspeakers. This range of SFs was chosen based on Cavagna et al. (1991) where the authors showed that such frequencies correspond to the range where subjects are able to run at all speeds. To remove the effect of learning and fatigue and secure statistical independency, the different speeds and frequencies were presented randomly. A one-hour training session was done at least two days prior to recordings. At the end of the training session all subjects were able to run within ±5% of the imposed frequency.

The instruction given during the trials was that each foot strike should correspond to a beat of the metronome. For each trial, the treadmill belt accelerated until the target speed was reached. After an auditory check by the experimenters ensuring that the subject was running approximately at the correct SF, the recording began and lasted 10 seconds. The belt then decelerated, and in total each trial lasted ≈ around 1 minute.

After each recording, a check of the average SF over the entire trial was done with a custom written algorithm (Matlab, Mathworks, 2019 Natick, Massachusetts, USA) that used the *fft* routine on the vertical ground reaction force waveform. If the computed SF did not match the required one ±6% of error, the participant was asked to repeat the trial.

Experimental setup

Participants ran on an instrumented treadmill (h/p/Cosmos, Germany - Arsalis, Belgium) with a belt surface of 1.6 x 0.65 m. The entire treadmill was mounted onto four strain-gauge force transducers that measure the three components of the GRF exerted by the treadmill under the foot (Willems and Gosseye 2013). Each transducer's analogue signals were amplified, low-pass filtered (4-pole Bessel filter with a -3dB cut-off frequency at 200 Hz) to avoid an aliasing effect during digitisation and recorded with a sampling rate of 1 kHz. After digitalisation, the force signals were filtered by a two-way 8^{th} order Bessel filter with a lowpass cut-off frequency at 10 Hz for the lateral F_x, 20 Hz for fore-aft F_y and 30 Hz for vertical F_z forces (Mesquita et al. 2020).

The electrical motor of the belt was also instrumented with an optical angle encoder to measure the speed of the belt (v_{belt}). When the participants ran on the

treadmill, the recorded average speed of the belt over a stride (V_{avg}) differed by 2.8 ±1.4% from the chosen speed and the instantaneous v_{belt} did not change by more than 5% of V_{avg}.

Bilateral, full-body three-dimensional (3D) kinematics was recorded at 200 Hz by means of a Qualisys system with thirteen cameras (12 Mocap OQUS 6+ cameras and 1 video MIQUS M1 camera, Qualisys, Sweden) placed around the treadmill. Participants were equipped with 29 retro-reflective markers glued onto the skin at the following positions: chin-neck intersect (Neck), sternum (Chest), superior surface of acromion (Shoulder), lateral epicondyle of humerus (Elbow), ulnar styloid process (Wrist), superior anterior iliac spine (Waist), superior posterior iliac spine (BackWaist), greater trochanter (GT), mid-thigh (Thigh), external condyle of femur (Knee), shin (Shank), lateral malleolus (Ankle), heel (Heel), fifth metatarsophalangeal joint (VM) and second metatarsophalangeal joint (IIM) on both sides of the body. Kinematic data were then oversampled at 1 kHz using the spline routine in Matlab. An oversampling of the kinematic data was chosen rather than a down sampling of the kinetic data to ensure that the force signal characteristics were not lost during data-processing. The kinematic data was filtered by the same filter with a lowpass cut-off frequency at 30 Hz.

Data processing

Data processing was performed *via* custom made programs written with LABVIEW (National Instruments 2019, Austin, Texas, USA) and Matlab software.

Assessment of General Gait Parameters

Fig. 2.1.1 illustrates the time curves of the vertical and fore-aft components of the GRF in two of the four speed classes and all frequency classes. A stride period is defined based from the foot contacts. A foot contact corresponds to the moment at which the vertical component of the ground reaction force (F_z) becomes greater than ten percent of *BW*. The stride period is defined as the time between a right foot contact and the next right foot contact and the step period is defined as the time between the foot contact of one leg until and the next foot contact of the contralateral leg. The effective contact time, t_{ce}, corresponds to the period during which $F_z \geq BW$ and the effective aerial time, t_{ae}, corresponds to the period during which $F_z < BW$ as in Cavagna et al. (2009). Furthermore, the contact phase (t_c), the period between the touch-down and take-off of the corresponding foot, can also be divided into an initial braking phase (t_{brake}) followed by a pushing phase (t_{push}). t_{brake} is defined as the time

spent decelerating the CoM during t_c and t_{push} as the time spent re-accelerating it preceding the take-off phase.

We considered valid strides when: (1) the average vertical force during the stride ($\overline{F_z}$) is within 5% of BW, (2) the sum of the increments and the sum of the decrements of the instantaneous velocity (v_y) of the CoM differed less than 25% as in Dewolf et al. (2016), (3) the step frequency was equal to the metronome step frequency ±5%. In total 2385 valid strides (4790 steps, 599 ± 75 steps per subject, mean ± SD) were selected.

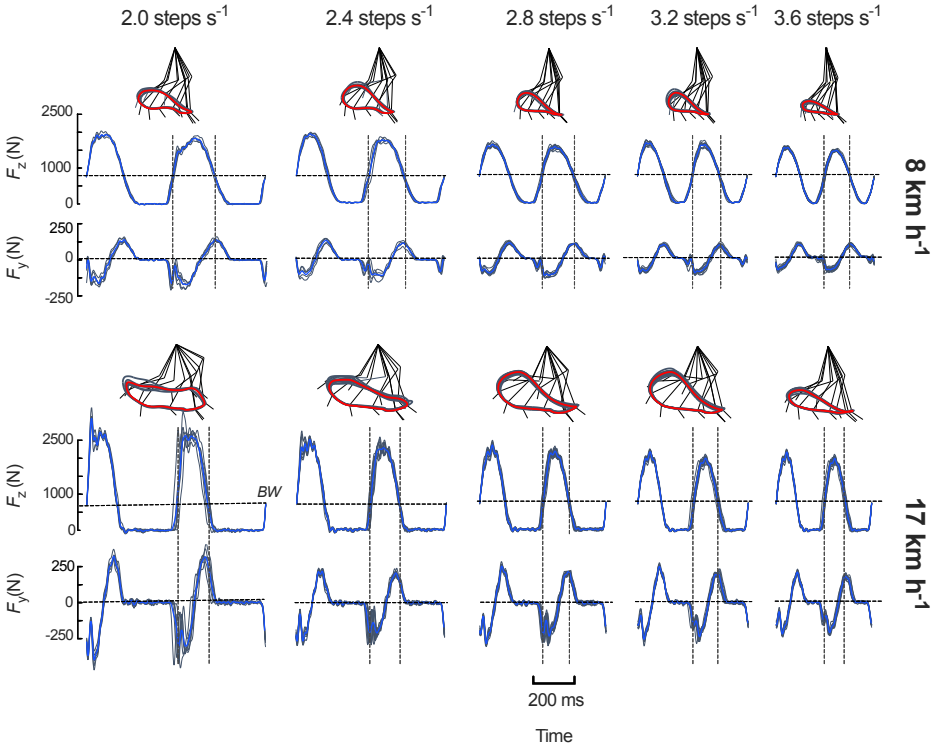

Fig. 2.1.1 *(A) Average (blue) and individual (grey) time-curves of the fore-aft (F_y) and vertical (F_z) components of the GRF done by one subject at each step frequency (SF) class at 08 and 17 km h^{-1}. In the upper left corner of each panel, a stick diagram indicates the position of the limb-segments relative to the GT landmark every 10% of a stride. The loop illustrates the trajectory of the ankle relative to the GT over one stride.*

Computation of Acceleration, Velocity and Vertical Displacement of the CoM

The acceleration, velocity and displacement of the CoM was calculated from the GRF as in Gosseye et al. (2010) and in Mesquita et al. (2020). Briefly, the fore-aft and vertical CoM accelerations were obtained respectively as $a_{\mathrm{f}} = \frac{F_y}{m}$ and $a_{\mathrm{v}} = \frac{F_z}{m} - g$. We did not consider the lateral component of the GRF since its contribution is negligible (Willems et al. 1995).

A time-integration of the a_{f}, and a_{V}-recordings give the fore-aft (v_{f}) and vertical (v_{V}) velocity changes of the CoM. Integrations are performed numerically by the trapezoidal method. An integration constant must be added to v_{f}, and v_{V} to obtain the components of the instantaneous velocities of the CoM relative to a reference frame fixed to the treadmill as in Gosseye et al. (2010). The vertical (S_{V}) displacement of the CoM relative to the treadmill is then computed by numerical integration of v_{V}. S_{v} can be further divided during the contact phase into two periods: after touchdown while the CoM is descending until its minimum ($S_{\mathrm{c,down}}$) and then once the CoM is rising until take-off ($S_{\mathrm{c,up}}$).

Computation of the External Work (E_{com}), Work (W_{ext}) and push-averaged power ($\dot{W}_{ext}$)

The energy of the CoM (E_{com}) done in respect to its environment was computed based on the fore-aft and vertical movements of the CoM. The energy due to the fore-aft movements of the CoM (E_{kf}) can be computed by: $E_{\mathrm{kf}} = \int F_{\mathrm{y}} \left(v_{\mathrm{f}} - V_{\mathrm{avg}}\right) \mathrm{d}t = \frac{1}{2}\, m \left(v_{\mathrm{f}} - V_{\mathrm{avg}}\right)^2$, where V_{avg} is the average speed of the treadmill. The energy of the CoM due to its vertical movements (E_{v}) can be computed by: $E_{\mathrm{v}} = \int (F_{\mathrm{z}}\, v_{\mathrm{v}})\ \mathrm{dt} = \frac{1}{2}\, m\, v_{\mathrm{v}}^2 + m\, g\, S_{\mathrm{v}}$. Then, the E_{com} is given by $E_{\mathrm{com}} = E_{\mathrm{kf}} + E_{\mathrm{v}}$.

Fig. 2.1.2A presents the time-curves of E_{kf}, E_{v} and E_{com} (blue curves) while running at 8 and 17 km h^{-1} in each frequency class. The positive external power done to move the CoM relative to the surroundings ($\dot{W}_{\mathrm{ext}}^{+}$) is then calculated as the sum of the positive increments from the E_{ext} - curve over one stride (W_{ext}^{+}), divided by the time of the stride (Fig. 2.1.2B). The average power done during the push phase ($\dot{W}_{\mathrm{ext,push}}$) is computed by dividing W_{ext}^{+} by the positive work phases, t_{push} (Table 2.1.2).

Computation of the Internal Power ($\dot{W}_{int}$)

The computation of the internal work done to accelerate and rotate the limbs relative to the CoM has been described in detail in Willems et al. (1995). Both legs were modelled as a multi-segmented limb formed by thigh, shank and foot segments. The upper body was modelled as a trunk, two arms and two forearm-hand segments (Dempster and Gaughran 1967). The internal energy of the i^{th} segment is given by: $E_{\mathrm{int}}^{\mathrm{i}} = \frac{1}{2}\left(m_{\mathrm{i}}\, V_{\mathrm{i}}'^{2} + I_{\mathrm{i}}\, \omega_{\mathrm{i}}^{2}\right)$ where m_{i} is the mass of the segment and I_{i} is its moment of inertia around its centre of mass, V_{i}' is the translational velocity of the segment's centre of mass relative to the CoM and ω_{i} is the rotational velocity of the segment. The energy of the segments of the same limbs were added to obtain the energy of each limb. This procedure assumes that energy transfers are only possible between segments of the same limb, but not among the limbs (Willems et al. 1995; Dewolf et al. 2019a). The internal energy time-curves (red curves) of the left and right upper-limbs (sum of upper-arm and lower-arm) and lower-limbs (sum of the thigh, shank and foot) while running at 8 and 17 km h^{-1} are presented in Fig. 2.1.2A. The positive internal power $\dot{W}_{\mathrm{int}}^{+}$, Fig. 2.1.2B, is calculated as the sum of the positive increments of the internal energy of the four limbs divided by the stride time.

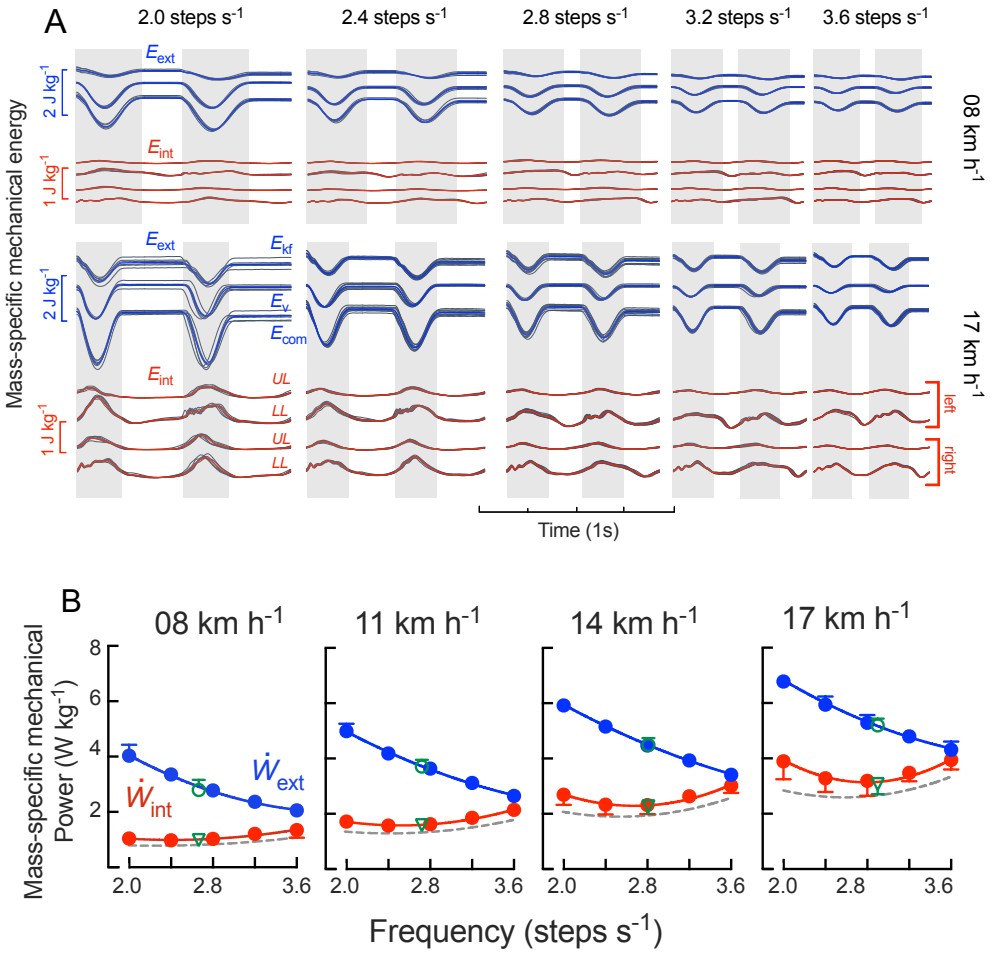

Fig. 2.1.2 *(A) Average (blue) and individual (grey) time-curves of the normalised external energy done by the CoM (E_{com}), the energy done to sustain the movements in the vertical direction (E_v) and the energy done to sustain the movements in the fore- aft direction (E_{kf}) at each step frequency. The four red and corresponding grey time-curves represent respectively, from top to bottom, the normalised internal energy of the: left upper limb (UL), left lower limb (LL), right upper limb (UL) and right lower limb (LL) relative to the CoM for each SF at both 08 and 17km h^{-1}. The grey contours in each panel correspond to the contact phases. Panel B shows the normalised mechanical external ($\dot{W}$ext, blue circles) and internal ($\dot{W}$int, red circles) power done by the CoM (W kg^{-1}) as a function of SF at different speeds. The points represent a grand mean and standard deviation at each step frequency. The green coloured open symbols represent the PSF grand mean and SD at different speeds. The grey dotted line represents the $\dot{W}_{int}$ of lower limb. The line which passes through all points is a quadratic non-linear regression as defined in Graphpad-Prism (Dotmatics, CA, USA).*

Speed (km h^{-1})	2.0 (steps s^{-1})	2.4 (steps s^{-1})	PSF (steps s^{-1})	2.8 (steps s^{-1})	3.2 (steps s^{-1})	3.6 (steps s^{-1})
Mass specific push-averaged power $\dot{W}_{ext}$ (W kg^{-1}) (mean ±SD)						
8	12.51 ±2.99	9.36 ±1.44	7.08 ± 1.28	7.20 ± 1.15	6.17 ±1.084	5.31 ± 1.27
11	17.76 ± 2.87	13.18 ± 1.56	11.02 ± 1.58	10.84 ± 0.77	8.79 ± 0.99	7.26 ± 1.26
14	23.61 ± 2.37	18.46 ± 1.97	14.62 ± 1.39	14.76 ± 0.70	12.11 ± 0.58	10.24 ± 1.12
17	29.25 ± 2.42	23.39 ± 2.35	18.11 ± 1.31	18.75 ± 1.23	16.10 ± 0.91	14.08 ± 1.18

Table 2.1.2 *Average and standard deviation mass-specific push-averaged power (W kg^{-1}).*

Computation of the Mechanical Stiffness

The mass-specific vertical stiffness (k_{vert}) was measured from the linear relation between a_v and S_v (Fig. 2.1.3). The slope of this linear relation was estimated as the ratio between the maximal vertical acceleration ($a_{v,max}$) of the CoM (whose event occurs close to the time at which the CoM reaches its lowest point) and the vertical displacement ($S_{v,ce}$) of the CoM during t_{ce} (Fig. 2.1.3): $k_{vert} = \frac{a_{v,max}}{S_{v,ce}}$.

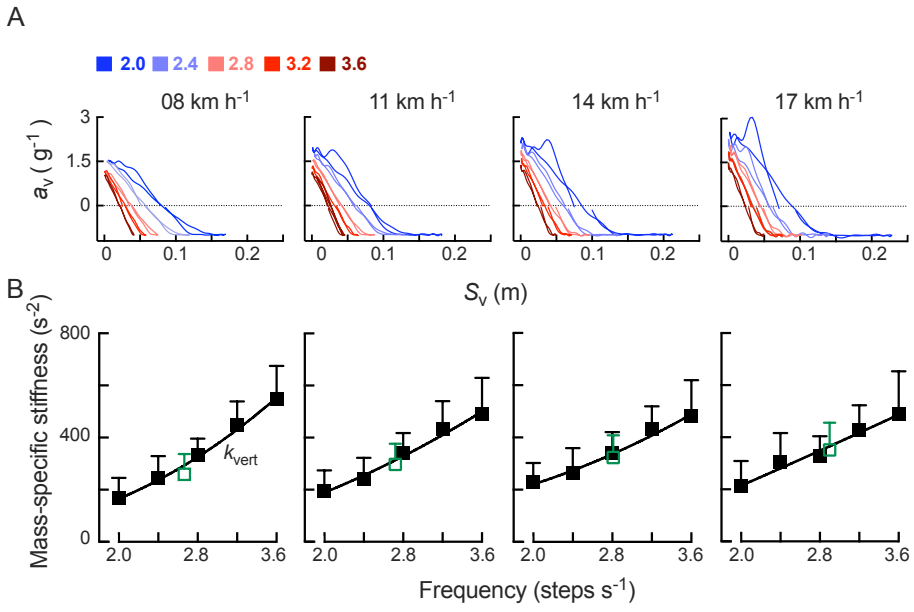

Fig. 2.1.3 *(A) Acceleration of the CoM, a_v (g^{-1}), as a function of the vertical displacement (S_v) at different speed classes. Each curve represents a specific step frequency class. Note, the vertical stiffness (k_{vert}) of the CoM is characterised by the slope of each curve. Panel (B) shows k_{vert} as a function SF at different speed classes. All other indications are as in Fig. 2B.*

Quantification of the Intersegmental Coordination via the Planar Covariance Law

For each limb segment, the elevation angles (θ) in the sagittal plane (*i.e.* the orientation of the segment in the sagittal plane relative to vertical) was computed by: $\theta = \arctan\left(\frac{y_p - y_d}{z_p - z_d}\right)$, where ($y_p$, z_p) and (y_d, z_d) are, respectively, the fore-aft (y) and vertical (z) coordinates of the proximal (subscript p) and distal (subscript d) markers of the segment. The joint angles (hip, knee, and ankle) were computed from the elevation angle of adjacent segments. The range of motion (ROM) during the stance and swing phases of each joint was computed as the difference between the maxima and the minima of each joint waveform over each period.

The phase relationship between the three angles was assessed by computing the phase lag between each elevation angles and a cosine function (*xcorr* routine in Matlab). The difference in phase lag between the shank and foot segments elevation angles are presented in the results.

For each trial, time-curves of the elevation angles of the thigh, shank and foot were time-interpolated over individual strides to fit a normalised 800-point time-base. The elevation angles waveforms of the left leg were shifted by 50% of the stride period. A first average was done across left and right strides separately, then both legs were pooled together. In each condition, the average waveforms of the elevation angles of the three lower-limb segments: thigh, shank and foot were computed across participants.

In each speed-frequency class, the inter-segmental coordination of the lower-limb segments was assessed using principal component analysis (PCA). This procedure has been described in detail in the literature (*e.g.* Borghese et al. 1996; Daffertshofer et al. 2004; Dewolf et al. 2018; Catavitello et al. 2018) and will only be explained briefly here. The centred thigh, shank, and foot elevation angles waveforms once plotted in a three-dimensional space form a loop which lies close to a plane. The best fitting plane is the one generated by the first two components extracted by the PCA performed on the covariance matrix of the three elevation angles waveforms (Daffertshofer et al. 2004; Ivanenko et al. 2008). The PCA returns the matrix of eigenvectors U with its associated eigenvalues (λ_1, λ_2, λ_3) rank-ordered from the highest to the lowest. The eigenvectors u_1 and u_2 generate the best fitting plane and the third eigenvector, u_3, orthogonal to the first two, defines the orientation of the plane. The components of the u_3 vector: u_{3t}, u_{3s}, and u_{3f} correspond to the direction cosines with the positive semi-axis of the thigh, shank and foot angular

coordinates, respectively (Fig. 2.1.6). The percentage of variance associated to the u_3 vector ($PV_3 = \lambda_3 / (\lambda_1+\lambda_2+\lambda_3)$) was used as a planarity index ($PV_3 = 0\%$ for maximum planarity).

Statistics

For each participant, the dynamic parameters (*e.g.* T, t_{ce} t_{ae}, L_{ce}, L_{ae}, k_{vert}) were averaged first across the right and left steps for each stride then averaged per stride, whereas the kinematic parameters (elevation angles, ROM, u_3, PV_3, *etc.*) were averaged directly across strides. Then descriptive statistical analysis was performed. First, the Shapiro-Wilk test was performed to verify normality. When the data did not meet the normal distribution criteria (Shapiro-Wilk's W-test, $p < 0.05$) non-parametric statistics were used for data analysis. A linear mixed effect model with *Bonferroni* post-hoc correction was used to assess the individual and interaction effects of frequency and speed on the calculated variables. When comparing means between two groups, for example when analysing the *on-off ground asymmetry,* a paired t-test was used. Statistical tests were run on IBM SPSS Statistics (PASW Statistics, 19, SPSS, IBM, Armonk, NY, USA). The results of the statistical tests were considered significant for a p-value <0.05. When a curve was drawn on figures, these were based on quadratic fits done on GraphPad Prism (GraphPad Software, LLC, Dotmatics, San Diego CA, USA).

Results

Effect of running frequency on the work and power done

External work and power. The external work done per step is much greater at low SFs than at high SFs ($p < 0.001$, fixed effect estimates between 2.0 and 3.6 steps s^{-1}: 0.71, $p < 0.001$; Fig. 2.1.2B). The mass-specific external power ($\dot{W}_{ext}$) is plotted in Fig. 2.1.2B, it decreases with speed and SF (F_{fq} =129.3, $p < 0.001$). The push-averaged mechanical power ($\dot{W}_{ext,push}$) was also greater at fast running speeds ($p < 0.001$) and greater at smaller SF as compared to higher SF ($F_{fq} = 16.7$, $p < 0.001$) (Table 2).

Internal work and power. The internal positive power increases when deviating from PSF (Fig. 2.1.2). Indeed, for each speed, the positive internal power is at its minimum between ± 2.4 and ± 2.8 steps s^{-1} (the *minima* are 2.39, 2.52, 2.68, 2.79 steps s^{-1} respectively at 8, 11, 14 and 17 km h^{-1}, based on a polynomial regression curve in Fig. 2.1.2B). The increase in W_{int} is greater when running at higher SFs and

low SFs compared to PSF (F_{fq} = 728.2, p < 0.001). Furthermore, the internal power ($\dot{W}_{int}$), as seen in Fig. 2.1.2, increases with both speed and frequency (F_{fq} = 24.2, p < 0.001). However, when analysed separately, we observed that the upper limb $\dot{W}_{int}$ increases with speed but decreases with frequency (F_{fq} = 18.45, p < 0.001).

Bouncing mechanism of running

Vertical stiffness. Fig. 2.1.3 illustrates the vertical GRF plotted as a function of the vertical displacement of the COM, showing a quasi-linear relationship. The mass-specific vertical stiffness was reduced with lower SF and increased with higher SF (p < 0.001, Fig. 2.1.3). At the PSF, k_{vert} increases with speed as in Cavagna et al. (1988), whereas throughout the frequency classes, k_{vert} does not vary much with speed. The increase of vertical stiffness is related to the vertical force applied to the ground. Indeed, the $F_{v,max}$ is greater at low SF as compared to high SF (F_{fq} = 956.9, p < 0.001; Fig. 2.1.1).

On-off ground asymmetry. When running at an imposed step frequency, the speed can only be changed by tuning the step length, L (Fig. 2.1.4). At a frequency of 2 step s^{-1}, L varies from ~1.1 m at 8 km h^{-1} to ~2.4 m at 17 km h^{-1}. The horizontal distance covered by the CoM during t_{ce}, *i.e.* L_{ce} ranges from 0.5 m at the lowest speed to 0.75 m at the highest speed, close to the maximal anatomical value previously determined by Cavagna et al. ~ 0.7m (1991). Since L_{ce} is limited, L is increased by increasing L_{ae} (L - L_{ce}). When speed increases, the period t_{ce} to cover the distance L_{ce} decreases and consequently, t_{ae} (T -t_{ce}) must increase accordingly. Subsequently, when running at low SFs, the bounce is asymmetric at all speeds, *i.e.* $L_{ce} < L_{ae}$ and $t_{ce} < t_{ae}$ (for t_{ce} , $t_{ae:}$ p<0.007 and for L_{ce} , L_{ae}: p<0.002 at slow speeds) and this asymmetry is more pronounced the higher the speed (for t_{ce} , t_{ae} and for L_{ce} , L_{ae}: p<0.001 at fast speeds).

At 3.6 step s^{-1}, L varies from ~0.6 m at 8 km h^{-1} to ~1.3 m at 17 km h^{-1}. At this frequency, L_{ce} ranges from 0.3 m at the lowest speed and 0.6 m at the highest speed, which is smaller than the anatomical limitation. For most speeds, $L_{ce} = L_{ae}$ (p > 0.05), and in turn $t_{ae} = t_{ce}$ (p > 0.05), except at 17 km h^{-1} where it becomes slightly asymmetric (p < 0.001 for both). Therefore, when running at a higher frequency, the bounce is symmetric in a larger range of speeds.

Landing-take off asymmetry. The timing of negative and positive work production during t_c varies with speed and step frequency (Fig. 2.1.4). In particular, t_{push} is modified by the SF (F = 776.4, p<0.001). Indeed, the timing during which muscles perform positive external work is extended during running with a lower SF

while it is decreased at a higher SF ($F = 776.4$, $p<0.001$). This landing-take off asymmetry is also reflected in the displacement of the COM during the contact phase. At low SFs and slow running speeds, the vertical downward displacement of the COM, $S_{c,down}$, is greater than its upward counterpart (Fig. 2.1.4), this difference lessens with increasing speed and SF.

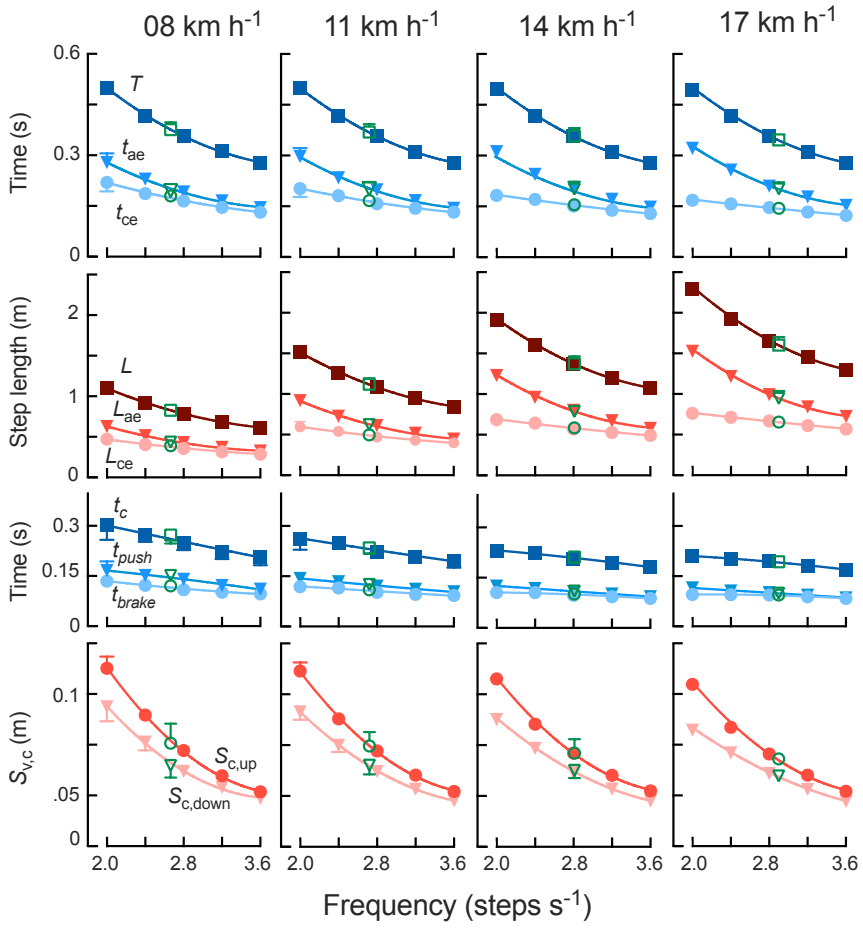

Fig. 2.1.4 Spatiotemporal and step length parameters presented as a function of SF at different speed classes. *The upper row presents the step time (T, dark blue squares), effective aerial time (t_{ae}, light blue circles) and effective contact time (t_{ce}, light blue triangles). The second row represents the corresponding step length (L, dark red squares), effective aerial length (L_{ae}, light red triangles) and effective contact length (L_{ce}, pink circles). The third and fourth rows show the spatiotemporal parameters and vertical displacement of the CoM, both occurring during the contact phase (t_c). In the top row, the t_c (dark blue squares) is divided into its brake (t_{brake}, light blue circles) and push phases (t_{push}, light blue triangles). In the bottom row the vertical displacement of the CoM during the contact phase is divided into the displacement done between the touch down and minimum height ($S_{c,down}$, pink triangles) and from the minimum until take-off height ($S_{c,up}$, red circles). All other indications are as in Fig. 2.1.2B.*

Kinematics of running

Intersegmental coordination. Fig. 2.1.5 illustrates the time-normalised elevation angular motion waveforms of the thigh, shank and foot over an entire stride at 8 and 17 km h^{-1} and in all frequency classes. Below each group of curves is depicted the corresponding, 3-dimensional view of the elevation angle trajectories along with the best fitting plane. At each speed, an increase of the step frequency corresponds to a rotation of the covariation plane (*i.e.* when reading Fig. 2.1.5 from left to right), whereas maintaining a fixed step frequency and increasing the speed (*i.e.* reading from top to bottom), the rotation is no longer evident. This is further shown in Fig. 2.1.6, where u_{3t}, the direction cosine of the third eigenvector which is orthogonal to the plane, increases with frequency but not with speed ($F_{fq} = 22.9$, $p < 0.001$; speed: $p = 0.8$). It can also be observed that at 2 step s^{-1}, the shape of the loop is drastically different from the other conditions and is speed dependent, changing from a drop-like shape at 8km h^{-1} to a quasi-ellipse at 17km h^{-1}, while at the other conditions the only observation is an enlargement of the loop whilst keeping a similar shape. u_{3s} slightly decreases with SF ($F = 5.44$, $p < 0.001$) and does not change with speed ($p = 1$). Concerning u_{3f}, there is a slight effect of SF ($F = 2.9$, $p = 0.02$) and of speed ($p < 0.001$). The latter is because there is a difference between 8 km h^{-1} and the other speeds (fixed effect estimate -0.32, $p < 0.014$, compared to 17 km h^{-1}).

The percentage of variance accounted for by the third eigenvector (PV_3) was used to quantify the planarity. Results show that the planarity was generally maintained for all speed and frequency classes (PV_3 ranged between 1.3% and 3.6%, overall minimum and maximum values respectively). Linear mixed model effect shows a slight interaction effect between the speed of progression and frequency ($p = 0.007$). However, when considering post-hoc correction PV3 is significantly lower at speeds above 14 km h^{-1} ($p < 0.001$) as compared to slower speeds. Furthermore, PV3 is lower at SFs below 2.8 steps s^{-1} compared to PSF ($p < 0.001$).

At 2.0 step s^{-1}, the movements of the shank and the foot are not in phase. When speeds and frequencies increase, the phase shift between the shank and foot elevation angles tends towards 0 meaning the movements of these two segments become gradually in phase (SF: $F = 10.6$, $p < 0.001$; speed: $p = 0.127$). The phase relationship between the thigh and shank elevation angles decreases with speed ($p<0.001$) and increases at the lowest frequencies as compared to PSF (SF: $F = 7.58$, $p < 0.001$).

Both the amplitude ratio and the time relationship characteristics between the elevation angles of two adjacent limb segments determine the lower-limb joint angle. For example, if the shank and foot elevation angles have the same amplitude and are

in phase, no motion would occur at the level of the ankle. Therefore, since a joint angle can be deduced from two adjacent elevation angles, the joint angles and their ROM are only presented in supplementary materials (Figs. 2.1.S1 and 2.1.S2).

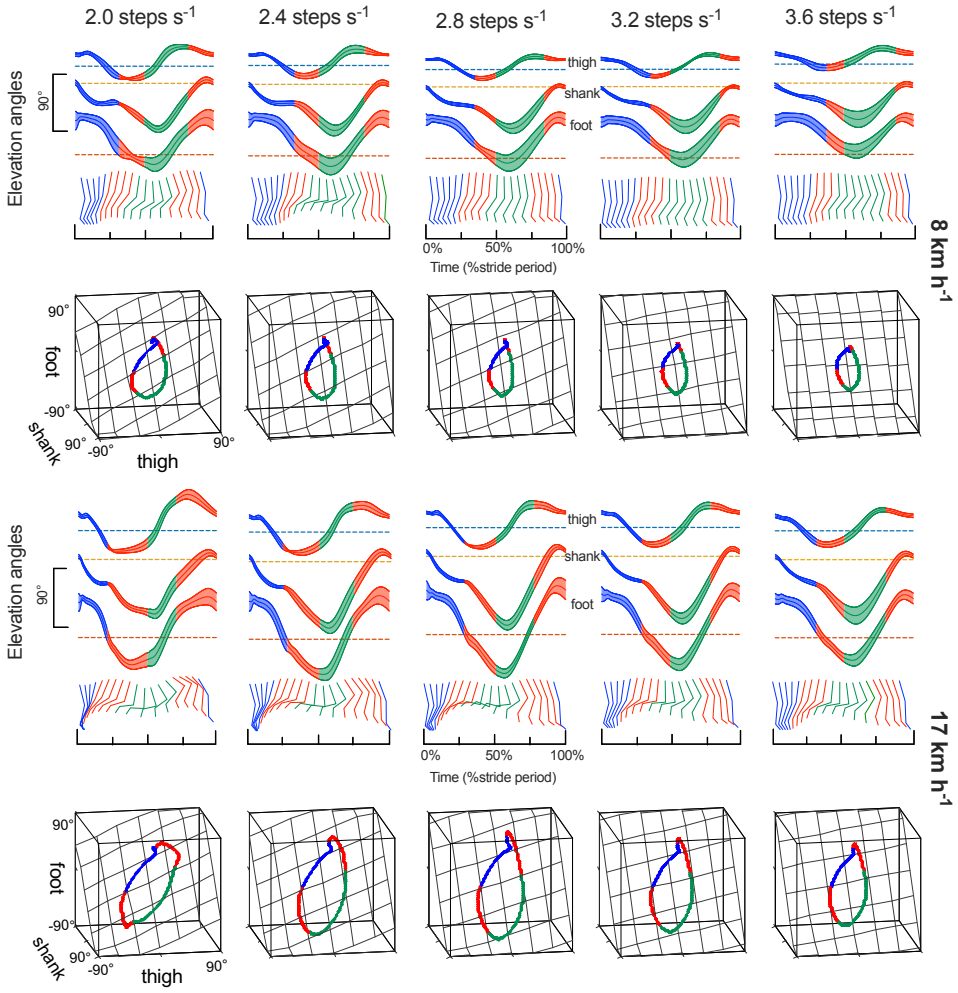

Fig. 2.1.5 *Time normalised average ± standard deviation cloud of the lower limb elevation angles done over a percentage of stride at different SF presented at both 08 and 17 km h^{-1}: thigh (top), shank (middle), and foot (bottom). The stride is cut into their four sequential temporal parts. (1) Blue corresponds to the contact time, followed by (2 and 4) the aerial phases in red, (3) the green represents the contact time of the other leg. The horizontal, respectively coloured, dashed line represents the neutral standing position of each segment. The stick figures below represent a typical trace of one subject taken every 5% of the stride, the colours represent the same temporal phases as the elevation angles. The cubes below show the average loop trajectories across all participants with superimposed the best fitting covariance planes (the grey grids).*

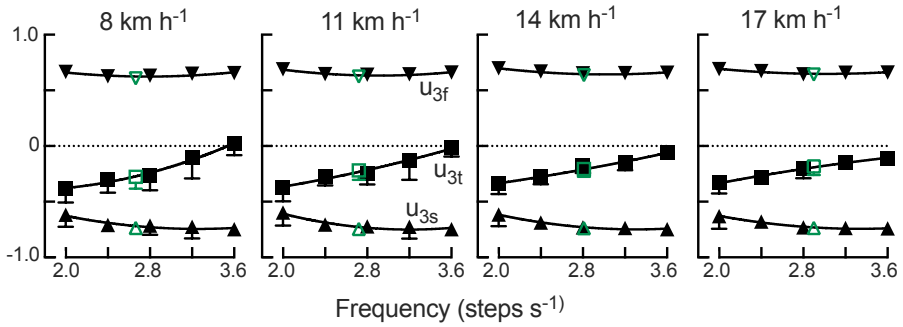

Fig. 2.1.6 *The third eigenvector direction cosines for the thigh (u_3t, squares), shank (u_3s, upper triangles) and foot (u_3f, downwards triangles) segments, of the normal to the covariation plane as a function of SF at different speeds. All other indications are as in Fig. 2.1.2B.*

Discussion

The effect of step frequency on the bouncing mechanism

When running speed increases, the PSF increases from 2.7 steps s^{-1} at 2.2 m s^{-1} to 2.9 steps s^{-1} at 4.7 m s^{-1}. Already well-documented in the literature (He et al. 1991; Cavagna et al. 1988), we observed an effect of speed on the vertical stiffness at PSF. Regarding a change in frequency at a given speed, a linear relationship between k_{vert} and SF has been documented at only one relatively slow speed of progression (*i.e.* 2.5 m s^{-1}) by Farley and González (1996). Here, by analysing various speed classes, we highlight another important finding. In each speed class, k_{vert} increases similarly with SF as observed in Farley and González. This result suggests that the adaption of k_{vert} to a particular speed reflects a change in the frequency chosen by the runner more than a change in the running speed itself. This is evidenced by the 'sliding' of the PSF values upon the frequency curves at different speed classes for k_{vert} as shown by the green square dots in Fig. 2.1.3B.

Similarly, the observation is also valid for the orientation of the covariance plane, which reflects the coordination between the lower-limb segments. Indeed, at the PSF an effect of speed has been observed or so, the orientation of the plane rotates as a function of speed (Ivanenko et al. 2007). However, as for k_{vert} when considering the whole data set of speeds and frequencies, we observed an increase of u_{3t} as a function of SF but not as a function of running speed. In other words, the effect of speed on u_{3t} at PSF could simply be due to a change in the preferred step frequency across speeds.

The choice of PSF, at the speeds studied in this paper, has been shown to be self-optimised by runners in a way that minimises both the mechanical and metabolic power of the runner (Cavagna et al. 1991; Burns et al. 2019). This is a central element in the development of an economical and safe running gait (Williams and Cavanagh 1987; Moore 2016; Folland et al. 2017). As explained in the recent review by Van Oeveren et al. (2021), debate exists whether SF is modified within trained/elite runners as compared to recreational/amateur runners: some authors show an increase of SF in athletes (Slawinski and Billat 2004; Nuñez Lisboa et al. 2021), others find a decrease (da Rosa et al. 2019) and still others find no significant differences between groups (Folland et al. 2017). In fact, the choice of PSF is highly dependent on the speed of progression, however better runners are shown to have a resonant step frequency (*i.e.* the natural frequency of the bouncing system) (Cavagna et al. 1991) that is increased as compared to amateur runners, as argued in da Rosa et al. (2019).

Running with a high step frequency

As described in Cavagna (2010), running with a step frequency higher than the PSF requires less important GRFs each step, both in the fore-aft and vertical direction (Fig. 2.1.1), thus less external work and power (Fig. 2.1.2) to move the CoM. On the contrary, the internal power, $\dot{W}_{\mathrm{int}}$, to move the limbs relative to the CoM is increased as the time to reset the limb is shorter and the limbs must be reset more often per unit time.

From a mechanical point of view, running with a higher step frequency seems to accentuate the elastic bounce of running. Indeed, the spring becomes stiffer as the vertical displacement is smaller and both the contact (t_c) and effective (t_{ce}) contact times are smaller (Farley and González 1996). Furthermore, producing smaller steps is also done by reducing the effective aerial phase (t_{ae}), which becomes shorter (Fig. 2.1.4). We observe here that the subjects spontaneously adopt a *symmetric rebound*, where the duration of the lower part and upper part of the vertical oscillation is about equal and the step frequency equals the natural frequency of the bouncing system (Cavagna et al. 1988). According to Cavagna (1997), tuning the step frequency to the natural frequency of the bouncing system results in a minimum of metabolic energy expenditure and in a maximum of the efficiency of conversion of stored energy into positive work.

The accentuation of the 'elastic bounce' in human running shows smaller differences between the 'braking phase', where elastic energy is stored into the muscle-tendon unit, and during the 'push phase', where elastic energy is released (Ruina et al. 2005; Cavagna 2009; Dewolf and Willems 2017a, 2019b). First, the

difference observed between the downward and upward displacements of the CoM during contact is reduced at higher SFs (Fig. 2.1.4), suggesting a smaller hysteresis in the force-length relationship of the spring leg. Second, the duration of the positive work production phase, t_{push} becomes similar to that of the negative work production phase, t_{brake}. The bounce of an elastic structure with no hysteresis would imply a $t_{push} \approx t_{brake}$ and $S_{c,down} \approx S_{c,up}$ (Cavagna 2009); therefore the modifications observed at high SFs are an expression of a more efficient use of elastic rebound, *i.e.* that the positive energy released approaches the negative energy stored. Nevertheless, when SF increases, the more efficient elastic rebound translates to less external work produced by the transformation of chemical energy into mechanical work but also comes with an increase of the internal work (Cavagna et al. 1991).

From a kinematic point of view, in order to perform a smaller step length, the ROM of the lower limb segments (elevation angles) and consequently of the joints is adapted. The reduction of step length with higher SF induces a reduction of the thigh elevation angle ROM (and in turn of the hip ROM) during both the contact and aerial phases (Fig. 2.1.5 and Fig. 2.1.S1). Furthermore, the ROM of the knee reflects the modifications brought about the amplitude and timing relationship of the thigh and shank segment elevation angles (Fig. 2.1.S1 and Fig. 2.1.5). During the contact phase, the knee ROM decreases to control the vertical stiffness of the lower limb (Ferris and Farley 1997; Günther and Blickhan 2002). During the aerial phase, it has been reported that runners with a higher SF have higher knee flexion during the swing phase (van Oeveren et al. 2021). At first glance, our results (Fig. S2) would disagree with these findings, however, at the speeds measured in this study, the normal ranges of PSF are on average always below 3 steps s^{-1} (Table 1). When the SF rises above 3 steps s^{-1} the time required for the aerial phase is too short for a runner to fully swing their leg and adequately bend their knee. Consequently, knee ROM decreases at higher SFs, despite its negative consequences on the W_{int} (Fig. 2.1.2). Additionally, as step length decreases, the phase relationship between shank and foot segments elevation angles tend to 0 (Fig. 2.1.5) and ankle motion decreases. It has been noted that ankle motion is primarily a consequence rather than a cause of leg motion (van Oeveren et al. 2021). Moreover, this reduction in ROM during the contact phase, as frequency increases, may contribute to the reduction of the *landing-take-off* asymmetry (Maykranz and Seyfarth 2014).

In addition to the modifications of joint angles, the changes in the phase relationships between the elevation angles of the lower limb segments are evidenced by changes in the third eigenvector, and in particular u_{3t} (Barliya et al. 2009; Bianchi et al. 1998). The eigenvector direction cosine, u_{3t} tends towards zero at the highest

SF which is most likely due to the reduction of the distance between the minima of the foot and shank segments that are more in-phase (Figs. 2.1.5 and 2.1.6). Because of the reduction of movement amplitude, we also observe that the loop amplitude decreases with increasing step frequency (Fig. 2.1.5).

Running at a low step frequency

Running with a step frequency lower than the PSF requires greater GRF in both the fore-aft and vertical direction to travel (Fig. 2.1.1), thus increasing the external work (and therefore the external power, Fig. 2.1.2). In turn, the internal power done over the step, $\dot{W}_{\mathrm{int}}$, is reduced as the time to reset the limb is longer and the limbs must be reset less often per unit time (Fig. 2.1.2). However, at the lowest SFs $\dot{W}_{\mathrm{int}}$ increases after reaching a minimum.

From a mechanical point of view, running with a step frequency lower than the PSF seems to lessen the effectiveness of the elastic rebound at any speed. Indeed, k_{vert} is reduced as the vertical displacement and the effective contact time (t_{ce}) increase. Furthermore, at a given speed for a runner to increase *SL*, they must lengthen both L_{ae} and L_{ce} until the latter reaches its physiological limit (~0.6-0.7 m) (Cavagna et al. 1988, 1991, 1997) (Fig. 2.1.4). Beyond this point, the only way of increasing L is by increasing L_{ae}. As a result, $t_{\mathrm{ce}} < t_{\mathrm{ae}}$ and the subjects adopt an *asymmetric rebound*.

The t_{ae}, t_{ce} asymmetry implies that the velocity at take-off and so the power produced during t_{push} must be increased. A greater push-averaged power ($\dot{W}_{\mathrm{ext,push}} = W_{\mathrm{ext}}/t_{\mathrm{push}}$) is therefore observed (Table 2). This is similar to uphill running or running against a horizontal traction force, where the push-average power must be increased (Dewolf et al. 2016; Mesquita et al. 2020), the increase of power is limited by (i) increasing the duration of the push at the expense of the duration of the brake (Fig. 2.1.4), and (ii) by reducing the downward displacement of the CoM as compared to its upward motion.

Running at a low SFs has consequences on the kinematic strategies adopted by the subject as evidenced partly by the larger and quasi-ellipse shaped loop (Fig. 2.1.5). Due to changes in the phase relationships between the elevation angle waveforms of the lower limb segments, the changes in u_{3t}, (Figs. 2.1.5 and 2.1.6) are evidence of an adapted kinematic strategy (plane rotation) when reducing SF. Particularly, u_{3t} decreases with lower SF, while u_{3s} decreases and u_{3f} remains relatively constant. Moreover, u_{3t} has been correlated with the mechanical energy expenditure during walking (*i.e.* the higher the third eigenvector, the higher the net

mechanical power) (Borghese et al. 1996; Grasso et al. 2000). This could imply that the rotation of the covariance plane is correlated with the net mechanical power produced to move the CoM in running. At slower step frequencies, the third eigenvector is furthest from 0, *i.e.* the plane rotates considerably at such SFs, potentially related to the fact that the net mechanical power developed to move the CoM forward is increased (Figs. 2.1.2, 2.1.5 and 2.1.6).

The lower limb and joint motion at touchdown have been reported to be similar at the level of the thigh, the knee and ankle for SFs ranging from 2.5 to 3.1 steps s^{-1} (Clarke et al. 1985). Whereas we also observed little to no modification at touchdown, the ROM during the contact phase is influenced by the SF. For example, the longer steps are a consequence of a modification of the thigh oscillation (and in turn the hip) during the contact phase (Fig. 2.1.5 and S2), even if this increase is limited by anatomical factors. A consequence of such limitations is that the thigh ROM increases mainly during the aerial phase. Also, during the contact phase, the knee ROM increases as the vertical displacement increases, indirectly controlling the reduction of lower limb stiffness with low SF. Concerning the ankle joint, the ROM during the contact phase also increases as SF decreases. The greater joint ROM, reflects the modification of the phase relationship between shank and foot segment elevation angles, may reflect a greater contribution of the muscle to the length change of the muscle-tendon unit during contact, thus deviating from an elastic rebound (Fig. 2.1.5, 2.1.S2).

During the swing phase, the subject sees their aerial peak knee flexion (and in turn the $ROM_{ta,}$ Fig. 2.1.S2) decrease as the SF decreases. A smaller knee flexion throughout the aerial phase leads to an increased inertia of the swing leg over the aerial phase (Willems et al. 1995). A greater swing leg moment could be used by the runner as a supplementary upwards impulse to the stance leg as it pushes off the ground (Seyfarth et al. 2022), to increase the propulsive forces in the fore-aft direction that are associated with running at lower SFs (Cavagna et al. 1991; Chang and Kram 1999).

Observations regarding the W_{int}

When considering for energy transfer between the segments of the same limb, our W_{int} results at PSF are respectively on average 12% and 14% lower than the results obtained in Willems et al. (1995) and Cavagna et al. (1991) during over-ground running but similar to Gosseye et al. (2010) during running on a treadmill. However, when not considering for energy transfer between segments our results are on average only 2.5% from Willems and colleagues. This difference could be due to differences

in movements of the limbs on a treadmill as compared to over-ground running (Miller et al. 2019; Van Hooren et al. 2020). In contrast with the results of Cavagna et al. (1991), our results show that the $\dot{W}_{\mathrm{int}}^{+}$ does not decrease linearly with decreasing SF. Here we observe that the internal work reaches a minimum at around 2.4 steps s^{-1} before rising again, especially at fast running speeds. These authors base this result on lower speeds. In fact, at the faster speeds the internal work was only measured at higher SFs (smallest SF 2.5 steps s^{-1} at 14 km h^{-1} and 3.2 steps s^{-1} at 17 km h^{-1}) and a regression curve was used to extrapolate the lower internal work results. Here, at low SF a greater contribution of the upper limbs increases the $\dot{W}_{\mathrm{int}}^{+}$ compared to PSF (Fig. 2.1.2A and B). This is visible in Fig. 2.1.2B as the difference between the power done by the lower limbs (dashed grey line) and the total $\dot{W}_{\mathrm{int}}^{+}$ (red lines and circles). Also, due to the greater knee extension during stance (Fig. 2.1.S1), the maximal velocity of the foot is greater at low SF as more distance needs to be travelled during the swing phase (Fig. 2.1.S3). Both the ipsilateral arm and the contralateral swing leg could be used by the runner as a supplementary upwards impulse to the stance leg (Seyfarth et al. 2022).

During a stride, the internal energy-time curve of each lower limb, as seen in Fig. 2.1.2, presents two peaks occurring during the two contact phases: a first peak when the lower limb itself is in contact with the ground and moves backwards relative to the trunk, a second peak when the opposite lower limb is in contact with the ground. In this case, the lower limb moves forwards relative to the trunk. During the two aerial phases, the internal energy of each limb is minimal, suggesting that the limbs are not moving a lot relative to the CoM. A similar phenomenon is observed at the level of the upper limbs: the kinetic energy of the upper limbs relative to the COM is higher during the contact phases than during the aerial phases. Although, due to the small mass of the upper limbs, the variation of their internal energy is smaller than in the lower limbs.

A proper synchronisation between the movements of the upper and lower limbs during running can be beneficial in terms of energetics and gait stability in locomotion. In the discussion of Willems et al. (1995), the authors argue that it is rather complicated to consider for energy transfer between the energy of the limb segments and the energy of the CoM without regarding for the feasibility of this transfer. The peaks present in the energy curves of the limb segment movements which correspond to the energy curve peaks based on the movements of the CoM could be evidence that a transfer between limb segment energy and CoM energy is in fact possible.

Limitations

Some limitations are present in this paper. Firstly, although the required number of steps is met to be able to reduce type I error, the sample size is rather small. Furthermore, all subjects were recreational amateur runners. The study did not compare untrained and trained runners whereas a lot of the literature distinguishes two groups. Secondly, the difference in our findings and the findings from Cavagna et al. (1991) concerning the W_{int} at the lowest frequencies and faster speeds do not match. This difference could be due to a result of the instruments used in data acquisition and analysis. Another possibility is that there are differences between the internal work of a subject when running over-ground and on a treadmill *e.g.* eventual energy transfers between internal and external work. This last limitation should therefore not be viewed as a limitation *per se* but rather as a starting point for further research comparing the differences between both.

Conclusion

To the best of our knowledge, this paper is the first, to compare SF and the bounce mechanics' spatiotemporal parameters and its relation to lower limb motion. Despite the extensive literature on SF and running, our results bring arguments that the adaption of k_{vert} to a particular speed reflects a change in the frequency chosen by the runner more than the running speed itself. This result is also extended to the motion and relation of the lower limb segments, as evidenced by the planar covariance law. When running at higher SF, running mechanics is best explained by the elastic bouncing model of running. Whereas when running at the lower SFs, running mechanics thus deviates from the bouncing model of running.

Acknowledgements

The authors would like to thank F. Desimpelaere for her contribution in the data collection and treatment during her time at the lab.

Supplementary Information

The average joint angles of all subjects throughout a stride at all step frequencies at 8 and 17 km h^{-1} are shown in the first figure of this document. The three plots show a time-normalised average curve of the ankle, knee and hip joint angles and standard deviation (respectively the thick centred line and coloured area around it) across all subjects. A greater ROM for each joint is observed at faster speeds and at slower step frequencies. It is further worth noting that the ankle movements are drastically reduced at the fastest speed and frequency.

The second figure breaks down the ROM of the thigh and both knee and ankle joints into their contact and swing phases. For both segment and joints the contact and swing ROM are speed and frequency dependant. However, whereas the ROM_{tc} seems to have a more systematic decrease with increasing frequency at both the ankle and knee angles, at low SFs the ROM in both joints is higher than PSF and at high SFs it is lower ($p < 0.001$) the change in frequency during the swing phase shows a constant decrease in the ankle joint ROM ($p < 0.001$ at all levels) while the ROM of the knee joint seems to change behaviour with increasing speeds. Due to the modification in both the shank and foot elevation angle ROM and the time synchronisation between these same both limbs, the behaviour of the joint ROM at both the knee and ankle are affected.

Note, ROM of the hip was not shown because although the variations of the trunk are affected by both speed and frequency ($p < 0.001$) its average orientation changes very little, a subject will slightly lean forwards both at low and high SFs with less than a 2° difference on average compared to PSF. Therefore, most variations on the hip ROM can be appreciated by the variations in the elevation angle of the thigh which sees an increase with speeds at PSF, as in Ivanenko et al. (2007). Compared to PSF, the ROM of the thigh decreases as a function of SF (Frequency tests: $thigh_{ta}$: $p<0.001$) During the contact phase the ROM decreases with increasing frequency at the level of the thigh (Frequency tests: $thigh_{tc}$: $p <0.001$). The ROM of the thigh during both the contact and aerial phases increase with speed (Speed tests for both $thigh_{tc}$ and $thigh_{ta}$, $p < 0.001$).

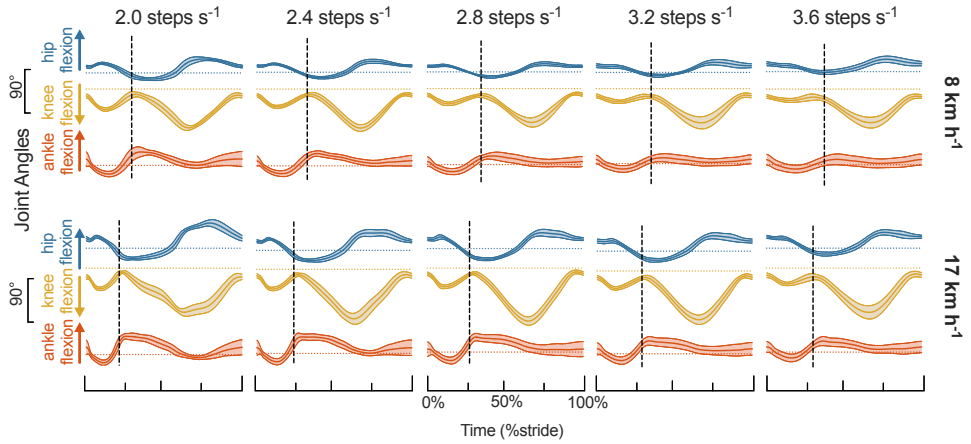

Fig. 2.1.S1 Joint Motion *Time normalised average ± standard deviation cloud traces of the angular displacement at the hip (blue), knee (yellow) and ankle (red) joints done over a percentage of stride at different SFs at both 08 and 17 km h^{-1}. The vertical dotted line shown in each figure corresponds to the end of the contact phase. The horizontal, correspondingly coloured, dashed line represents the neutral standing position of each joint.*

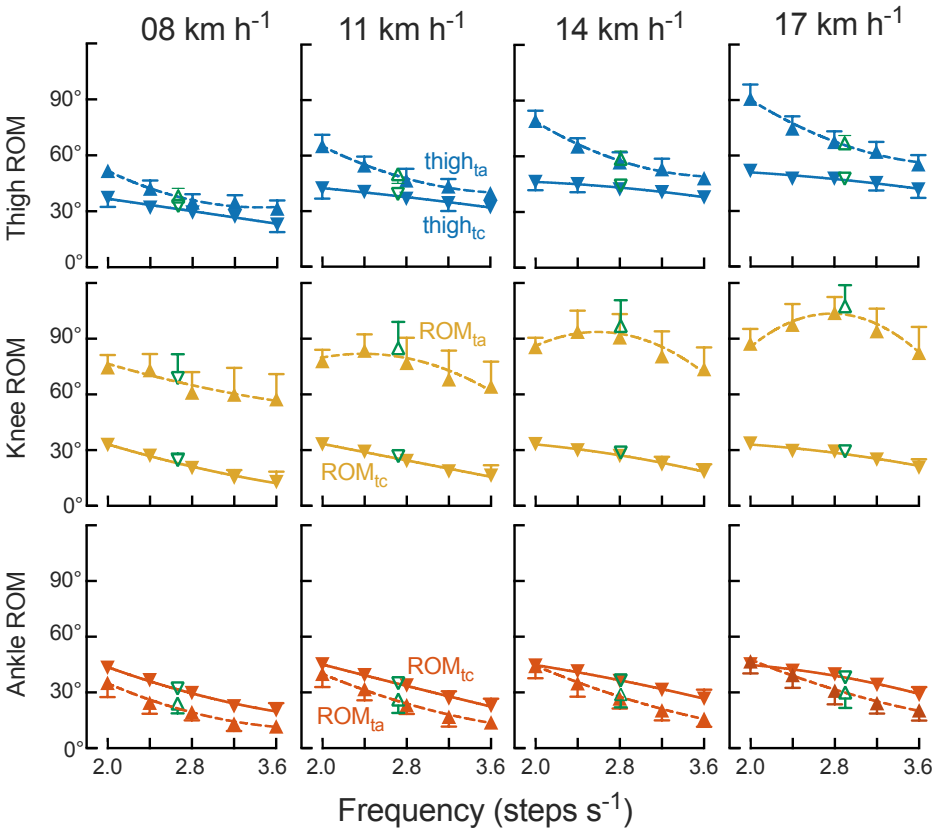

Fig. 2.1.S2 Range of Motion *Thigh (upper row), knee (middle row) and ankle (lower row) ROMs divided into their contact and aerial phases (distinguished by tc and ta subscripts) as a function of SF at different speed classes. All other indications are as in Fig. 2.1.2B.*

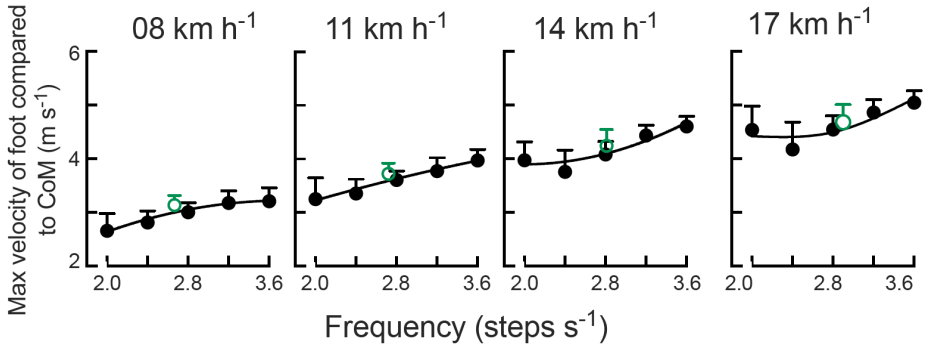

Fig. 2.1.S3 Maximum velocity of the foot compared to the CoM *as a function of SF at different all different speeds. All other indications are as in Fig. 2.1.2B..*

2.2 Kinetics and mechanical work done to move the body centre of mass along a curve

Raphael M. Mesquita, Patrick A. Willems, Arthur H. Dewolf & Giovanna Catavitello

PLoS ONE (2024) 19(2): e0298790.

Keywords: running, turning centre of mass, mechanical work, ground reaction force

List of Abbreviations

a_x, a_y, a_z:	Lateral, fore-aft and vertical component of the acceleration of the CoM in the *o-x-y-z* reference frame.
BW:	Body weight.
CoM:	Body centre of mass.
c_x, c_y, c_z:	Lateral, fore aft and vertical constants when integrating the acceleration to get the velocity.
δ:	Angle between the vector v_h and the y-axis.
δ_{TD}, δ_{TO}:	Angle between the vector v_h and the y-axis respectively at *TD* and *TO*.
E_{com} :	Total energy of the CoM due to its movements relative to the surroundings.
E_X, E_Y :	Kinetic energy of the CoM due to its velocity along the X- and the Y-axis.
E_z :	Kinetic and potential energy of the CoM due to its vertical movements.
F_x, F_y, F_z :	Lateral, fore aft and vertical components of the GRF in the *o-x-y-z* reference frame.
F_X, F_Y, F_z:	Lateral, fore aft and vertical components of the GRF in the *O-X-Y-z* reference frame.
GRF:	Ground reaction force.
m:	Body mass.
MTU :	Muscle tendon unit
o-x-y-z:	Inertial reference frame fixed to the laboratory. During straight-line running, *x* points in the lateral direction, *y* in the fore aft direction and the *z*-axis is vertical.
O-X-Y-z :	Inertial reference frame that changes at each foot contact: *O* is the position of the foot at the instant *TD*, the *Y*-axis point in the direction of v_h at *TD*, the *X*-axis is perpendicular to the *Y*-axis and the *z*-axis is vertical.
PL_{cx}, PL_{cy} :	Coordinates in the transverse plane of the point $\boldsymbol{PL_c}$ located inside the pelvis i.e. at the centroid of the triangle <SAT_L, SAT_R, S2>.
R_{th} :	Theoretical radius determined by the running lanes.

R:	Actual radius of curvature calculated by a circular fit on the (PL_{cx}, PL_{cy}) coordinates during the strides analysed.
r:	Instantaneous radius of curvature i.e. actual distance between the points (x_o, y_o) and (PL_{cx}, PL_{cy}) at each instant of the stride.
%Recovery :	Percentage of energy recovered through the transduction between E_X, E_Y and E_Z.
SAT_L, SAT_R, S2:	Reflective markers placed respectively at the left and right anterior superior iliac tuberosity and at the level of the second sacral vertebra.
S_z :	Vertical displacement of the CoM.
SLR :	Straight-line run.
θ :	Angle between the tangent to the circle and the *y*-axis.
θ_{TD}, θ_{TO}:	Angle between the tangent to the circle and the *y*-axis respectively at *TD* and *TO*.
t_c and t_a:	Duration of the phases of contact with the ground and the aerial phases.
TD:	Touch down *i.e.* instant when the foot touches the ground.
TO:	Take off *i.e.* instant when the foot leaves the ground.
v_x, v_y, v_z :	lateral, fore aft and vertical component of the velocity of the CoM in the *o-x-y-z* reference frame.
v_X, v_Y, v_z :	lateral, fore aft and vertical component of the velocity of the CoM in the *O-X-Y-z* reference frame.
v_h :	Velocity vector of the CoM in the transverse plane
W_{com} :	Work done to sustain the movements of the CoM relative to the surroundings.
W_{com}^+ :	Positive work done to sustain the movements of the CoM relative to the surroundings.
W_X^+, W_Y^+, W_z^+ :	Positive work necessary to sustain movements of the CoM respectively in the *X*-, *Y*- and *z*-directions. The positive and negative superscripts indicate the increments of work.
x_o, y_o :	Coordinates of the centre of the circle in the *o-x-y-z* reference frame, calculated from a circular regression.

Introduction

In the laboratory, human locomotion is mostly analysed in a "steady state" condition *i.e.* while moving on a straight line, at an average constant speed, on a level and firm terrain (Cavagna et al. 1991; Willems et al. 1995; Alexander 2002; Mesquita et al. 2024a). In nature (Usherwood and Wilson 2006; Wilson et al. 2013b, a), in daily life or during sport activities (Gabbett et al. 2008; Minetti et al. 2011; Taylor et al. 2017), this steady state situation appears rather infrequently. External factors and/or circumstances often require modifying the gait pattern to accelerate/decelerate the body (Van Caekenberghe et al. 2013; Dewolf et al. 2020b; Mesquita et al. 2020), to move on a soft yielding ground (Lejeune et al. 1998; Dewolf et al. 2019c), to move upwards or downwards (Dewolf et al. 2016; Dewolf and Willems 2017b), to leap over an obstacle (Mauroy et al. 2014), *etc*. Most studies on human locomotion are done in a straight line, whereas daily, one rarely moves in only one direction.

When running, one can change direction in different ways (Dos'Santos et al. 2019). For example, a runner can gradually change the direction of progression, step by step, *e.g.* when running on an athletic track (curved running) (Churchill et al. 2011, 2016; Judson et al. 2019, 2020a). Alternatively, the runner can change direction abruptly during a transition phase (lasting 1-3 steps), as in various multidirectional team sports (cutting manoeuvres (Zamparo et al. 2016, 2019; Dos'Santos et al. 2019; Padulo et al. 2023)). Although some principles and specific hypotheses have been investigated for various modes of locomotion while changing direction (Greene 1985, 1987; Hamill et al. 1987; Hase and Stein 1999; Chang and Kram 2007; Segal et al. 2008; Qiao et al. 2014; Churchill et al. 2016; Dos'Santos et al. 2019) the picture is not yet complete regarding the biomechanics of curved running in humans.

To the best of our knowledge, the trajectory and potential adaptions of the centre of mass of the body (CoM) when running along a curve and the work done by the muscle-tendon unit (MTU) to sustain its movements (W_{com}) have not yet been analysed. Indeed, since wind resistance is negligible and the foot is not skidding on the ground (Cavagna 1975; Lejeune et al. 1998), essentially all the work done by the MTU relative to the CoM (classically called $W_{ext} = W_{com} + W_{env}$ (Cavagna 1975; Peyré-Tartaruga et al. 2021)) is done to sustain its movements (W_{com}) rather than to move it against the environment (W_{env}), therefore $W_{com} = W_{ext}$.

A further understanding of the constraints and adaptions of the CoM mechanics while running on a curve may have practical implications in various fields, including sports performance, injury prevention, and rehabilitation (Peyré-Tartaruga et al. 2021). To date, regarding kinetic variables, only the description of the ground

reaction forces during curved running has been documented in the literature, most of which has focused on sprint mechanics performed at maximal velocity on an athletic track curve where the minimal radius of curvature for an outdoor track is of 36.5 m (Jain 1980; Greene 1985; Churchill et al. 2011, 2016, 2019; Judson et al. 2019, 2020a) or when running in curves with radii smaller than 6 m (Chang and Kram 2007).

When running in a curved path, the velocity of the CoM must be deflected each step in the transverse plane (Greene 1985) and a net lateral force, opposite to the side one wishes to move, must be exerted on the ground. The magnitude of this force depends, among others, on the velocity of progression and on the radius of the circular path (Greene 1985; Quinn 2009). In the frame of this paper, we aim to answer four questions/hypotheses to better understand the mechanisms underlying curved running.

First, running consists of a succession of contact phases interrupted by flight phases. In the latter no lateral force acts upon the body and so the CoM movements are uniformly rectilinear in the horizontal plane (Cavagna et al. 1976). When running in a curve, an "over-deflection" should occur during the contact phase to compensate for the rectilinear motion during the aerial phase and keep the runner on the circular trajectory. This over-deflection should be countered by an increased braking fore-aft force which prevents inappropriate rotation, thus allowing the runner to maintain the running trajectory (Qiao et al. 2014).

A second question concerns a possible asymmetry between the inner and outer lower limbs. Indeed, while turning, the runner feels an apparent centrifugal force directed outwards, causing the subject to lean inwards to maintain balance (Greene 1985). Consequently, one might expect that the two lower limbs exert different lateral forces since the inner limb is pushing on the lateral side of the foot, whereas the outer limb pushes with the medial side of the foot. This asymmetry has been described when running at sprinting speeds on an athletic track (Churchill et al. 2016). The question arises as to which extent this asymmetry also persists at slower speeds and shorter radii of curvature?

The third goal of this paper is to study the effect of running speed and radius of curvature on the muscular work (W_{com}) done while running on a circular arc. To identify the sources of W_{com}, the work done to sustain the forward movements of the CoM (W_Y), the work done to sustain its vertical movements (W_z), and the work done to modify the direction of progression (W_X) were also measured.

When running on a straight line (SLR), W_{com} is assessed from the forces exerted by the ground under the foot in the fore aft (y-axis), lateral (x-axis) and vertical (z-axis) directions (Cavagna et al. 1988; Willems et al. 1995). When running along a curve, using a fixed referential attached to the laboratory makes no physiological sense since the fore aft and lateral directions no longer correspond to the y- and x-directions. It is therefore necessary to use a referential which rotates with the runner. A first solution should be to rotate the frame of reference at each instant so that the Y-axis of the new reference frame is tangent to the circular trajectory that the runner follows and the X-axis is pointed towards the centre of the circle. However, in this case, it is difficult to separate the work done to move the CoM in the axis of progression (W_Y) from the work necessary to modify the direction of progression (W_X) (see supplementary material).

As the foot is fixed on the ground during most of the contact phase (Mesquita et al. 2024a) (Fig 2.2.S4), we propose to use a referential that rotates only once per step: at each foot contact. The origin of the referential is then placed at the position where the foot touches the ground and is oriented in a way where one of the axes is in the direction of the velocity vector in the transverse plane at the instant of touch down. In this new O-X-Y-z referential, the Y-axis lies in the direction of progression and the X-axis points inwards. In this referential frame, W_Y corresponds to the work done to sustain the movements of the CoM in the fore-aft direction and W_X to the work done to sustain the lateral movements of the CoM in the referential of the runner.

Fourth, when running on a straight line most of the movement is done in the sagittal plane and the work to sustain the lateral movements of the CoM is negligible (Cavagna et al. 1963; Dewolf et al. 2016). The energy of the CoM due to its fore-aft velocity (E_y) and the energy due to its vertical movements (E_z) are in phase (Cavagna et al. 1976). Part of the kinetic and potential energy lost during the braking phase can be stored to be reused to accelerate and elevate the CoM during the second part of contact, as in a spring-mass system bouncing on the ground (Cavagna et al. 1976). When turning, the work to sustain the lateral movements of the CoM is no longer negligible since a lateral force must be exerted during the entire contact phase to deflect the trajectory of the CoM. Therefore, part of the kinetic and potential energy lost during the first part of contact when the CoM is decelerated and lowered in the sagittal plane (braking phase) could be used to redirect the CoM in the lateral direction.

To answer these four questions, the forces that the ground exerts under the feet and the movements of the pelvis were recorded during 1-4 strides (2-8 steps) while running in curves where the radius of curvature was of either 6 m or 18 m, at different

speeds ranging from 2 to 6 m s^{-1}. Based on these data, the trajectory of the CoM and its energy were computed. From there, W_X, W_Y, W_z and W_{com} were assessed. Results were compared with those obtained while running on a straight line.

Materials & Methods

Participants and experimental procedure

Eleven recreational healthy male runners (height: 1.81 ± 0.03m, mass: 74.91 ± 5.38 kg, age: 24.64 ±2.91 years, mean ± SD) participated in the study. The participants were all amateur-level runners with 10km personal bests ranging from 33 – 45 minutes and were recruited through informal person-to-person communication channels. Informed written consent was obtained, and the study followed the guidelines of the Declaration of Helsinki. All procedures were accepted by the UCLouvain Ethical Committee (B403201940199). Power analysis was performed using GLIMMPSE 3.1.2. (Kreidler et al. 2013) (Denver Colorado, USA) to estimate a sufficient number of participants required to avoid type II error (Power 1-ß: 0.8, minimum sample size: 9 participants).

Participants took part in two sessions 6 weeks apart. First, they were asked to run at different speeds, ranging from 2 to 6 m s^{-1} (~7 to 22 km h^{-1}), on a circular path (radius of curvature 18 m) instrumented with 16 force plates. Second, they were asked to run on a 6 m radius curved path, and on a treadmill, for comparison with SLR. The equipment used to record data is explained in the section below. The six-week period interval between the two data collection sessions was necessary to reconfigure the force plates.

Participants ran in a 20 m long straight corridor before arriving in the curved path. They took at least one step in the curve before the measurements were taken. Participants were first asked to run at intermediate speeds (around 12-14 km h^{-1}), then at fast speeds (between 16 and 18 km h^{-1}), followed by slow speeds (between 8 and 10 km h^{-1}), and finally at the maximum speed that they could reach. After each trial, the average velocity of the runner, v_h (explained below) and number valid of strides were checked and communicated to the participant. Trials were considered valid if they contained at least one stride (two successive steps) where v_h remained constant, *i.e.* if the sum of the decrements of v_h differed less than 25% of the increments over a complete stride. Rest periods were allowed between the trials, at the runner's convenience, to avoid fatigue-bias.

Experimental set-up

During the experiments, two types of variables were measured. First, the reaction forces that the ground exerts under the foot (GRF) were evaluated using force platforms (kinetic variables). Second, the movements of the pelvis were recorded using high-speed infrared cameras (kinematic variables). Both systems are described in length below. Two pairs of photocells were placed at the level of the neck, ~6 m apart, at each end of the running track. These cells both triggered and stopped the acquisition of kinetic and kinematic data.

Measurement of kinetic variables during curved running

For the curved running sessions, 16 custom built force plates of 1 m x 1 m each were placed side by side in the configurations illustrated in Fig. 2.2.1A & 2.2.2A. The circular paths bended to the right. To guide the runner during curved running, a 0.5 m wide lane was delimited by two white stripes. The characteristics of the force plates are described in detail in Genin et al. (Genin et al. 2010) and are only presented briefly here. Each plate measured the three components of the GRF by means of four force transducers placed under each corner of the plate surface. Each plate possessed its own data acquisition system comprising amplifiers, anti-aliasing low-pass filters (4-pole Bessel filter with a -3 dB cut-off frequency of 200 Hz), a 16-bit analogue-to-digital converter sampling at 1 kHz and a micro-controller (Rabbit Semiconductor, Davis, CA, USA). The 16 plates were connected to a central PC *via* ethernet using the TCP/IP protocol.

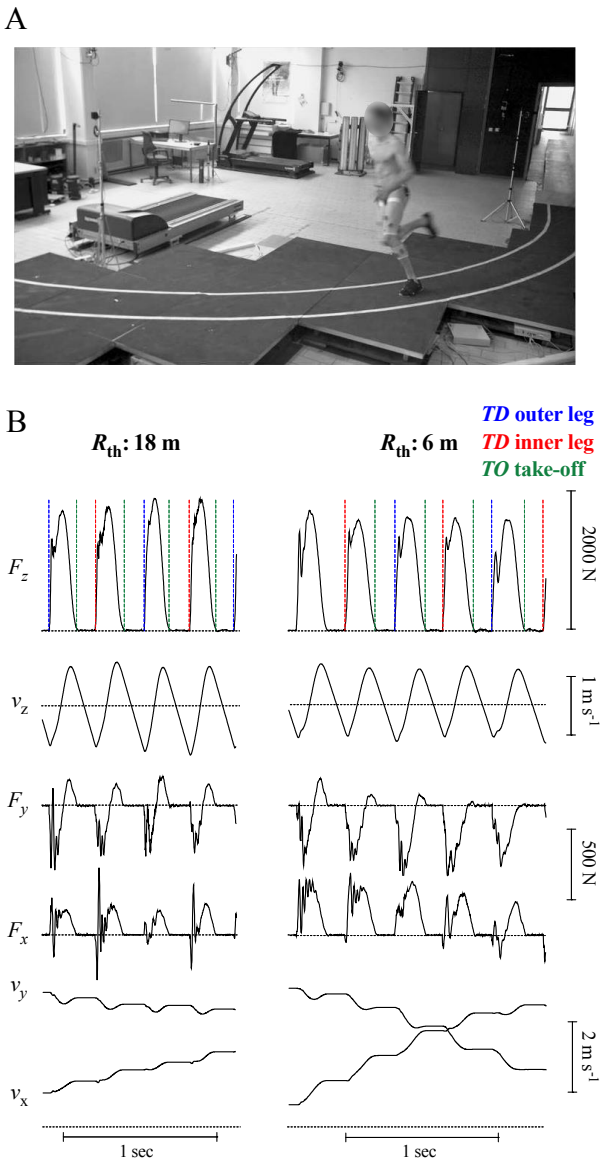

Fig. 2.2.1 Image of the set-up and typical traces. Panel A: *Image of the 16 (1x1 m) force plate set-up for the 6 m radius of curvature. A 0.5 m track is drawn over the to guide the runner.* ***Panel B:*** *typical traces of the three components of the GRF and of the velocity of the CoM relative an inertial reference frame attached to the lab. For both radii of curvature, variables were recorded over entire trials on one subject (body mass: 65.1 kg, height: 1.78 m) running at 14 km h^{-1}. From top to bottom: vertical component of the GRF (F_z) and of the velocity (v_z), components of GRF in the transverse plane along the y- and the x-axis (respectively F_y and F_x). Further below, the two components of the horizontal velocities along the y-axis (v_y) and the x-axis (v_x). The dashed vertical lines drawn over F_z correspond to the time of touchdown of the inner leg (red) and of the outer leg (blue) and of the time of take-off of both legs (green).*

Measurement of kinetic variables during straight-line running

During SLR, the GRF were measured by means of an instrumented treadmill, which consisted of a modified commercial treadmill (h/p/Comos-Stellar, Germany) mounted on four force transducers (Arsalis, Belgium). Since the whole body of the treadmill (including the motor) was mounted on the transducers, these were measuring the three components of the GRF exerted by the treadmill under the foot (Willems and Gosseye 2013). A more in-depth description of the treadmill can be found here (Mesquita et al. 2024a). The signals were amplified, low-pass filtered (4-pole Bessel filter with a -3 dB cut-off frequency at 200 Hz) and digitized by a 16-bit analogue-to-digital converter (National Instrument, PCI-MIO-16E-4) at 1000 Hz.

Measurement of kinematic variables

Bilateral, full-body three-dimensional (3D) kinematics were recorded by means of a Qualisys system (Gothenburg, Sweden) equipped with 12 Mocap OQUS 6+ cameras placed around the running track or the treadmill, plus one video Miqus M1 camera. Participants were equipped with 43 retro-reflective markers glued onto the skin according to the Qualisys sports marker set disposition. In the frame of this study, only the markers placed on the left and right anterior superior iliac tuberosity (SAT_L and SAT_R) and at the level of the second sacral vertebra (S2) were used. Kinematics were recorded at a sampling rate of 100-240 Hz and oversampled during post-processing at 1 kHz to match the sampling frequency of the kinetic data. An oversampling of the kinematic data was chosen rather than a down sampling of the kinetic data to ensure that the force signal characteristics were not lost during data-processing.

Data processing

In this manuscript, we used two different reference frames. The first *o-x-y-z* is fixed in the laboratory and was used to compute and analyse the trajectory of the CoM. The second *O-X-Y-z* changed orientations at each foot contact and was used to assess the work done to move the CoM relative to the surroundings.

Measurement of the contact and aerial period

The lower part of Fig. 2.2.1B illustrates the time-curves of the vertical (F_z), fore-aft (F_y) and medio-lateral (F_x) components of the GRF measured between the two photocells while running on an 18 m (left) and 6 m curve (right). The contact phase (t_c) corresponds to the period during which $F_z \geq 30\ N$ and the aerial phase (t_a) to the

remaining period. The dotted lines drawn on F_z indicate the heel-strike of the outer leg (blue), the heel-strike of the inner leg (red) and the take-off instant (green).

Assessment of the centre of mass movement in the transverse plane

The CoM displacement in the transverse plane was computed from the position of a point (PL_c) placed approximatively in the centre of the pelvis. Since the movements of the trunk relative to those of the CoM are small (Willems et al. 1995), one can consider that the displacement of PL_c is similar to the displacement of the CoM. (see Fig. 2.2.S1 in the supplementary material).

At each instant, the position of PL_c in the transverse plane (*i.e.* the centroid of the triangle) was computed from the SAT_R, SAT_L and S2 markers (Fig. 2.2.2B, upper right corner):

$$PL_{cx} = \frac{SAT_{Rx} + SAT_{Lx} + S2_x}{3}$$

and

$$PL_{cy} = \frac{SAT_{Ry} + SAT_{Ly} + S2_y}{3}. \quad (1)$$

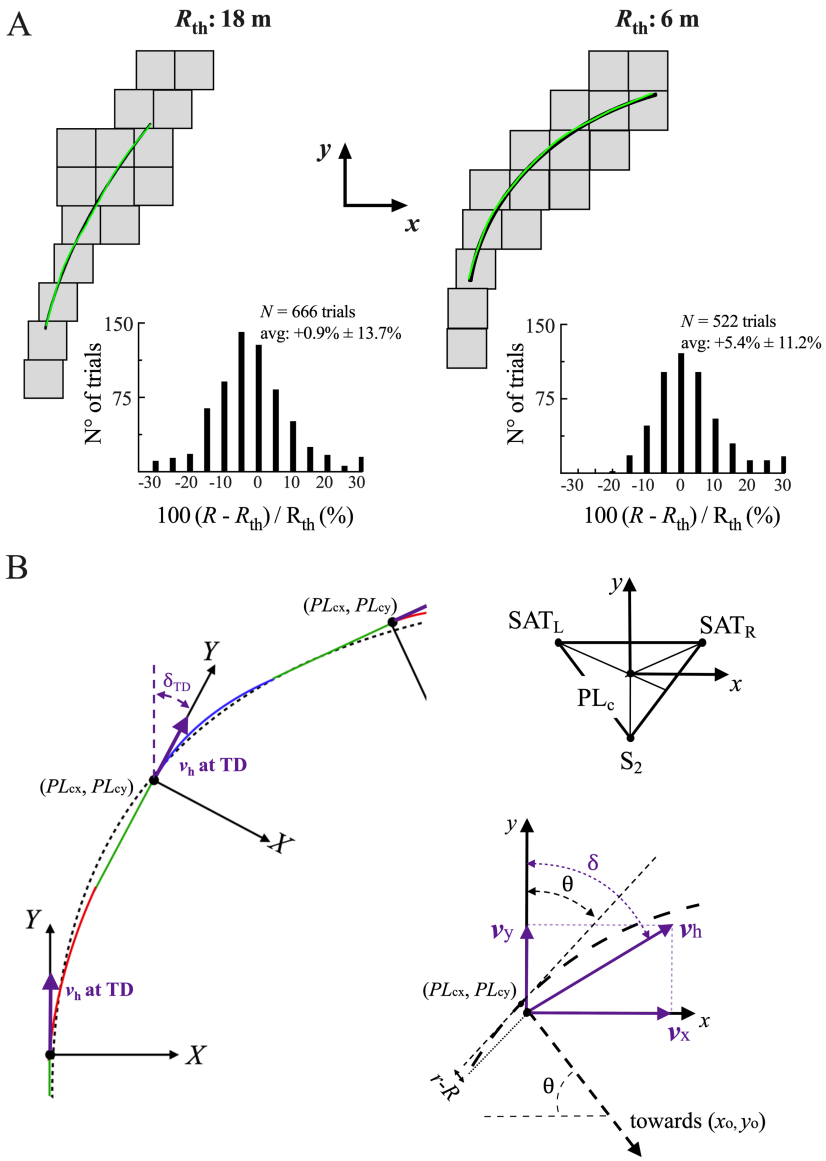

Fig. 2.2.2 Force plate disposition and experimental considerations. Panel A: *Disposition of the 16 (1x1 m) force plates for both the 18 m and 6 m radii of curvature. For both radii of curvature, the theoretical radius R_{th} (black line) is drawn over the diagram of the force platforms superimposed with the trajectory computed from radius R (green line). Note, R is obtained by fitting a circular curve through the points PL_c. The frequency distributions of $(R-R_{th})/ R_{th}$ is shown beside this as a histogram.* ***Panel B****: The upper left diagram of the panel shows the position of PL_c relative to the three markers glued on the skin of the subject (see Assessment of the movement of the CoM in the transverse plane, in the Methods section). The lower left diagram illustrates how the two angles δ and θ are computed (see eq. 7 and 8). The left diagram illustrates how the referential O-X-Y-z is rotated at each foot contact (see Computation of the work, in the Methods section).*

The displacement of the CoM can also be calculated *via* the double integration of the GRF. This signal gives the displacement and not the position of the CoM. To obtain the CoM's position, one has to use integration constants, which require knowing the initial and final position of the runner over the recorded distance. When running in a straight line, the positions of the start and end triggers can be used as the integration constant (Cavagna et al. 1991). However, although the width of the lane in which the subject was asked to stay in was relatively small as compared to the regulatory width of an athletic track lane (1.22 m (World Athletics 2019)), if the runner began on the inside or outside of the lane could change the distance covered in either direction considerably.

For the same reason, while the runner's average trajectory should be equal to the theoretical radius (R_{th}) determined by the running lane curvature (*i.e.* 18 m or 6 m), they could deviate from this desired radius of curvature. As a result, the radius of curvature based on the runner's trajectory was measured in each trial by fitting a circular regression to the (PL_{cx}, PL_{cy}) coordinates over the strides analysed to obtain the actual radius of curvature (R) and the position of the centre of the circle (x_o, y_o). An example of the difference between the R-curve and the R_{th}-curve is illustrated on the diagram of the force-plates in Fig. 2.2.2A. For each trial, the difference between R and the theoretical radius (R_{th}= 6 or 18 m) was computed.

To assess the oscillation of the CoM around the circular trajectory, the distance between PL_c and the centre of the circle was calculated at each instant of the stride. The difference between this "instantaneous" radius of curvature (r) and the radius R was thus obtained by:

$$r - R = \sqrt{(PLC_{cx} - x_o)^2 + (PLC_{cy} - y_o)^2} - R\,. \qquad (2)$$

Computation of acceleration velocity and displacement of the centre of mass

Below we presented the method to compute the acceleration, velocity and displacement of the CoM from the force platform signal relative to an inertial reference frame fixed to the lab (the method to compute these variables on a treadmill are presented in Gosseye et al. (2010).

The acceleration components in the three directions of space were obtained respectively as:

$$a_x = \frac{F_x}{m},\ a_y = \frac{F_y}{m},\ \text{and}\ a_z = \frac{F_z - BW}{m}, \qquad (3)$$

where m is the mass of the body and BW is its weight.

A time-integration of a_x, a_y, and a_z between t_1, the beginning and t_2, the end of the analysed stride(s) gave the velocity changes of the CoM in the three directions of space plus integration constants (Fig. 2.2.1B):

$$v_x = \int_{t_1}^{t2} a_x \, dt + c_x,$$

$$v_y = \int_{t_1}^{t2} a_y \, dt + c_y,$$

$$v_z = \int_{t_1}^{t2} a_z \, dt + c_z. \quad (4)$$

Since the subject moved on the level, the average vertical velocity of the CoM over a complete number of strides is equal to zero and the integration constant c_z is nil. Next, the vertical displacement (S_z) of the CoM was computed by time-integration of v_z.

The integration constants c_x and c_y were determined by dividing the distance travelled by the point PL_c during the strides analysed in the x- and y-direction (respectively ΔPL_{cx} and ΔPL_{cy}) by the duration of the strides (T_{tot}):

$$c_x = \Delta PL_{cx}/T_{tot}$$

and

$$c_y = \Delta PL_{cy}/T_{tot}. \quad (5)$$

At each instant, the magnitude of the velocity vector in the horizontal plane (v_h) was computed as:

$$v_h = \sqrt{v_x^2 + v_y^2}\,. \quad (6)$$

and its orientation relative to the inertial reference frame of the lab was measured as (Fig. 2.2.2B, lower right corner):

$$\delta = \operatorname{atan}\frac{v_x}{v_y}\,. \quad (7)$$

The angle θ between the tangent of the circle and the x-axis of the lab's referential was also measured:

$$\theta = 180° - \operatorname{atan}\frac{PL_{cy} - y_o}{PL_{cx} - x_o}\,. \quad (8)$$

If $\delta = \theta$, v_h had the same direction as the tangent of the circle. If $\delta < \theta$, v_h was directed outside the trajectory of the circular path and if $\delta > \theta$, v_h looked inwards.

Computation of the work

Here we presented a method to assess the muscular work done each step to move the CoM (W_{com}) while running in a curve. To validate our method, we also computed E_{com} in two other ways. These results are presented in the supplementary material (see Fig. 2.2.S2) and show that E_{com} gives identical values for the three methods. However, the method chosen here allowed to better identify the different sources of work in W_{com}, *i.e.* to distinguish between the work done to move the CoM forwards, upwards and to change its direction in the transverse plane.

At the last instant prior to the contact phase, the reference frame was rotated around the vertical *z*-axis so that the *Y*-axis of the new reference frame corresponded to the direction of the velocity vector v_h at touch-down (*TD*), which was roughly the direction of v_h during the previous aerial phase (Fig. 2.2.2B, left). The *X*-axis was perpendicular to that direction. During the contact phase, the reference frame was maintained fixed until the next *TD*. Placing the reference frame relative to the runner allowed to separately assess the work done during the contact phase to maintain the movements of the CoM in the direction of progression (W_Y), the work done to deflect the trajectory of the CoM laterally (W_X) and the work necessary to move the CoM vertically (W_z).

δ_{TD} was defined as the angle at *TD* between the velocity vector v_h and the reference frame of the lab (eq. 7 and Fig. 2.2.2B). The components of the GRF (F_X, F_Y) and of v_h (v_X, v_Y) in the transverse plane relative to the new reference frame are computed at each instant of the step by:

$$\begin{pmatrix} F_X \\ F_Y \end{pmatrix} = \begin{pmatrix} F_x \cos\delta_{TD} - F_y \sin\delta_{TD} \\ F_x \sin\delta_{TD} + F_y \cos\delta_{TD} \end{pmatrix}, \quad (9)$$

and

$$\begin{pmatrix} v_X \\ v_Y \end{pmatrix} = \begin{pmatrix} v_x \cos\delta_{TD} - v_y \sin\delta_{TD}, \\ v_x \sin\delta_{TD} + v_y \cos\delta_{TD} \end{pmatrix}. \quad (10)$$

The energy of the CoM due to the velocity changes in the *X*-, the *Y*- and the *z*-directions are computed as:

$$E_X = \int F_X \, v_X \, dt = \frac{1}{2} \, m \, {v_X}^2 , \quad (11)$$

$$E_Y = \int F_Y \, v_Y \, dt = \frac{1}{2} \, m \, {v_Y}^2 , \quad (12)$$

$$E_z = \int (F_z - m\,g) \, v_z \, dt = \frac{1}{2} \, m \, v_z^2 + m \, g \, S_z , \quad (13)$$

and the total energy of the CoM by:

$$E_{\mathrm{com}} = E_{\mathrm{X}} + E_{\mathrm{Y}} + E_{\mathrm{z}} \,. \tag{14}$$

The positive and negative work done, W_{com}^{+} and W_{com}^{-} were respectively the sum of the positive and negative increments of the E_{com}-curve. To minimise errors due to noise, the increments in mechanical energy were considered to represent positive/negative work done only if the time between two successive maxima/minima was greater than 20 ms. Similarly, W_{Y}^{+} and W_{Y}^{-}, which represent roughly the work to sustain the movements of the CoM in the direction of progression were computed from the positive and negative increments of the E_{Y}-curve; and W_{X}^{+} and W_{X}^{-} represent roughly the work done to deflect the CoM laterally were evaluated from the positive and negative increments of the E_{X}-curve. Finally, the work W_{z}^{+} and W_{z}^{-} done to move the CoM vertically were computed from the positive and negative increments of the E_z-curve. The mass specific and step normalised positive (W_{Y}^{+}, W_{X}^{+}, W_{z}^{+} and W_{com}^{+}) and negative (W_{Y}^{-}, W_{X}^{-}, W_{z}^{-} and W_{com}^{-}) works were normalised by the subject mass and step length (Cavagna et al. 1976; Peyré-Tartaruga et al. 2021; Mesquita et al. 2024a). Energy transduction between the E_{X}-, E_{Y}- and E_z-curves were assessed as *%Recovery* (Mesquita et al. 2020):

$$\%Recovery = 100 \left[1 - \frac{W_{\mathrm{com}}^{+} + |W_{\mathrm{com}}^{-}|}{W_{\mathrm{l}}^{+} + |W_{\mathrm{l}}^{-}| + W_{\mathrm{f}}^{+} + |W_{\mathrm{f}}^{-}| + W_{\mathrm{z}}^{+} + |W_{\mathrm{z}}^{-}|}\right]. \tag{15}$$

Selection of the analysed steps

Over the strides selected, care was taken to select inner and outer steps where the subject was not accelerating nor decelerating and where the vertical velocity was not drifting. Therefore, the magnitude of the velocity vector in the horizontal plane (v_{h} - equation 6) and in the vertical direction (v_{z} - equation 4) were checked before analysis. Steps were considered suitable for analysis if the sum of the increments and the sum of the decrements of v_{h} and of v_{z} differed less than 25% (Mesquita et al. 2020). In total, 4863 steps were analysed: 2545 outer steps and 2318 inner steps from a total of 6380 steps (3152 inner and 3228 outer steps).

Statistics

For each participant, the different parameters were first averaged for all left and right steps over one trial. Then descriptive statistical analysis was performed. First, a Shapiro-Wilk test was performed to verify normality. A linear mixed effect model with *Bonferroni* post-hoc correction was used to assess the individual and interaction effects of radius and speed on the calculated variables with IBM SPSS Statistics

(PASW Statistics, 19, SPSS, IBM, Armonk, NY, USA). To analyse the eventual inner-outer limb asymmetry between the variables a paired t-test (t) was used, along with a Cohen's d (d) value to analyse the effect size and interpreted as follows: < 0.19 = trivial, 0.20-0.59 = small, 0.60-1.19 = moderate, 1.20-1.99 = large, > 2.00 = very large (Hopkins et al. 2009). When figures were presented by speed-class, the inter-subject grand means were shown at the following speed classes ([6,8), [8, 10), [10,12), [12, 14), [14, 16), [16, 18), [18, 20), [20, 22)), these groups were only used for the figures and not used for statistical tests.

Results

Actual radius of curvature of the runner

Although the width of the lane in which participants were asked to run in was small (0.5m) as compared to that of an athletic track, runners could deviate from the desired radius of curvature. The distribution of the actual radius of curvature (R) compared to R_{th} was quantified and presented in Fig. 2.2.2A. At 18 m, R was on average 0.9% ± 13.7% higher than the R_{th}. At 6 m, R was on average 5.4% ± 11.2% higher than R_{th}. Across all trials, the coefficient of determination (r^2) of the curved regression fit was of 0.99 and the RMSE was of 0.015 m on average.

Deviation from a circular trajectory

Note that despite the high coefficient of determination, the trajectory of the CoM deviates from the perfect circular path (Fig. 2.2.3 left) and it exhibits a roughly similar progression at all speeds on the two curvatures (Fig. 2.2.S3). The right column of Fig. 2.2.3 presents the evolution of the angles δ and θ during the stride, which also present a similar pattern in all situations.

At TD on the inner leg, the CoM is located outside of the curve as indicated by the positive r-R (Figs. 2.2.3 left and Fig. 2.2.4B), whereas at TD on the outer leg, r-R is negative, indicating that the CoM is located inside the curve ($t = -30.1$, $p < 0.001$, $d = -0.9$). When speed increases, $|r\text{-}R|$ at TD increases ($F = 9.315$, $p < 0.001$) both on the inner and outer leg.

Fig. 2.2.4C presents the differences δ_{TO}-δ_{TD} and θ_{TO}-θ_{TD}. Except at very low speeds (≤ 8 km h^{-1}), δ_{TO}-δ_{TD} > θ_{TO}-θ_{TD}. The difference δ_{TO}-δ_{TD} increases with speed ($F = 79.9$, $p<0.001$) and when the curvature decreases ($F = 1455.6$, $p <0.001$). Furthermore, δ_{TO}-δ_{TD} is greater for the inner-leg as compared to the outer leg ($t= -10.6$, $p <0.001$). Note that when the body touches the ground, the vector v_h is

increasingly directed outside the circle (δ - θ < 0) at all speeds (on average at 8 km h^{-1}, δ_{TD} - θ_{TD} ~ -1° and ~ -3° at 22 km h^{-1}; speed: F= 21.52, p<0.001), except at TD on the inner leg when speeds ≤ 8 km h^{-1}. When the body leaves the ground, v_h is directed inside the circle at all speeds and curvatures (speed: F= 44.6, p<0.001; radius: F=43.8, p<0.001), again except for the slowest speeds.

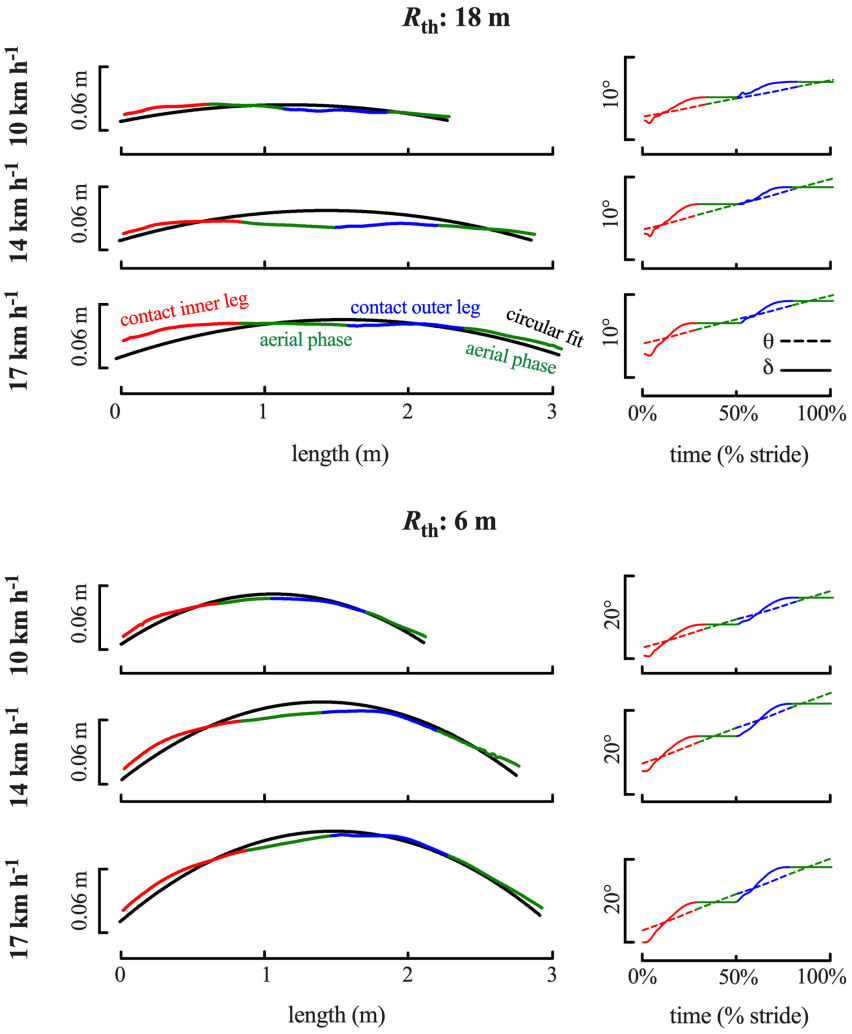

Fig. 2.2.3 PL_c oscillation around the circular fit and angle deviations. *The left panels illustrate the typical traces of the oscillation of PL_c over one stride around the circular fit, R (black line), for the same subject as in Fig. 2.2.1. In each panel, the circular path is rotated so that the cord of the arch defined by the first and last point of the stride is horizontal. The vertical scale is amplified to accentuate the oscillation around the curve. The right panels represent the temporal changes of the angles δ (continuous line) and θ (interrupted line) over the strides presented in the left panel. Colours are the same as in Fig. 2.2.1.*

Spatiotemporal parameters

Fig. 2.2.4A shows the effect of running speed and curvature on the contact (t_c) aerial (t_a) and step (T) period. Regarding the effect of speed, below 10 km h^{-1}, t_a represents less than 30% of T. When speed increases, t_c decreases ($F = 166.6$, $p < 0.001$) whereas t_a increases ($F = 60.9$, $p < 0.001$). At speeds above 15 km h^{-1}, both t_a and t_c decrease. On an 18 m curvature, t_a is approximately equal to t_c, whereas on a 6 m curvature, t_a is less than t_c.

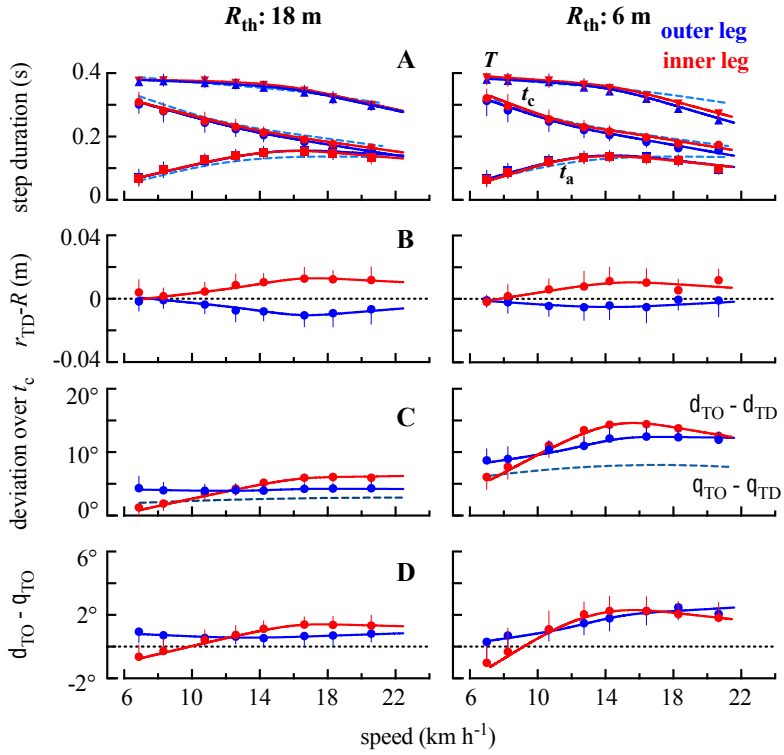

***Fig. 2.2.4 Comparisons between running at 18 m, 6 m and on a straight line. Panel A**: Effect of running speed on the time of contact (t_c) and aerial time (t_a) of steps on of the inner (red) and outer (blue) while running a curve of 18 (left) and 6 m (right) radius. **Panel B**: Effect of speed on the difference between the "instantaneous" radius at touch down, r_{TD}, and the radius described by the circular fit of the PL_c trajectory, R. **Panel C:** The difference between the angles δ (continuous line) and θ (interrupted line) at take-off (subscript TD) and touch down (subscript TO). **Panel D:** The difference between δ and θ at take-off. In each panel, the continuous lines represent spline functions fitted on all the data.*

Regarding the effect of the curvature, when running on a circular path, t_c is slightly reduced as compared to t_c during SLR ($F = 4.86$, $p = 0.01$), however no difference between the two radii is evidenced (*post-hoc* $p = 0.335$). On the contrary,

a significant effect of the curvature on t_a is observed (F = 8.3, p = 0.002): t_a is smaller at 6 m as compared to 18 m (*post-hoc* p = 0.008). This last difference is mainly highlighted at high speeds.

Work to move the centre of mass relative to the surroundings

Fig. 2.2.5A presents the three components of the GRF signal relative to the *O-X-Y-z* reference frame of steps of a subject running at 14 km h^{-1} (same subject than in Fig. 2.2.1). The *X*-component (which is always directed towards the inside of the curve) increases when the radius of curvature decreases. On a 6m radius of curvature, a difference between the inner and the outer limb occurs.

Fig. 2.2.5B presents the energy changes due to the movements in the three directions of space plus the total energy of the CoM during the same steps as in Fig. 2.2.5A. The increments of the E_{com}-curves represent the positive work done to move the CoM (W_{com}^{+}), whereas the increments of E_z, E_X and E_Y represent the positive work necessary to move the CoM along the *z*-, *X*- and *Y*-axes (respectively W_z^{+}, W_X^{+} and W_Y^{+}).

The two panels on last row of Fig. 2.2.6 show the effect of speed and of radius of curvature on W_{com}^{+}: both variables have a significant effect on W_{com}^{+} (speed: F = 7.05, p <0.001 radius: F = 23.2, p = 0.002). W_{com}^{+} decreases with speed in all curves. Whereas, when comparing running on a curve to SLR, W_{com}^{+} is greater on a 6 m radius curve than during SLR (*post-hoc* p < 0.001) and is not significantly different on an 18 m radius curve compared to SLR (Fig. 2.2.6, lower panels).

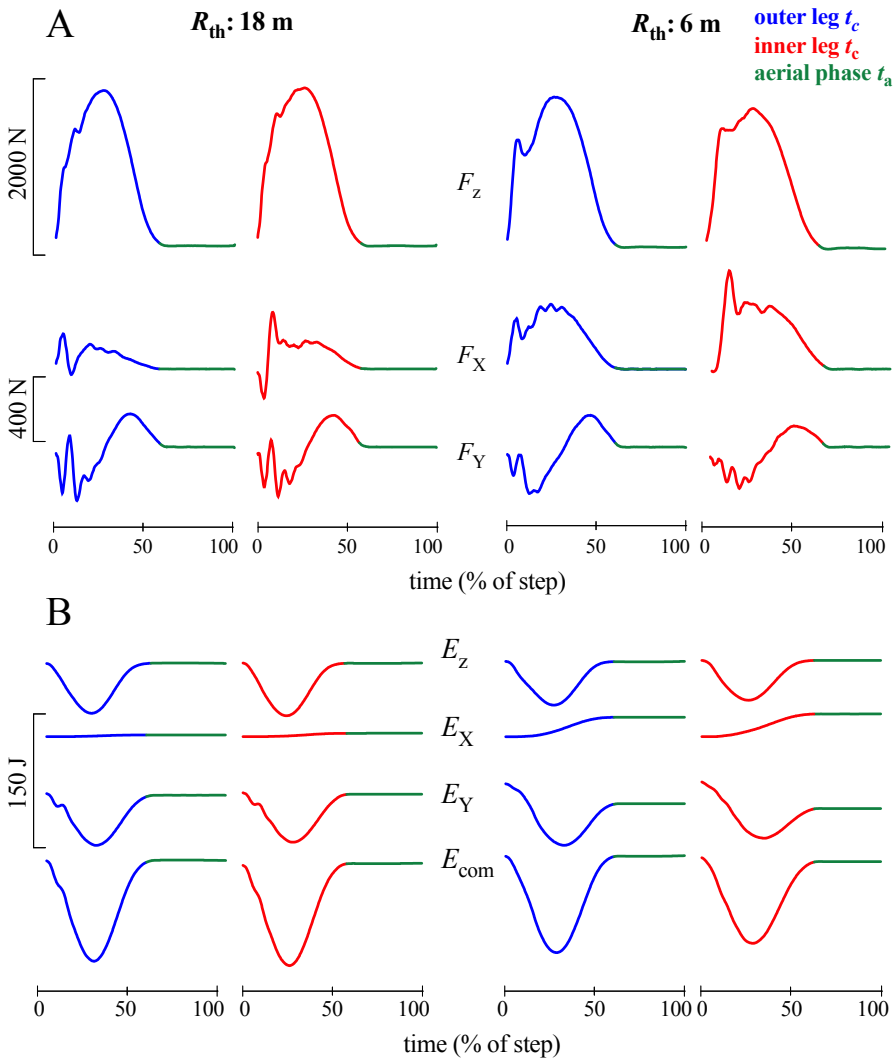

Fig. 2.2.5 Rotated referential forces and energies. Panel A: *The time-evolution of the three components of the GRF (F_Z, F_Y and F_X) recorded in the O-X-Y-z inertial reference frame during one step on the outer (blue) and inner leg (red) while running at 14 km $^{-1}$ on a curve with an 18 m (left) and 6 m radii (right). The green line represents the average aerial phase for each trace. The thin lines are the individual traces recorded on the same subject than in Fig. 2.2.1. The thick line is the average of all the steps.* ***Panel B****: Energy-time curves of the CoM on all the same steps than in panel A. E_z is the potential plus kinetic energy of the CoM due to its vertical movements, E_X and E_Y are the kinetic energies due to the velocity of the CoM along the X- and the Y-axis, respectively. E_{com} is the total energy of the CoM (E_{com}= E_z+ E_X+E_Y). In both panels, time is expressed as a percentage of the step period.*

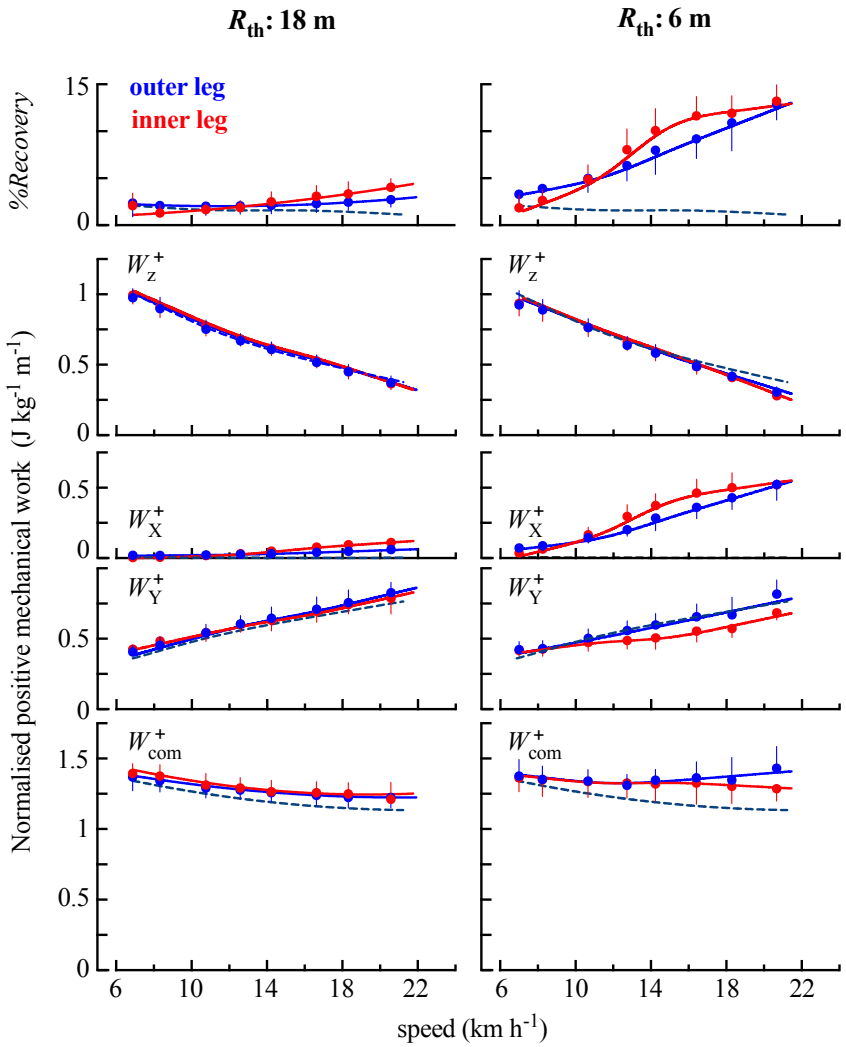

Fig. 2.2.6 %Recovery and work done to sustain the centre of mass movements. *%Recovery and work done on the inner (red) and outer (blue) limb for both radii of curvature as a function of speed. The upper panels present energy recovered through the transduction between E_X, E_Y and E_z. The four panels below present the mass-specific positive work normalised per unit distance. From top to bottom row 2 presents the work necessary to sustain the movements of the CoM respectively in the vertical direction (W_z), row 3: along the X-axis (W_X) and row 4: along the Y-axis (W_Y). The bottom panel represents the work done to sustain the movements of the CoM relative to the surroundings. The interrupted lines represent spline fits for the left foot during SLR. Other indications are as in Fig. 2.2.4.*

The work W_z^+ decreases when running speed increases ($F = 320.3$, $p<0.001$) but is not modified by the radius of curvature ($F = 2$, $p=0.156$) (Fig. 2.2.6 second row from above). W_X^+ is negligible during SLR (Fig. 2.2.S2), whereas, when running on

a curve, W_X^+ increases both with speed of progression (F= 95.2, p <0.001) and with radius of curvature (F=2109.9, p<0.05). The work W_Y^+ increases with running speed (F = 40.9, p<0.001) and with radius of curvature (F=119.1, p<0.001). This last difference is seen when comparing each radius class with another (*post-hoc* p<0.001).

Both W_Y^+ and W_X^+ are different on the inner and the outer limb ($W_Y{}^+$: t = 10.61, p<0.001, W_X^+: t = -12.3, p <0.001), with moderate effect sizes in both cases (W_Y^+: d = 0.53, W_X^+: d = - 0.56). Only a small difference was observed regarding the work to move the CoM vertically ($W_z{}^+$: t = -6.47, p <0.001, d = -0.2), and no difference between the inner and outer limb was evidenced for W_{com}^+ (t = -0.47, p =0.637).

Transfer in energy used to deflect the centre of mass

The %*Recovery* (Fig. 2.2.6, upper panel) increases both as a function of speed (F = 26.63, p<0.001) and as a function of radius of curvature (F = 731.8, p <0.001). On an 18 m curvature, the %*Recovery* is always lower than 5%, as in SLR, whereas on a 6 m curvature at higher speeds, one can recover about 12% of energy.

Discussion

The results of the present study provide insight into the biomechanics of running along a curve and shed light on the adaptations that occur in response to changes in speed and radius of curvature. The implications of these findings within the broader context of sport sciences will be considered upon.

When instructed to run at different speeds inside a circular path marked on the ground (Figs. 2.2.1A and 2.2.2A), participants kept a circular trajectory, as evidenced by the strong coefficient of determination of the circular fit applied to the PL_c trajectory (r^2= 0.99). However, the mean value of the actual radius curvature (R) is 1% greater than the theoretical R_{th} on an 18 m curvature and more than 5% greater on a 6 m curvature (histogram in Fig. 2.2.2A). This means that despite the ground markings delimiting a smaller corridor than on an athletic track (0.5 m vs. 1.22 m), most participants follow a curve greater than R_{th} by entering the curve on the outer limit, leaning inside to the apex and finishing close of the outer limit. This strategy reduces the detrimental effects of curvature especially at high running speeds on tight curves (Greene 1985; Quinn 2009). This fact is well known by trainers when they compare running performances between inside and outside lanes (Jain 1980), or between outdoor and indoor venues.

Running is defined by unipedal stance phases followed by flight phases (Cavagna et al. 1976). Following Newton's second law, during the flight phase the CoM describes a uniform rectilinear motion which deviates from a circular path (Fig. 2.2.3). Therefore, the rectilinear motion during the aerial phases needs to be "over-compensated" during the contact phases. This is done by applying a lateral GRF which increases when the curvature decreases (Fig. 2.2.5A).

In both legs, $\delta<\theta$ at TD (Fig. 2.2.3 right), indicating that v_h is directed outwards. Around mid-contact, δ becomes greater than θ, indicating that v_h is directed inwards during the second part of t_c. During contact, the v_h vector is thus reoriented. The difference θ_{TO}-θ_{TD} represents the angle covered along the circular path *i.e.* the rotation of the tangent to the circle during t_c. The actual rotation of v_h during t_c (*i.e.* δ_{TO}-δ_{TD}) is greater than θ_{TO}-θ_{TD} (Fig. 2.2.4C), which clearly shows that there is an "over-compensation" of the rotation during t_c.

At slow running speeds, as in SLR (Dewolf et al. 2016), t_c represents more than 70% of the step period (Fig. 2.2.4A). As a result, the deviations due to the linear trajectory during t_a are small (δ_{TO}- $\delta_{TD} \simeq \theta_{TO}$-$\theta_{TD}$ Fig. 2.2.4C). With increasing speed, the "over-compensation" during t_c increases. It is interesting to note that at high speeds, on a 6 m curvature, t_a is shortened (Fig. 2.2.4A), most likely to best follow the circular path and to contain the increase of lateral force during t_c. A decrease in t_a has been reported at very high running speeds (9.3 m s^{-1}) as the inner leg has "less room" (*sic*) to perform its swing phase (Churchill et al. 2016). Furthermore at high speed bend sprinting, differences in the contact period (t_c) between the inner and outer limb have also been reported (Churchill et al. 2016). In the present study, we did not find any statistical difference in t_c between the two limbs. This apparent discrepancy is most likely due to the fact our participants did not run faster than 5.8 m s^{-1} (Fig. 2.2.4A).

When the body leaves the ground, the vector v_h is directed towards the inside of the circle (except at TD on the inner leg with speeds ≤ 8 km h^{-1}). This strategy reduces the deviation (r-R) from the circular path; the difference δ- θ is positive at take-off (Fig. 2.2.4D), suggesting that the runner directs the velocity vector towards the inside of the circle at the end of the support phase.

An asymmetry in the GRF between the inner and outer limb has already been described although the results sometimes seem contradictory. When running on a 1-6m curve, Chang and Kram (2007) found that the outer limb produces greater peak lateral forces than the inner limb. In smaller radii the outer leg performs a cutting manoeuvre, performing greater lateral impulses than the inner leg (Rand and Ohtsuki

2000; Churchill et al. 2016; Dos'Santos et al. 2019). When running at 6 m s^{-1} on a radius of 31.5 m curvature, Hamill et al. (Hamill et al. 1987) observed larger peak lateral forces on the inner rather than the outer leg. Churchill et al (Churchill et al. 2016) found a greater inward force in the inner rather than outer limb when running at high speeds on an athletic track. In addition, athletes have shown greater muscular demand in the medial gastrocnemius of the inner than the outer leg (Pietraszewski et al. 2021).

In the present study, an asymmetry between the inner and outer leg is observed at all speeds on the two curvatures (Figs. 2.2.3 left and S3). During stance on the inner limb, the CoM tends to be located outside the circular path, whereas on the outer limb, the CoM tends to be located inside. In both legs, the CoM tends to move closer to the circular trajectory during t_c (Fig. 2.2.S3). During the aerial phase following the inner limb contact, the CoM tends to be located inside the circular path, whereas during the aerial phase following the outer limb contact, the CoM tends to be located outside. This may be explained by the role each limb plays in the redirection of the trajectory of the runner. At very slow speeds, the rotation of the velocity vector (δ_{TO}-δ_{TD}) during t_c, is mostly done by the outer leg (Fig. 2.2.4C). However, as speed increases, the reorientation done by the inner leg during t_c becomes greater than that of the outer leg.

Where the study of the GRFs during running while turning is not novel, observing the outcomes on the CoM mechanics over multiple strides and over different radii has, to the best of our knowledge, never been explored before. Previous studies collected the GRF on a small number of force platforms (1 or 2) placed tangentially to the circle. In the present situation, where multiple force platforms were placed side-by-side over a circular trajectory, the resolution of the GRF into components that have a fixed referential has no physiological sense. Indeed, as runners lose energy in one axis which are compensated by gaining energy in another (Figs. 2.2.1B& 2.2.S2), neither axis provides physiological information as to what the runner is experiencing during their trial. Instead, a rotating referential that follows the direction of progression is best suited to distinguish between the forces necessary to push the runner inwards or outwards in the direction of the centre of the circle and accelerate and decelerate the runner in an axis facing the tangent of the circle at TD.

As compared to SLR, W_{com}^{+} is greater during curved running and increases as the radius decreases (Fig. 2.2.6). This increase is mainly due to an augmentation of W_X^{+}, which roughly represents the work done to deflect the trajectory of the CoM laterally, while W_z^{+} and W_Y^{+} remain approximately the same. On a 6 m curve, at

speeds above 12 km h^{-1}, W_X^+ is greater on the inner leg than on the outer leg. However, the increase in W_X^+ is roughly compensated by a decrease in W_Y^+. Consequently, the work necessary to move the CoM in the transverse plane ($\simeq W_X^+ + W_Y^+$) is approximately the same in the inner and outer limb. This observation suggests that the inner and outer limb play different roles in maintaining balance and controlling the trajectory while running in a curve: the inner limb is doing more work than the outer limb to deviate the CoM laterally whereas the outer limb is doing more work to accelerate the CoM forwards. This difference between the two limbs disappears on larger curves (18 m), at least at speeds below 22 km h^{-1}.

The energy recovered through the transduction between E_X, E_Y and E_z represents less than 5% of the work done in SLR, similar to previous studies (Cavagna et al. 1976; Gosseye et al. 2010; Mesquita et al. 2020). In running while turning, during the first part of contact, the E_X-curve is no longer in phase with the E_Y- and E_z-curves (Fig. 2.2.5), which allows for energy transduction. Indeed, E_X increases continuously during contact, whereas the E_Y- and E_z-curves are decreasing during the first part of contact (braking phase) before increasing during the second part. Part of the energy lost during the braking phase could be recovered to increase the velocity (and thus the kinetic energy) of the CoM in the lateral direction (Fig. 2.2.6). A similar phenomenon has been observed during uphill running (Dewolf et al. 2016): where part of the energy lost during the braking phase is used to increase the potential energy of the CoM each step.

Limitations

One of the limitations of this study is that SLR was performed on a treadmill whereas curved running was performed on the ground. However, it was deemed the best option considering the lack of time and the amount work to change the configuration of the platform. Although this difference in data collection may slightly bias the results, the results that we obtained on SLR are in agreement with previous results obtained on overground running (Cavagna et al. 1976, 1988; Willems et al. 1995).

The movements of the CoM are assimilated to the movements of the pelvis delimited by three markers glued on the skin. Though the movements of the CoM relative to the pelvis are small (Willems et al. 1995) (Fig. 2.2.S1), the present study does not take these movements into account. Furthermore, it has been shown that the external work measured based on the movements of the pelvis was overestimated as compared to the measurement based on GRF (Pavei et al. 2017). Although, this is not applicable here, it is worth noting that these movements are not exactly the same.

One of the main objectives of this study is to analyse the trajectory of the CoM/pelvis, focusing particularly on the movements of this point in the transverse plane, without considering the movements of the body segments. In a near future, it would be interesting to analyse also the movements of the body segments in 3-D to understand how a change in direction of the CoM and the rotation of the body are generated by the movement of these segments.

Conclusion and Perspectives

As compared to SLR, W_{com} is increased by up to 25% depending on the running speed and radius of curvature. Furthermore, the in-depth analysis of the CoM trajectory highlights an "over-deflection" during the contact phase to counter the rectilinear motion of CoM during the aerial phases. We also show that the inner and outer leg play a different role in this "over-deflection": the inner leg tends to deflect the trajectory of the CoM more that the outer leg, whereas the outer leg plays a more important role in accelerating the CoM forwards.

Indeed, the identification of asymmetries between the inner and outer limbs provides insight into potential strategies for optimising performance and minimising injury risk. Future investigations should consider the limb movements, their intersegmental coordination and internal work (Willems et al. 1995) used to re-accelerate and reorient the velocity vector. These have been previously shown in cutting manoeuvres to contribute significantly in the amount of total mechanical energy done by the runner (Zamparo et al. 2019). Such quantifications of these biomechanical constraints in running while turning may have practical implications in various fields, including sports performance, injury prevention, and rehabilitation.

Supplementary Information

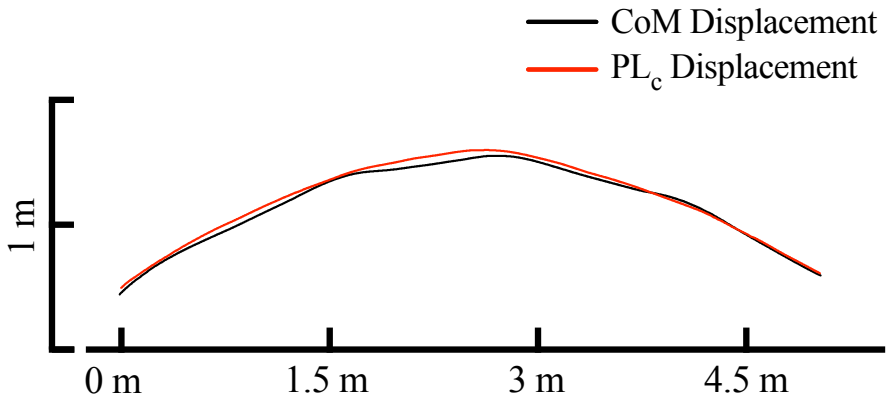

Fig. 2.2.S1 *The rotated oscillation of PL_c (in red) over two strides and the rotated displacement of the CoM (in black) calculated as the double integration of the horizontal GRF using the initial and final positions of the PL_c and the duration of the trial (T_{tot}) as the integration constant for (p_x, p_y). The trace is run at 14 km h^{-1} and on a 6 m radius of curvature and is from the same trial as in Fig 2.2.1B. The scales are asymmetrical to accentuate the oscillations around the curve.*

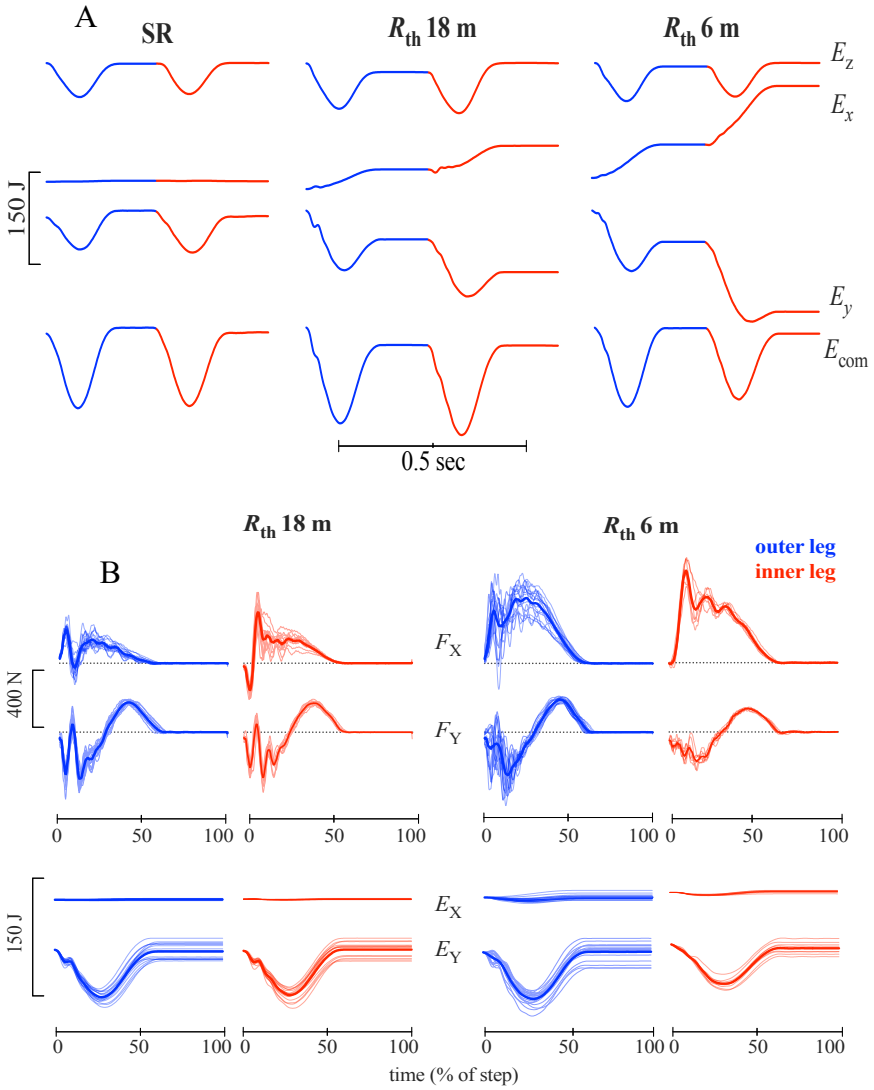

Fig. 2.2.S2 *(**A**) The typical energy traces (J) of one stride in the o-x-y-z referential from the first right stride used in Fig. 2.2.1 at both radii plus the typical trace of one stride from when the subject ran on a treadmill at the same speed (14 km h^{-1}). The blue represents the outer leg and red the inner. E_z is the energy done to sustain the vertical movements of the CoM. E_x is the energy done to sustain the medio-lateral movements of the CoM and E_y, similarly but for the fore-aft movements. E_{com} is the sum of all three first curves. (**B**) The time-normalised rotated GRFs (F_Y and F_X, expressed in Newtons) for every inner (red) and outer step (blue) done at 14 km $^{-1}$ for the 18 m and 6 m radii based on the continuously rotated referential using the θ- angle as explained below. The time-normalised typical energy traces (J) of E_X and E_Y for all the steps at the same speed calculated similarly from F_X, F_Y forces above.*

Classic method: Computation of external energy relative to a fixed referential frame

When running along a circular path, the *y*-direction no longer corresponds to the fore-aft direction of progression. Let's take, for example, a subject that runs on a 90° circular curve turning to the right. If the external referential is fixed to the lab, the subject runs in the *y*-direction at the beginning of the curve, and in the *x*- direction at the end of the curve. Thus, the CoM progressively gains velocity along the *x* axis and loses velocity along the *y*-axis. In other words, during the movement, the kinetic energy E_y (equation 11) is decreasing while the kinetic energy E_x (equation 10) is increasing (Fig. 2.2.S2A) The energy of the CoM due to its vertical movement (E_z) is not affected by the turn.

In this case, the total work W_{com} is correctly measured, however the division of the work into W_x and W_y has no physiological meaning, and the distinction between the work done to sustain the motion of the CoM in the direction of progression (W_f) and in the lateral direction (W_l, *i.e.* in the direction perpendicular of the axis of progression) is not possible.

Continuous rotation of the forces: Computation of the external energy relative to a referential frame rotating at each instant of the step

In this second approach one a more obvious solution for rotating the referential should be to rotate the frame of reference at each instant so that the *Y*-axis of the new reference frame is tangent to the circular trajectory that the runner follows, and that the *X*-axis is pointed towards the centre of the circle. However, in this case, it is difficult to separate the work done to move the CoM in the axis of progression (W_f) from the work necessary to modify the direction of progression (W_l). The θ-angle is used for this rotation:

$$\theta = 180° - \operatorname{atan}\frac{PLC_{cy} - y_o}{PLC_{cx} - x_o}.$$

The two horizontal components of the GRF in the frame *O*-*X*-*Y* were computed as:

$$(F_X\ F_Y) = \begin{pmatrix} \cos\theta & -\sin\theta \\ \sin\theta & \cos\theta \end{pmatrix} \begin{pmatrix} F_x \\ F_y \end{pmatrix}.$$

Similarly, the two horizontal components of the velocity of the CoM were computed as:

$$(v_X\ v_Y) = \begin{pmatrix} \cos\theta & -\sin\theta \\ \sin\theta & \cos\theta \end{pmatrix} \begin{pmatrix} v_x \\ v_y \end{pmatrix}.$$

Then the energy of the CoM due to the velocity changes in the *Y*-axis, and the *X*-axis were computed using equations similar to equations (6) and (7) in the new reference frame:

$$E_Y = \int F_Y \, v_Y \, \mathrm{d}t \; = \frac{1}{2} \, m \, {v_\mathrm{Y}}^2 \, ,$$

$$E_X = \int F_X \, v_X \, \mathrm{d}t = \frac{1}{2} \, m \, {v_\mathrm{X}}^2 \, ,$$

Note that because we are using *R* and not *r* for the calculation of θ, there is a slight amount of energy done in the centripetal axis. If one were to consider the centripetal axis at each instant, no energy is done as the force and velocity vectors are orthogonal. Nevertheless, nearly all of the energy done in the horizontal plane is done in the direction tangent to the circle. Second, the energy of the CoM due to its vertical movement (E_z) is not affected by the turn. The total energy of the CoM (E_{com}) is then computed by:

$$E_{\mathrm{com}} = E_\mathrm{Y} + \; E_\mathrm{X} + E_z.$$

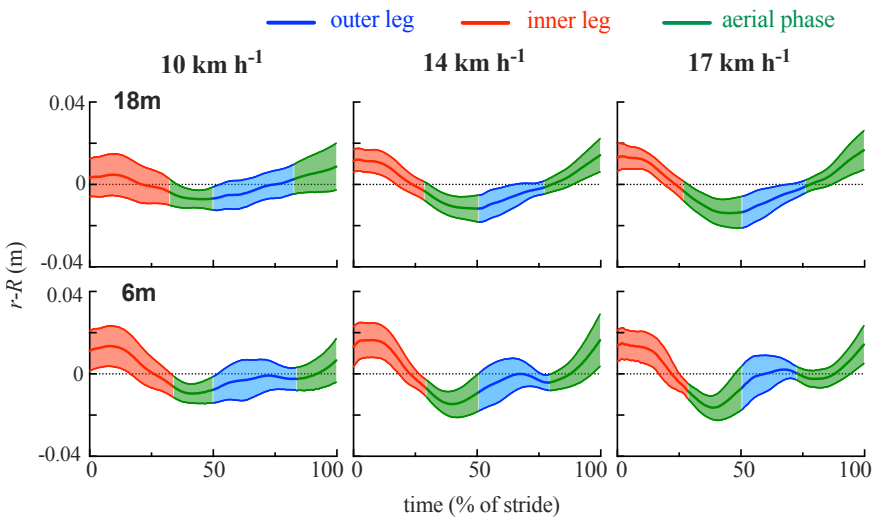

Fig 2.2. S3 *The average difference between the 'instantaneous' radius, r, and the actual radius R (r-R) calculated by the circular fit from the movements of PL_c as explained in the methods, plotted as a function of time. The top panels show three different speeds (10, 14 and 17 km h^{-1}) when running on an 18 m curve, whereas below the same speeds are shown for a 6 m curve. The average trace (thick line) is calculated over all participants and the cloud around is the standard deviation. Time is expressed in a percentage of the stride period. The traces start on the inner leg TD where the distance between r and R is at its highest (in red), before the CoM trajectory approaches the circle and the distance between both is reduced prior to the aerial phase (green trace). This is followed by the outer step (blue trace) which has a similar negative distance to R than the inner leg and is also progressively directed inwards prior to the second aerial phase. Note, during the aerial phase the CoM is travelling in a rectilinear motion. Here above, the aerial phase curves because we are looking at a difference between the CoM trajectory and the curve. Therefore, if the CoM begins its flight close to the circle and continues straight whereas the curve bends then the distance between both increases.*

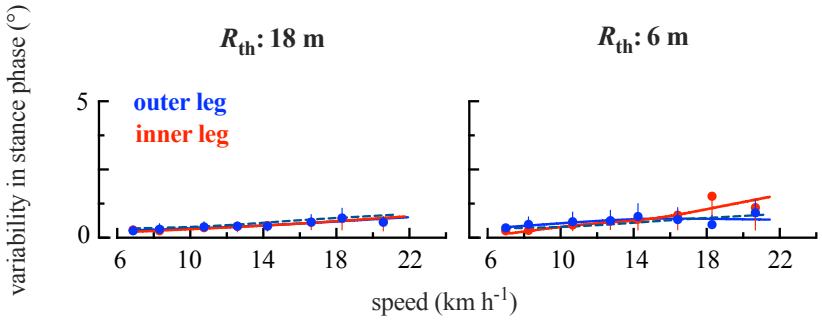

Fig 2.2.S4 *The variation of foot angle (τ) in the horizontal plane while the foot was flat on the ground as a function of speed at both radii of curvature. τ was defined as the angle formed between the x-y position of the markers placed on the 5th metatarsal, the heel and the horizontal. The variation was measured as the standard deviation of τ between the point when the heel touches the ground until when the heel lifted off the ground by 0.05m, or so when the foot was flat on the ground. This was chosen as a means to verify that the foot was not skidding or rotating over the ground rather than measuring the ankle-roll over the toes during contact. All other indications are as in Fig 2.2.4.*

2.3 Kinematic and motor coordination of the inner and outer limb in running while turning

Raphael M. Mesquita, Patrick A. Willems, Arthur H. Dewolf

Medicine & Science in Sport & Exercise (Submitted)

Keywords: running, curved running, kinematic coordination, inner outer limb difference

Introduction

Human locomotion requires structured coordinated bilateral motion to execute functional movement patterns. To manage this complexity, the central nervous system (CNS) simplifies control by reducing the degrees of freedom, producing a coordinated response involving both limb movements and muscular activation (Bernstein 1967). This coordinated motion allows the system to continuously adapt to the evolving biomechanical demands of everyday life.

Habitually, locomotion is studied in controlled, linear, and symmetrical conditions, such as walking or running on a treadmill at constant speeds over multiple strides. However, in nature, such situations are probably rather infrequent. Humans must constantly adjust to changes in speed, terrain, obstacles, and direction (Alexander 2002). In a recent study, we collected the present data and examined how the body's centre of mass (CoM) adapts when running on curves with radii ranging from 6 - 18 m at constant speeds of 07 - 22 km h^{-1} (Mesquita et al. 2024b). Our findings show that the work required to sustain the CoM movements increased by approximately 25% at the highest speeds, largely due to the added work needed to manage the lateral movements. Furthermore, while the overall work to maintain CoM motion is roughly balanced between both limbs, the inner limb performs more work to redirect the CoM inward, whereas the outer limb primarily handles braking and acceleration in the fore-aft direction.

The body functions as a dynamical system, where the position of the CoM and its movements depend among others on the overall configuration and coordination of the lower limb segments (Ivanenko et al. 2008). Consequently, inner and outer limb differences in force production (Chang and Kram 2007; Churchill et al. 2016), limb kinematics (Alt et al. 2015), joint dynamics (Luo and Stefanyshyn 2012) and muscular demand (Fílter et al. 2020; Pietraszewski et al. 2021) will have different outcomes on the positioning and thus power output of the CoM as it aims to maintain constant speed motion while running on a curve.

Although these limb differences have been examined in the studies mentioned above, these analyses predominantly focussed on sprint mechanics at maximal velocity on an athletic track, where the minimum radius of curvature is at least of 36.5 m (Churchill et al. 2011, 2016; Judson et al. 2020a), or on running curves with radii smaller than 6 m (Chang and Kram 2007; Luo and Stefanyshyn 2012). Given that the joint moments and power sheds light into the biomechanical constraints of running, an in-depth analysis of the lower limb coordination during an asymmetrical running task, using kinematics and a multi-muscle approach could provide insight on

athletic training, injury prevention, and biomechanical modelling of non-linear gait. Thus, our aim was to analyse the differences in inner/outer limb coordination patterns when running on curves with increasing speeds. We supposed that the differences observed *via* the analyses mentioned above, would highlight the distinct roles each limb has in running while turning.

In this paper, lower limb coordination was evaluated through three main approaches: joint dynamics, intersegmental coordination, and muscular activity of the lower limb muscles. In the first approach, the movements of the lower limb can be assimilated by a multi-jointed system composed of torsional spring/motors which either store/release or produce/absorb energy over the contact phase (Qiao et al. 2017). During straight-line running (SLR), the lower limb joints in the sagittal plane (relative to the vertical) modulate the running motion through a proximal-to-distal distribution of energy production/absorption: the proximal joints produce energy whereas the distal joints operate as springs or energy absorbers (Daley et al. 2007; Orendurff et al. 2018). When adapting to different situations, *e.g.* accelerative running, the energy production shifts to the distal joints (McGowan et al. 2005). These differences help coordinate the overall leg function (Qiao et al. 2017).

When running in a curve, frontal plane motion is no longer negligeable, as the limb must push inward with each step. Therefore, understanding the role of hip abductors/adductors when running, muscles which move the limbs in the frontal plane, is necessary to comprehend how the lower limb coordinates for leg function. Movement should therefore be analysed in both planes of motion. We hypothesised that in the sagittal plane, the proximal-to-distal modulation would shift towards the distal segments, as the hip joint also needs to accommodate the increased frontal plane motion. We expected this shift to intensify with increasing speed and decreasing radius of curvature. Additionally, we predicted that the inner and outer limbs would adapt differently during curved running, given their distinct roles in contributing to the mechanical work of the CoM (Mesquita et al. 2024b).

In the second approach, the segmental motion and intersegmental coordination was also analysed *via* the planar covariation method (Borghese et al. 1996; Bianchi et al. 1998). In running, the elevation angles of the foot, shank, and thigh in the sagittal plane follow a coordinated pattern, forming a closed-loop trajectory over a stride when plotted one versus the others. These three angular movements covary along a plane, effectively reducing the degrees of freedom of the locomotor system to two: limb length and limb orientation (Poppele et al. 2002; Ivanenko et al. 2008). The orientation of the covariation plane, along with the characteristics of the loop, defines a general kinematic pattern of locomotion. This pattern adapts to different

locomotor conditions (Dewolf et al. 2018), adjusts with changes in speed (Ivanenko et al. 2007; Mesquita et al. 2024a) and mechanical demands (Dewolf et al. 2018; Dewolf, 2020b). Considering that the CNS controls both limb length and orientation (Poppele et al. 2002) and that plane orientation is limb function specific (Catavitello et al. 2015, 2018), when limbs have different functions we expected that the plane describing the motion of the inner limb would progressively diverge from that of the outer limb as the radius of curvature decreased.

In the third approach, to assess the muscular demands of each limb during curved running, we analysed the neuromuscular control of gait. The coordination of lower limb muscular activity depends on both the spatial and temporal organisation of muscle activation (Yakovenko et al. 2002; Ivanenko et al. 2006; Martino et al. 2014). During curved sprints, the muscular demand has been shown to be limb specific, for example the inner limb adductor and plantar-flexor muscles show higher mean and peak activity over a stride in curved sprinting (Fílter et al. 2020; Pietraszewski et al. 2021). We anticipated differences in the spatial and temporal activation patterns between the two limbs, and that these differences would become more pronounced as the radius of curvature decreased and the running speed increased.

The role that each limb has to continuously maintain a curved trajectory, oppositely to a cutting-curved turn, has been extensively documented (Chang and Kram 2007; Churchill et al. 2011; Viellehner et al. 2016; Dos'Santos et al. 2019). At curves with a large radius (above 6 m), the inner limb has been shown to play a larger role redirecting the CoM, whereas the outer limb primarily handles braking/acceleration in the fore-aft direction (Churchill et al. 2011; Heinrich et al. 2015; Ishimura and Sakurai 2015; Mesquita et al. 2024b). Thus, observing how each limb distributed load within its joints, how it programs its segment configuration to adapt a curve, and how the muscles need to adapt to this change in strategy, provides deeper insight into the biomechanical strategies employed during turning.

Materials & Methods

Participants and experimental procedure

The present experimental protocol was adapted from Mesquita et al. (2024b) (chapter 2.2.2), and as such, similar sections were summarised. Eleven recreational male runners (height: 1.81 ± 0.03m, mass: 74.91 ± 5.38 kg, age: 24.64 ±2.91 years, mean ± SD) participated in the study. Informed written consent was obtained in accordance with the Declaration of Helsinki, and the study was approved by the UCLouvain Ethical Committee (B403201940199).

Participants attended two sessions spaced six weeks apart. In the first session, they ran at speeds ranging from 7 to 22 km h^{-1} on a circular track with a radius of 18 m, which was instrumented with 16 force platforms (described below). In the second session, participants ran on a curved path with a 6 m radius and on a treadmill, allowing for comparison with straight-line running. The six-week interval was required to reconfigure the force plates.

Each trial began with participants running along a 20 m straight corridor before entering the curved path, ensuring that they took at least one step on the curve prior to data collection. Participants were first asked to run at intermediate speeds (around 12-14 km h^{-1}), then at fast speeds (between 16 and 18 km h^{-1}), followed by slow speeds (between 8 and 10 km h^{-1}), and finally at the maximum speed that they could reach. After each trial, the runner's average horizontal velocity and the validity of strides were verified and communicated to the participant. Rest periods were provided as needed to prevent fatigue-related bias.

A trial was considered valid if it included at least one stride (two consecutive steps) in which the horizontal velocity (v_h), calculated by the ground reaction forces, remained constant over a complete stride (Mesquita et al. 2024b). A stride began when the vertical component of the ground reaction force became greater than 30 N on one foot and ended when the same foot touched the ground for the following stride: a total of 1021 strides were analysed.

Experimental set-up

The present study measured three types of variables. First, the kinematic movements of body limb segments were captured using high-speed infrared cameras. Second, surface electromyographic (EMG) activity in both lower limbs was recorded via 24 surface electrodes. Third, the ground reaction force (GRF) was measured and has been detailed extensively in our previous work (Mesquita et al. 2024b). Two pairs of

photocells were positioned ~6 m apart at each end of the running track, at level with the neck. These cells were used to trigger and stop the data acquisition for all three systems simultaneously.

Measurement of kinetic variables during curved running

For the curved running sessions, 16 custom-built force plates of 1 m x 1 m each were arranged side by side in an 18 m and 6 m curved configuration. The circular paths curved to the right and the runner followed a 0.5 m wide lane delimited by two white stripes. Each force plate measured the three components of the GRF by means of four force transducers placed under each corner of the plate surface. Detailed characteristics of the force plates are provided in Genin et al. (2010). During SLR, the GRF was measured with an instrumented treadmill (h/p/Comos-Stellar, Germany) mounted on four force transducers (Arsalis, Belgium). A more in-depth description of the treadmill can be found in (Mesquita et al. 2024a).

Measurement of kinematic variables

Bilateral, full-body three-dimensional (3D) kinematics were recorded by means of a Qualisys system (Gothenburg, Sweden) equipped with 12 “Mocap OQUS 6+” cameras placed around the running track or the treadmill, plus one video “Miqus M1” camera. Participants were equipped with 43 retro-reflective markers glued onto the skin according to the Qualisys sports marker set disposition. Symmetrical markers for the upper limbs and trunk were placed on the left and right temples, acromia, mid-arm on the biceps brachii, lateral and medial humeral epicondyles, styloid processes of ulna and radius, second metacarpal-phalangeal joints. For the lower limbs, symmetrical markers were placed on the left and right superior anterior iliac spines, iliac tuberosities, greater trochanters, mid-frontal thighs, lateral femoral condyles, mid-frontal shanks, lateral malleoli and on the second and fifth metatarsal-phalangeal joints. Furthermore, asymmetrical markers were placed on the front of the head, sternal manubrium, T2 and T12 and S2 spinous processes. Kinematics were recorded at a sampling rate of 100-240 Hz and oversampled during post-processing at 1 kHz to match the sampling frequency of the kinetic data. An oversampling of the kinematic data was chosen rather than a down sampling of the kinetic data to ensure that the force signal characteristics were not lost during data-processing and to avoid aliasing effects.

Measurement of EMG variables

The EMG activity of 12 bilateral lower limb muscles was recorded at 2.15 kHz with a Delsys Trigno surface electrode system of (Natick, MA, USA). Two EMG protocols (A and B) were established to increase the number of muscles recorded. In both protocols, 10/12 muscles per protocol were the same; the gluteus maximus (Gmax), rectus femoris (ReFe), sartorius (Sart), gracilis (Grac), semi-tendinosum (SeTe), biceps femoris (BiFe), medial gastrocnemius (MeGa), lateral gastrocnemius (LaGa), tibialis anterior (TiAn), peroneus longues (PeLo) of both limbs were always recorded. The muscles that differed between protocols were the tensor fascia latae (TeFL) and vastus medialis (VaMe) for protocol A and gluteus medius (Gmed) and vastus lateralis (VaLa) for protocol B. After preparing the shaved skin with alcohol, we placed EMG electrodes based on the SENIAM protocol (seniam.org), the European project on surface EMG. To this end, we located the muscle bellies by means of palpation and oriented the electrodes along the main direction of the fibres (Winter 2009). The raw EMG signals were down sampled to 1 kHz during post processing to match the other types of data.

Data analysis

All data were separated into the following speed classes based on the average v_h (in km h^{-1}): [6,8[, [8, 10[, [10,12[, [12, 14[, [14, 16[, [16, 18[, [18, 20[. As subjects had to freely match speeds according to vocal guides, when less than half of the participants covered the speeds in the class, the group was removed from the analysis. One class in treadmill running needed to be removed. Without this data point, speed classes counted on average 9.6 ± 2.1 subjects. The analysis was performed *via* custom-written programs using LABVIEW (National Instruments 2021, Austin, TX, USA) and Matlab software (MathWorks r2019a, Natick, MA, USA).

Referential rotation

In our previous paper (Mesquita et al. 2024b) we presented a method for rotating ground reaction forces from a reference frame *o-x-y-z* fixed to the lab to a reference frame *O- X- Y- z* that moves as the runner turns. This method allowed us to better distinguish between the work done to move the CoM forwards and the work done to push the CoM inward, relative to the runner. To achieve this, we calculated a virtual position for the centre of the pelvis in the transverse plane, P_c, as the centroid of a triangle between the right and left ASIS and S2 markers. We then ran a circular fit on the movement of P_c in the transverse plane to determine the radius of the curve

covered by the subject over the trial and rotated the transverse plane forces by the angle (θ) formed by the *o-x* axis, the position of P_c and the centre of a circle.

Here, we rotated the forces and kinematic marker positions based on the instantaneous θ_j-angle. In this way, the (*x,y*) positions of each marker (*i*) in the fixed reference frame were rotated at each instant (*j*) of the stride to give a lateral and fore-aft, respectively (*X,Y*) position relative to a non-inertial reference frame:

$$\begin{pmatrix} X_{i,j} \\ Y_{i,j} \end{pmatrix} = \begin{pmatrix} x_{i,j}\cos\theta_j - y_{i,j}\sin\theta_j \\ x_{i,j}\sin\theta_j + y_{i,j}\cos\theta_j \end{pmatrix}.$$

This rotation is possible given the angular displacement covered by the outer and inner limb are symmetric over a step (Fig. 2.3.S1A). Note, the vertical axis was not rotated compared to body pitch as to maintain a reference perpendicular to the ground. From these rotated marker positions, the elevation angles in the rotated frontal (*O-X-z*) and sagittal (*O-Y-z*) plane, *i.e.* the orientation of the limb segments of both lower limbs relative to vertical were computed. For each trial, the segment motion time-curves were segmented by stride and time-normalised to fit a standardised 400-point time-base. For each speed and radius class, the average across-stride values were computed separately for each limb and for each subject.

Computation of joint moment and work

By combining both the rotated kinematic and kinetic variables, the net muscular moments of the lower limb joints were evaluated in the sagittal and frontal plane over the contact phase by an inverse dynamic method (Mauroy et al. 2014).

In the sagittal plane, the lower limbs were modelled as a multi-segmented limb formed by thigh, shank and foot segments. Each segment being in motion equates to: $\sum_i \vec{F}_i - m_s\vec{a}_s = 0$, where $\vec{F}$ is the *i*th force applied on the segment, m_s is the segment mass and $\vec{a}_s$ is the double time derivative of the segment's centre of mass displacement, obtained *via* the Dempster and Gaugran tables from Winter (2009). Note, that the fictious forces due to the referential rotation accounted for less than 2% of the total force over the contact phase and were therefore neglected. The torque generated around each joint, ankle, knee, and hip, can be computed as: $\sum_i \vec{d}_i \times \vec{F}_i + \sum_i \vec{M}_j - I_s\,\vec{\alpha}_s = 0$, where $\vec{d}_i$ is the lever arm of $\vec{F}_i$, $\vec{M}_j$ is the net muscular moment applied on the joint, I_s is the moment of inertia of the segment and $\vec{\alpha}_s$ is the angular acceleration of the segment, both relative to the sagittal plane (*O- Y- z)*. The net muscular power generated at each joint (P_j) was calculated as: $P_j = \vec{M}_j\,\omega_j$. Where ω_j is the time derivative of the angle formed between two segments. Accordingly,

the muscular energy done at the joint level per limb ($E_{\mathrm{j,i}}$), was determined by the time-integration of the summed joint power: $E_{\mathrm{j,i}} = \int P_{\mathrm{j,i}}\,\mathrm{d}t$. The positive/negative joint work done at each joint for each limb, $W_{\mathrm{j,i}}^{+/-}$, is calculated as the sum of the positive/negative increments of this curve.

In the frontal plane, given that the angular displacement of the ankle was not significantly different between limbs during sprinting (Judson et al. 2020b), that the knee motion in the frontal plane is an accessory movement and that error is accumulated per rising joint level (Winter 2009): only the joint moment of the hip was computed by considering the lower limb as a single segment which comes in contact with the floor. Given the fictitious forces, due to the reference rotation, the forces explaining segment motion were equal to $\sum_i \vec{F}_i - m_s\vec{a}_s = \vec{F}_{\mathrm{fict}}$, where $\vec{F}_{\mathrm{fict}}$ was the centripetal force apparent due to the non-inertial reference frame and was proportional to the square angular velocity of frame rotation and the position of the segment relative to the centre of the reference frame. The other fictious forces were neglected. From this, the joint moment, power and positive/negative work at the hip in the frontal plane was then computed similarly to the sagittal plane.

Range of motion and intersegmental coordination

In each speed and radius class, the average waveforms of the elevation angles of the three lower-limb segments—thigh, shank, and foot—were computed across participants. The segment range of motion (ROM) over a stride was computed as the difference between the maxima and the minima elevation angle over the period.

The inter-segmental coordination of the lower-limb segments was analysed using principal component analysis (PCA), a method previously described in detail (Borghese et al. 1996; Ivanenko et al. 2008; Catavitello et al. 2018). Briefly, when the centred thigh, shank, and foot elevation angles are plotted in three-dimensional space, they form a closed-loop trajectory that lies near a plane. The best-fitting plane is defined by the first two principal components obtained from the PCA of the covariance matrix of the three elevation angle waveforms (Daffertshofer et al. 2004; Ivanenko et al. 2008). The PCA returns a matrix of eigenvectors u with associated eigenvalues (λ1, λ2, λ3) ordered from the largest to the smallest. The first two eigenvectors, u_1 and u_2 generate the best fitting plane while the third eigenvector, u_3, orthogonal to the plane, defines its orientation. The components of u_3: u_3t, u_3s and u_3f correspond to the direction cosines with the positive semi-axis of the thigh, shank and foot angular coordinates. The percentage of variance associated to vectors u_1, u_2, u_3 are respectively PV1, PV2 and PV3 and are computed as the ratio of each

eigenvalue to the total eigenvalue sum (*e.g.* PV3 = λ3/ (λ1 + λ2 + λ3)). PV3 was used as an index of planarity, with PV3 = 0% indicating maximum planarity.

EMG analysis

The raw EMG signals were visually inspected for amplifier saturation and noise artefacts. The signals were then high-pass filtered (30 Hz), rectified and low-pass filtered (10 Hz) with a zero-lag fourth-order Butterworth filter to obtain each muscle's linear envelope (Dewolf et al. 2020a). Signals were then cut by stride and the geometric average of all strides of the same speed and radius class was calculated per subject. The geometric average was chosen as it is less sensitive to outliers and thus further reduces noise in the signal (Linssen et al. 1993). The signals were time-normalised to 400 points and to reduce residual baseline noise, the minimum signal for each envelope was subtracted (La Scaleia et al. 2014). This gave us a 28x400 matrix (muscles from both protocols x time-normalisation) per speed class, per radius class and per subject. The waveform amplitudes were also normalised based on the maximum values for each muscle per subject when running on the treadmill at all speeds. As the 18 m curve was done on a different day than the 6 m and treadmill runs, due to skin impedance and electrode placement the amplitude normalisation for the former should not be considered precise (Burden et al. 2003). Therefore, all amplitude analyses (*e.g.* mean muscular activity and full width at half maximum) were only compared between the 6 m and treadmill trials.

The centre of activity (CoA) was computed per muscle as in Martino et al. (2014) by using circular statistics and plotted in polar coordinates (polar direction denoted the instant *t* of the stride cycle expressed an angle (α) going from 0 to 360°). The CoA of the EMG waveform was calculated as the angle of the vector (1st trigonometric moment) that points to the centre of mass of that circular distribution using the following formula:

$$\mathrm{CoA} = \tan^{-1}\left(\frac{\sum_{t=1}^{400} \sin \alpha_t \times \mathrm{EMG}_t}{\sum_{t=1}^{400} \cos \alpha_t \times \mathrm{EMG}_t}\right).$$

Furthermore, for each EMG waveform per trial, the full width at half maximum (FWHM) was calculated as the duration during which the muscular activity exceeded the half of its maximum over one stride (Martino et al. 2014).

Statistics

For each participant, the different parameters were first averaged for all inner and outer steps over one trial. Then descriptive statistical analysis was performed. A Shapiro-Wilk test was performed to verify normality on linear data. Then, a linear mixed effect model with pairwise comparison and Bonferroni post-hoc correction was used to compute the individual effects of radius, speed and limb on the calculated variables. A power analysis, conducted using GLIMMPSE 3.1.2 (Denver, Colorado, USA), confirmed that a sample size of 10 participants was required to achieve adequate statistical power (1- ß = 0.872) and avoid a type II error when considering this model for joint dynamics, intersegmental coordination and muscular activity variables.

For circular data, *i.e.* CoA, the mean resultant length (r) was evaluated for each variable. For data which were concentrated appropriately ($r > 0.5$) a Watson-Williams test was performed with pairwise comparison and a Bonferonni post-hoc correction was used to compute factor effects. Statistical tests were run on IBM SPSS Statistics (PASW Statistic 27, NY, USA) for linear data and on Matlab for circular data. The results of the statistical tests were considered significant for a p-value < 0.05.

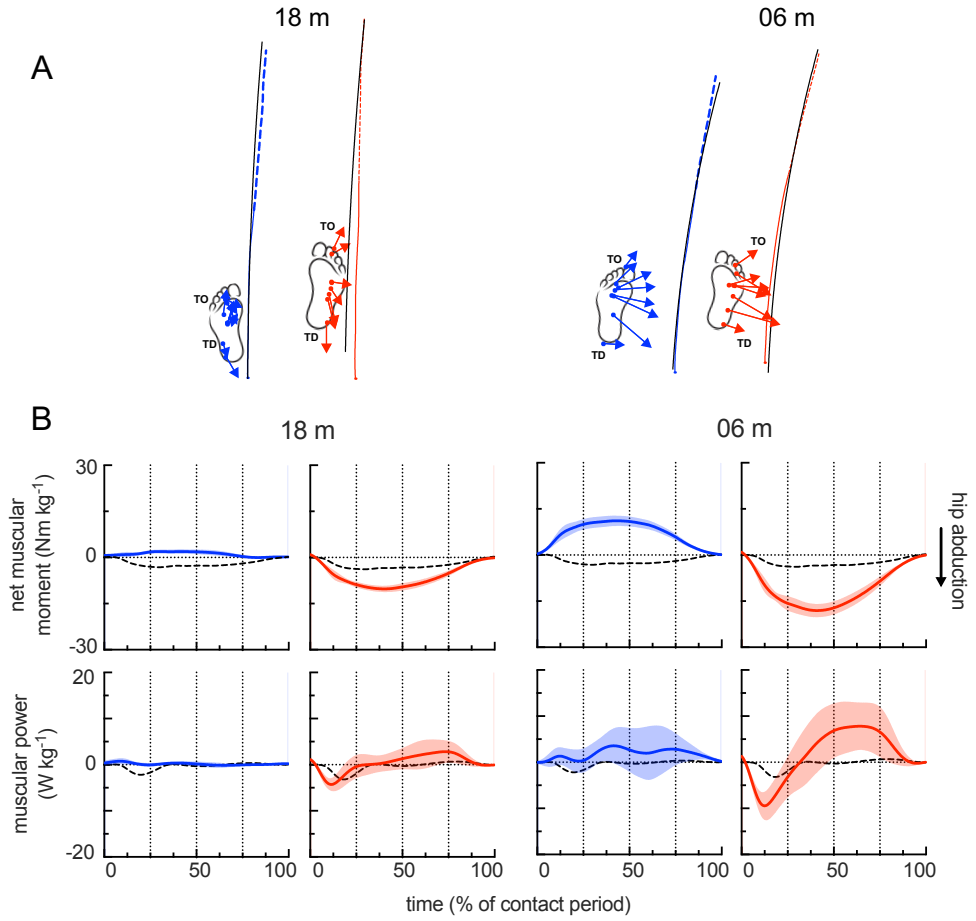

Fig 2.3.1 A) *Typical trace of the evolution of the component of the GRF vector in the transverse plane every 10% of the stance period (about ~19 ms between each point) when running at 17 km h^{-1} on the 18 m-curve (left) and 6 m-curve (right). Each point represents the position centre of pressure position (COP), calculated as in (Dewolf et al. 2018). Note that the feet remain largely fixed over stance (Mesquita et al. 2024b). When the threshold to compute the COP was not attained, neither the COP nor the GRF vector were plotted (i.e. when the GRF is smaller than 150 N). The position of the inner (red) and outer foot (blue) are plotted relative to the circular fit computed on the displacement of P_c (black thin line) over the entire trial. The red (inner) and blue (outer) lines are the actual movements of P_c over the full step presented here (contact phase: filled line, aerial phase: dashed line) (see Methods section).* ***B)*** *Net muscular moments and muscular power developed in the frontal plane by the inner (red) and outer (blue) hip joints during stance at 17 km h^{-1} for both radii of curvature. Time is normalised in percent of the contact period. Continuous lines represent the average and coloured surface the standard deviation. The dashed black line corresponds to the respective limb in SLR. The dotted vertical lines break the stance phase into 25%-time phases.*

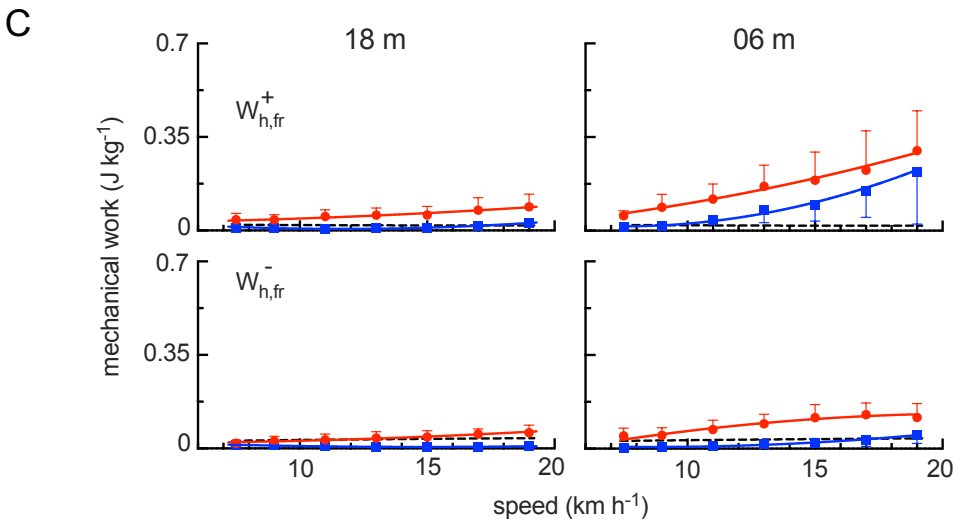

Fig 2.3.1 C) *Positive ($W^{+}_{h,fr}$) and negative ($W^{-}_{h,fr}$) average and standard deviation of the hip mechanical work done to sustain its movements in the frontal plane for the inner (red circles) and outer (blue squares) limbs at both radii of curvature as a function of speed. The continuous lines following the average points, are a quadratic fit of the data over all speeds. The dashed continuous black lines are the fits on the right limb SLR data. Note that positive work done by the inner limb is done by the abductor muscles, whereas outer limb positive work is done by the hip adductors.*

Results

Position of the feet relative to the trajectory of the pelvis

Fig. 2.3.1A illustrates a typical trace of the evolution of the component of the GRF vector in the transverse plane. The point of application of this vector is placed on the centre of pressure position (COP) each 10% of step, along with the position of the inner and outer feet during stance. The COP was computed as in Dewolf et al. (2018). The lines on each panel represent the trajectory of the point P_c in the transverse plane. On an 18 m-curve, the outer foot landed near the outer edge of the P_c trajectory, suggesting that the outer limb contributed little to pushing the CoM inward with the forces primarily oriented in the fore-aft direction. In contrast, the inner foot also landed on the outer edge of the P_c trajectory, creating a larger moment arm. This positioning allowed the limb to orient its forces both in the fore-aft and inward direction. On a 6 m-curve, the pattern remained similar, however both feet landed further from the P_c trajectory. This shift suggests that the outer limb adducted to push itself inwards, while the inner limb abducted to direct its forces inwards.

Work done at the level of the hip in the frontal plane

In the frontal plane during SLR, as the foot touched the ground, the hip abductors contracted eccentrically to control the adduction of the lower limb (Fig. 2.3.1B). As the lower limb returned to its initial position, the hip abductors contracted isometrically to stabilise the hip throughout the rest of the contact phase. This explains the near-zero power observed in the frontal plane, as minimal lateral movement occurs, there was little power required for sustaining lateral motion of the lower limb.

In curved running, like SLR, the inner limb underwent an initial eccentric contraction to control adduction, followed by concentric contraction of the hip abductors, pushing the body inward during the stance phase. For the outer limb, the hip adductors contracted concentrically as the body bent inward. The outer limb's contribution in the frontal plane depended on the curve's radius. At 18 m, the lower limb remained beneath the centre of rotation, resulting in negligible frontal plane movement, however as the radius decreased, the hip adducted the limb concentrically.

Overall, the inner limb abductors performed more positive work than the outer limb adductors to push the body inward ($F = 86.49$, $p < 0.001$) during the contact phase. Both the positive and negative work done to sustain the frontal motion increased with speed ($W^{+}_{h,fr}$: $F = 12.80$, $p < 0.001$; $W^{-}_{h,fr}$: $F = 9.69$, $p < 0.001$) and as the radius of curvature decreased ($W^{+}_{h,fr}$: $F = 94.40$, $p < 0.001$; $W^{-}_{h,fr}$: $F = 74.78$, $p < 0.001$).

Work done at the level of the ankle, knee and hip in the sagittal plane

In curved running, the positive work done at the ankle increased compared to SLR ($F = 287.86$, $p < 0.001$, post-hoc $p < 0.001$), while negative work decreased ($F = 65.62$, $p < 0.001$, post-hoc $p < 0.001$) (Fig. 2.3.2). Runners did more positive (*i.e.* propulsive) work and less negative (*i.e.* braking) work in curved running than in SLR, though no significant differences were found between the two radii of curvature ($p = 1$ for both positive and negative work). Additionally, the inner and outer ankle generated the same amount of propulsive work ($F = 0.70$, $p = 0.79$), but the outer ankle performed significantly less braking work than the inner ankle ($F = 106.60$, $p < 0.001$), with this difference becoming more pronounced as the radius decreased.

At a radius of 6 m, the knee reached maximum flexion earlier in the contact phase, leading to an increase in eccentric work by the knee extensors compared to SLR ($F = 13.29$, $p < 0.001$, post-hoc < 0.001), though no significant change occurred

at the larger radius ($p = 1$) (Figs. 2.3.2 & 2.3.S3A). The knee then extended through a concentric contraction of the knee extensors during the second part of the stance phase. In curved running, the positive/negative work ratio was ≈1, indicating an increase in positive work to extend the knee compared to SLR where the ratio was on average 0.35 across all speeds ($F = 479.03$, $p < 0.001$). However, positive work did not differ between radii (post-hoc $p = 0.016$). Comparing the inner and outer limbs, the inner knee performed less negative work than the outer knee ($F = 14.26$, $p < 0.001$) but both knees performed the same amount of positive work ($F = 5.64$, $p = 0.018$).

The hip joint sagittal motion changed pattern between SLR and curved running. In SLR, as the subject touched the ground, the hip extensors contracted isometrically during weight acceptance followed by a small concentric contraction, controlling the hip over the stance. In curved running, the isometric portion of the hip motion was controlled by both hip flexors and extensors. Over the second portion of the stance, the hip flexors eccentrically contracted to slow hip extension. The amount of negative work done at the hip increased as the radius decreased ($F = 55.73$, $p < 0.001$) and was greater in the outer compared to the inner hip ($F = 57.70$, $p < 0.001$).

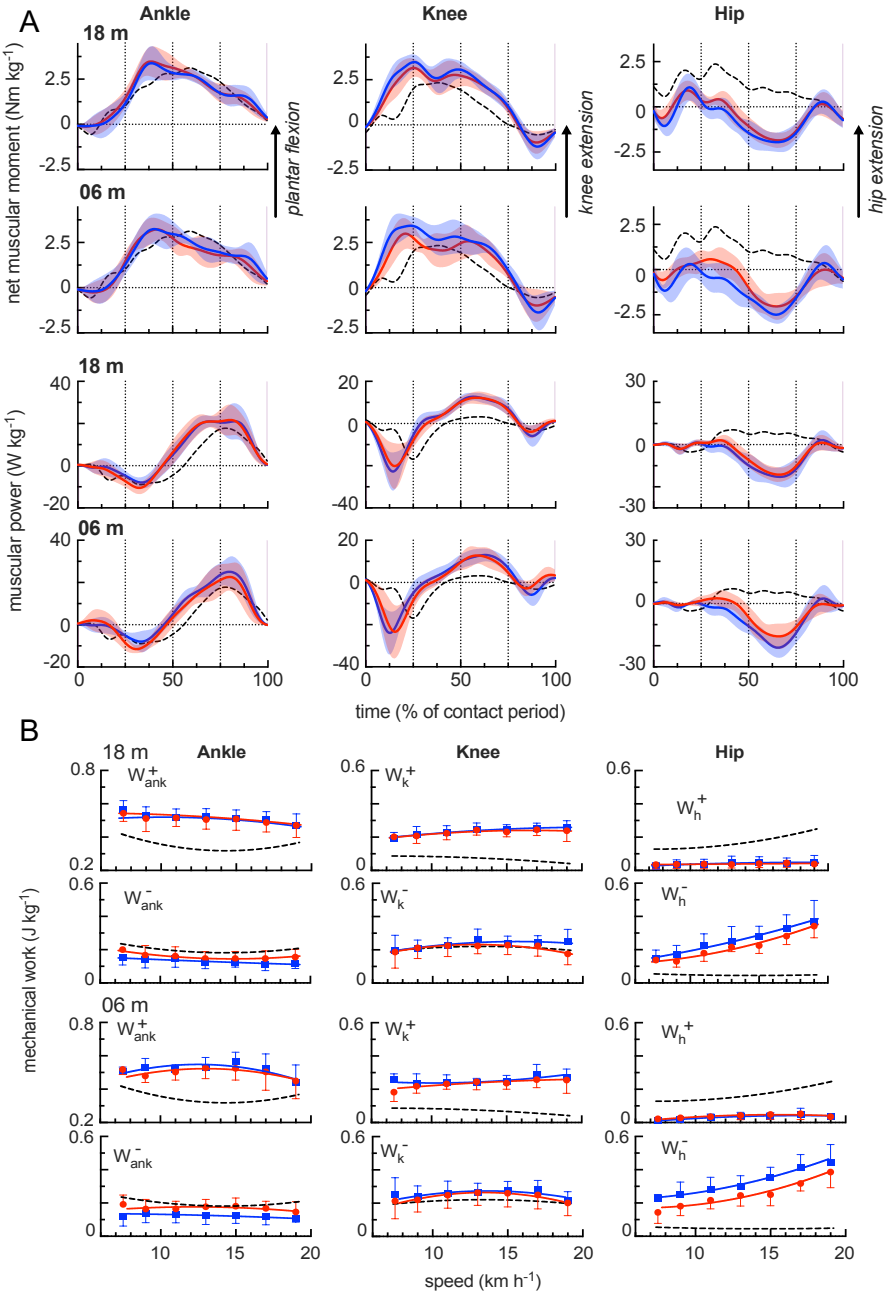

Fig 2.3.2 A) *Net muscular moments and muscular powers performed in the sagittal plane by the inner and outer ankle, knee and hip joints during stance while running at 17 km h^{-1} on both radii of curvature. All other indications are as is in Fig. 2.3.1B.* ***B)*** *Positive (superscript +) and negative (superscript -) mechanical work done to sustain the movements of the ankle (W^{+}_{ank}), knee (W^{+}_{k}) and hip (W^{+}_{ank}) joints in the sagittal plane. All other indications are as in Fig. 2.3.1C.*

Intersegmental coordination & range of motion

Fig. 2.3.3A shows the time-normalised elevation angles of the thigh, shank, and foot for both limbs over a stride at 17 km h^{-1} in SLR and on the two radii of curvature. Below are the corresponding 3D-plots of these elevation angles, along with the best-fitting planes for the inner and outer limbs and their projections on the thigh-foot plane (Figs. 2.3.3B & C). The ROM of each lower limb segment increased with speed (thigh: $F = 918.25$, $p < 0.001$; shank: $F = 720.04$, $p < 0.001$; foot: $F = 350.21$, $p < 0.001$) (Fig. 2.3.S3B). The ROM of the thigh and shank increased at the 6 m as compared to SLR ($F = 27.87$, $p < 0.001$; shank: $F = 6.501$, $p = 0.002$; post-hoc $p < 0.007$) but not when comparing 18 m and SLR (thigh: $p = 0.129$, shank: $p = 1$). When comparing limbs, the inner thigh and shank had a greater ROM than their outer counterparts (thigh: $F = 37.10$, $p < 0.001$; shank: $F = 9.88$, $p = 0.002$). The foot ROM, however, did not change significantly with radius (radius $F = 0.71$, $p = 0.49$, limb: $F = 0.86$, $p = 0.35$) (Figs. 2.3.3C & 2.3.S3B).

As the radius of curvature decreased, especially at higher speeds, the rotation of the covariation plane differed between the inner and outer limbs (Fig. 2.3.3B). This is further shown by the inner limb u_3t component, orthogonal to the plane (Fig. 2.3.3D, left), which progressively dissociated from the outer limb as the radius increased (limb effect: $F = 94.68$, $p < 0.001$, radius*limb effect: $F = 11.90$, $p < 0.001$). The inner limb relied less on PV1 (limb effect: $F = 54.12$, $p < 0.001$) and had a higher percentage of variance explained by PV2 (limb effect: $F = 26.69$, $p < 0.001$) compared to the outer limb (Fig. 2.3.3D, right).

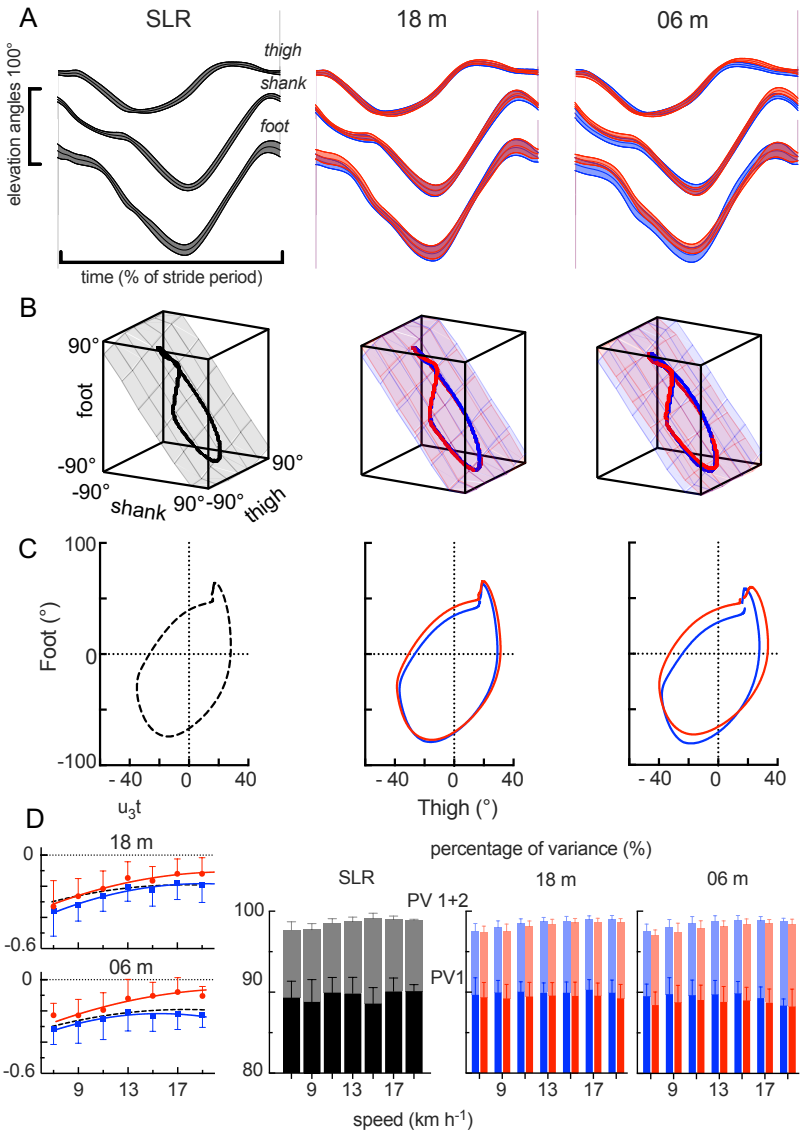

Fig 2.3.3 A) *Elevation angles of the thigh, shank, and foot for the inner and outer limbs over a step at 17 km h^{-1} in SLR, 18 m and 6 m curves. Traces begin at foot contact.* ***B)*** *3D-plots of the elevation angles of Fig. 2.3.3A, along with the best-fitting planes for the inner and outer limbs. In SLR, only the right limb is presented.* ***C)*** *The projections of each 3D-plot on the thigh-foot plane over a stride.* ***D)*** *left side: direction cosine for the thigh of the third eigenvector u_3t averages and standard deviations at both radii of curvature as a function of speeds. Other indications are as in Fig. 2.3.1C. right side: percentage of variance (average and standard deviations) explained by the first eigenvector (PV1) and percentage of variance explained by the first and second eigenvector (PV1+2) for inner (red) and outer (blue) limbs for 18 m and 6 m curves as a function of speeds. For SLR the right limb is presented.*

Muscular activity and coordination

Fig. 2.3.4 shows the time-normalised average muscle activity and standard deviation for 14 bilateral muscles in the inner (right) and outer (left) limbs, during one stride of running on a 6 m-curve and on SLR at 17 km h^{-1}. Qualitatively, some of the muscles which stand out by their increased activity are those involved in hip motion, *e.g.* sartorius and gracilis. Furthermore, almost all muscles appear to anticipate their activity peaks compared to SLR.

Quantitative analysis (Fig. 2.3.5) of the FWHM, CoA and mean muscular activity were computed. All muscles, except the gracilis and tibialis anterior, had a concentrated burst of activity, providing a coherent CoA value. These two muscles remained active throughout most of the stride, making CoA analysis unreliable. The CoA was anticipated with speed for most of the muscles (Gmed, SeTe, BiFe, VaLa, VaMe, LaGa, MeGa, PeLo $p < 0.050$). As the radius decreased, all muscles anticipated their CoA ($p < 0.005$). The inner limb Sart ($p < 0.001$), SeTe ($p < 0.049$), BiFe ($p < 0.049$) showed more anticipation compared to the outer limb. Oppositely, the CoA of the outer limb PeLo ($p < 0.001$) was more pre-activated.

The FWHM of several muscles (Gmed, TFL, Sart, Grac, SeTe, BiFe, MeGa, LaGa, TiAn, PeLo) decreased with increasing speed ($p < 0.035$), while the mean muscular activity of all muscles increased ($p < 0.050$). Between SLR and running on a 6 m curve, the FWHM increased for the Grac, BiFe, MeGa, LaGa, TiAn and PeLo ($p < 0.040$) and the mean muscular activity increased for Gmax, VaLa, ReFe, SeTe, BiFe, LaGa and PeLo ($p < 0.025$). Regarding limb differences, the inner limb showed greater FWHM for Gmed, VaLa, MeGa, LaGa, and TiAn ($p < 0.03$), while the outer limb had greater FWHM for BiFe ($p < 0.009$). Mean muscle activity was higher in the inner limb Grac ($p < 0.008$), and higher in the outer limb Sart, BiFe, MeGa, LaGa, and PeLo ($p < 0.05$).

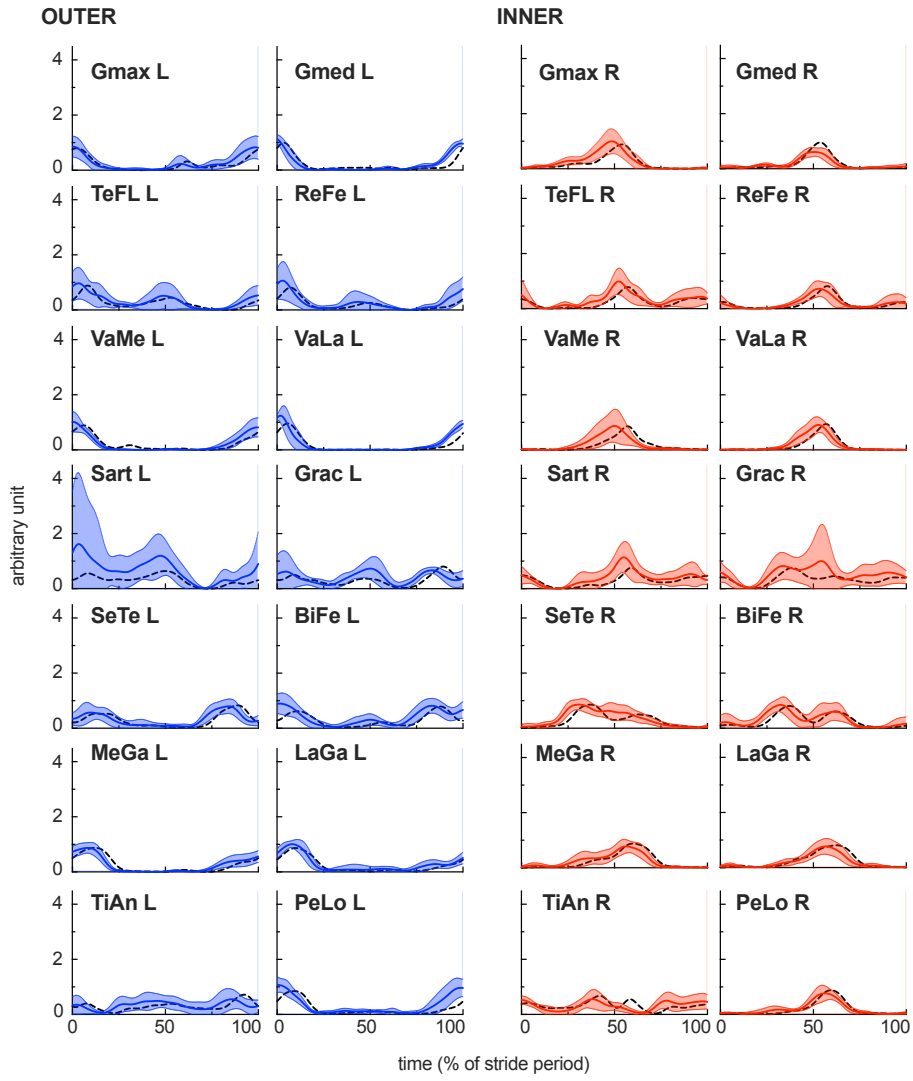

Fig 2.3.4 *Linear envelopes of the EMG of the 14 bilateral lower limb muscles of the outer (left) and inner (right) limbs over a stride while running on a 6 m-curve at 17 km h^{-1}. The coloured surface and continuous line represent the average ± 1 SD of these envelopes. The dashed lines correspond to the same muscles in SLR. Muscular activity is normalised by the maximum value obtained when confounding on speeds during SLR. The stride begins at the outer, left, foot contact when running.*

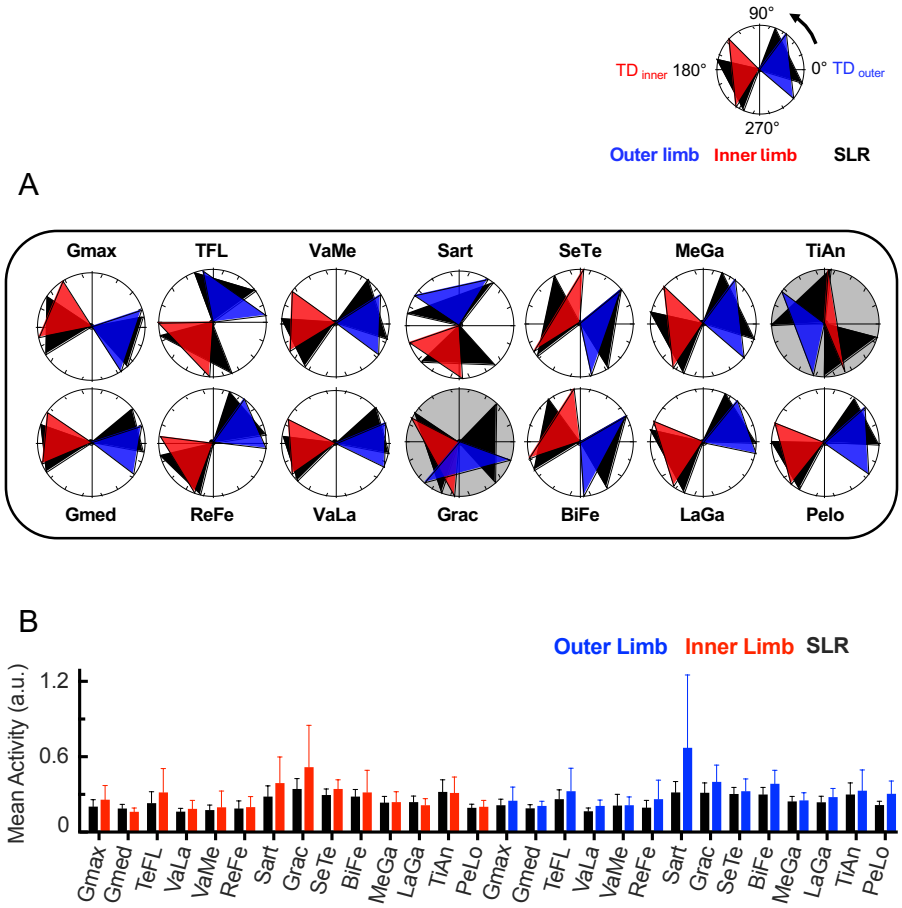

Fig 2.3.5 *Characteristics of the EMG activity during running on a 6 m-curve and SLR at 17 km h^{-1}.* ***A)*** *Centre of activity (CoA) and full width at half maximum (FWHM) of the bilateral lower limb muscles. The direction of the centre of each triangle corresponds to the CoA of each muscle and the length of the base of each triangle corresponds to the FWHM for both limbs (similar colours as Fig. 2.3.4) and in SLR (black triangles). The polar direction corresponds to the relative time over a stride. At 0° the timing corresponds to the outer left foot touch down and time progresses counterclockwise. Grey circles are because the EMG activity was dispersed throughout the entire stride and not concentrated enough for the CoA circular statistics.* ***B)*** *Mean muscular activity for the 14 bilateral lower limb muscles.*

Discussion

This paper analysed the effect of the radius and speed of locomotion on the neuromechanical coordination of the lower limb in curved running, as compared to straight-line running. Specifically, it analysed the joint dynamics, intersegmental coordination and muscular activity of the inner and outer limb when running on two different radii of curvature (18 m and 6 m) at speeds ranging from 7-19 km h^{-1} to further understand the different roles of the inner and outer limb. We confirmed that the inner limb primarily managed lateral redirection of the body, relying on increased joint compliance and enhanced muscular activation in the hip abductors to accommodate the greater lateral forces. In contrast, the outer limb contributed more to propulsion and stabilisation to drive forward motion. In the following paragraphs, we described successively the difference between SLR and running while turning, and the outer and inner limb differences.

Kinematic, joint and limb coordination

When running in a straight-line, joint coordination follows a proximal-to-distal gradient of neuromechanical control. The proximal, hip muscles, drive the gait while the distal, ankle muscles, act like a spring, storing and releasing elastic energy over the contact phase (Roberts and Azizi 2011; Qiao et al. 2017). This allows the hip joint to control limb retraction and produce net mechanical work over the gait (Biewener and Daley 2007; Daley et al. 2007). The knee, set between the proximal and distal joints, functions as a damper, modulating the overall lower limb stiffness and reacting to the force balance between the joints (Biewener and Daley 2007; Lieberman et al. 2015; Qiao et al. 2017). Note, the ankle spring-like behaviour has been shown to vary depending the foot strike pattern (Ahn et al. 2014; Almeida et al. 2015), with heel strikers shifting more from a spring to motor behaviour, possibly due to a greater amount of negative work being dissipated in the soft tissues and not stored in the elastic tendons (Dewolf et al. 2024).

When running on a curve, our results show that the ankle joint deviated from a spring-like behaviour, exhibiting a greater net positive work balance than in SLR (Fig. 2.3.2). Instead, as compared to SLR, at the knee level, an equivalence was observed between positive and negative work, and the knee no longer behaved like a damper. At the hip, more negative than positive work was present (Fig. 2.3.2B). This shift in joint energy production to the distal joint aligned with our hypothesis that the ankle adapts to the increased force production required in curved running by shifting from a spring-like to motor behaviour, similar to that observed in accelerative or

decelerative running (McGowan et al. 2005; Bezodis et al. 2008). Also, the proximal-to-distal shift in positive mechanical work production could likely be due to the lower limb being angled during the stance phase to accommodate for the lateral redirection of the body, which forced the hip to lose its effectiveness in generating power in the sagittal plane (Churchill et al. 2011). Initially, both hip flexors and extensors stabilised the lower limb through weight acceptance, as in SLR (Mauroy et al. 2014), after which the flexors eccentrically contracted to control hip extension.

When considered separately, the inner and outer limbs adjusted their sagittal plane motion and coordination differently when running on a curve. Consistent with previous findings, we confirmed that the inner limb played a greater role in turning, while the outer limb primarily stabilised and maintained forward motion of the CoM as already shown by Hamill et al. (1987), Viellehner et al. (2016) and Mesquita et al. (2024b). We showed that the outer limb ankle drove fore-aft motion more than the inner limb by performing less negative braking work (Fig. 2.3.2). This could be related to the modification of foot-ground interaction. Indeed, after the initial heel touchdown phase the GRF vector shifted to the ball of the outer foot for the remainder of the stance, whereas the inner limb distributed its force across the entire foot (Fig. 2.3.1A). The increased propulsive torque in the ankle was carried upwards to the knee and hip, increasing torque and work production at those joints as well (Fig. 2.3.2). This is consistent with the rise in momentum observed in the outer limb during curved sprinting (Ishimura and Sakurai 2015).

The specific role of the inner limb became clearer when examining the frontal plane hip moments. Frontal plane dynamics showed increasing inner-outer asymmetry, as each hip joint had a distinct role in pushing the body inward. The inner limb abductors produced both eccentric and concentric contractions throughout the stance, and the limb remained more adducted compared to the outer limb (Figs. 2.3.1 & 2.3.S2). This greater inner limb adduction angle during the stance also explained why the inner hip was in a less advantageous angle to control fore-aft motion, consistent with what is observed in maximal speed sprinting (Churchill et al. 2011; Alt et al. 2015). At larger radii, the outer limb stabilised the lower limb isometrically and did not directly contribute to inward propulsion. However, as the radius of curvature decreased, the outer limb also aided in inward propulsion through concentric hip adductor contractions. While research on frontal plane joint dynamics is limited, previous documentation highlighted that the inner hip is generally "highly loaded" and has an important role in stabilising the non-sagittal plane movement (*sic*) (Luo and Stefanyshyn 2012; Heinrich et al. 2015; Viellehner et al. 2016).

Regarding the kinematic coordination of the lower limb segments (Fig. 2.3.3), the ROM of the thigh and shank of both limbs increased at the smallest radius of curvature as compared to SLR (Fig. 2.3.S3). In terms of the covariance planes, when both limbs were considered, segment coordination in the sagittal plane did not differ from SLR. This emphasizes the robustness of the planar covariance law in the sagittal plane segment angular motion (Ivanenko et al. 2008; Lacquaniti et al. 2012). Additionally, it also confirmed previous observations that sprint curving dynamics do not substantially alter sagittal plane dynamics (Ishimura and Sakurai 2015) (Fig. 2.3.3).

By looking at the outer and inner segmental coordination, differences in the movement programming between limbs emerged. The coordination loops (Fig. 2.3.3C & D) revealed that the outer limb followed the long axis more closely, which is better explained by the first eigenvector (increased PV1), whereas the inner limb aligned more with the wide axis, better explained by the second eigenvector (increased PV2). This suggested that the outer limb's movement was primarily governed by variations in limb orientation while the inner limb's motion was more influenced by telescopic length changes (Ivanenko et al. 2008), indicating distinct strategies in limbs for managing the curved running motion. This was consistent with observations that limb function affects the plane orientation (Catavitello et al. 2015, 2018).

Such distinct roles of the inner and outer limbs during curved running led to differences in how each limb sought gait stability in the sagittal plane. At the ankle, the inner limb exhibited greater angular displacement compared to the outer limb (Fig. 2.3.S3A). This increased displacement, coupled with a similar net muscular moment (Fig. 2.3.2A), suggested that the inner ankle was more compliant (less stiff) than the outer ankle. Greater compliance increases the stability of a segment (Daley and Usherwood 2010). In contrast, the outer ankle showed increased stiffness, consistent with its primary role in driving the body forward rather than inward. Similar observations are noted at the proximal joints, where the outer knee and hip displayed greater muscular moments than their inner counterparts for similar joint displacements, further indicating stiffer outer limb joints. The combination of a stiffer outer limb and a more compliant inner limb provides a balance of opposing factors, which aligns with the findings of Qiao and Jindrich (2014).

Muscular Coordination

When running on a curve, the lower limb muscular activation patterns were not substantially different from SLR as in previous studies on curved walking (Courtine and Schieppati 2003). However, in line with our hypothesis, systematic temporal and spatial changes were observed when running on a curve (Fig. 2.3.4 & 5). Firstly, as running speed increased, muscles showed increased mean activity and decreased FWHM, resulting in concentrated burst lengths with increased amplitudes (Kyröläinen et al. 2005; Cappellini et al. 2006). These findings supported the hypothesis for a speed-dependant control of locomotion (Biewener and Daley 2007; Dewolf et al. 2020a).

Additionally, compared to SLR, as the radius of curvature decreased, all muscles exhibited an anticipatory activation pattern relative to their CoA. This anticipatory behaviour may be attributed to a heightened sensitivity of the muscle spindles, which stimulate the tendomuscular systems to better tolerate and absorb higher impact loads (Gollhofer and Kyröläinen 1991; Kyröläinen et al. 2005). For example, Kyröläinen et al. (2005) showed that an anticipated muscle activation subsequently facilitated the A - motoneurons resulting in increased EMG activities of the knee extensor and plantar flexor muscles with increasing running speed. Furthermore, in curved running, the mean activity and FWHM increased for the muscles involved in controlling the hip and ankle joints, supporting the kinematic control of gait discussed above. Both the pre-activation and increased mean activity could be linked to the anticipated and increased negative power peaks observed at the ankle and knee joints in the sagittal plane and increased negative peak observed at the hip in the frontal plane (Fig. 2.3.1B & 2A).

When comparing the left and right side of the body, the hip muscles of the inner limb (Sart, SeTe, BiFe) exhibited an earlier peak burst of activity compared to their outer counterparts, stabilising and propelling the body both inward and forward. The frontal plane joint kinematics showed that the inner limb initially slowed its adduction, then abducted the segment throughout the remainder of the stance phase (Fig. 2.3.1B & S2). After foot take-off, the limb benefited from the centripetal force, which aided in its adduction as it is pushed outward. The inner limb then used the momentum generated by the contralateral limb ground contact to swing back inwards (limb abduction) and prepared for its following contact phase (Fig 2.3.S2). Consequently, the pre-activation of the hip muscles accommodated the increased lateral load. Additionally, the Grac increased its mean muscular activity, contracting eccentrically at the end of the swing phase to control hip abduction and then concentrically throughout the contact phase. The heightened activity of the adductor

muscles in the inner limb has also been documented in studies on curved sprints (Fílter et al. 2020).

The outer limb was more abducted than in SLR and compared to the inner limb. It maintained a quasi-static frontal motion throughout the contact phase. At foot take-off the hip adductors contracted concentrically to counter the centripetal force. They were then aided by the inner limb momentum over the contralateral ground contact and centripetal force to abduct back to its programmed touchdown position. Given that the adductors contract concentrically over both the stance and aerial phase, the Grac muscular activity did not show a specific burst throughout the stride, explaining the dispersity and incoherent CoA analysis as well as the lesser contribution of the muscle compared to its inner counterpart (Fig. 2.3.5A) (Fílter et al. 2020).

In the sagittal plane both limbs adjusted their muscular coordination spatially and temporally to accommodate for their separate roles in the turning motion. Indeed, the mean activity of the outer limb was greater at the level of the hip (Sart, BiFe), corresponding to the increased deceleration of the outer hip throughout the stance (Fig 2.3.2A). Specifically, the Sart exhibited heightened mean activity over the stance phase, as the hip flexors contracted eccentrically to control hip extension. The increased outer BiFe mean activity agreed with the observations of Fílter et al. (2020) and can be explained by the muscle's more prevalent role in hip extension at the end of swing and initial contact phase, as compared to the other hamstring muscles (Mesquita et al. 2024c; Van Wingerden et al. 1993).

Contrary to the findings of Pietrazewski et al. (2021), we showed increased muscular activity in the outer rather than inner limb plantar flexors. This difference suggests that the increased braking moment and energy absorption observed in the inner limb, was most likely handled by the increased FWHM of the TiAn and inner plantar flexor muscles (Fig. 2.3.4 & 5), but also by the muscles that control the metatarsal-phalangeal joints (Judson et al. 2020b). Furthermore, increased TiAn activation has been shown to counter ankle imbalance when the COP is shifted laterally (van Leeuwen et al. 2021). In the outer limb, the PeLo demonstrated higher pre-activation and greater mean activity. Pre-activation of the PeLo has been shown to increase ankle stability when the COP experiences a medial shift (Fig. 2.3.1A) (Baur et al. 2010; Ortega et al. 2024).

From a stability perspective, we showed that firstly, the inner limb was more compliant during the stance compared to the stiffer outer limb. This finding was also supported by the higher activity in the outer *vs.* inner gastrocnemius muscles. A more compliant musculotendon complex increases energy absorption allowing for a more

efficient motion (less net-work production). In contrast, a stiffer tendon, accompanied by increased muscular activity, is capable of releasing more energy back into the system (Daley 2013; Kyröläinen et al. 2005). Secondly, the increased FWHM in the inner limb may indicate an enhanced search for stability similar to observations made when running on slippery surfaces or rough terrain (Cappellini et al. 2010; Santuz et al. 2018).

During the 400 m Paris Olympics semi-final, Alexander Doom, the indoor 400 m world champion, stopped his race during the second curve due to injury in his inner adductor muscles. Sprinters which are required to turn at high speeds (200 m and 400 m runners) have been reported in having a 3:1 prevalence in posterior hip and thigh injuries of the inner compared to outer limb (Ayres and Gottlieb 2006; Edouard et al. 2020). In fact, Ayres and Gottlieb go on to explain that this difference may reflect the increased stress created by inward lean while turning. Recognising such vulnerabilities is crucial for both athletes and trainers, as targeted interventions and training modifications may reduce these risks, supporting better long-term performance and injury prevention (Exell et al. 2012).

Limitations & perspectives

As the 18 m curve was done on a different day than the 6 m and treadmill trials, the amplitude comparisons between curved and SLR were only done between trials run on the same day and excluded the 18 m curve, a better configuration would have been to combine curved and SLR in each configuration.

A second limitation of this study is that the SLR condition was done on a treadmill and not overground. Thus, despite most outcomes between treadmill and overground running being largely comparable (Van Hooren et al. 2020), it did add some bias to our results, for example the hip angular dynamics show some variability in touchdown and take-off angles (Kerdok et al. 2002; Hardin et al. 2004; Van Hooren et al. 2020). As explained above, limb positioning influences the tendon length and could change joint mechanical properties (Gabaldón et al. 2004), thus a comparison for the apparent differences between SLR and curved running could be due simply due this discrepancy.

Third, in our discussion we argued that the inner and outer limb showed changes in muscular moments for a same angular displacement, or *vice-versa*, which indicated a change in joint stiffnesses. We did not however directly measure the stiffness of the lower limb nor of the joints directly. A lessened stiffness in one plane could also be due to the spring bending in a different plane. A future study should

take these observations into account to measure both joint and global lower limb stiffness, accounting for the limb movements by considering the 3D motion of the lower limb spring.

Conclusion

In conclusion, this study demonstrated that running on a curve modified the neuromechanical coordination of the lower limbs, with distinct roles for the inner and outer limbs. The inner limb primarily managed lateral redirection of the body, relying on increased joint compliance and enhanced muscular activation in the hip abductors to accommodate the greater lateral forces. In contrast, the outer limb contributed more to propulsion and stabilisation to drive forward motion. This deeper understanding of limb function in curved running could inform future research on athletic training, rehabilitation, and biomechanical modelling of non-linear gait.

Supplementary Information

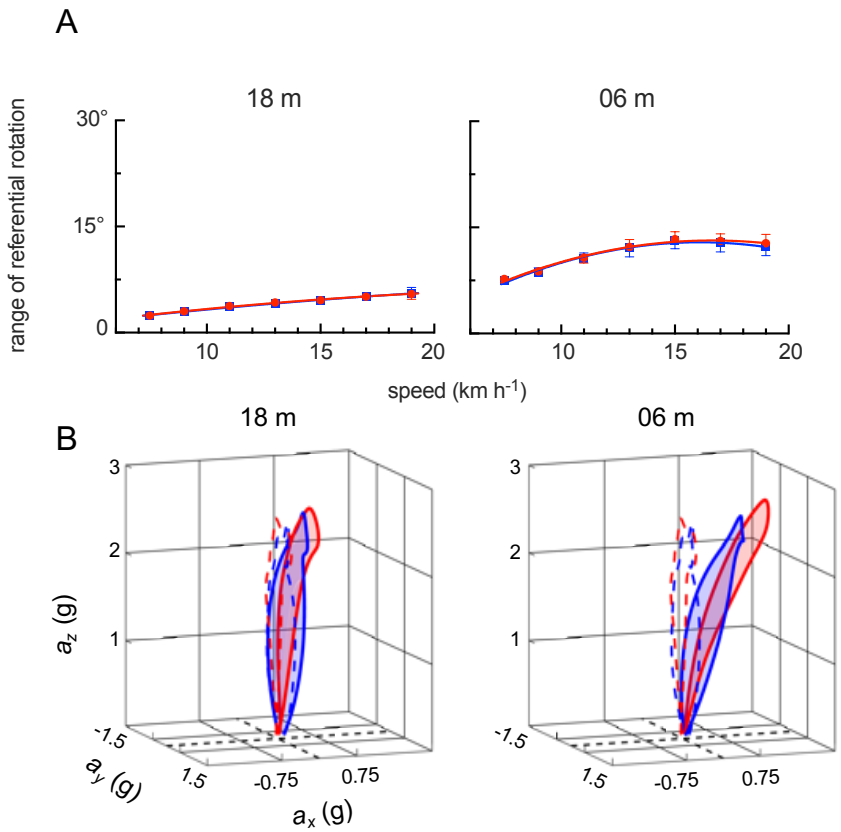

Fig 2.3.S1 A) *Average ± SD reference frame angular rotation covered over an inner (red) and outer (blue) step for both radii as a function of speed.* ***S1B)*** *3D-average plots of the acceleration vector normalised by the gravitational acceleration of the inner and outer limbs at both radii of curvature and in SLR (corresponding-coloured dashed lines).*

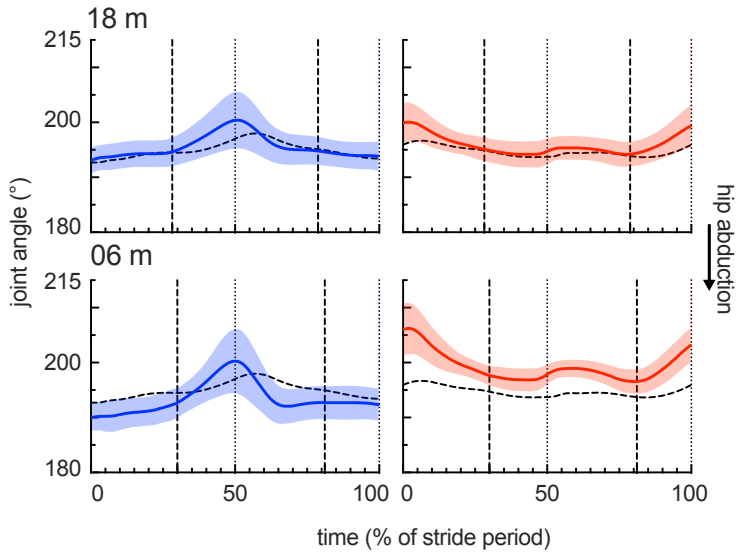

Fig 2.3.S2 A) *Adduction-abduction angle of the hip in the frontal plane for both limbs (other indications as in Fig. 2.3.1B) over one stride beginning at the outer foot contact for both radii of curvatures and in SLR (black dashed lines, showing the right limb). The vertical dashed lines correspond to the foot take-off of either limb. Foot contact is at 0%, 50%, and 100% of the stride and are represented by dotted lines.*

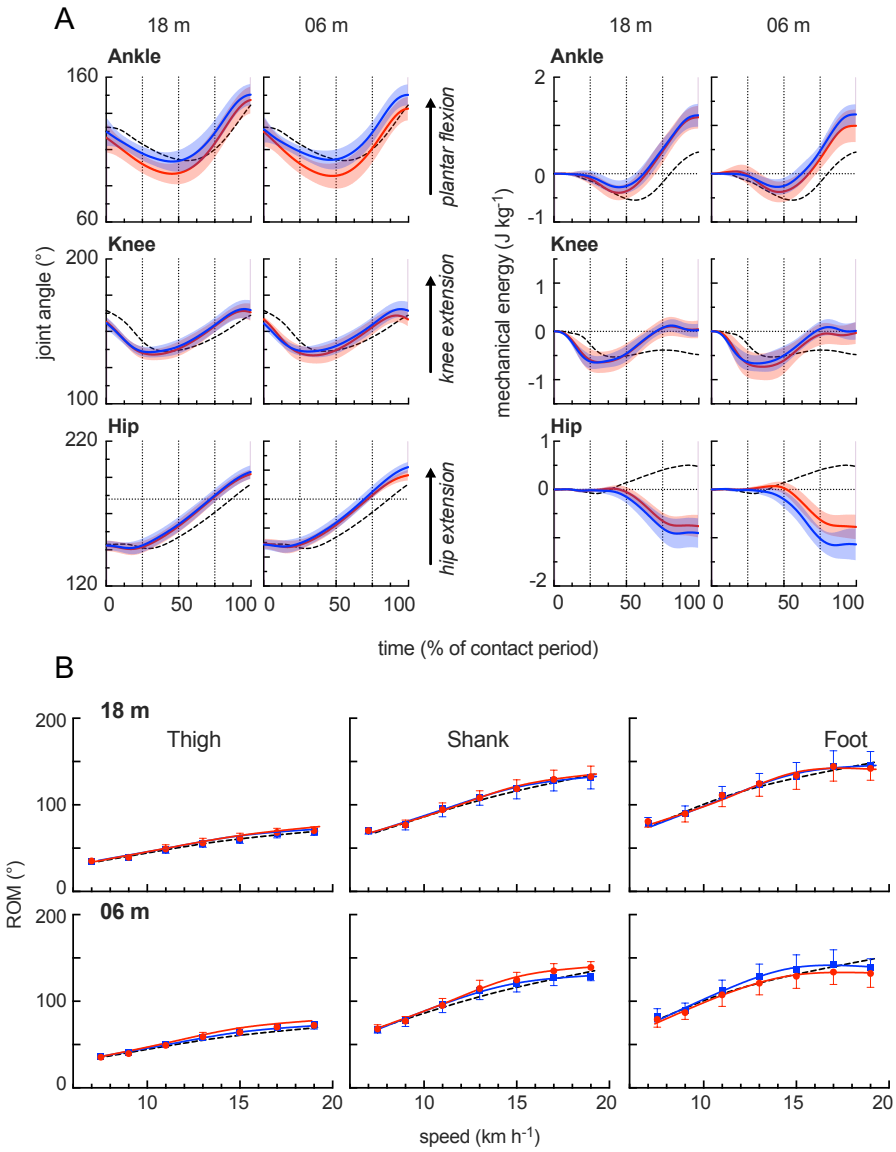

Fig 2.3.S3 A) *Left: Plantar - dorsi flexion angle of the ankle, flexion - extension angle of the knee and the hip in the sagittal plane for both limbs (similar indications as Fig. 2.3.1B) over the stance phase for both radii of curvatures and in SLR (corresponding-black lines). Right: Time normalised average and standard deviation of the mechanical energy of each lower limb joint. All other indications as in the left side.* ***S3B)*** *Range of angular motion of the thigh, shank and foot segments. All other indications are as in Fig. 2.3.1C.*

Chapter 3. Gait modifications with environmental perturbations

During locomotion at a constant average speed on a firm level ground, when wind speed is considered negligible and the foot is not skidding on the ground, almost no energy is dissipated into the environment and muscles do as much negative as positive work. However, in nature situations like these are rather infrequent. In the latter, part of the energy produced by the muscles is used to do work against the environment and an imbalance occurs between positive and negative mechanical work done. This is the case in situations such as in locomotion on a slope (Dewolf et al. 2016), or when moving on sand (Lejeune et al. 1998).

In this chapter, we compared three situations where positive and negative muscular work done are not equal. First, we compared running with/against tractive forces to running on a slope. Second, we compared running in the wind with running with a tractive force. These comparisons are possible due to the hypothesis emitted by di Prampero that running while accelerating is equivalent to running uphill.

In 2005, di Prampero hypothesised that, because of the similar body lean when accelerating on flat terrain and when running at constant speed on an uphill slope, the two situations were metabolically comparable (Fig. 3.0.1).

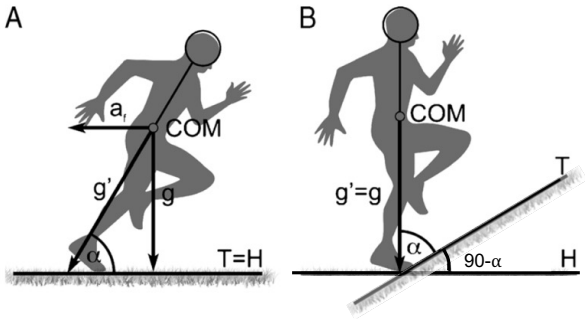

Fig. 3.0.1 *Simplified view of the forces acting on a subject during accelerated running. The runner's body is represented by a straight line. T, terrain; H, horizontal; g, acceleration of gravity; af, forward acceleration; g', vectorial sum of af and g. Accelerated running on flat terrain (**A**) is equivalent to constant speed uphill running (**B**) wherein the angle of the terrain T with the horizontal H (90 - α) is such that to the angle of the subject's body with the terrain (α) over ground and on slope are the same. Adapted from Osgnach et al. 2010.*

The study introduced the concept of an "equivalent slope" that a runner experiences depending on their acceleration overground, defined as the slope that runners would have to use at constant speed to yield a similar energy cost. Despite

numerous simplifying assumptions, the authors evaluated oxygen consumption, metabolic cost and power during accelerated running and successfully correlated it with the metabolic cost and power of slope running (di Prampero et al. 2005).

Comparison of running with a tractive force and running on a slope

Maintaining constant accelerations over a large period of time is no easy task. Indeed, running while accelerating on a treadmill is not mechanically comparable to running while accelerating on the ground (Van Caekenberghe et al. 2013). Furthermore, in overground accelerations, the velocity of progression changes continuously, modifying the velocity of contraction of the muscles and their contractile properties (Cavagna et al. 1971). Therefore, we hypothesised that rather than continuous sprinting, running with a constant force which hindered the movements of the CoM while maintaining a constant speed would be an equivalent situation to accelerative bouts, without the downfalls that acceleration faces on treadmills.

Given that running while accelerating is metabolically equivalent to running on a slope, we decided to compare the mechanical findings of Dewolf et al. (2016) in running uphill to running against a constant force hindering the movements the CoM. Both are situations where muscles produce more positive work than the negative work that they must dissipate per step. Furthermore, we also compared running with an aiding tractive force to running downhill, where the opposite is true and more negative work must be dissipated than positive work restored per step. We hypothesised that the imbalance between positive and negative work done would modify the bouncing mechanism of running as muscles must perform/dissipate additional work over each step as they were being either hindered or pushed by the environment while maintaining constant average velocity.

The purpose of this section, 3.1, was to (1) investigate the mechanical energy-changes of the CoM throughout the step during running with increasing hindering and aiding tractive forces at different speeds; and (2) compare these changes to those observed when running on a slope. Ground reaction forces were measured on 8 subjects running on an instrumented treadmill at different speeds against tractive forces of different magnitudes equivalent to a percentage of the subject's BW.

As compared to unperturbed running, running against/with a tractive force increased/decreased positive external work by ~20-70% and decreased/increased negative work by ~40-60%, depending on speed and tractive force. The external power to maintain forward motion against a tractive force was contained by increasing the push phase and step frequency. When running with an aiding force, the external power during the brake phase was limited by increasing its duration.

Furthermore, the aerial time was increased to reduce the power required to reset the limbs each step. Our results showed that the bouncing mechanism of running against/with a hindering/aiding tractive force was equivalent to that of running on a positive/negative slope. These findings provided interesting alternative training methods which simulate the mechanical load of slope running on level ground, this could be a useful alternative for runners who do not have the opportunity to train in mountain terrain for example. This study was published in the *European Journal of Applied Physiology* (Fig. 3.0.2).

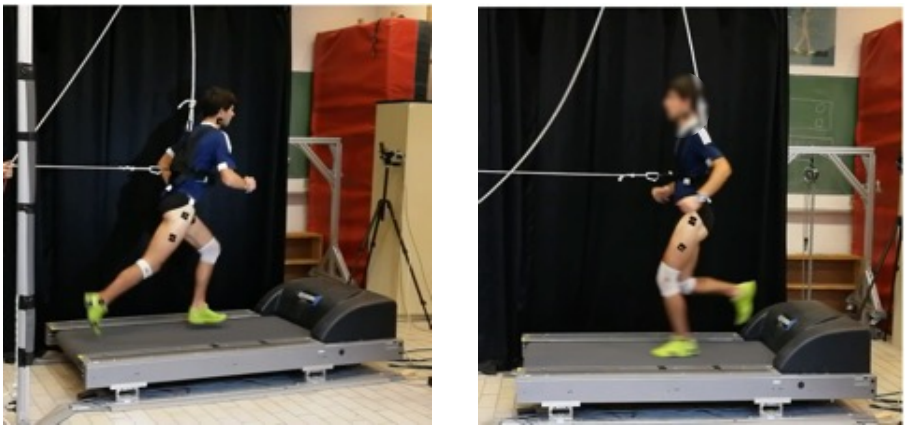

Fig. 3.0.2 *Subject running at 14 km h^{-1} on a treadmill against a hindering (left) and aiding tractive force equivalent to 15% of their body weight. The black spots are Velcro patches with retro-reflective markers glued on them to create a contrast which improved precision in the data acquisition of the 2D cameras used previously in the lab (unpublished data).*

Comparison of running in the wind and running with a tractive force

In the second scenario (3.2), air resistance - or drag - is an external force against which the MTUs do work. In laboratory settings, human locomotion encounters minimal opposition from air resistance. However, moving in nature often requires overcoming airflow. Here, the drag force exerted on the body by different headwind or tailwind speeds (between 0 &15 m s^{-1}) was measured during walking at 1.5 m s^{-1} and running at 4 m s^{-1}. To our knowledge, the biomechanical effect of drag in human locomotion had only been evaluated by simulations (Hill 1928; Polidori et al. 2020; Schickhofer and Hanson 2021; Beaumont et al. 2021).

Data were collected on eight male subjects using an instrumented treadmill placed in a wind tunnel. From the ground reaction forces, the drag and external work done to overcome wind resistance and to sustain the motion of the centre of mass of the body were measured. Drag increased with wind speed: a 15 m s^{-1} headwind exerted a drag of ~60 N in walking and ~50 N in running. The same tailwind exerted

-55 N of drag in both gaits. At this wind speed, the work done to overcome the airflow represented ~80% of the external work in walking and ~50% in running. Furthermore, in the presence of fast wind speeds, subjects altered their drag area (C_dA) by adapting their posture to limit the increase in air friction.

Moving in the wind modified the ratio between positive and negative external work performed. The modifications observed when moving with a head- or tailwind have been compared with moving uphill or downhill and tractive running. The present findings may have implications for optimising aerodynamic performance in competitive running, whether in sprints or marathons. This paper was published in the *Journal of Applied Physiology* (Fig. 3.0.3).

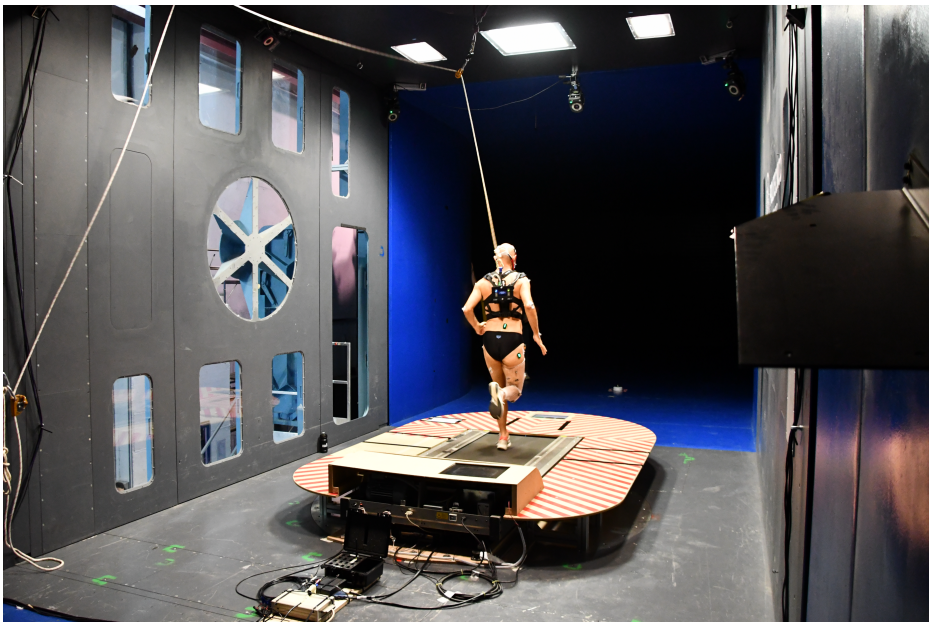

Fig. 3.0.3 *Subject running on a treadmill in the wind tunnel (with no wind) in the Politecnico University of Milan. The wooden structure which surrounded, but did not touch, the treadmill assured that the subject would encounter laminar (un-turbulent) airflow during their trial. The subject is equipped with markers, EMGs on the right limb and a K5 – metabolic system. Note, the treadmill motor is also covered, providing shielding for the EMG base (black box on the floor) which needed to be in the same room as the subject for optimal recording.*

3.1 The bouncing mechanism of running against hindering, or with aiding traction forces - A comparison with running on a slope

Raphael. M. Mesquita, Arthur. H. Dewolf, Giovanna Catavitello, Cristian Osgnach, Pietro E. di Prampero, Patrick. A. Willems

European Journal of Applied Physiology (2020) 120(7), 1575-1589.

Keywords: Body centre of mass, Locomotion, External work, Pulling force, Propulsive and Braking force

List of Abbreviations

$\boldsymbol{a_l, a_f, a_v}$	lateral, fore-aft and vertical accelerations of the *CoM*
$\boldsymbol{\bar{a}_{v,ce}, \bar{a}_{v,ae}}$	average vertical acceleration of the CoM during the t_{ce} and t_{ae}
ATF, HTF	aiding traction force, hindering traction force
BW	body weight
$BW_{//}$	component of the body weight vector parallel to the slope of the terrain
CoM	centre of mass of the body
$E_{com} = E_{kf} + E_v$	mechanical energy of the CoM due to its movements relative to the surroundings
$\boldsymbol{E_{kf}}$	kinetic energy of the CoM due to its fore-aft velocity
E_v	mechanical energy of the CoM due to its vertical movements
f_s	natural frequency of the body bouncing system
$\boldsymbol{\bar{F}_{brake}, \bar{F}_{push}}$	average forces during the negative (brake) and positive (push) work phases
F_f	resultant of the fore-aft forces applied on the body
F_{tr}	horizontal component of the traction force
F_l, F_h, F_v	lateral, horizontal and vertical components of the *GRF*
$\boldsymbol{\bar{F}_h}$	average of F_h over a stride
$\boldsymbol{\bar{F}_v}$	average of F_v over a stride
g	acceleration of gravity
GRF	ground reaction force
k	stiffness of the elastic structures responsible for the rebound
m	body mass

$\overline{\boldsymbol{P}}_{\mathrm{f}}$	average power spent to maintain the fore-aft movements of the CoM
$\overline{\boldsymbol{P}}_{\boldsymbol{s}}$	average power spent on a slope
$\overline{\boldsymbol{P}}_{\mathrm{tr}}$	average power spent to overcome the traction force
$\overline{\boldsymbol{P}}_{\mathrm{v}}$	average power spent to maintain the vertical movements of the CoM
%R	percentage of energy transduction between E_{v} and W_{f}
$\boldsymbol{s}_{\mathbf{v}}$	vertical displacement of the CoM
T	step period
t_{ae}, t_{ce}	effective aerial time and effective contact time, i.e. respectively the period during which $F_{\mathrm{v}} < BW$, and $F_{\mathrm{v}} > BW$
t_{a}, t_{c}	aerial time and contact time
t_{push}, t_{brake}	duration of W_{ext}^{+} and W_{ext}^{-}
Unperturbed running	Running on the level at a constant average speed, without a traction force
$\boldsymbol{v}_{\mathbf{belt}}$	speed of the treadmill belt
$\boldsymbol{V}_{\mathbf{belt}}$	average speed of the treadmill belt over a stride
$\boldsymbol{v}_{\mathbf{l}}$, $\boldsymbol{v}_{\mathbf{f}}$, $\boldsymbol{v}_{\mathbf{v}}$	lateral, fore-aft and vertical components of the velocity of the CoM
$\overline{\boldsymbol{v}}_{\mathrm{f}}$	average of v_{f} over a stride
$\overline{\boldsymbol{v}}_{\mathrm{v}}$	average of v_{v} over a stride
$\boldsymbol{W}_{\mathbf{ext}}$	external work, *i.e.* the work done to sustain the movements of the CoM relative to the surroundings plus the work done on/by the traction force
$\boldsymbol{W}_{\mathbf{ext}}^{+}$, $\boldsymbol{W}_{\mathbf{ext}}^{-}$	positive and negative work phases of W_{ext}

$\dot{\boldsymbol{W}}_{\text{ext}}$	external power, *i.e.* the time-derivative of W_{ext}
$\dot{\boldsymbol{W}}_{\text{int}}$	internal power, *i.e.* the power necessary to move the limbs relative to CoM
$\boldsymbol{W}_{\mathbf{f}}$	work done at each instant to sustain the fore-aft movements of the CoM plus the work to overcome the traction force
$\boldsymbol{W}_{\mathbf{f}}^{+}, \boldsymbol{W}_{\mathbf{f}}^{-}$	positive and negative work phases of W_{f}
$\boldsymbol{W}_{\mathbf{v}}^{+}, \boldsymbol{W}_{\mathbf{v}}^{-}$	positive and negative work done to sustain the vertical movements CoM relative to the surroundings
$\boldsymbol{W}_{\mathbf{tr}}$	external work done on/by the traction force

Introduction

When running on the level on firm ground, since the foot is not skidding and wind resistance is negligible, muscles perform as much positive as negative external work to move the body relative to the environment (Cavagna et al. 1976). In this situation, the movement of the centre of mass of the body (CoM) can be compared to a mass mounted on a spring, bouncing on the ground (Cavagna et al. 1988). When running uphill or downhill, positive and negative muscular work done are not anymore equal (Minetti et al. 1994) since gravitational potential energy of the CoM must be increased/decreased each step due to slope. This unbalance between positive and negative external work modifies the bouncing mechanism of running (Dewolf et al. 2016).

As running on a slope, running at a constant speed with a horizontal traction force which either hinders or aids the forward motion of the subject will also disturb the ratio of positive and negative work done. This unbalance will most likely also modify the bouncing mechanism of running. Indeed, in this case, muscles must perform/dissipate additional work each step to maintain the average kinetic energy of the CoM constant.

To the best of our knowledge, no studies have examined the bouncing mechanism while running either with or against a horizontal force. The purpose of this study is to analyse the changes in the bouncing mechanism of running brought about by an aiding/hindering horizontal force. Therefore, we used a subject pulling system (SPS) that generates a horizontal aiding (ATF) or hindering (HTF) force of 5-15% of body weight (*BW*). We expect the four following characteristics of the bouncing mechanism to be affected by the horizontal force.

First, when running with a HTF/ATF, the CoM tends to decelerate/accelerate during the step and muscles must produce/dissipate energy to keep the average speed of progression constant. We hypothesise that on one hand, the unbalance between positive and negative work done to sustain the motion of the CoM (W_{ext}^{+} and W_{ext}^{-}) will, to a certain extent, jeopardise the bouncing mechanism of running. On the other hand, we hypothesise that, when running against a HTF, the reduction of the negative work will restrain the increase in positive external work due to traction. The contrary will be true during running with an ATF: a reduction of the positive work will limit the increase in the negative work due to traction. In other words, the amount of energy that can be stored and released in the elastic structures of the lower-limb will be reduced when the traction increases either forwards or backwards.

Second, during running, the vertical movements of the CoM can be compared to a mass mounted on a spring that bounces on the ground. From a mechanical point of view, this spring-mass system oscillates around an equilibrium point at which the vertical component of the GRF (F_v) is equal to body weight (BW) (Cavagna et al. 1988). The natural frequency of the bouncing system (f_s) depends on the body mass (m) and the stiffness of the elastic structures responsible for the rebound (k): $f_s = \frac{1}{2\pi}\sqrt{\frac{k}{m}}$. At all running speeds, the period t_{ce} represents the duration of half the period of the oscillation of the bouncing system, i.e. $t_{ce} = \pi\sqrt{\frac{m}{k}}$. The period t_{ae} represents the other half of the oscillation of the bouncing system only if the aerial phase is nil. Indeed, if the body leaves the ground, the elastic model is no longer valid because the restoring force is no longer proportional to the displacement (since the vertical acceleration is constant).

When running on the level, the vertical momentum lost and gained during t_{ce} must equal the vertical momentum lost and gained during t_{ae}. Consequently,

$$\bar{a}_{v,ce}\, t_{ce} = \bar{a}_{v,ae}\, t_{ae}\ , \qquad (1)$$

where $\bar{a}_{v,ce}$ and $\bar{a}_{v,ae}$ are the average vertical accelerations during t_{ce} and t_{ae}, respectively. At slow speeds, $\bar{a}_{v,ce} = \bar{a}_{v,ae}$ and the rebound is symmetric i.e. $t_{ce} \approx t_{ae}$ (called the *on-off ground symmetry*, (Cavagna 2009)). At speeds around 3-3.5m s^{-1}, $\bar{a}_{v,ce}$ becomes greater than 1g; whereas $\bar{a}_{v,ae}$ cannot exceed 1g. Consequently, $t_{ae} > t_{ce}$ and the step becomes asymmetric (Cavagna et al, 1988, Schepens et al. 1998). For a given t_{ce}, an *on-off ground symmetry* requires a smaller $\bar{a}_{v,ce}$, which in turn reduces the external power ($\dot{W}_{ext}$) to move the CoM relative to the environment (Cavagna et al. 1991), whereas an *on-off ground asymmetry* requires a greater $\bar{a}_{v,ce}$; however, due to a longer t_{ae}, the step period is increased and results in a smaller internal power ($\dot{W}_{int}$) necessary to reset the limbs at each step (Cavagna et al. 1988).

As compared to *unperturbed running*, running with/against a traction force requires additional external positive/negative power to overcome the traction force. We hypothesise that this situation will be similar to running on a positive/negative slope. Therefore, to limit the increase in $\dot{W}_{ext}$, we expect that, when running against a HTF, the step will remain symmetric above 3-3.5 m s^{-1} (Dewolf et al. 2016). In contrast, when running with an ATF, we expect - because maximal muscle forces are greater during eccentric than concentric contractions - that t_{ae} becomes greater than t_{ce} at speeds lower than 3-3.5 m s^{-1}. In other words, we hypothesise that with an ATF the *on-off ground* asymmetry appears at lower speeds. In this way, the time to reset

the limbs is increased and therefore the $\dot{W}_{\mathrm{int}}$ during the swing phase - rather than the $\dot{W}_{\mathrm{ext}}$ - is limited as compared to *unperturbed running* (Cavagna 2009).

Third, if an unbalance between W_{ext}^{+} and W_{ext}^{-} is present, we expect that the duration of the negative (brake) and positive (push) work phases (respectively t_{brake} and t_{push}) will be modified, as compared to *unperturbed* running. While the spring-mass system assumes the same characteristics of the spring during the storage and release of energy, *i.e.* a ratio $t_{\mathrm{brake}}/t_{\mathrm{push}}$ equal to 1, an asymmetry between the braking and pushing time reflects a deviation from the elastic behaviour of the spring-mass model (Cavagna 2006; Maykranz and Seyfarth 2014; Dewolf and Willems 2017b, 2019b). When a traction force hinders the forward movement of the CoM, we hypothesise that the duration of t_{brake} will be shortened while that of t_{push} will be lengthened to contain the increase in $\dot{W}_{\mathrm{ext}}^{+}$. In this case, the ratio $t_{\mathrm{brake}}/t_{\mathrm{push}}$ would tend towards zero when the running speed and the traction force increase. In contrast, when the subject is being aided in his movement, the duration of t_{push} will be shortened and t_{brake} lengthened to contain the increase in $\dot{W}_{\mathrm{ext}}^{-}$. In this case, the ratio $t_{\mathrm{brake}}/t_{\mathrm{push}}$ would become greater than 1 when the running speed and the traction force increase.

Fourth, without traction, the energy fluctuations of the CoM due to its fore-aft movements (E_{kf}) and those due to its vertical movements (E_{v}) are in phase (Cavagna et al. 1976). Consequently, there is little possibility for energy transduction between the E_{kf}- and the E_{v}-curves. When running with a hindering/aiding traction force, we expect that the moment at which E_{v} is minimal will occur around mid-stance, as in *unperturbed* running. However, the moment at which E_{kf} is minimal will change with the direction and the amplitude of the traction force: this minimum will shift towards touch-down with an increasing hindering force, and towards the take-off with an increasing aiding force. Consequently, an energy exchange can occur between the minimum of these two curves (Cavagna et al. 2008a), which could reduce the external work (W_{ext}), hence increasing the *%Recovery* (*%R*), as defined by Cavagna et al. (2008a) (see below and equation 11).

To test these four hypotheses, the rebound of the body was analysed on eight subjects running on a treadmill at different speeds with backward/forward traction forces of different magnitudes. Then, the mechanism of running - where the average orientation of the GRF is tilted to counteract the hindering/aiding force - is compared to that of running on a slope - where the angle between the average GRF and the terrain is also modified (Gottschall and Kram 2005; Dewolf et al. 2016).

Materials & Methods

Subjects and experimental procedure

Eight recreational male runners participated in the study. They were all students at the UCLouvain-Belgium (average age: 20.94 ±1.57 years). Their mass was comprised between 60 and 85 kg (mean ±SD: 72.76 ±5.57 kg) and their height between 1.7 and 1.9 m (1.81 ±0.05 m). Informed written consent was obtained. Studies followed guidelines of the Declaration of Helsinki and all procedures were accepted by the UCLouvain (B403201838331).

All subjects ran on an instrumented treadmill at five different constant speeds of: 2.22, 2.78, 3.33, 3.89 and 4.44 m s $^{-1}$ (which corresponds to 8, 10, 12, 14 and 16 km h $^{-1}$), while being pulled by a HTF/ATF. The magnitudes of the traction force were selected to be able to compare the present results with those obtained while running on a slope in Dewolf et al. (2016). When standing on a slope, the *BW* vector can be broken down into a component perpendicular and another parallel ($BW_{//}$) to the ground. Here, the magnitudes of traction force represented 0%, 5%, 10% and 15% of *BW*, which corresponded to $BW_{//}$, i.e. to the sine of the studied slopes (0, 3, 6 and 9°). To remove the effect of learning and of fatigue, the magnitude of the traction was selected in a different order for each subject; then for each traction, the speeds were selected randomly.

Experimental setup

Experiments were conducted on a commercial treadmill (h/p/Cosmos, Germany) with a belt surface of 1.6 x 0.65 m. The entire treadmill was mounted onto four strain-gage force transducers (Arsalis, Belgium). Because the whole body of the treadmill (including the motor) was mounted on the transducers, these were measuring the three components of the *GRF* exerted by the treadmill under the foot (Willems and Gosseye 2013). The signal was amplified, low-pass filtered (4-pole Bessel filter with a -3dB cut-off frequency at 200 Hz).

The electrical motor of the belt was instrumented with an optical angle encoder to measure the speed of the belt (v_{belt}). The average speed of the belt over a stride (V_{belt}) differed by 2.8 ±1.4% from the chosen speed and the instantaneous v_{belt} did not change by more than 5% of V_{belt}.

The traction system was similar to the ones proposed by Lloyd and Zacks (1972) and by Asmussen and Bonde-Petersen (1974) . The horizontal traction force was generated by a weight attached to a harness *via* an elastic rope and a pulley. The point

of application of the rope on the harness was located at ~60 % of the subject's height from the ground (*i.e.* close to the centre of gravity of the projected area of the body on the coronal plane). The pulley was mounted on a force transducer that measured the traction force (F_{tr}). In order to keep the rope horizontal despite the vertical movements of the runner, the pulley was placed at the level of the fixation point on the harness, three meters behind/in front of the subject. In this way, the angle between the rope and the horizontal varied by less than ± 2°. Therefore, the change in this angle was not taken into account. Due to friction and inertia, F_{tr} varied within ± 0.5% *BW* during a step.

The lateral (F_l), fore-aft (F_h) and vertical (F_v) components of *GRF* and the traction force (F_{tr}) were digitized by a 16-bit analogue-to-digital converter at a sampling frequency of 1 kHz. Acquisition and data processing were performed *via* custom made programs using LABVIEW (National Instruments 2014, Austin, Texas, USA).

Data analysis

All trials analysed began with a right step. Strides were divided according to the beginning of t_{ce}, *i.e.* when F_v becomes greater than *BW* (Dewolf et al. 2016). Foot contact was determined at a threshold of F_v > 10N. During trials, between 4 and 32 steps were analysed per condition and for all subjects a total of 6324 steps were analysed (Padulo et al. 2014).

Acceleration, Velocity and Vertical displacement of the CoM

Calculations for the acceleration, velocity and displacement of the CoM were done as seen in (Padulo et al. 2014). Therefore, this method is only explained in brief. Since air friction was negligible, the three forces applied to the body were the body weight (*BW*), the *GRF* and the traction force (F_{tr}). Acceleration in the lateral (a_l), fore-aft (a_f) and vertical (a_v) directions was obtained by:

$$a_l = \frac{F_l}{m}, \tag{2}$$

$$a_f = \frac{F_f}{m} = \frac{F_h + F_{tr}}{m}, \tag{3}$$

$$a_v = \frac{F_v - \overline{F_v}}{m}, \tag{4}$$

where m is the body mass, F_f is the resultant force of F_h and F_{tr}, $\overline{F_v}$ is the average vertical force over a stride. When running on a flat terrain, $\overline{F_v} \approx BW$; if $\overline{F_v}$ varied from *BW* by more 5%, the stride was not analysed.

Accelerations were time-integrated by the trapezoidal method to determine the variations of vertical (v_v), fore-aft (v_f) and lateral (v_l) velocities of the CoM plus an integration constant. In the fore-aft direction, since the subject was running at an average constant speed, the integration constant was considered to be equal to the average speed of the belt over a stride (V_{belt}). In the lateral and vertical direction, the integration constants of v_l and v_v were equal to zero, on the assumption that the CoM returns to its initial lateral position and height at the end of each stride. The vertical displacement of the CoM (s_v) was then computed by time integration of v_v. A typical trace of F_v, F_h & F_{tr} and of v_v & v_f is presented in Fig. 2.3.1.

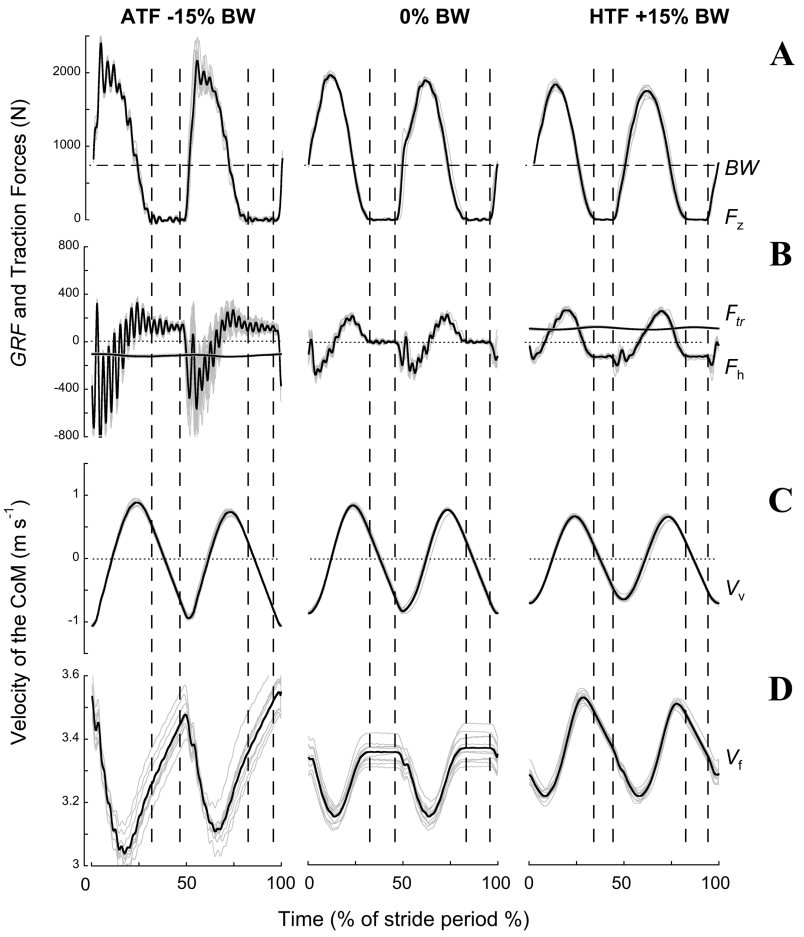

Fig. 2.3.1 *Time-traces of (**A**) the vertical (F_v) and (**B**) fore-aft (F_h) components of ground reaction force and of (**C**) the vertical (V_v) and (**D**) fore-aft (V_f) components of the velocity of the CoM. The black lines are obtained by averaging all the consecutive steps (light grey lines) of a subject (mass: 77.8 kg, height: 1.85 m) running at 3.3 m s^{-1} with no traction force (0% BW), with an ATF (-15% BW) or an HTF (+15% BW). The time is expressed as a percentage of the stride period (T, which equals 0.751 s at 0% BW, 0.739 s at -15% BW and 0.665 s at +15% BW). These traces were cut according to the beginning of t_{ce} and filtered by an 8^{th} order Bessel filter with a cut-off frequency of 25Hz. The vertical striped lines represent the aerial phase in each step. In panel **A**, the horizontal dotted line indicates the body weight, BW. In panel **B**, F_{tr} is the traction force. Note that when running with a HTF/ATF, the fore-aft velocity of the CoM decreases/increases during the aerial phase since the traction force is pulling the runner backwards/forwards.*

Energy of the CoM, external work and %Recovery

The energy of the CoM in respect to the environment (E_{com}, Fig. 2.3.2) was calculated as the algebraic sum of the energy due to the vertical movements, E_{v}, and that due to the fore-aft movements, E_{kf} (Schepens et al. 1998):

$$E_{\mathrm{com}} = E_{\mathrm{v}} + E_{\mathrm{kf}}, \tag{5}$$

where

$$E_{\mathrm{v}} = m\ g\ s_{\mathrm{v}} + \frac{1}{2} m\ v_{\mathrm{v}}^2, \tag{6}$$

$$E_{\mathrm{kf}} = \frac{1}{2}\ m\ v_{\mathrm{f}}^2. \tag{7}$$

The energy due to the lateral movement of the CoM was neglected (Cavagna et al. 1963). Since the work done by the foot on the belt accounted for less than 3% of E_{com}it was not considered in this study.

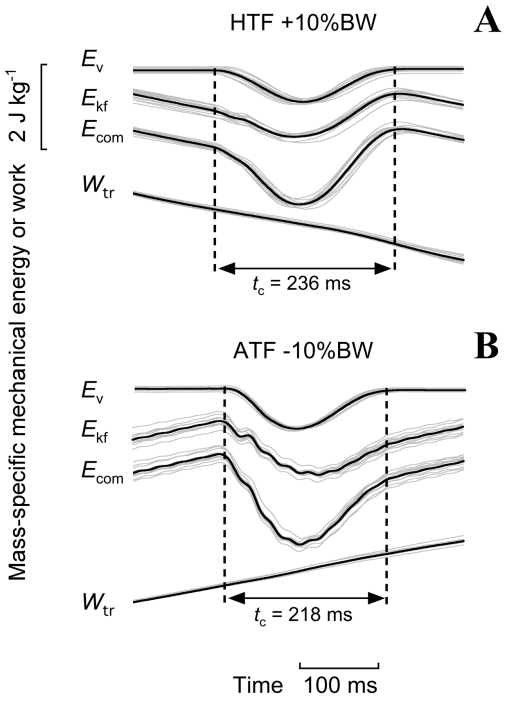

Fig. 2.3.2 *Typical traces of the mass-specific mechanical energy or work while running at 3.9 m s^{-1} against a HTF (**A**) and with an ATF (**B**). From top to bottom, curves represent the energy of the CoM due to its vertical movements (E_v) and to its fore-aft movements (E_{kf}). The curve E_{com} represents the total energy of the CoM ($E_{com} = E_v + E_{kf}$) and W_{tr} is the work done by/against the traction force. The vertical dotted lines delimit the contact phase. Same subject than in Fig. 2.3.1. Other indications as in Fig. 2.3.1.*

Along the fore-aft axis, even when running without any traction force (*unperturbed running*), the interaction of the foot with the ground induces a deceleration of the CoM during the first part of the contact phase, which requires to reaccelerate the CoM during the second part of the contact. When running with a HTF/ATF, work must be done during the contact phase not only to sustain the kinetic energy changes of the CoM but also to counteract the traction force. The work done on/by the traction force (Fig. 2.3.2) was calculated as:

$$W_{\mathrm{tr}} = \int F_{\mathrm{tr}}\ v_{\mathrm{belt}}\,\mathrm{d}t\ , \tag{8}$$

and the work done at each instant to sustain the movements of the CoM in the fore-aft direction (W_{f}) as the sum of the E_{kf} and the W_{tr} curves:

$$W_{\mathrm{f}} = E_{\mathrm{kf}} + W_{\mathrm{tr}}\ . \tag{9}$$

In turn, the work done by the forces applied externally to the body (W_{ext}) was computed as the algebraic sum of the E_{v} and the W_{f} curves:

$$W_{\mathrm{ext}} = E_{\mathrm{v}} + W_{\mathrm{f}}\ . \tag{10}$$

Positive (W_{f}^{+}, W_{v}^{+} and W_{ext}^{+}) and negative (W_{f}^{-}, W_{v}^{-} and W_{ext}^{-}) works were computed by summing the increments and the absolute value of the decrements of the W_{f}, E_{v} and W_{ext} curves, respectively. Energy transduction between E_{v} and W_{f} was assessed as *%R* (Cavagna et al. 2008a):

$$\%R = \frac{W_{\mathrm{f}}^{+}+|W_{\mathrm{f}}^{-}|+W_{\mathrm{v}}^{+}+|W_{\mathrm{v}}^{-}|-(W_{\mathrm{ext}}^{+}+W_{\mathrm{ext}}^{-})}{W_{\mathrm{f}}^{+}+|W_{\mathrm{f}}^{-}|+W_{\mathrm{v}}^{+}+|W_{\mathrm{v}}^{-}|}\ . \tag{11}$$

Statistics

All of the step data from one condition were averaged per subject to obtain the grand average and grand standard deviation which was then grouped into traction and speed classes. In order to analyse the effect speed and traction on their interaction, a two-way ANOVA with Bonferroni *post-hoc* correction was used (PASW Statistics, 19, SPSS, IBM, Armonk, NY, USA).

We estimated the minimal numbers of strides required to minimise the type I error for the 7 traction classes (α= 0.05, 1–β= 0.8, f size = 0.25) using an a priori G*Power test (Faul et al. 2007). Each traction class should totalise at least 224 strides. When running this same test for the 5 speed classes, the number of strides analysed should be higher than 195 in the same conditions. Note that our sample size for the 7 traction classes or for the 5 speed classes is equal to 276.

Results

Positive and Negative Work Done

When running without a traction force, the E_v- and E_{kf}-time curves vary in phase and $W_{ext}^{+} \approx W_f^{+} + W_v^{+}$. Furthermore, muscles are doing as much positive as negative work and $W_v^{+} \approx W_v^{-}$, $W_f^{+} \approx W_f^{-}$ and $W_{ext}^{+} \approx W_{ext}^{-}$. When running with a traction force, W_v^{+} is still approximately equal to W_v^{-} (Fig. 2.3.3) and both decrease with increasing speed against all traction forces. At +15% *BW,* $W_v^{+/-}$ are significantly lower than during *unperturbed running* (for both W_v^{+} and W_v^{-}: *post-hoc* Bonferroni $p < 0.001$).

Contrary to W_v^{+} and W_v^{-}, both W_f^{+} and W_f^{-} increase as a function of speed at all traction forces (W_f^{-}: $F= 155.6$, $p < 0.001$; W_f^{+}: $F= 192.7$, $p < 0.001$). When running against a HTF, W_f^{-} decreases ($F= 3810.8$ $p < 0.001$) and W_f^{+} increases ($F= 3710$, $p <0.001$), as compared to *unperturbed running*. When running with an ATF, the opposite is true: W_f^{-} increases with the magnitude of F_{tr}, whereas W_f^{+} decreases (in both cases, $F= 3811$, $p <0.001$). Consequently, the gap between W_f^{-} and W_f^{+} becomes larger when the magnitude of F_{tr} augments.

The external works W_{ext}^{+} and W_{ext}^{-} decrease slightly with increasing speed (W_{ext}^{+}: F= 20.26, p <0.001; W_{ext}^{-}: F= 17.56, p <0.001). As the magnitude of the F_{tr} increases, the difference between W_{ext}^{-} and W_{ext}^{+} become larger (Fig. 2.3.3).

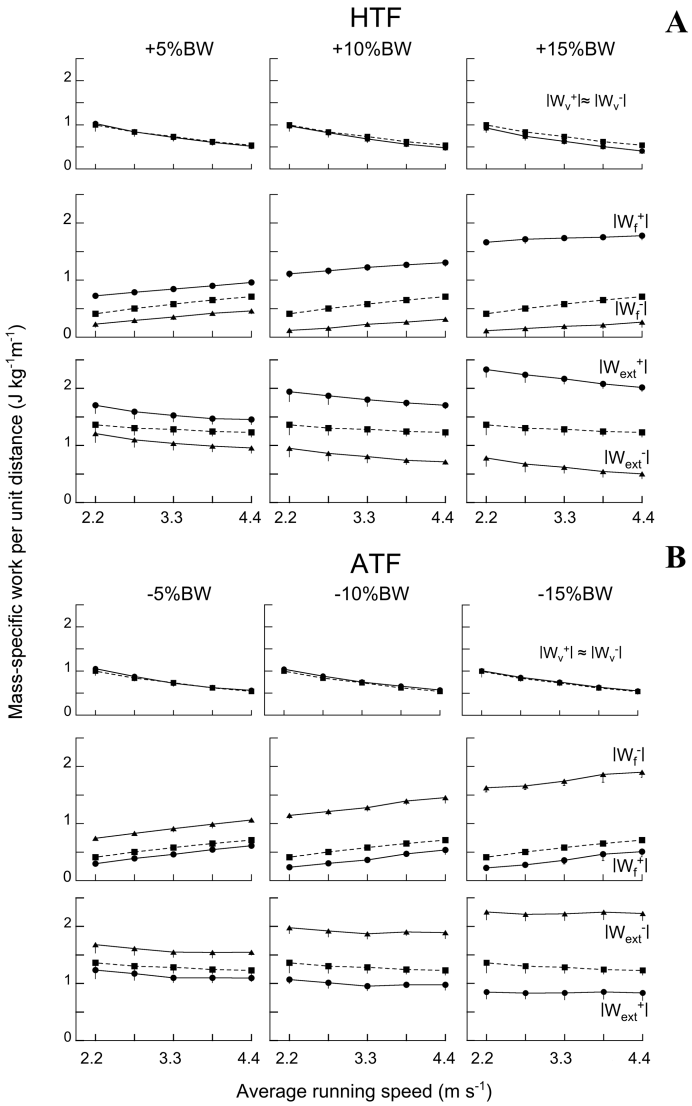

Fig. 2.3.3 *Mass-specific mechanical work per unit distance (J kg^{-1} m^{-1}). Each traction force displays positive (closed circles, superscript +) and negative (closed triangles, superscript -) mechanical work done each step as a function of speed. The striped line on each graph represents the corresponding positive and negative work on when running without an additional horizontal traction force. W_v is the work done to sustain the vertical movements of the CoM, W_f is the work done to sustain its fore-aft movements and W_{ext} is the work to maintain the movement of the CoM relative to the surroundings. Since the subject is running on the level, $|W_v^+| = |W_v^-|$. Against a HTF (**A**), there is more $|W_f^+|$ than $|W_f^-|$. Consequently, $|W_{ext}^+| > |W_{ext}^-|$. Against an ATF (**B**), more $|W_f^-|$ than $|W_f^+|$ is being done. Consequently $|W_{ext}^+| < |W_{ext}^-|$. Symbols and bars represent the grand mean of the subjects (n=8) and the standard deviations (when bars extended beyond the symbols) respectively. These data were plotted via Kaleidagraph 4.5. Note that when running unperturbed, W_{ext}^+ and W_{ext}^- are about equal at all speeds, as in Willems et al. (1995).*

Duration of the different phases of step

When running without a traction force, the step period (T) decreases with speed (Fig. 2.3.4A) and the *on-off asymmetry* (i.e. $t_{ae} > t_{ce}$) occurs at speeds above 3-3.5 m s^{-1}, as in Cavagna (2009). When running with a HTF, T decreases significantly as compared to running without traction, due to a shortening of the aerial time (t_a) ($F = 7.90$, $p < 0.001$). In contrast, when running with an ATF, T does not vary because contact time (t_c) decreases ($F = 4.01$, $p < 0.001$) whereas t_a increases ($F = 29.09$, $p < 0.001$; Fig. 2.3.4A) with the increasing traction.

When running with a traction force, as compared to *unperturbed running*, the relationship between t_{ce} and traction force is not modified ($F = 1.805$, $p > 0.05$). When the magnitude of HTF augments, t_{ae} decreases ($F = 12.48$, $p < 0.01$) and tends towards t_{ce}. At +10% & +15% BW, $t_{ce} = t_{ae}$ at all speeds. Oppositely, at any magnitude of ATF, t_{ae} does not change with speed, as compared to *unperturbed running*.

When running against a HTF, $t_{push} > t_{brake}$ at all speeds, however the difference between t_{push} and t_{brake} decreases as speed increases. When running with an $|ATF| > 5\%\ BW$ at speeds greater than ~2.2 m s^{-1}, $t_{brake} > t_{push}$ signifying that the subjects spend more time braking than accelerating the CoM forwards.

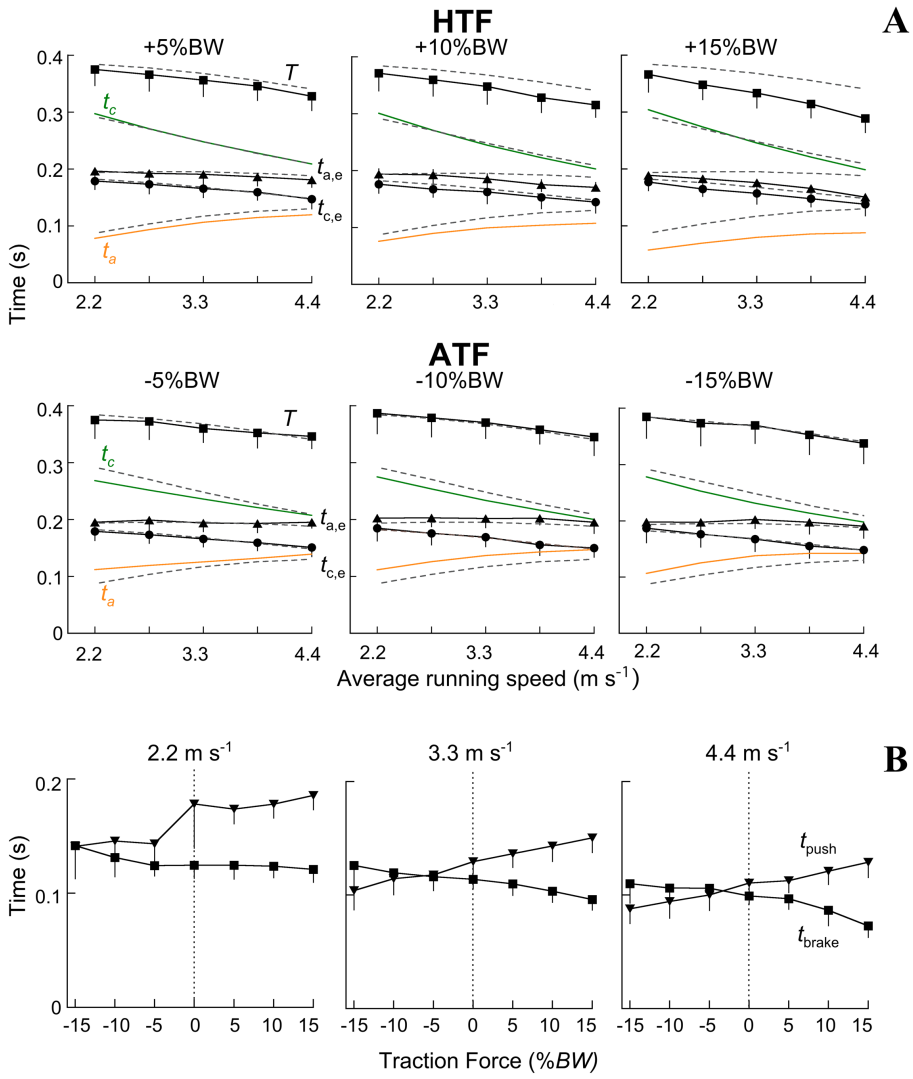

Fig. 2.3.4 (A) *Step durations as a function of speed at each traction force. Step period T (closed squares), effective aerial time t_{ae} (closed triangles) and effective contact time t_{ce} (closed circles) are shown in black. The green and orange curves are weighted mean (Kaleidagraph 4.5) of the contact t_c and aerial t_a time, respectively. The interrupted lines were fitted through the data obtained when running unperturbed.* ***(B)*** *Time required to brake (t_{brake}, closed squares) and accelerate (t_{push}, closed triangles) the CoM as a function of traction force when running at 2.2, 3.3 and 4.4 m s^{-1}. Other indications as in Fig. 2.3.3. Note that when running unperturbed, results obtained on step durations (T, t_{ce}, t_{ae}, t_c and t_a) are similar to those of Cavagna 2005.*

Energy transduction

When running without any traction force, since air friction is negligible, E_{kf} does not change during the aerial phase and the E_v- and E_{kf}-curves change in phase during contact. When running against/with a traction force, as muscles are not able to counter F_{tr} when the feet are not on the ground, E_{kf} decreases/increase during the aerial phase (Fig. 2.3.2). Therefore, during contact, muscles must compensate the loss/gain in E_{kf} and $W_f^+ > W_f^-$ (or $W_f^+ < W_f^-$); this modification causes a shift between the minimums of the E_v- and E_{kf}-curves.

Consequently, during the period in which E_v and W_f are out of phase, an exchange between these two curves might occur (Figs. 2.3.5 & 6). With an ATF, the W_f-energy lost during the grey zone in Fig. 2.3.5 & 6 can be used to increase the height of the CoM, whereas against a HTF, the E_v-energy lost during the grey zone can be used move the CoM forwards. When the applied force becomes greater, the duration between the two minima is lengthened.

The *%R* expresses the relative amount of energy that could be recovered by an exchange between E_v and W_f, and vice versa. At a given speed, *%R* increases with the magnitude of the hindering/aiding force (Fig. 2.3.6A). When running at 2.2 m s^{-1}, *%R* reaches a maximum of ~ 20% at -15% *BW* and of ~16% at +15% *BW*. When speed increases, *%R* at a given traction force is reduced. This might be explained by the fact that the period during which the energy transduction can occur is reduced when speed increases (Fig. 2.3.6B). Note also that *%R* is significantly higher at negative traction forces compared to positive traction forces.

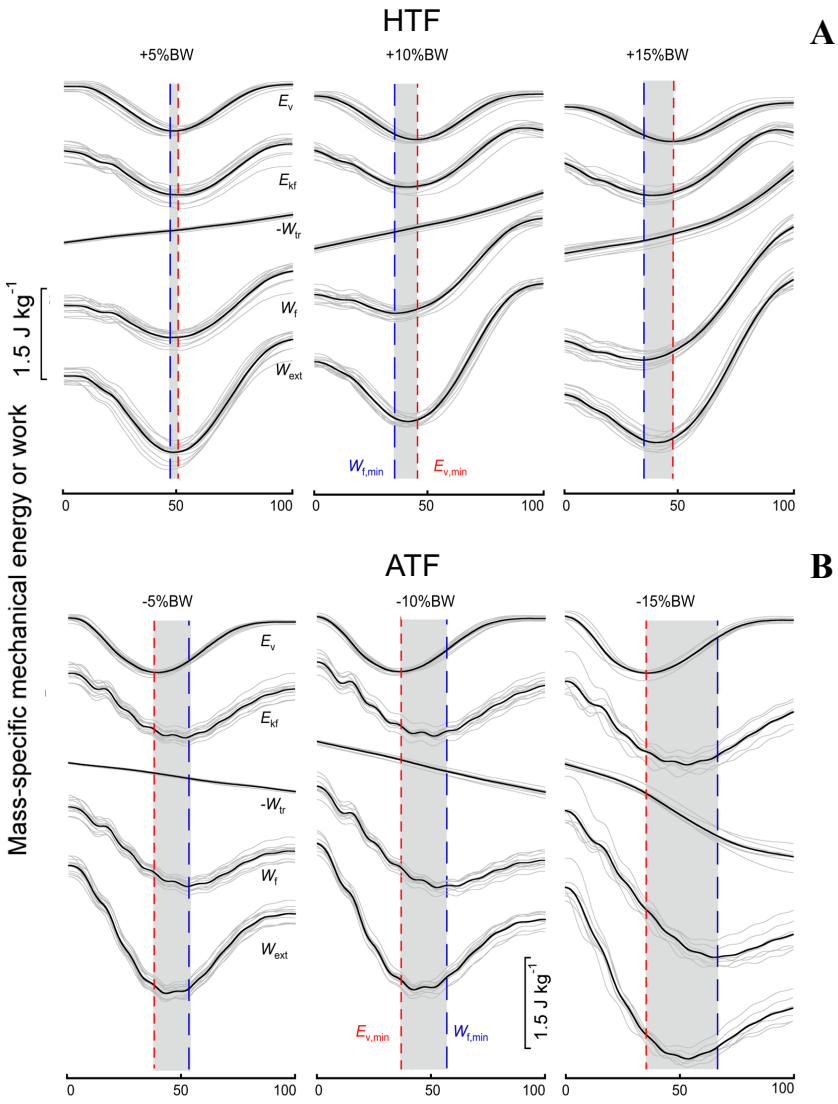

Fig. 2.3.5 *Typical time-traces of the mass-specific mechanical energy or work while running at 3.9 m s^{-1} against a HTF (**A**) and with an ATF (**B**). The upper three panels display from left to right an increasing HTF (+5%, +10%, +15% BW). The bottom three, depict an increasing ATF (-5%, -10%, -15% BW). From top to bottom, curves represent the energy of the CoM due to its vertical movements (E_v) and to its fore-aft movements (E_{kf}). The curve $-W_{tr}$ is the work done by the subject to counteract the traction force; W_f is the work done to maintain the forwards motion of the CoM and W_{ext} is work done by the muscles to maintain the movements of the CoM relative to the surroundings. The dashed dark blue and red vertical lines represent respectively the minima of W_f and E_v (respectively $W_{f,min}$ and $E_{v,min}$). Note that against a HTF, $W_{f,min}$ precedes $E_{v,min}$ whereas it follows $E_{v,min}$ with an ATF. The greyed area between the two dashed lines corresponds to the period in which energy transduction takes place. The contact period, t_c equals 0.234 s at +5% BW, 0.236 s at +10 % BW, 0.222 s at +15% BW, 0.220 s at -5% BW, 0.218 s at -10 % BW and 0.219 s at -15% BW. Other indications as in Fig. 2.3.2.*

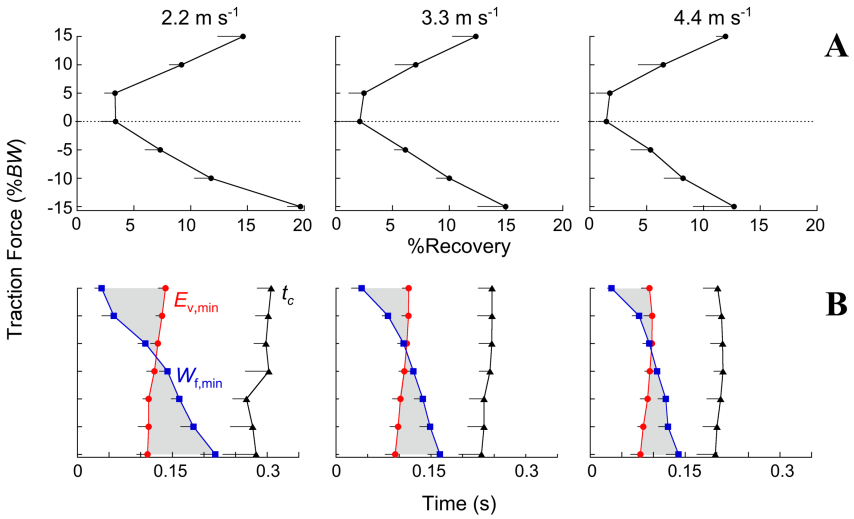

Fig. 2.3.6 *(**A**) Energy recovered through an energy exchange between W_f and E_v (%Recovery) as a function of the traction force. (**B**) The contact period t_c, and the duration between $E_{v,min}$ and $W_{f,min}$ (or vice versa) when running at 2.2, 3.3, 4.4 m s^{-1}. The grey area corresponds to the period in which an energy transduction is possible (same greyed area as in Fig. 2.3.5. Note that in this figure the independent variables are presented on the abscissa.*

Comparison of running against traction with running on a slope

In this study, we have compared the ratio W_{ext}^{-}/W_{ext}, the average vertical acceleration during t_{ce}, *i.e.* $\bar{a}_{v,ce}$ and the ratio t_{brake}/t_{push} between running with/against a traction force and running on a negative/positive slope. These last data were obtained from Dewolf et al. (2016).

As seen in Fig. 2.3.7A, the ratio W_{ext}^{-}/W_{ext} presents equivalent values in both conditions. Note that when running *unperturbed* on the level at a constant average speed, this ratio is equal to 0.5 and does not vary with increasing speed. Downhill / with an ATF this ratio increases above 0.5 and does not change with speed; on an uphill/against a HTF the ratio falls below 0.5.

In all conditions, $\bar{a}_{v,ce}$ increases with running speed. As compared to unperturbed running, $\bar{a}_{v,ce}$ while running with an ATF or on a negative slope increases when the magnitude of the traction force/slope increases (Fig. 2.3.7B). On the contrary when running with a HTF or on a positive slope, $\bar{a}_{v,ce}$ decreases when the magnitude of the traction force/slope increases.

When the traction is hindering the forward motion of the runner, the t_{brake}/t_{push} ratio decreases similarly when the magnitude of the traction and the slope increases (Fig. 2.3.7C). With an ATF or during downhill running, t_{brake}/t_{push} increases with the magnitude of the traction/slope.

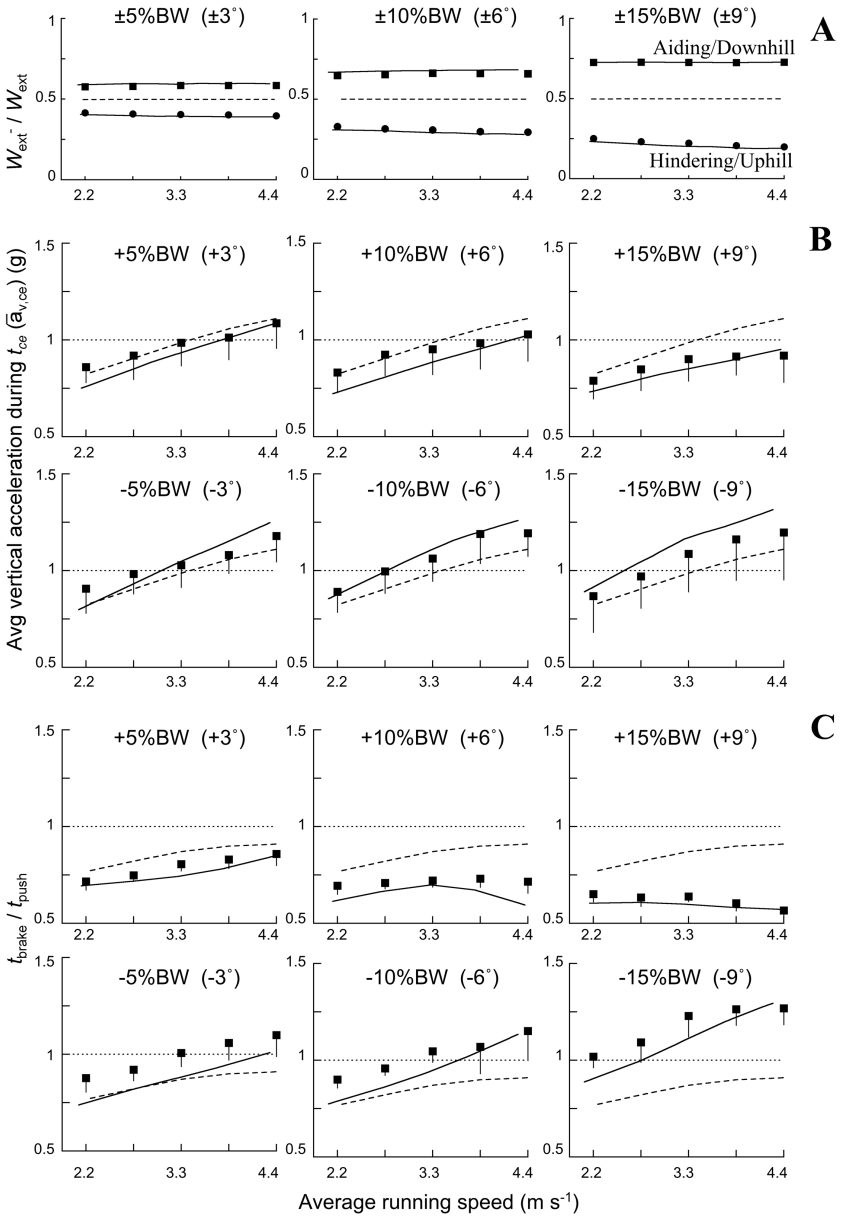

Fig. 2.3.7 *Comparisons between data obtained while running unperturbed (dashed lines), on the level against/with a traction force (filled symbols) and on a positive/negative slope (continuous lines). Data on a slope are from Dewolf et al. (2016).* ***(A)*** *Ratio W_{ext}^{-}/W_{ext} when running with an ATF (filled squares) and against a HTF (filled circles).* ***(B)*** *Average vertical acceleration of the CoM during t_{ce} ($\bar{a}_{v,ce}$). When $\bar{a}_{v,ce}$ goes beyond 1g, step becomes asymmetric (i.e. $t_{ce} < t_{ae}$).* ***(C)*** *Ratio between t_{brake} and t_{push}. If t_{brake}/t_{push} increases above 1, more time is spent braking than accelerating the movement of the CoM. Other indications as in Fig. 2.3.4.*

Discussion

The mechanism of running on a firm and flat terrain can be compared to a mass mounted on a spring that bounces on the ground. This mechanism is modified in the presence of external factors such as for example, the slope (Dewolf et al. 2016) or the nature of the terrain (Lejeune et al. 1998; Ferris et al. 1998; Dewolf and Willems 2019c). In the present study, we have analysed how a horizontal traction force applied to the trunk of the runner affects the bouncing mechanism of running. Our results show that a horizontal traction force modifies the unbalance between positive and negative work done to sustain the motion of the CoM, the *on-off ground asymmetry*, the ratio t_{brake}/t_{push} and the phase shift between the E_v- and E_{kf}-curves. We also showed that, as in walking (Dewolf et al. 2020b), some similarities exist between running with/against a traction force and running uphill and downhill.

In the first section of the discussion, we will examine how these variables affect the bounce of the spring-mass system during running with a traction force. We will show that these modifications are tuned to limit the increase in the positive or negative muscular power. In a second section, these modifications will be compared to the ones observed when running on a slope.

How to limit the increase in power due to the traction force?

In presence of a horizontal traction force, an imbalance between W_f^+ and W_f^- increases gradually as force increases; whereas W_v^+ and W_v^- remain about equal to the values observed when running without a traction force (Fig. 2.3.3). When running against a HTF, the imbalance between W_f^- and W_f^+ is tipped towards W_f^+. The opposite is observed when running with an ATF. Therefore, the imbalance between W_{ext}^+ and W_{ext}^- is brought on by the imbalances between W_f^+ and W_f^-.

The imbalance between positive and negative work done is also accompanied by an imbalance in the duration of the work production in order to reduce the power necessary to sustain the movement of the CoM (Fig. 2.3.5). Indeed, when running against a horizontal traction force, the duration of W_f^+ is lengthened and that of W_f^- is shortened. The contrary is observed when running with ATF: the duration of W_f^- is lengthened and that of W_f^+ is shortened. However, in both situations, the durations of W_v^+ and W_v^- are less affected by the traction.

The changes in the duration of W_f^+ and of W_f^- without changes in the durations of W_v^+ and W_v^- will have two consequences on the positive and negative muscular power ($\dot{W}_{ext}^+$ and $\dot{W}_{ext}^-$). First, the duration of t_{push} with a HTF and of t_{brake} with an ATF

will be increased (Fig. 2.3.4B) as compared to *unperturbed* running, with the consequence that the increase in $\dot{W}_{ext}^{+}$ with a HTF and of $\dot{W}_{ext}^{-}$ with an ATF will be contained. Second, since the W_f- and E_v-curves are no longer in phase and energy exchange between these two curves will occur (Fig. 2.3.6). However, this energy transduction mechanism saves at best 20% of W_{ext}.

As compared to *unperturbed* running, t_{ce} is not affected by a HTF, whereas t_{ae} decreases when the HTF increases. This reduction of t_{ae} is due, at least in part, to a reduction of t_a, which occurs for the following reason. When running *unperturbed*, the fore-aft velocity of the CoM (v_f) remains constant during t_a. On the contrary, when running against a HTF, the traction reduces v_f during t_a. Consequently, the longer the aerial phase, the greater the work required to reaccelerate the CoM (W_f^+) during contact. In other words, a short t_a reduces W_f^+. Since at a given speed, t_{ce} does not change and t_{ae} becomes shorter, the step period T is reduced. Consequently, (1) the step remains symmetrical (i.e. $t_{ce} \approx t_{ae}$) at higher speeds than in *unperturbed* running (Fig. 2.3.4) and (2) the step frequency at a given speed is increased, which reduces the $\dot{W}_{ext}$ (Cavagna et al. 1991).

As compared to unperturbed running, both t_{ce} and t_{ae} (and thus T) are not affected by an ATF (Fig. 2.3.4) and the *on-off ground symmetry* is not modified. On the contrary, t_a increases whereas t_c is reduced. These results are in agreement with those observed during 'unweighted running' (He et al. 1991; Chang et al. 2001). Furthermore as compared to unperturbed running, $\bar{a}_{v,ce}$ increases with an ATF (Fig. 2.3.7B); this is made possible by increased eccentric muscular contractions during landing.

Is running against traction similar to running on a slope?

In 2005, di Prampero et al. (2005) hypothesised that if a subject is running at constant speed on an incline, the angle between the runner and the slope is equivalent to the angle formed by a runner tilting forwards while accelerating constantly on the level. If we were to replace this acceleration by a constant force pulling the subject backwards while running at a constant speed on the level, the subject should consequently tilt forwards in a similar way (Fig. 2.3.8).

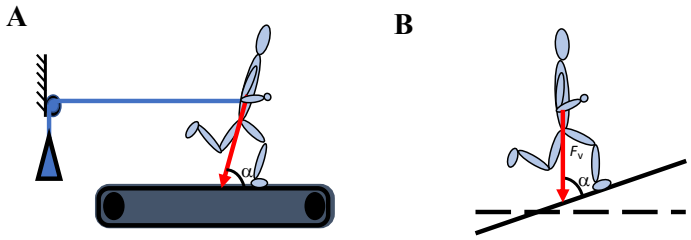

Fig. 2.3.8 *Schema illustrating that the angle between a subject and level ground when running against a traction force (**A**) is equivalent to the angle between the subject and the slope when running uphill (**B**). Modified from di Prampero et al. (2005).*

When running at constant speed on a slope, the average fore-aft component of the *GRF* over a step ($\bar{F}_h$) is nil and its average vertical component ($\bar{F}_v$) is equal to BW. In addition, the average fore-aft component of the velocity of the CoM $\bar{v}_f = v_{belt} \cos\theta$, where θ is the slope of the terrain and $\bar{v}_v = v_{belt} \sin\theta$. Consequently, the average power ($\bar{P}_s$) spent on a slope to maintain the fore-aft ($\bar{P}_f$) and vertical ($\bar{P}_v$) movement of the CoM is given by:

$$\bar{P}_s = \bar{P}_f + \bar{P}_v = \bar{F}_h\,\bar{v}_f + \bar{F}_v\,\bar{v}_v = 0 + BW\,\bar{v}_f\,\tan\theta \qquad (12)$$

When running at constant speed with a traction force, $\bar{F}_h$ is equal to the average traction force ($\bar{F}_{tr}$, expressed as a percentage p of BW) and $\bar{F}_v = BW$. The $\bar{v}_f$ represents the average horizontal speed of progression whereas $\bar{v}_v = 0$ since the subject is running on the level. Consequently, the average power ($\bar{P}_{tr}$) spent to run against/with a traction force is given by:

$$\bar{P}_{tr} = \bar{P}_f + \bar{P}_v = \bar{F}_h\,\bar{v}_f + \bar{F}_v\,\bar{v}_v = p\,BW\,\bar{v}_f + 0 \qquad (13)$$

Since tan (3°)≈ 0.05, tan (6°)≈ 0.10 and tan (9°)≈ 0.15, the average power spent on a ±3°, ±6° and ±9° slope are roughly equivalent to the power spent with a traction force of ±5%BW, ±10%BW, ±15%BW, respectively.

As compared to running *unperturbed*, in one case, net $\dot{W}_{ext}$ must be performed to change the potential energy to the CoM whereas in the other case, net $\dot{W}_{ext}$ must be performed to maintain the fore-aft movement of the CoM. It should be noted that W^+_{ext} and W^-_{ext} present equivalent values in the present study as those observed by Dewolf et al. (2016) when running on a slope. Therefore, as predicted by equation (12) and (13), the variations brought on vertically by the slope ($W_{v,slope}$) are similar to those brought on horizontally by a traction force ($W_{f,tr}$). As seen in Fig. 2.3.7A, the ratio between W^-_{ext}/W_{ext} describes this similarity. Note that when running on the level *unperturbed* this ratio is equal to 0.5 and does not vary with increasing speed.

Downhill/with an ATF this ratio increases above 0.5 and does not change with speed; on an uphill/against a HTF the ratio falls below 0.5.

When running with a HTF, $\bar{a}_{v,ce}$ decreases when the magnitude of the traction force increases. A comparable behaviour is observed when running uphill (Dewolf et al. 2016): the *on-off ground symmetry* is maintained at higher speeds to limit the increase in required force production and so the $\dot{W}_{ext}$. Similarly, as compared to young runners, elderly adults running present an $\bar{a}_{v,ce}$ that is 40% lower (Cavagna et al. 2008a), which can be attributed to a loss of muscular strength with age.

Furthermore, the ratio between concentric and eccentric muscular contractions are similar when running with a traction force and on a slope. The t_{brake}/t_{push} ratio decreases similarly when both the magnitude of the HTF and the positive slope of the terrain increase (Fig. 2.3.7C). Likewise, t_{brake}/t_{push} increases when both the magnitude of the ATF and the negative slope of the terrain increase.

Prior to the present study, Chang and Kram (1999) also compared running at 14 km h^{-1} with/against a pulling force to running on a slope. They concluded that although both conditions resemble each other "qualitatively*"* they are rather different "quantitively". Indeed, they found that when running against a horizontal impeding force the step frequency does not change whereas it increases when running on a positive slope (Minetti et al. 1994; Dewolf et al. 2016). Therefore, these authors argued that the internal work required to move the limbs according to the CoM (W_{int}) will not vary against a traction force but will increase with slope. However, in the present study, we observe that the stride frequency increases with the magnitude of the hindering force. An explanation for which Chang and Kram did not observe a significant change in stride frequency can be because they only measured HTFs up to +6% *BW*, whereas significant increase in stride frequency is observed if the HTF is equal or greater than +10% *BW*.

In summary, the changes in the bouncing mechanism observed when running with a hindering/aiding force are similar to the ones observed when running on slope. In both cases, the duration of positive/negative power production is lengthened to limit this increase in power. Furthermore, the additional work done is limited by transforming kinetic into potential energy and *vice versa*. This energy transduction allows to reduce the additional work by 15-20%, depending on the magnitude of traction force or on the inclination of the terrain. In a near future, it would be interesting to extend the comparison to an accelerating/decelerating situation and to analyse - in a wind tunnel for example - if running against/with the wind is comparable to running with a hindering/aiding force.

3.2 Biomechanics of Human Locomotion in the Wind

Raphael M. Mesquita, Patrick A. Willems, Giovanna Catavitello,
Giuseppe Gibertini, Valentina Natalucci, Francesco Luciano,
Alberto E. Minetti, Gaspare Pavei, Arthur H. Dewolf

Journal of Applied Physiology (2024) 137(3), 616-628.

Keywords: Aerodynamics, external work, locomotion, wind tunnel

Introduction

Locomotion enables living beings to move from one point to another traversing a medium which typically offers resistance to their forward motion: bacteria travel through extracellular fluid, fish through water, birds through air, *etc*. (Tucker 1975). When moving on land, most animals use their limbs to support their weight, propel themselves forward and exert force to overcome inertia and counter air resistance. In this case, external work (W_{ext}) is done (i) against air resistance and (ii) during interaction of the body with the ground (Cavagna et al. 1976). Additionally, because in legged locomotion the limbs must constantly be 'reset' for the following step, internal work (W_{int}) is also required to move the limbs relative to the centre of mass (*CoM*) (Cavagna et al. 1977).

Air resistance - or drag - is an external force against which the muscle-tendon units (MTU) do work. Its magnitude is directly related to the drag area (C_dA) *i.e.* the projected frontal area facing the airflow (A) multiplied by the drag coefficient (C_d), and by the dynamic pressure generated by the air moving around the body at a certain speed (Hoerner 1965). In turn, the product of the drag and the distance covered represents W_{drag}, the work required to overcome the resistance of the medium. Secondly, the interaction of the body with the ground is responsible for the remaining portion of external work. If the feet are not skidding, no work is done against frictional forces on the ground. Therefore, the ground reaction force (*GRF*) is responsible for the kinetic and potential energy changes of the *CoM* during each step (Cavagna et al. 1976). Consequently, the MTUs mainly perform work to sustain the movements of the *CoM* relative to the surroundings (W_{com}) (Cavagna et al. 1976).

When moving in still air, the speed of the relative airflow generated is equal to the subject's moving speed. In human locomotion, this speed is generally low *i.e.* less than 25 km h^{-1}, equating to negligible drag: *e.g.* at 21 km h^{-1}, the magnitude of air resistance represents ~6 N (Pugh 1970, 1971; Davies 1980; Schickhofer and Hanson 2021; Pecchiari et al. 2023). As a result, the work done to sustain the movements of the *CoM* against drag (W_{drag}) represents only a small fraction of the total positive work ($W_{tot} = W_{ext} + W_{int}$) done during locomotion: < 3% in walking and < 10% in running (di Prampero 1986). Consequently, as a first approximation, W_{drag} is negligible in still air - except at high running speeds (Hill 1928; Pugh 1971). However, in the presence of faster head- or tailwind, the additional external force generated by the airflow will hinder/aid the progression of the person and will most likely also alter the walking and running gait mechanics.

The first goal of our study was to quantify the drag exerted on the subject at different wind speeds (ranging from −15 to +15 m s^{-1}) while walking at 1.5 m s^{-1} and

running at 4 m s^{-1}. To our knowledge, air resistance in human locomotion has only been evaluated using simulations such as computational fluid dynamics (CFD) models, manikins which simulate the human body (Inoue et al. 2016; Polidori et al. 2020; Schickhofer and Hanson 2021; Forte et al. 2022; Marro et al. 2023; Fernandes et al. 2023) or investigated *via* experimental studies *e.g.* by using external tractive devices to pull on the subject and thus hindering or aiding progression (Lloyd and Zacks 1972; Chang and Kram 1999; Mesquita et al. 2020; Da Silva et al. 2022). Regarding human locomotion, CFD simulations have, amongst others, studied the drag applied on the body and their respective segments (Schickhofer and Hanson 2021; Forte et al. 2022), and the effect of multiple runner formations on running performance (Polidori et al. 2020; Beaumont et al. 2021; Valsecchi et al. 2022; Da Silva et al. 2022; Marro et al. 2023; Fernandes et al. 2023). However, little full-scale experimental data have been collected in a wind tunnel (Pugh 1970, 1971; Davies 1980). Moreover, to the best of our knowledge, there have been no studies investigating the biomechanical adjustments of locomotion when moving against the wind.

Here, in a novel approach, the aerodynamic drag of humans walking and running on a treadmill in a wind tunnel, was measured *via* the ground reaction forces (Pecchiari et al. 2023). This investigation is of current relevance (Polidori et al. 2020; Marro et al. 2023; Fernandes et al. 2023), especially in the field of sports science where the official marathon world record is on the brink of passing below the 2-hour mark (World Athletics 2023). We anticipated that as an adaption to the increased resistive force, subjects would adjust their posture, and consequently their C_dA, to reduce air resistance. This phenomenon is commonly observed in various organisms experiencing flow influences (Vogel 1994).

The second goal of the present study was to analyse the effect of drag on the pendular mechanism of walking and the bouncing mechanism of running. When moving in still air, since $W_{drag} \approx 0$, one can state that the positive (W_{ext}^{+}) and negative (W_{ext}^{-}) work done are about equal (Cavagna 2010). When wind speed increases, the W_{ext} should increase. In the case of headwind, W_{drag} is positive and slows the *CoM*. Consequently, $W_{ext}^{+} > W_{ext}^{-}$, meaning that MTUs do more positive than negative work to maintain a constant average speed of progression. In the opposite situation (*i.e.* tailwind), the flowing air does work on the subject and $W_{ext}^{-} > W_{ext}^{+}$, meaning that MTUs do more negative than positive work. This hypothesis is based on what occurs when moving against a hindering/aiding tractive force pulling on the *CoM* (Dewolf et al. 2020b; Mesquita et al. 2020). One may expect that the deviation from a 1.0 ratio between positive and negative work will affect the pendulum-like mechanism of walking and bouncing mechanism of running (Cavagna 2010). Indeed,

these models are characterised by a phase lag between the kinetic energy of the *CoM* due to its fore-aft motion (E_{kf}) and the energy due to its vertical motion (E_v) (Cavagna et al. 1976). When moving in still air on a flat terrain, the time course of E_{kf} and E_v are out of phase during walking and in phase during running. In the presence of linear head- or tailwind, E_v will most likely not change, as the external force is applied in the fore-aft direction. On the contrary, the amplitude of positive work to accelerate the *CoM* will be greater/smaller than the negative work to decelerate the *CoM*. This situation may be similar to walking/running on a slope (Minetti et al. 1993, 1994; Dewolf et al. 2016, 2017b), when the ratio between negative and positive work changes, their respective durations are also modified, inducing a change in the phase shift between E_v and E_{kf}. Therefore we hypothesised that, as in walking/running against an external tractive force or on a slope (Minetti et al. 1993, 1994; Dewolf et al. 2020b; Mesquita et al. 2020; Da Silva et al. 2022), the phase relationship will change and modify the energy transduction between kinetic and potential energy (Cavagna et al. 2002).

To achieve these goals, we evaluated eight subjects walking at 1.5 m s^{-1} and running at 4 m s^{-1} on an instrumented treadmill in a wind tunnel against different head- and tailwind blowing at different speeds. The *GRF* was recorded, and the mechanics of the *CoM* applied against head- and tailwind forces were analysed.

Materials & Methods

Experimental setup

The experimental setup described here was also used in the context of a recently published study (Pecchiari et al. 2023). An instrumented treadmill (Stellar ®, h/p/Cosmos, Germany - Arsalis, Belgium) with a belt surface of 1.6 x 0.65 m was fixed in the centre of a 4 m wide x 6 m long x 3.84 m high wind tunnel at the GVPM, Politecnico di Milano (Italy). The wind tunnel free stream turbulent level was less than 0.1%. The treadmill was aligned so that its long axis was parallel to the direction of the wind. To ensure a smooth (more laminar) flow around the athlete, a wooden floor structure was built around the treadmill and was oriented so that the wind first touched the subject before reaching the treadmill motor. In this way the motor wake did not affect the test (Figs. 3.2.1 & S1 in Supplementary Material). The flow disturbances introduced by the test rig were checked prior to athlete testing. In summary, the unavoidable turbulent boundary layer over the floor affected a region of less than 20 cm over the ground and that these differences in the local dynamic pressures (in respect to the reference value taken at 1 m over the floor) were

sufficiently small to allow for an estimation of a maximum error of 3% on the body total drag due to the wind non-uniformity.

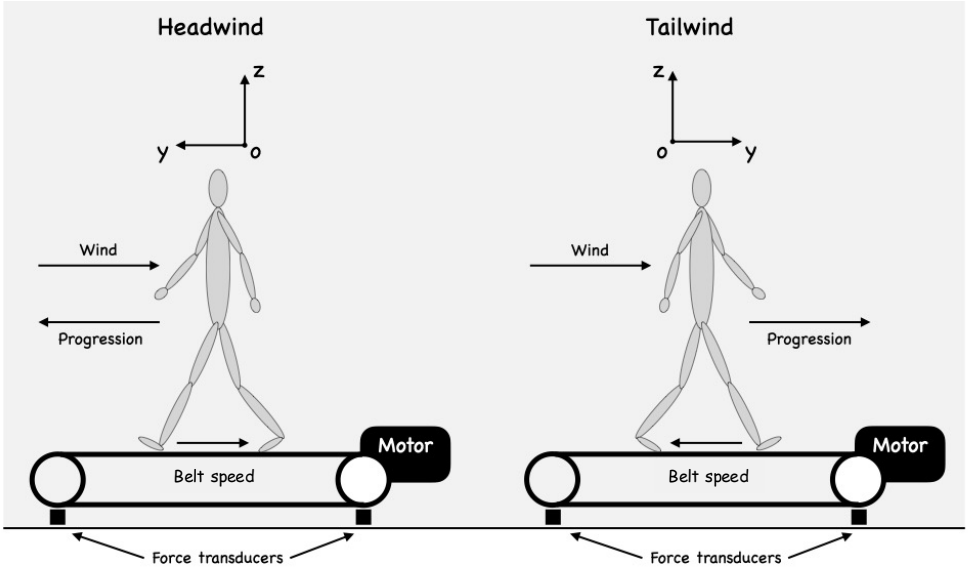

Fig. 3.2.1 *Illustration of the direction of the speed belt and of the forces applied to the subject when moving either with a head- or tailwind. In either wind direction, the wind first touched the subject before touching the motor, as such the motor wake did not affect the test conditions.*

Four strain-gauge force transducers placed under the body of the treadmill measured the three components of the *GRF*. The force transducers were shielded by a thin aluminium plate to prevent wind from directly applying a force to the sensors. Prior to the data collection, the strain gauges were calibrated and the cross talk between vertical, F_z and fore-aft F_f components of the *GRF* components were evaluated and remained on average below 0.5% (Dierick et al. 2004). Furthermore, prior to each recording, the force offset was removed from the signal. The transducer's analogue signals were amplified, low-pass filtered (4-pole Bessel filter with a - 3dB cut-off frequency at 200 Hz) to avoid an aliasing effect during digitization and recorded with a sampling rate of 1 kHz (Winter 2009). After digitization, the *GRF* signals were filtered by a two-way 8th order Bessel filter with a lowpass cut-off frequency at 10 Hz for the lateral F_x, 20 Hz for F_y and 30 Hz for F_z (Mesquita et al. 2024a). A typical trace of the vertical and fore-aft components of the *GRF* is shown during walking (Fig. 3.2.2A) and during running (Fig. 3.2.3A).

The electrical motor of the belt was also instrumented with an optical angle encoder (h/p/Cosmos, Germany - Arsalis, Belgium) to measure the instantaneous

velocity of the belt (v_{belt}). When the participants walked or ran on the treadmill, the recorded average velocity of the belt over a stride (V_{avg}) differed by 2.8 ±1.4% from the chosen speed and the instantaneous v_{belt} did not change by more than 6% of V_{avg}.

Bilateral, full-body three-dimensional kinematics were recorded at 250 Hz by means of a VICON system (Oxford, United Kingdom) with 8 cameras (6 MX-13 and 2 T20-S) placed around the treadmill. Participants were equipped with 18 retro-reflective markers glued onto the skin. In the context of this study only the markers glued on the zygomatic arch, shoulder and greater trochanter were used to measure the angle between the long axis of the trunk and the horizontal. Kinematic data were then oversampled at 1 kHz using a linear interpolation function in LABVIEW. The kinematic data were filtered by the same lowpass filter as the ground reaction forces (cut-off frequency at 30 Hz). An oversampling of the kinematic data was chosen rather than a down sampling of the kinetic data to ensure that the force signal characteristics were not lost during data-processing. Subjects also wore a face mask together with a portable gas analyser on their back (K5, COSMED, Rome, Italy). The metabolic data will be a part of a forthcoming study.

Participants and experimental procedure

Eight professional or semi-professional male runners (height: 1.77 ± 0.05 m, mass: 66 ± 7 kg, age: 31.2 ± 6.2 years, Personal Best 10000 m: 31'20" ± 1'12" mean ± SD) participated in the study. The number of subjects chosen was based on an *a priori* statistical power analysis using G*Power (Faul et al. 2007) from results of a previous study which focused on similar variables (Mesquita et al. 2020). Informed written consent of each subject was obtained and the study followed the guidelines of the Declaration of Helsinki. Subjects consented to having their photos published. All procedures were accepted by the local ethics committee (Politecnico di Milano, n°16/2022).

Participants walked at 1.5 m s^{-1} and ran at 4 m s^{-1} on the instrumented treadmill, wearing a bathing suit and their usual, conventional running shoes (Figs. 3.2.2C and 3C). The subjects walked and ran in still air and against ten different head- (denominated as +) and tailwind (−) velocities of 0, ±5, ±7.5, ±10, ±12.5 and ±15 m s^{-1}.

The experimental protocol involved participants walking and running in both wind directions at a given wind speed before switching to the next randomly chosen wind speed.

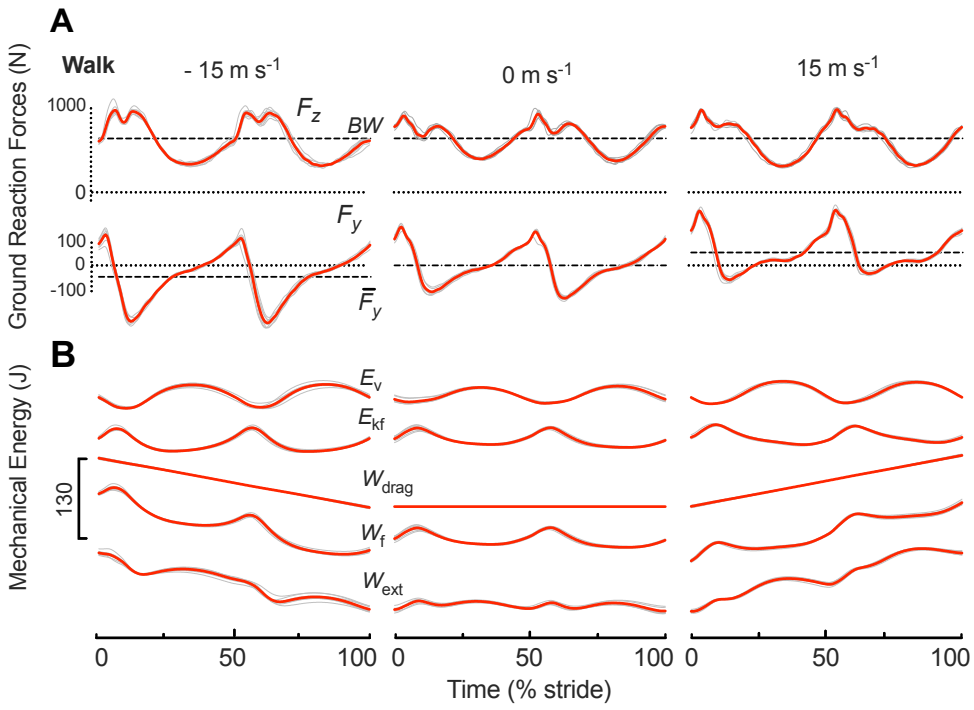

Fig. 3.2.2 Panel A: *Typical traces of the vertical (F_z) and fore-aft (F_y) component of the GRF as a function of time (in % of the stride period) of one subject (mass: 64 kg, height: 1.75 m) walking at 1.5 m s^{-1} with a tailwind speed of -15 m s^{-1}, without a wind force, and with a headwind speed of 15 m s^{-1}. The grey traces represent all strides recorded during one trial normalised in % of stride and the red line represents the average of all strides. When the subject is not on the treadmill, F_z and F_y = 0 (dotted line). The dashed horizontal lines represent the average ground reaction forces when the subject walks or runs on the treadmill: in the vertical direction, this line corresponds to the subject's body weight (BW), whereas in the fore-aft direction the dashed line ($\bar{F}_y$) corresponds to the opposite of the drag force ($\bar{F}_d$).* ***Panel B:*** *The mechanical energy of the CoM (in J) from the same traces as in panel A. From top to bottom: E_v, is the energy due to the vertical movements of the CoM. E_{kf} is the energy due to the changes in its fore-aft velocity, W_{drag} is the work done by the subject against the wind, W_f is the work done to sustain the fore-aft movements of the CoM ($W_f = E_{kf} + W_{drag}$), and W_{ext} is the work done to sustain the progression of the CoM in the wind ($W_{ext} = E_v + W_f$).*

Fig 3.2.2 Panel C: *a picture of a subject walking in the wind tunnel (here without wind) on the instrumented treadmill setup designed to reduce turbulence around the runner.*

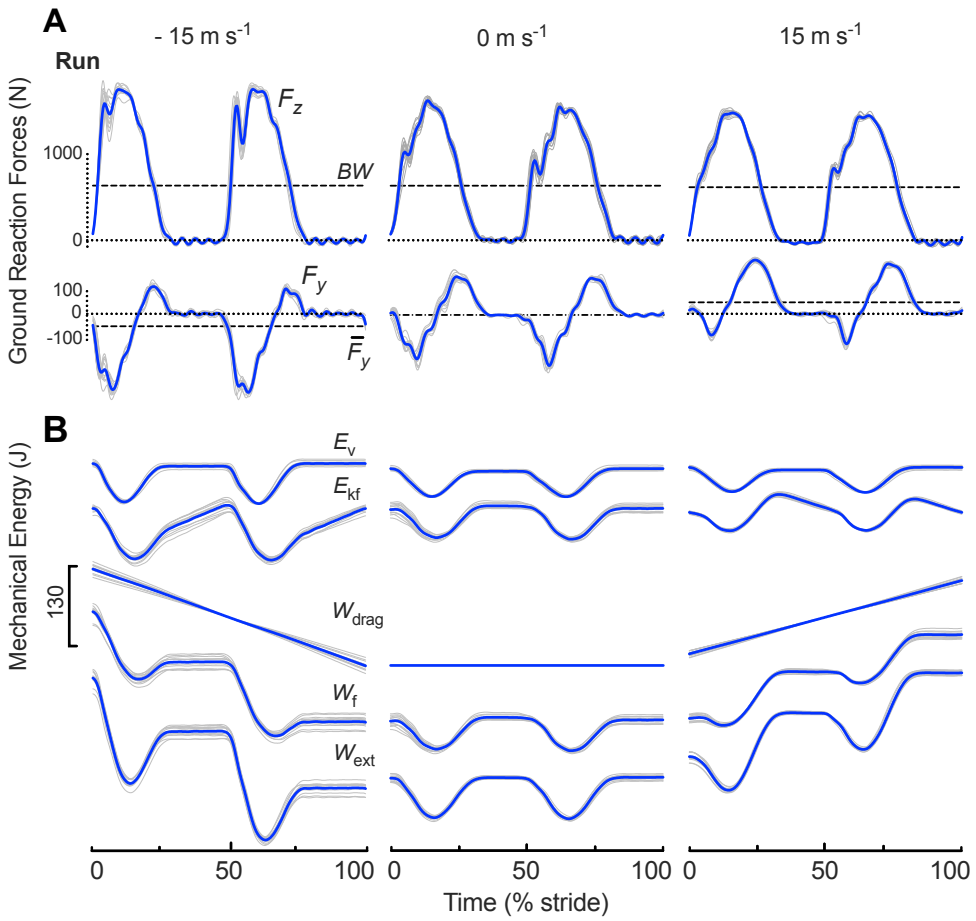

Fig. 3.2.3 Panel A: *Typical traces of the vertical (F_z) and fore-aft (F_y) forces of one subject (mass: 64 kg, height: 1.75 m) running at 4.5 m s^{-1} without a wind force and with tail and headwind speeds of ±15 m s^{-1} (tail: –, head: +).* ***Panel B:*** *Mechanical energy of the CoM (in J) from the same traces as in panel A. All other indications are as in Fig. 3.2.2.*

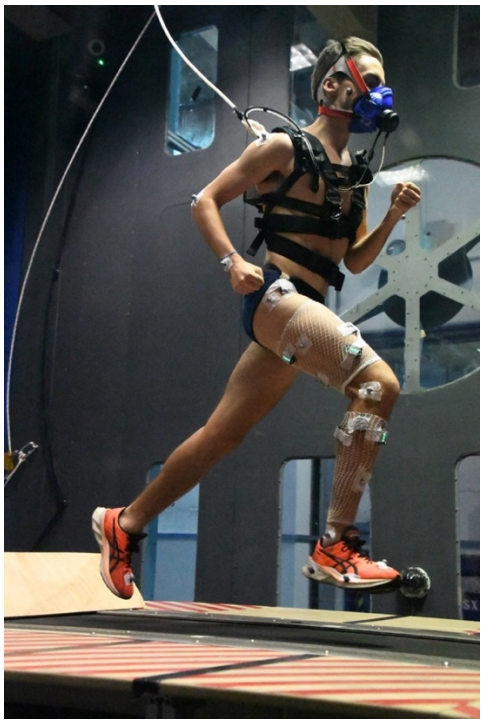

Fig 3.2.3 Panel C: *picture of a subject running in the wind tunnel against a headwind.*

Data processing

Data processing was performed *via* custom-made programs written with LABVIEW (National Instruments 2019, Austin, Texas, USA). In both gait patterns, strides were defined as a succession of a right followed by a left step. A step started at foot contact, determined at the threshold when $F_z > 30\ N$ and ended when the contralateral foot touched the ground (the instant before $F_z > 30\ N$) (Da Silva et al. 2022; Mesquita et al. 2024b).

Acceleration, Velocity and Vertical displacement of the CoM

Calculations for the acceleration, velocity and displacement of the *CoM* were done as in Gosseye et al. (2010), Mesquita et al. (2020) and Dewolf et al. (2020b) and will, therefore only be briefly explained here. The lateral component of the *GRF* was not considered since its contribution to the external work is negligible (Cavagna et al. 1963, 1976).

When moving in the wind on the level, the following forces were applied to the body: the body weight (*BW*), the *GRF* (*F*) and the drag (F_d). In this case, over an

integral number of strides, the average fore-aft *GRF* ($\overline{F}_y$) was equal and opposite to F_d and the average vertical *GRF* ($\overline{F}_z$) was equal to *BW*.

The acceleration of the *CoM* in the fore aft (a_y) and vertical (a_z) directions relative to a fixed reference frame attached to the wind tunnel was given as:

$$a_y = \frac{F_y - \overline{F}_y}{m}, \text{ and } a_z = \frac{F_z - \overline{F}_z}{m},$$

where m is the body mass. A time-integration of the a_y, and a_Z-curves by the trapezoidal method gave the fore-aft and vertical velocity changes of the *CoM* plus their respective integration constants (Cavagna, 1975; Mesquita et al. 2024b).

To be included in the study, the strides had to fulfil the two following criteria, as in Dewolf et al. (2016): (1) the average vertical force during a complete stride ($\overline{F}_z$) had to be within 10% of *BW*, (2) the sum of the increments and sum of the decrements of the instantaneous *CoM* fore-aft velocity had to differ less than 25%. In total, between 13 and 84 strides were analysed per condition and per subject. A total of 8850 strides were analysed (5443 strides for the running trials and 3307 strides for the walking trials, *i.e.* 1111± 68 strides per subject, mean ± SD).

External mechanical work (W_{ext})

The external power ($\dot{W}_{ext}$) developed during each step by the forces applied to the body was computed as the algebraic sum of the power developed by the *GRF* ($\dot{W}_{com}$), plus the power developed to counter the drag ($\dot{W}_{drag}$). From these, the time integral of $\dot{W}_{com}$ and $\dot{W}_{drag}$ give, respectively, the work done to sustain the movements of the *CoM* (W_{com}) and work done against the drag (W_{drag}). The sum of W_{com} and W_{drag} gives the external work, W_{ext}, similar to the methods proposed in (Mesquita et al. 2020).

The two first curves of Figs. 3.2.2B and 3B represent typical traces of the energy done to sustain the fore-aft and vertical movements of the *CoM*, respectively E_{kf} and E_v during one stride of walking and one stride of running, computed as in (Cavagna et al. 1976; Willems et al. 1995). The middle curves of Figs. 3.2.2B and 3B represent W_{drag}, the work done by the subject on the wind:

$$W_{drag} = \int_{t_1}^{t_2} \overline{F}_y \, v_{belt} \, dt. \quad (1)$$

When moving against a wind force, the work (W_f) was done during the contact phase to sustain the kinetic energy changes of the *CoM* but also to counteract the drag:

$$W_f = E_{kf} + W_{drag}. \quad (2)$$

The bottom curve represents the external energy of the *CoM*, which was computed as the sum of the E_v- and E_{kf}-curves plus the curve W_{drag}.

$$W_{ext} = E_v + E_{kf} + W_{drag}. \quad (3)$$

Positive (W_f^+, W_v^+ and W_{ext}^+) and negative (W_f^-, W_v^- and W_{ext}^-) work were computed by respectively summing the increments and the absolute value of the decrements of the W_f, E_v and W_{ext} curves, respectively. An in-depth description of the method is available in the supplementary materials.

Aerodynamic parameters

The drag applied to a subject, F_d, is dependent on the drag area, C_dA, *i.e.* the projected frontal area of the subject (A) multiplied by the drag coefficient (C_d) and by the dynamic air pressure of the moving air stream (q) (Hoerner 1965; Pugh 1970, 1971; Davies 1980). As the subject moved at constant speed, the magnitude of the average fore-aft ground reaction force ($\overline{F_y}$) computed over an integral number of strides was equal to $|F_d|$. Consequently, the C_dA of the subject was given as:

$$C_dA = \frac{\overline{F_y}}{q}. \quad (4)$$

In turn, q could be evaluated as the kinetic energy per unit volume of a moving solid body $q = 0.5\,\rho\,u^2$, where ρ was the air density and u the wind speed. In turn, the air density ρ was computed by: $\frac{p}{RT}$, where p is the static air pressure, R is the gas constant and T is the air temperature. The instantaneous values of these variables (u, q, p, and T) were recorded at 1kHz during trials. Wind speed, u, deviated from the nominal wind speed on average by 2 ± 0.4% over all trials. The average wind speed, U, was similar between walking and running ($F = 1.14$, $p < 0.344$), air density was on average at 1.137 ± 0.005 kg m^{-3}, and the average temperature was 28.3 ± 1.3°C (301.54°K) over all trials.

%Recovery, drag ratio and phase lag

Energy transduction between the W_f- and E_v-curves in both walking and running were assessed by the *%recover*y as in (Cavagna et al. 2002). The drag ratio (D_r) was obtained by dividing the work done to overcome drag (W_{drag}) by the external work (W_{ext}).

$$D_r = \frac{w_{drag}^{+/-}}{W_{ext}^{+/-}}, \quad (5)$$

in the case of headwind, the D_r was the ratio between the sum of the positive increments whereas in the case of tailwind, the negative increments were used.

The phase ϕ, expressed in degrees, evaluated the lag between the maximum of W_f (t_f) and the minimum of E_v (t_v) in walking and between the minimum of W_f (t_f) and the minimum of E_v (t_v) in running:

$$\phi = 360 \frac{t_f - t_v}{ST}. \quad (6)$$

where ST is the step period.

Statistics

For each participant, the different variables were first averaged across the right and left steps for each stride then averaged per stride. Descriptive statistical analyses were performed. First, a Shapiro-Wilk test was performed to verify normality. Then, a linear mixed effect model assessed the effect of wind speed on the calculated variables. Depending on the lowest Akaike Information Criterion either U or U^2 was used for the wind effect. For each comparison, the F and p values for the fixed effect were reported. To analyse eventual differences in the aerodynamic variables between walking and running, all data were pooled together and the effect of wind, walking/running speed and their interaction were analysed. Statistical tests were run on IBM SPSS Statistics (PASW Statistic 27, NY, USA). The results of the statistical tests were considered significant for a p-value<0.05.

Results

Drag as a function of wind speed

As wind speed increases, the magnitude of the drag, $|F_d|$ increased (Fig. 3.2.4A) both in walking ($F = 1195.02$, $p<0.001$) and in running ($F = 1317.03$, $p<0.001$). However, at a given wind speed, the drag $|F_d|$ was greater in walking than in running ($F = 92.56$, $p < 0.001$) and this difference was marked at the fastest wind speeds (regression curve of $|F_d|$ as a function of the instantaneous wind speed u, for running: $|F_d| = 0.85 - 0.108\ u + 0.239\ u^2$, $r^2 = 0.986$ and for walking: $|F_d| = 0.635 + 0.055u + 0.265u^2$, $r^2 = 0.986$) (95% IC intervals show difference between walking and running for headwinds ≥ 10 m s^{-1}). Note also that similar trends were observed for the F_d versus U relation for both head- and tailwinds (Table S1 in Supplementary Material).

The dynamic air pressure (q) increased with the square of wind speed and was not different between head- and tailwinds (*post-hoc* test always equal $p = 1$ between equivalent head- and tailwind speeds; regression curve for running: $q = -0.03 - 6.9610^{-4}\ u + 0.578\ u^2$, $r^2 = 0.999$ and for walking: $q = -0.03 - 4.45\ 10^{-5}\ u + 0.578\ u^2$, $r^2 = 0.999$). The C_dA decreased as a function of increasing wind speed (Fig. 3.2.4B) both in walking ($F = 6.25$, $p < 0.001$) and in running ($F = 23.89$, $p<0.001$). With headwind, C_dA was greater in walking than in running (*post-hoc* effect between +5 and +15 m s^{-1} $p<0.001$). On the contrary with tailwinds faster than -5 m s^{-1}, there was no significant difference between the two gaits (*post-hoc* between -7.5 and -10, -12.5 and -15 $p=1$). Without wind, the trunk was vertical during walking and slightly leaned forwards (5°) during running (Fig. 3.2.4C). Both in walking and in running, the trunk tilted forward (≈11° for both) with headwind and backward (≈5° for both) with tailwind ($F = 112.77$, $p<0.001$ for running and $F = 217.61$, $p<0.001$ for walking).

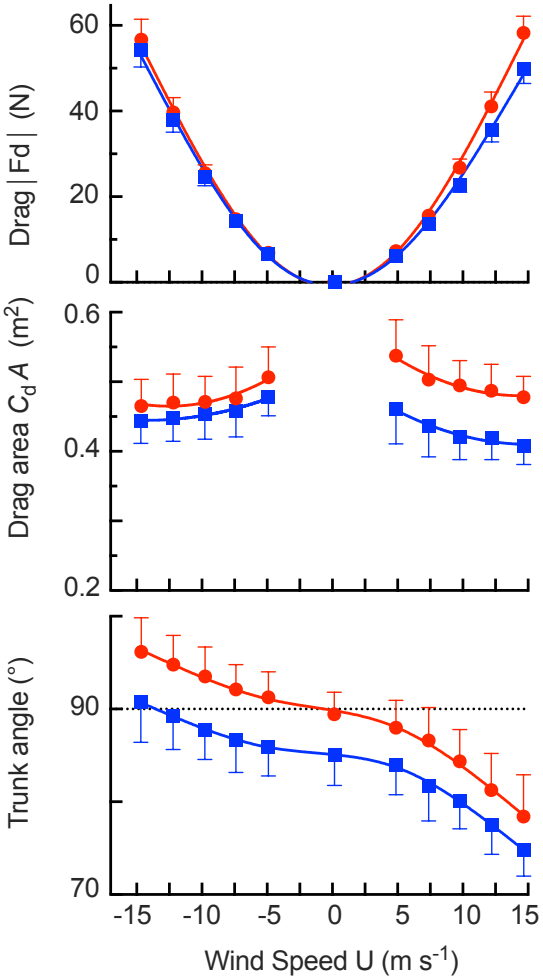

Fig. 3.2.4 *Aerodynamic variables in walking (red circles) and running (blue squares) as a function of wind speed (U in m s^{-1}). **Panel A:** Magnitude of drag (in N) in both walking and running. **Panel B:** Drag area (C_dA) is computed from equation 4. No values are expressed when wind speed is nil, since in equation 4, the wind speed U is part of the denominator and C_dA mathematically tends towards infinity when the wind speed tends to zero. **Panel C:** Trunk angle (expressed in degrees) in walking and running. In each panel, the points are the average of the data measured on all steps of all subjects. The vertical bars indicate the standard deviation of the mean and are drawn when they exceed the size of the symbol. Filled and dashed lines are spline functions with four notches from all data points. These data are plotted via Graphpad Prism 10 (GraphPad Software, Boston, USA).*

Step length and external work while walking and running in the wind

Wind speed had a significant effect on the step length (Fig 3.2.S2 in Supplementary Material) both in walking ($F=8.13$, $p<0.001$) and in running ($F=14.98$, $p<0.001$). In walking, step length decreased by about 5% when comparing no wind and – 15 m s^{-1} (*post-hoc* $p<0.001$). Conversely, in running step length decreased with increasing headwind ($p<0.001$ between 15 m s^{-1} and no wind).

The magnitude of the work done to overcome wind resistance ($|W_{drag}|$) is presented in Fig. 3.2.5C. The muscle-tendon units did positive work against headwind and negative work against tailwind. In both directions, $|W_{drag}|$ increased with wind speed ($F = 4134.44$ in walking and $F = 1360.72$ in running, $p<0.001$). Note also that when normalised by distance travelled, W_{drag} was slightly greater in walking than in running ($F = 3.01$, $p<0.001$).

When walking or running in the wind, since the subject is moving on level ground, $W_v^+ \approx W_v^-$ (Figs. 3.2.2, 3 & 5A). However, in walking both W_v^+ and W_v^- increased as wind speed increased (W_v^-: $F= 35.32$, $p < 0.001$; W_v^+: $F= 35.32$, $p<0.001$); whereas the effect of wind on either variable was much smaller in running (W_v^-: $F= 8.85$ $p<0.001$, W_v^+: $F= 8.88$, $p<0.001$).

In both gaits, head- and tailwind speed influenced the positive (W_f^+) and negative (W_f^-) work done to move the *CoM* forwards (for W_f^+: $F= 867.45$ in walking and $F= 1034.28$ in running, $p<0.001$ and for W_f^-: $F= 1643.28$ in walking and $F= 1005.77$ in running, $p<0.001$). As compared to walking and running with no wind, when headwind increased, W_f^- decreased, while W_f^+ increased (Fig. 3.2.5B). Conversely, with a tailwind, W_f^- increased with wind speed whereas W_f^+ decreased. In both gaits, the net increase in W_f (*i.e.* $\left|W_f^+ - |W_f^-|\right|$) was about equal to $|W_{drag}|$ (Fig. 3.2.5C).

In walking as in running, the effect of wind on W_{ext}^+ and W_{ext}^- was similar to the one observed on W_f^+ and W_f^- (Figs. 3.2.2, 3 & 5D), meaning that W_{ext}^+ increased with faster headwinds and decreased with faster tailwinds ($F= 388.01.45$, $p < 0.001$), whereas W_{ext}^- decreased with increasing headwinds and increased with increasing tailwind ($F= 547.11$, $p<0.001$). Note that in both gaits, the duration of the positive work phases (t_{push}) increased when the headwind speed increased and decreased when tailwind speed increased. Inversely, the duration of the negative work phases decreased when the headwind speed increased and increased when tailwind speed increased (see Fig. 3.2.S3).

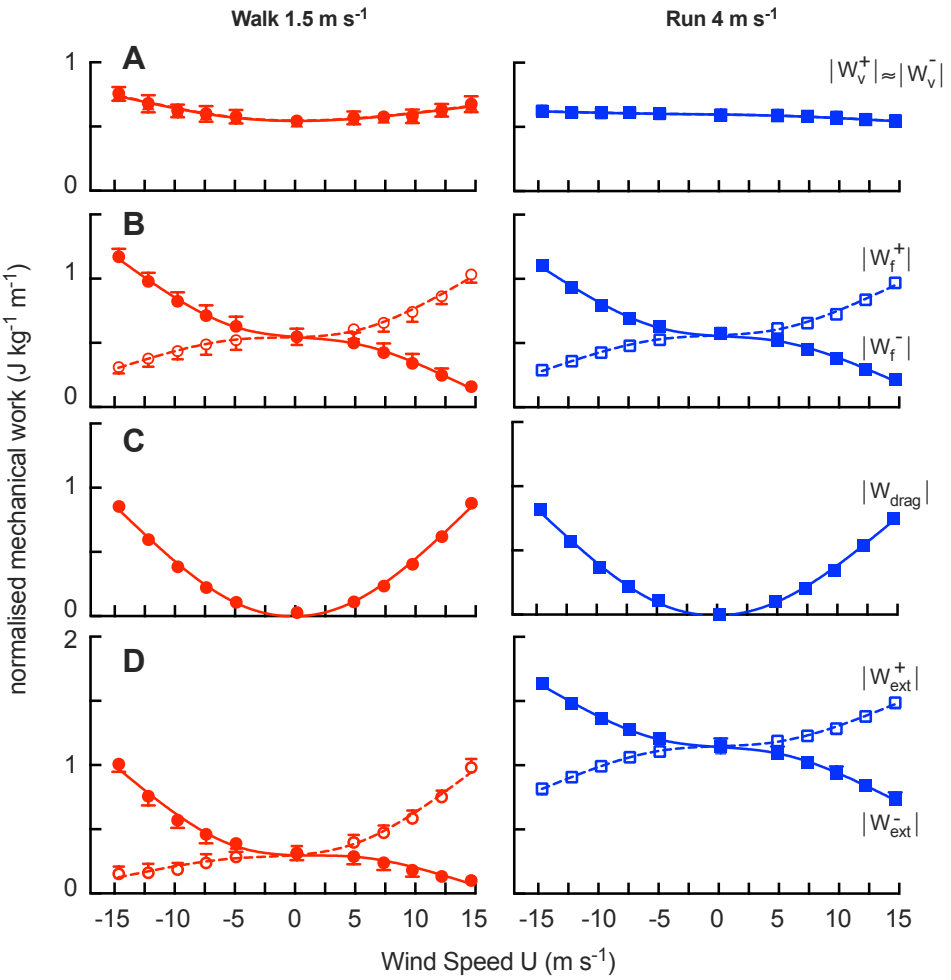

Fig. 3.2.5 Magnitude of the mass-specific mechanical work per unit distance (J kg-1 m-1) in walking (red circles) and running (blue squares) as a function of the average wind speed (U). Open symbols represent positive work (superscript, +) and closed symbols, negative work (superscript, -). **Panel A**: W_v is the work done to sustain the vertical movements of the CoM. **Panel B**: W_f is the work the sum of the work done to sustain its fore-aft movements of the CoM plus the work done against the wind. **Panel C**: is the work done against the wind. **Panel D**: external work (W_{ext}) done to maintain the movements of the CoM relative to the surroundings. Other indications as in Fig. 3.2.4.

%*Recovery*, drag ratio and phase shift between W_f and E_v

The drag ratio ($D_r = \frac{W_{drag}}{W_{ext}}$) increased as a function of wind speed in both walking and running (in walking: F = 536.03, p<0.001, in running: F = 1148.70, p < 0.001). This increase was greater in walking than in running as evidenced by the interaction effect observed between wind speed and moving speed (F = 26.74, p<0.001) (Fig. 3.2.6A).

In both gaits, wind had a significant effect on the phase shift (ϕ) between the minimum of W_f and the maximum of E_v in walking (F = 97.95, p<0.001) and the minima of both W_f and E_v in running (F = 434.78, p<0.001) (Fig. 3.2.6B) Without wind, ϕ was close to 0° when walking (phase opposition) at 1.5 m s^{-1} and when running at 4 m s^{-1} (in phase). In walking, the W_f- and E_v-curves were perfectly out of phase (ϕ= 0°) with a tailwind of ~5 m s^{-1}. When the tailwind decreased and became a headwind, the lag between the two minima increased. When the tailwind became greater than ~5 m s^{-1}, the lag between the two minima was reduced.

In running, the W_f- and E_v-curves were perfectly in phase (*i.e.* ϕ= 0°) with a headwind of ~10 m s^{-1}. When the headwind increased, the minimum of E_v occurred later than the minimum of W_f. On the contrary, if the headwind slowed or if the tailwind got faster, the minimum of E_v occurred before the minimum of W_f.

In walking, when wind speed increased the %*recovery* decreased (F = 26.02, p<0.001) (Fig. 3.2.6C). The *%recovery* was at its peak at 0 m s^{-1} and followed a curvilinear decrease with both head- and tailwinds. In running, %*recovery* increased with increasing wind speed (F = 65.05, p<0.001) principally with tailwinds (*post-hoc* between 0 wind and all tailwind speeds p<0.001). Against headwinds, the *%recovery* at 0 wind significantly differed only at +15 m s^{-1} (*post-hoc* p<0.001) (Fig. 3.2.6D).

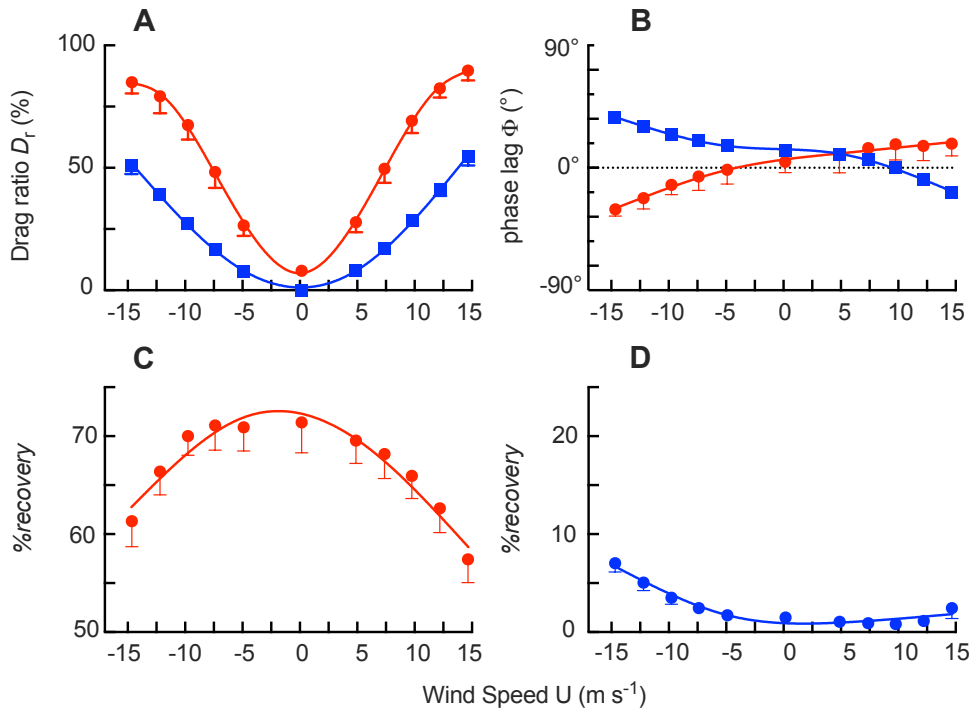

Fig.3.2.6 *Drag ratio, D_r (**Panel A**) and phase lag, ϕ (**Panel B**) in walking and in running as a function of wind speed. Energy recovered through energy transduction between W_f and E_v (%recovery) as a function of the wind speed in walking (**Panel C**) and in running (**Panel D**). Other indications as in Fig. 3.2.4.*

Discussion

In the present study, we analysed the effects of wind (ranging from -15 to +15 m s^{-1}) on the external work (W_{ext}) and on the mechanics of locomotion when walking at 1.5 m s^{-1} and running at 4 m s^{-1}. In this section, we will first discuss how aerodynamic variables change during human locomotion against head- and tailwinds. We will then analyse how the ratio between negative and positive work, the drag ratio, and the phase lag change with increasing wind. Then, we will consider practical implications of our results and compare these to two situations where the ratio between negative and positive work is imbalanced: moving against tractive forces and moving on a slope.

Aerodynamics of walking and running in the wind

While the study of locomotion against wind forces is not novel (Hill 1928; Pugh 1970; Davies 1980; Inoue et al. 2016), the direct measurement of drag *via* the *GRF*

is innovative. This method was based on the following principle: when the average speed of progression does not change over an integral number of strides, the average fore-aft acceleration of the *CoM* is nil and the magnitude of the average fore-aft component of the *GRF* is equal to the drag force.

In the present study, we assumed that the drag remained constant during the stride. In other words, we considered that the movements of the limbs during the stride (the turbulence of which is often referred as 'Active Drag') do not significantly change the projected frontal area of the subject. This assumption was also made by Pugh (1971) and Davies (1980). In fact, the positioning of the limbs generates little variation of C_dA (Schickhofer and Hanson 2021; Fernandes et al. 2023). Similar observations were made in cycling where the pedalling motion of the lower limbs has negligible effect on the C_dA (Crouch et al. 2016).

With increasing wind speeds, the drag force exhibits a quadratic rise, reaching approximately 50-60 N at the highest wind speeds (Fig. 3.2.4). These results are similar to the CFD simulations of Schickhofer and Hanson (2021), who obtain a drag force of 18.45 N at 10 m s^{-1}, compared to our experimental result of 22.4 N. When wind speed increases further, *i.e.* at 15 m s^{-1}, slight differences appear in F_d between walking and running. Furthermore, when applying Davies' equation to estimate the projected area, our results for C_d vary between 0.89 - 1.05 similar to previously documented values (Pugh 1971; Davies 1980; Valsecchi et al. 2022).

Given the similar average wind speed and consistent air density of 1.137 kg m^{-3} ± 0.005 kg m^{-3} across all trials, the observed difference in F_d can be attributed solely to a change in C_dA, which decreases more with increasing wind velocities in running than in walking (Fig. 3.2.4 & Table S1 in Supplementary Material). In turn, this difference in C_dA between the two gaits may be attributed, at least partially, to the more forward-leaning posture of the trunk, which reduces the projected frontal area of the runner. Furthermore, this increased trunk flexion, associated with shorter steps and higher step frequency (Fig. 3.2.S2), is a trait generally associated with initial *CoM* acceleration (Nagahara et al. 2018), decreased push averaged power (Cavagna et al. 1991; Mesquita et al. 2024a) and is related to running economy and performance (Novacheck 1998; Folland et al. 2017; van Oeveren et al. 2021; Warrener et al. 2021). Van Oeveren et al. (2021) explain that a greater trunk lean likely increases propulsion, tilts the *GRF* vector further, and shifts the centre of mass forward. Nonetheless, running performance is typically associated with a more upright trunk posture, whereas novice runners, especially when fatigued, tend to lean their trunks more. Furthermore, increased trunk lean, due to its role on

the pelvis, is linked with several running injuries (Bramah et al. 2018; Mendiguchia et al. 2021).

Improving aerodynamics during walking and running has received little attention in sports science, as it would not lead to major improvements of performance. However aerodynamics are rather important in sports such as speed skating and cycling where speeds, and hence drag forces, are greater (di Prampero 1986). However, when the limits of performance are nearly reached, even small changes can improve running time (Hoogkamer et al. 2018). Indeed, in the past twenty years the marathon record has improved by 3.6% between Paul Tergat's 2:04:55 and Kelvin Kiptum's 2:00:35. For example, although hypothetical, decreasing drag by drafting behind another athlete decreases the drag coefficient (C_d) by 9.7%, potentially saving up to 535 s over an entire marathon run at 4.7 m s^{-1} (Valsecchi et al. 2022). Note that this improvement will be speed and distance between runner dependent (Pugh 1971; Polidori et al. 2020; Schickhofer and Hanson 2021; Beaumont et al. 2021; Fernandes et al. 2023). In light of this, we would argue that prior to modifying one's gait, elite athletes should look at improving their drafting technique (*e.g.* by improving racing strategy (Hoogkamer et al. 2017), adapted clothing (Kyle and Caiozzo 1986).

Positive and negative external work, drag ratio and phase lag while walking and running in the wind

Headwinds impede forward progression. Therefore, to maintain the average speed of progression constant from one stride to the next, $W_f^+ > W_f^-$ and $W_{ext}^+ > W_{ext}^-$ (Figs. 3.2.2, 3 & 5). Conversely, tailwinds aid forward progression and $W_{ext}^- > W_{ext}^+$. Additionally, in walking when head- or tailwind increases, W_v increases. This could be explained by the drag generating a lift force accelerating the *CoM* upwards, at certain moments of the stride, and thus increasing the vertical motion of the CoM (Davies 1980). In running, the vertical movements of the *CoM* are slightly reduced at the fastest headwind speed as compared to running without wind. When running against fast headwinds, Davies (1980) reports that subjects "lean" on the wind flow and tuck their head in, reducing the vertical movement of the *CoM*. Consistently, our measurements show a ~12% increase in the forward trunk inclination at the fastest wind speed.

When walking in the presence of increasing headwind, due to W_{drag}, the angle ϕ becomes greater than 0°, showing that the minimum of W_f occurs later in the step than the minimum of E_v. As a result, the periods during which the W_f- and E_v-curves

increase together becomes longer and the percentage of energy transduction (%*recovery*) between energy W_f and $E_{v,}$ decreases from 65% to 55% (Fig. 3.2.6C & D). In presence of increasing tailwind, the angle ϕ decreases and becomes smaller than 0°, demonstrating that the minimum of W_f occurs earlier in the step than the minimum of $E_{v.}$ As a result, the periods during which the W_f- and E_v-curves decrease together becomes longer and the %*recovery* decreases from 65% to 55% (Fig. 3.2.6C & D). When running in presence of increasing headwind, the angle ϕ decreases and becomes smaller than 0°, showing that the periods during which the W_f-curve increases while the E_v-curve decreases gets longer, allowing energy transduction between the two curves. In presence of increasing headwind, the angle ϕ becomes greater than 0°, showing that the periods during which the W_f-curve decreases while the E_v-curve increases, allowing for energy transduction between the two curves. Therefore, when ϕ deviates from 0° (in both directions), the %*recovery* increases slightly (Fig. 3.2.6C & D).

Effect of the wind on the drag ratio

When walking or running on a treadmill, humans move through still air which offers negligeable resistance to their forward motion. Consequently, the product of the drag times the distance covered is small as compared to the total muscular work done to move the body and the drag ratio, $D_r = \frac{W_{drag}}{W_{ext}}$, is close to zero (Fig. 3.2.6A). On the contrary, in fast winds, the drag ratio, increases up to ~80% of W_{ext} in walking and ~50% in running (Fig. 3.2.6A), suggesting that the fraction of work done against the environment increases if the medium crossed offers a greater resistance/assistance to forward motion. However, with increasing wind speed, the ratio between $|W_{ext}^{-}|$ and W_{ext}^{+} deviates from 1.0, and with it, a reduction of the energy-saving pendular mechanism of walking and bouncing mechanism of running are observed (Fig. 3.2.6C & D). This has been observed in other situations (Davies 1980; Cavagna 2010; Zamparo et al. 2016). We also observed that both in walking and in running, the duration of the push phase (t_{push}, *i.e.* the duration of the positive work production) increases when the headwind speed increases whereas the duration of the brake phase (t_{brake}) increases when the tailwind speed increases (Fig. 3.2.S3). This increase in t_{push} when running against the wind and of t_{brake} when running with the wind reduces the average positive power developed during the positive/negative work phase, respectively.

Furthermore, an increase in D_r together with the imbalance in the positive/negative external work could modify the overall efficiency of locomotion

(Cavagna 2010; Peyré-Tartaruga and Coertjens 2018). Indeed, against drag forces generated by wind, the 'apparent' efficiency decreases towards efficiencies observed in slope running (Davies 1980). Note that this last study, based on 3 subjects, showed considerable variability in their data, mostly due to subject heterogeneity and to the small sample size. Also, those results are affected by the included determinants of the total mechanical work and its 'apparent' nature due to elastic contribution of tendons, which is small in walking but considerable in running (Cavagna et al. 1977; Farris and Sawicki 2012; Minetti et al. 1993, 1994; Monte et al. 2020, 2021). The effect of D_r on the efficiency of locomotion could be tested (1) by measuring the internal and thus the total muscular work done during locomotion in the wind and (2) evaluating the energy expenditure during walking and running with head and tail winds blowing at the same speed.

Practical considerations about the mechanics of wind locomotion

Transposing locomotion in the wind tunnel to overground locomotion.

Note that when walking or running on the ground instead of a treadmill, the "apparent wind" speed, as known in sailing (Anderson 2008) should be corrected to the "true wind" speed; the wind that the subject experiences while moving. For example, running on the treadmill at 4 m s^{-1} with a headwind of 15 m s^{-1} corresponds to running on the ground at 4 m s^{-1} with a true wind of 11 m s^{-1}. Moreover, when running on the ground at 4 m s^{-1} with a tailwind of 4 m s^{-1} corresponds to running on the treadmill with no wind. When simulating overground locomotion, using a treadmill in a wind tunnel, both with head- and tailwinds, the speed of the belt should be subtracted from the wind speed to match ecological conditions. This concept should be acknowledged when transposing our findings to field tests, such as drag formations (Polidori et al. 2020; Beaumont et al. 2021; Valsecchi et al. 2022; Da Silva et al. 2022; Marro et al. 2023; Fernandes et al. 2023).

Comparison to locomotion on a slope

Previous studies have shown, both in walking (Dewolf et al. 2020b) and in running (Mesquita et al. 2020), that the W_{ext} while moving on a slope of n% (0%<n<15%) (Dewolf et al. 2016, 2017b) is equivalent to W_{ext} while moving on the level with a horizontal tractive force representing n% of BW. From a metabolic standpoint, similarities have been documented between walking-running with head and tailwind and walking-running uphill and downhill (Davies 1980) however no consensus exists (Pugh 1971). When moving in the wind, if the drag is expressed as a percentage of

BW or as a function of squared wind speed, we observe similarities between the magnitude of the drag and both the equivalent slope (Dewolf et al. 2016, 2017b) and the magnitude of tractive force (Dewolf et al. 2020b; Mesquita et al. 2020) in both types of locomotive strategies. For an in-depth discussion on the matter, the reader is invited to consult the supplementary materials (Figs. 3.2.S4 and S5 Supplementary Material).

Inclining the treadmill by 1% compensates for the lack of air resistance

Jones and Doust (1996) proposed that in order to (metabolically) compensate for the lack of air resistance during treadmill running, researchers should incline a treadmill by 1% to be able to compare their results to overground running. Despite the paper's popularity, systematic reviews like those of Miller et al. and Van Hooren et al. (Miller et al. 2019; Van Hooren et al. 2020) have shown that during efforts below 18 km h^{-1}, no difference in oxygen consumption is observed between level treadmill and overground running. The last authors explain that as air resistance increases with the square of wind speed, when running at high speeds the overground $\dot{V}O_2$ more closely matches treadmill running with a 1% incline. Based on the regression curve for $|F_d|$ presented in our results, at the speeds covered in Jones and Doust (1996), a 66 kg person (the average subject mass in the present study) running at 2.92 m s^{-1} would experience a "true" drag force of 2.36 N, corresponding to an incline 0.36% (di Prampero et al. 2005; Mesquita and Dewolf 2022). At 5 m s^{-1} the drag is at 6.07 N (corresponding to 0.93% incline). Fig. 3.2.S6 shows the increase in drag, expressed in %BW, as a function of running speed.

Running records in sprint races are not considered with wind speeds above 2 m s^{-1}.

Based on the quadratic nature of wind and drag, winds of about 2 m s^{-1} would have little impact on road races; however, when running speed is much higher (~10 m s^{-1} for an elite sprinter compared to 5.8 m s^{-1} for an elite marathoner) even small changes in wind speed have an important effect on the drag as is the case in faster sports such as cycling or speed skating.

Per World Athletics Competition Rule 31.14.3 (World Athletics 2024): "For performances made outdoors up to and including 200m [...] if the wind velocity, measured in the direction of running, averages more than 2 meters per second, the performance will not be ratified". When we apply our findings to Usain Bolt's record average speed of 10.43 m s^{-1} (Taylor and Beneke 2012), the drag force in a system with no wind would be approximately 25.5 N, about 2.7% of Bolt's 94 kg (Bolt's

projected frontal area is not considered). Supposing that Bolt had run with an added 2 m s^{-1} tailwind to the system, his drag would have been of 16.7 N (1.8% of BW) for a resultant wind speed of 8.43 m s^{-1}. Assuming Bolt maintains the same total mechanical power (~50 W kg^{-1}) (di Prampero et al. 2023), we can approximate an increase of 1.9% in running speed (equation Se3).

Perspective for future research based on comparable methods.

Wind tunnel studies are rather useful in understanding the relationship between the drag force applied to a runner and wind speed, based on the biomechanical adjustments of the drag area. However, wind tunnel testing requires substantial time and resources and therefore, cost-effective alternatives have been used to advance research without necessarily relying on the former, such as computational fluid dynamics (CFD) simulations or tractive devices that hinder/aid progression. For example, in the study of Da Silva et al. (Da Silva et al. 2022), the gross metabolic power was calculated when running against tractive forces ranging from 0-8 N which simulated running against impeding air resistance. The authors justified this range based on several CFD studies which estimated that drag forces on elite marathoners were between 6.6 -7.94 N (Polidori et al. 2020; Schickhofer and Hanson 2021; Beaumont et al. 2021). Based on our results, elite marathoners running at the official marathon record speed of 5.83 m s^{-1} experience a drag of ~8.1 N (~1.4% of *BW* for Eliud Kipchoge's 58 kg), a comparable result. Therefore, even if the kinematic intricacies of locomotion in the wind are difficult to capture using such cost-effective alternatives, they provide results that may be of interest to sports scientists.

Limitations

As the time required to match the nominal wind speed once changed was long, trials were only randomised by wind speed. This experimental protocol may have incurred fatigue and habituation bias to our results. Furthermore, although our sample size was decided based on a power analysis, timing, and funding constraints, it nevertheless remains small and composed of only male subjects. Thirdly, the subjects in our study are all professional or semi-professional athletes which is interesting when comparing our results to those of Pugh (1970) and Davies (1980) which both had experienced runners in their studies. However, in the studies of mechanical changes in slope locomotion (Dewolf et al. 2016, 2017b) and against tractive forces (Dewolf et al. 2020b; Mesquita et al. 2020) the subjects recorded were recreational runners making direct comparisons more difficult. Lastly, the method used here does not allow us to measure the individual limb *GRFs* during walking's double contact

phase, which is possible, among others with a split-belt treadmill. Therefore, one cannot directly calculate the simultaneous work done by each limb during the walking step-to-step transition (Donelan et al. 2002).

Conclusion

In conclusion, our findings expand our understanding of the interaction between wind and the biomechanics of human locomotion. Wind increases external work, alters the balance of positive/negative work, and adjusts the subject's C_dA. Locomotion in the wind shares similarities with walking and running on slopes or with a tractive force, albeit with the external force distributed across the frontal area of the body. This study offers insights for optimising performance, particularly in running, potentially aiding in breaking the official 2-hour marathon barrier. Moreover, understanding how gait is modified against external forces furthers our understanding on how one adapts the two fundamental locomotion mechanisms and provides part of the puzzle for understanding locomotor efficiency changes.

Supplementary Information

Fig. 3.2.S1 3D-drawing of the wooden platform around treadmill

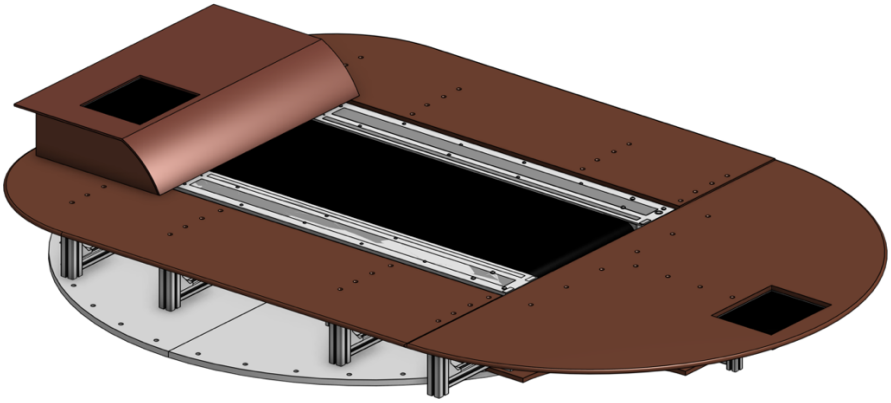

In-depth description of the method to compute the external work done

Computation of the acceleration, velocity and vertical displacement of the CoM

Calculations for the acceleration, velocity and displacement of the *CoM* were done as in Gosseye et al. (2010), Mesquita et al. (2020) and Dewolf et al. (2020b) and will, therefore, only be briefly explained here. The lateral component of the *GRF* was not considered since its contribution to the external work is negligible (Cavagna et al. 1963, 1976).

When moving in the wind on the level, the following forces were applied to the body: the body weight (*BW*), the *GRF* and the drag (F_d). In this case, over a complete number of strides, the average fore-aft ground reaction force ($\overline{F_y}$) was equal and opposite to F_d and the average vertical ground reaction force ($\overline{F_z}$) was equal to *BW*.

The acceleration of the *CoM* in the fore aft (a_y) and vertical (a_z) directions relative to a fixed reference frame attached to the wind tunnel was given as:

$$a_y = \frac{F_y - \overline{F_y}}{m}, \text{ and } a_z = \frac{F_z - \overline{F_z}}{m},$$

where m is the body mass. A time-integration of the a_y and a_z-curves by the trapezoidal method gave the fore-aft (V_y) and vertical (V_z) velocity changes of the *CoM* plus an integration constant. In the *y*-direction, since the subject moved at an average constant speed equal to the average treadmill belt speed (V_{avg}), the integration constant was computed so that the absolute value of the average horizontal velocity of the *CoM* equaled the absolute value V_{avg}. This computation did not consider the variation of the instantaneous belt velocity around V_{avg}. Indeed, since the work done by the subject to accelerate and decelerate the treadmill belt accounted for less than 3% of W_{com} (Dewolf et al. 2016) it was not considered in this study.

In the *z*-direction, since the subject is moving over level ground, it was assumed that over a full stride the upward displacement of the CoM is equal to its downward displacement, therefore the integration constant for V_z is equal to zero. Based on the latter, the vertical displacement of the *CoM* (S_z) was then computed by the time-integration of V_z (Cavagna 1975).

Calculations of External mechanical work (W_{ext}) and power ($\dot{W}_{ext}$)

The external power ($\dot{W}_{ext}$) developed during each step by the external forces applied to the body was computed as the algebraic sum of the power developed by the *GRF* ($\dot{W}_{com}$) plus the power developed to counter the drag ($\dot{W}_{drag}$).

$$\dot{W}_{ext} = \dot{W}_{com} + \dot{W}_{drag} = F\,V + \overline{F}_y\,v_{belt}\,, \qquad \text{(Se1)}$$

where F is the resultant vector of the forces exerted by the ground under the feet (*i.e.* the *GRF* vector), V is the velocity vector of the *CoM* relative to the fixed reference frame of the lab and $\overline{F}_y$ and v_{belt} are respectively the average horizontal ground reaction force and the average velocity of the belt, during a given step. The external work done during a step was then given as:

$$W_{ext} = \int_{t_1}^{t_2}\left(F\,V + \overline{F}_y\,v_{belt}\right)\,dt\,, \qquad \text{(Se2)}$$

where t_1 and t_2 were respectively the time at the beginning and end of the step. This equation considered the possible exchanges between the two sources of energy: the muscle-tendon unit and the wind.

In turn, the power done to sustain the *CoM* movements ($\dot{W}_{com}$) could be subdivided into two parts:

$$\dot{W}_{com} = F_y\,V_y + F_z\,V_z = F_y\,V_y + m\,(g + a_z)\,V_z, \qquad \text{(Se3)}$$

since $\int F\ V\,dt = \int F\,\frac{dS}{dt}\,dt = \int F\ dS$, the work W_{com} was computed as:

$$W_{com} = \int_{t_1}^{t_2} F_y\ dS_y + \int_{t1}^{t2} m\,(g + a_z)\ dS_z. \qquad \text{(Se4)}$$

At each instant of the step, the energy of the *CoM* (E_{com}) relative to a reference frame which lies parallel the treadmill belt surface was computed as:

$$E_{com} = \int F_y\ dS_y + \int m\,(g + a_z)\ dS_z = \frac{1}{2}\,m\,V_y^2 + m\,g\,S_z + \frac{1}{2}\,m\,V_z^2$$

$$E_{com} = E_{kf} + E_p + E_{kv} = E_{kf} + E_v \qquad \text{(Se5)}$$

where E_{kf} and E_{kv} were the kinetic energies of the *CoM* respectively due to its fore-aft and vertical velocities, and E_p was its potential energy and $E_v = E_p + E_{kv}$, the energy due to its vertical movements.

The two first curves of Figs. 3.2.2B and 3.2.3B represent typical traces of E_{kf} and E_v respectively during one stride of walking and one stride of running. The middle curves of Figs. 3.2.2B and 3B represent W_{drag}, the work done by the subject on the wind:

$$W_{\text{drag}} = \int_{t_1}^{t_2} \overline{F}_{\text{y}}\, v_{\text{belt}}\ \text{dt}. \qquad \text{(Se6)}$$

When moving against a wind force, the work (W_{f}) was done by muscle-tendon units during the contact phase to sustain the kinetic energy changes of the lower limb interaction with the ground but also to counteract the drag:

$$W_{\text{f}} = E_{\text{kf}} + W_{\text{drag}}. \qquad \text{(Se7)}$$

The bottom curve represents the external energy of the *CoM*, which was computed as the sum of the E_{v}- and E_{kf}-curves plus the curve W_{drag}.

$$W_{\text{ext}} = E_{\text{v}} + E_{\text{kf}} + W_{\text{drag}}. \qquad \text{(Se8)}$$

Positive (W_{f}^{+}, W_{v}^{+} and W_{ext}^{+}) and negative (W_{f}^{-}, W_{v}^{-} and W_{ext}^{-}) work were computed by respectively summing the increments and the absolute value of the decrements of the W_{f}, E_{v} and W_{ext} curves, respectively.

Fig. 3.2.S2 Step length in walking and running

In running (blue curves), step length, calculated as the magnitude of the average belt velocity multiplied by the step period, decreases as a function of increasing headwind ($F=14.98$, $p<0.001$), this difference is only marked at the highest headwind speeds (*post-hoc* $p<0.001$ between 12.5 and 15 m s^{-1} winds as compared to no wind). In walking, the contrary is true: step length tends to decrease ($F=8.13$, $p<0.001$) and is only different from no wind at the highest tailwind speeds (*post-hoc* $p<0.001$ between -15 m s^{-1} and no wind). These differences in step length are similar to those observed when walking and running against an external pulling tractive force (Dewolf et al. 2020b; Mesquita et al. 2020).

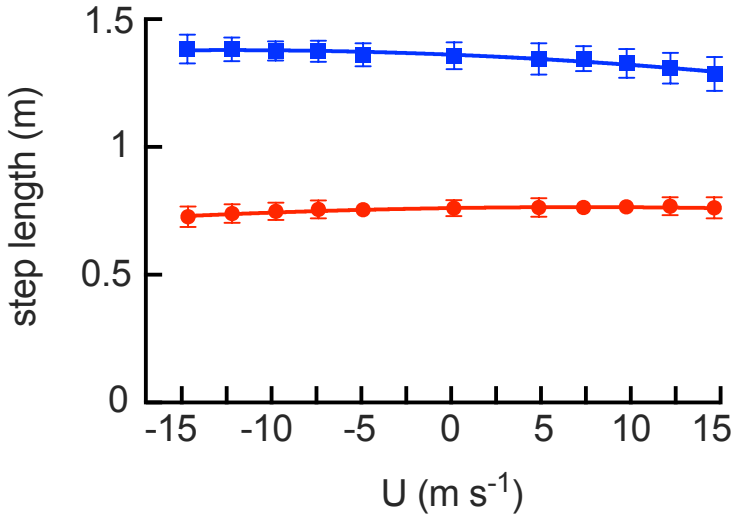

Step length as a function of wind speed. All marks, colours and symbols are the same as Fig. 3.2.3.

Fig. 3.2.S3 Duration of the positive (t_{push}) and negative (t_{brake}) work phase as a function of wind speed

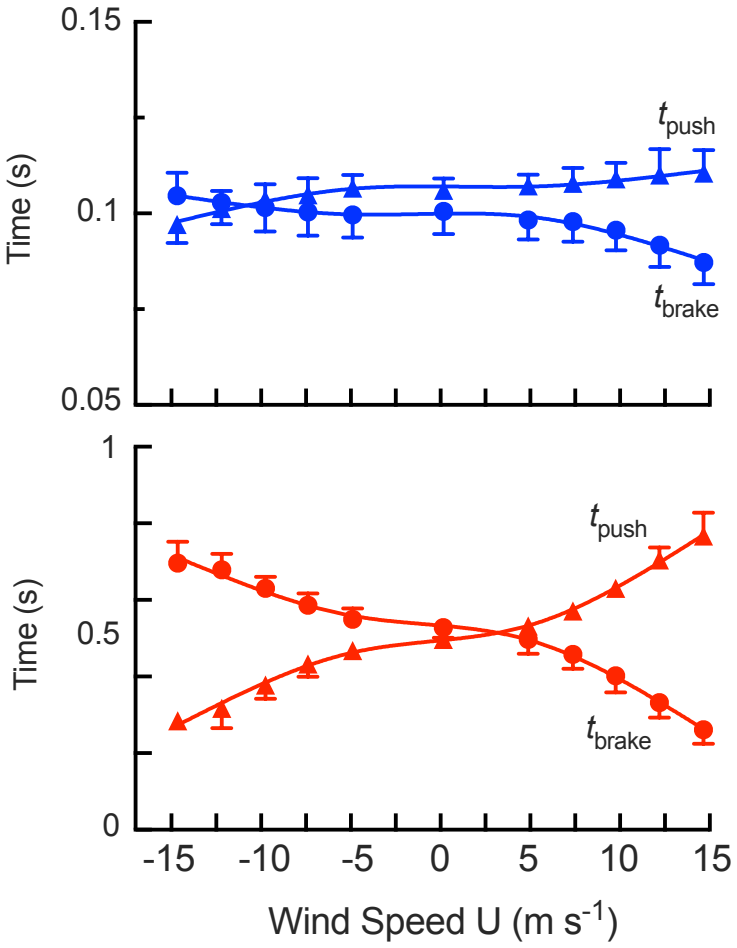

Duration of the positive work phase (t_{push}, triangle) and the negative work phase (t_{brake}, circles) during one step while running at 4 m s^{-1} (blue) and walking at 1.5 m s^{-1} (red) as a function of wind speed. During a running step, there was one positive work phase during which MTUs provided energy to lift and accelerate the *CoM* and one negative work phase during which MTUs absorbed energy to lower and decelerate the *CoM*. During a walking step, there were two phases of positive work: one during which the *CoM* is accelerated forwards (phase *a*) and one during which the *CoM* is elevated (phase *b*). In this case, $t_{push} = a + b$. Similarly, t_{brake} is the sum of

duration of the negative work phase during which the *CoM* is lowered plus the duration of the negative work phase during which the *CoM* is decelerated.

When running in still air, t_{push} is slightly longer than t_{brake} because MTUs can develop greater force during eccentric contraction than concentric contraction. When headwind speed increases t_{push} increases while t_{brake} decreases. With increasing tailwind, t_{push} decreases while t_{brake} increases. However, t_{push} becomes smaller than t_{brake} with only strong tailwinds.

When walking in still air, t_{push} and t_{brake} are about equal. With headwinds, $t_{push} > t_{brake}$ whereas with tailwinds $t_{push} < t_{brake}$. In both directions, the difference between t_{push} and t_{brake} increases with wind speed. In both gaits, with headwinds, the longer t_{push} allows MTUs to produce energy over a longer time, thus reducing the average power developed during the push. In the same manner, with tailwinds, the longer t_{brake} allow to reduce the average power developed during the brake period.

Comparison of moving uphill and downhill and moving with a headwind and tailwind.

As compared to moving in still air, in the presence of wind, additional positive/negative work must be done to maintain the average horizontal speed of the *CoM* constant from one stride to the next. Similarly, when moving on a slope additional positive/negative work must be done to raise/lower the *CoM* in the vertical direction. From a metabolic standpoint, similarities have been documented between walking-running with head and tailwind and walking-running uphill and downhill (Davies 1980) however no consensus exists. Here we have addressed these issues from a mechanical point of view.

Firstly, we can draw parallels in the vertical *GRF* reported in slope running and their characteristic foot fall patterns, *i.e.* greater heel strike impacts in downhill running vs. forefoot striking in uphill running (Gottschall and Kram 2005) and the vertical *GRF* observed here (Fig. 3.2.3). Secondly, when comparing our data in the wind with those of Dewolf et al. (2016) for running and Dewolf et al. (2017b) for walking on a slope, we found certain degrees of commonalties in the amount of positive/negative external work performed. Indeed, if the drag is expressed as a percentage of *BW* or as a function of squared wind speed, U^2, and if the change in slope is expressed as a percentage of the forward displacement, the external work W_{ext}^{+} and W_{ext}^{-} done when head- or tailwind increases is similar to the W_{ext}^{+} and W_{ext}^{-} when a positive or negative slope gets steeper (Fig. 3.2.S4A & B). The net work ($\Delta W_{ext} = |W_{ext}^{+} - W_{ext}^{-}|$) done against the drag, expressed as a function of U^2 (F_d is related to the square of *u,* equation 4) and on a slope both similarly increase linearly

(Fig. 3.2.S4C). Note also that the ratio between the negative external work and the total external work done in running *i.e.* $\frac{|W_{ext}^-|}{|W_{ext}^-|+W_{ext}^+}$ as a function of U^2 (Fig. 3.2.S4D) shows a similar relationship to the one described by Minetti et al.(1994) while running on a slope. A similar relationship was also observed between $\frac{|W_{ext}^-|}{|W_{ext}^-|+W_{ext}^+}$ while walking on a slope (Minetti et al. 1993) and while walking on the level with a horizontal tractive force (Dewolf et al. 2020b). In other words, external work in slope locomotion and when moving against/with a pulling tractive force is proportional to the square of wind speed.

The similarity between wind and slope observed from the metabolic point of view by Davies (1980), may thus be explained by the similar work done in both situations. This may seem peculiar since when moving in the wind, muscle tendon units (MTUs) do work each step to overcome a rather small force (F_d <10% *BW*) over a long distance, whereas when moving on slope, MTUs do work each step against an important force (*BW*) over a shorter distance. The fact that the curves of Fig. 3.2.S4, obtained in the two situations, are very close to each other suggests that metabolic energy consumption and gait pattern are related to the work done rather than to the magnitude force developed. Furthermore, the direction of the force exerted doesn't influence the amount of external work done.

Note also that the W_{ext} measured in the wind is slightly lower than W_{ext} when moving on a slope (Fig. 3.2.S4). In our study, as in Pugh (1971) and in Davies (1980), experimental subjects were professional or semi-professional runners. However, the analysis of mechanical changes in slope locomotion (Dewolf et al. 2016, 2017b), were done on recreational runners, making direct comparisons more difficult. Indeed, it is well known that with running experience, the mechanical work performed decreases (Bianchi et al. 1998; Zagatto et al. 2023). Previous studies have shown, both in walking (Dewolf et al. 2020b) and in running (Mesquita et al. 2020), that W_{ext} while moving on a slope of *n*% (0%<*n*<15%) is equivalent to W_{ext} while moving on the level, with a horizontal tractive force representing *n*% of *BW*. When moving in the wind, we also observe a similarity between the magnitude of the drag and the magnitude of the tractive force (Fig. 3.2.S4 in Supplementary Material). The small difference in W_{ext} between wind and tractive force may be firstly due to F_d being applied to the whole body, whereas the tractive force is only applied on a point close to the position of the *CoM*.

Fig. 3.2.S4 Comparison of moving uphill and downhill and moving with a headwind and tailwind.

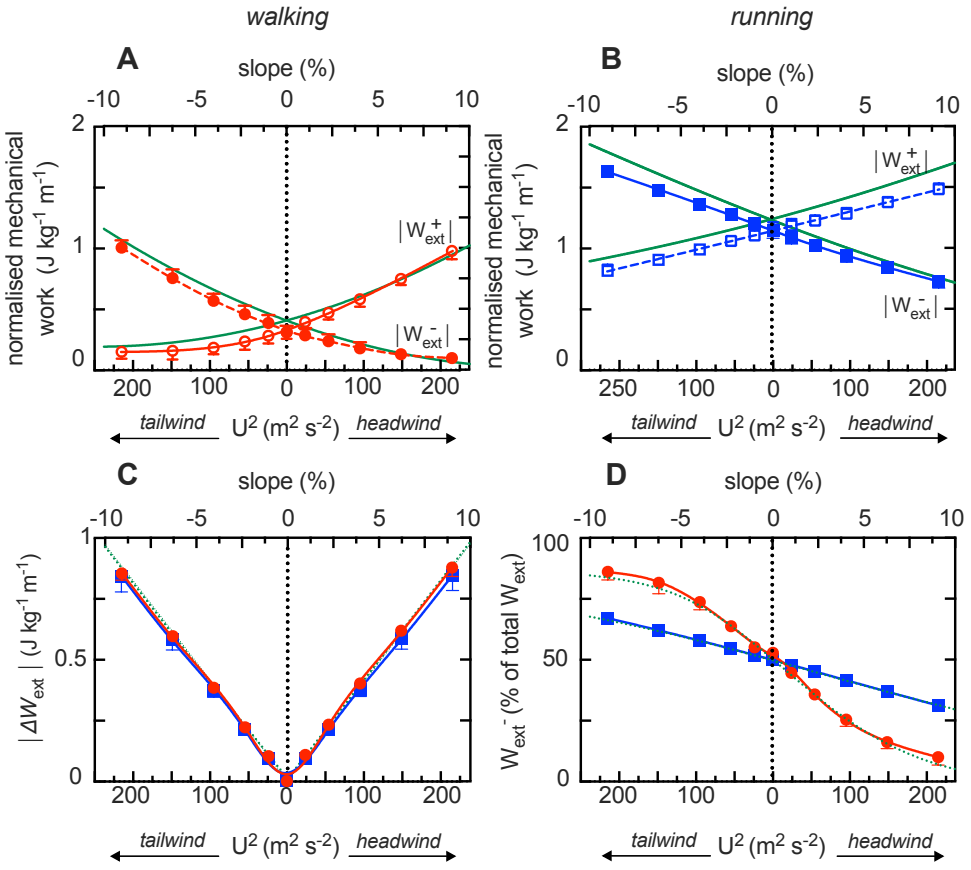

Comparison of moving uphill and downhill and moving with a headwind and tailwind. *For the slope, data are presented as a function of the percentage of inclination. For the wind, since drag is proportional to the square of wind speed, data are presented as a function of U^2 multiplied by the direction of the wind. Red and blue lines and symbols correspond respectively to walking and running in the wind. The green lines correspond to slope locomotion.* ***Panels A and B)*** *Comparison between the mass-specific external work done per unit distance in walking and running.* ***Panel C)*** *Comparison between the net mechanical work done ($\Delta W_{ext} = |W_{ext}^{+} - W_{ext}^{-}|$).* ***Panel D)*** *Ratio between the negative external work and the total external work computed as $\frac{|W_{ext}^{-}|}{|W_{ext}^{-}|+W_{ext}^{+}}$ in walking and running. Slope data are from Dewolf et al. (2017b) for walking and Dewolf et al. (2016) for running.*

Fig. 3.2.S5 Comparison between walking and running in the wind and with a tractive force

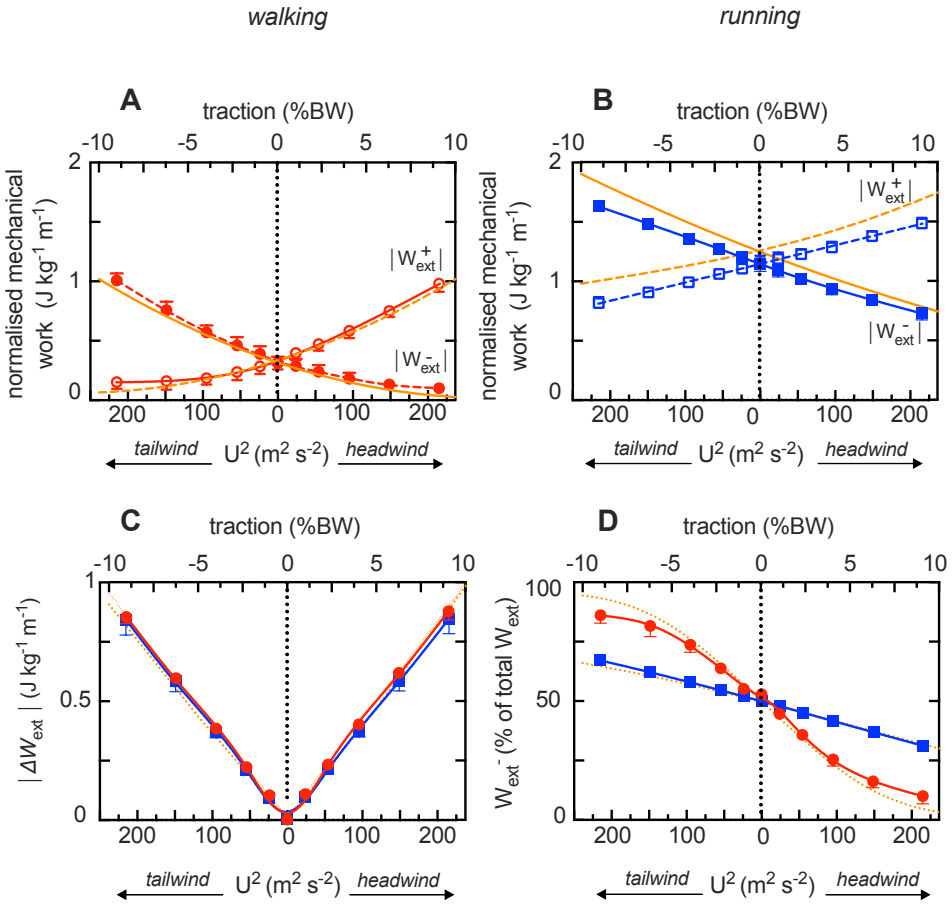

Comparison of moving with a hindering/aiding tractive force and moving with a headwind and tailwind. *For the tractive, data are presented as a function of the percentage of body weight. For the wind, since drag is proportional to the square of wind speed, data are presented as a function of U^2 multiplied by the direction of the wind. Red and blue lines and symbols correspond respectively to walking and running in the wind. The orange lines correspond to locomotion against a tractive force.* ***Panels A and B)*** *Comparison between the mass-specific external work done per unit distance in walking and running.* ***Panel C)*** *Comparison between the net mechanical work done ($\Delta W_{ext} = |W^+_{ext} - W^-_{ext}|$).* ***Panel D:*** *Ratio between the negative external work and the total external work computed as $\frac{|W^-_{ext}|}{|W^-_{ext}|+W^+_{ext}}$ in walking and running. tractive data are from Dewolf et al. (2020b) for walking and Mesquita et al. (2020) for running.*

Fig. 3.2.S6 Drag force expressed in %BW as a function of the headwind speed while running overground

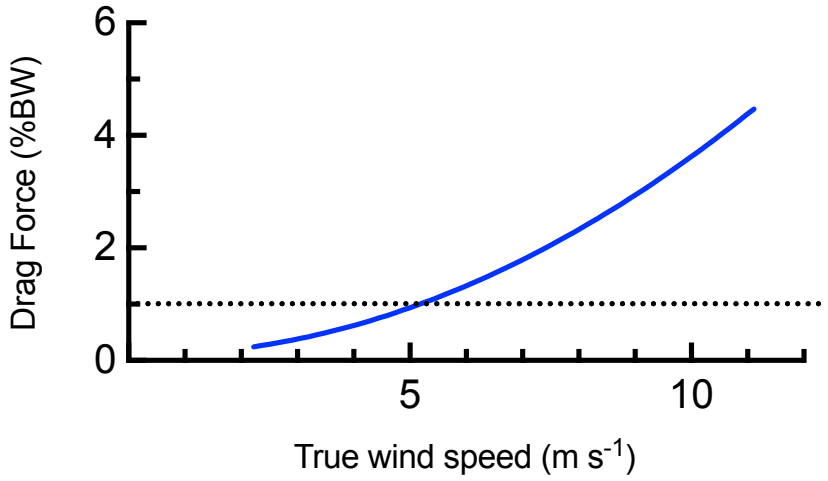

Transposition of the results obtained on a treadmill in a wind tunnel to overground running against the wind

The figure represents the drag force expressed as a percentage of the subject average body weight (647.46 N) calculated when running at 4 m s^{-1} as a function of the true wind speed when running on the ground (i.e. the wind speed in the tunnel minus the speed of the treadmill belt). The dotted line represents 1% of *BW* which corresponds to a 1% incline of the treadmill.

Suppose that we are running on the ground in still air. The blue curve here above will then represent the drag of the apparent wind speed generated by the movement of the subject.

Jones and Doust proposed that a 1% incline of the treadmill would simulate overground running in still air (Jones and Doust 1996). As shown here and explained in Van Hooren et al. (2020), a 1% incline corresponds to a drag force at ~5 m s^{-1}. These results show that a 1% incline overestimates the drag force in still air when moving at speeds below ~5 m s^{-1} and underestimates this drag force when moving at higher velocities.

Table 3.2.S1

Wind Speed (m s $^{-1}$)	Walk Run	Wind direction	F_d (N)	C_dA (m^2)	Trunk incl. (°)
0	W	/	0.15±0.48	/	89.43±2.3
	R		0.16±0.77	/	85.07±3.3
5	W	Tail	-6.90±0.58	0.51±0.04	91.25±2.7
	R		-6.53±0.39	0.48±0.03	85.92±3.1
	W	Head	7.29±0.70	0.54±0.05	88.00±2.3
	R		6.26±0.77	0.46±0.05	83.98±3.2
7.5	W	Tail	-14.76±1.40	0.48±0.04	92.12±2.6
	R		-14.21±1.16	0.46±0.04	86.70±3.5
	W	Head	15.56±1.51	0.50±0.05	86.60±3.5
	R		13.53±1.39	0.44±0.04	81.7±3.76
10	W	Tail	-25.48±1.96	0.47±0.04	93.52±3.1
	R		-24.59±2.01	0.45±0.03	87.77±3.2
	W	Head	22.76±2.03	0.49±0.05	84.36±3.4
	R		22.82±1.82	0.42±0.03	80.08±2.9
12.5	W	Tail	-39.65±3.49	0.47±0.04	94.79±3.1
	R		-37.96±2.90	0.45±0.03	89.21±3.5
	W	Head	41.10±3.34	0.49±0.03	81.26±3.9
	R		35.50±2.71	0.42±0.03	77.55±3.2
15	W	Tail	-56.69±4.76	0.46±0.04	96.17±3.6
	R		-54.21±3.90	0.44±0.03	85.51±4.3
	W	Head	58.27±3.85	0.48±0.03	78.40±4.5
	R		49.87±3.43	0.41±0.03	74.84±2.8

Average and standard deviation of the drag (N), C_dA (m^2) and trunk inclination as compared to the horizontal (°) in walking (W) and running (R) against head and tail winds as a function of wind speed.

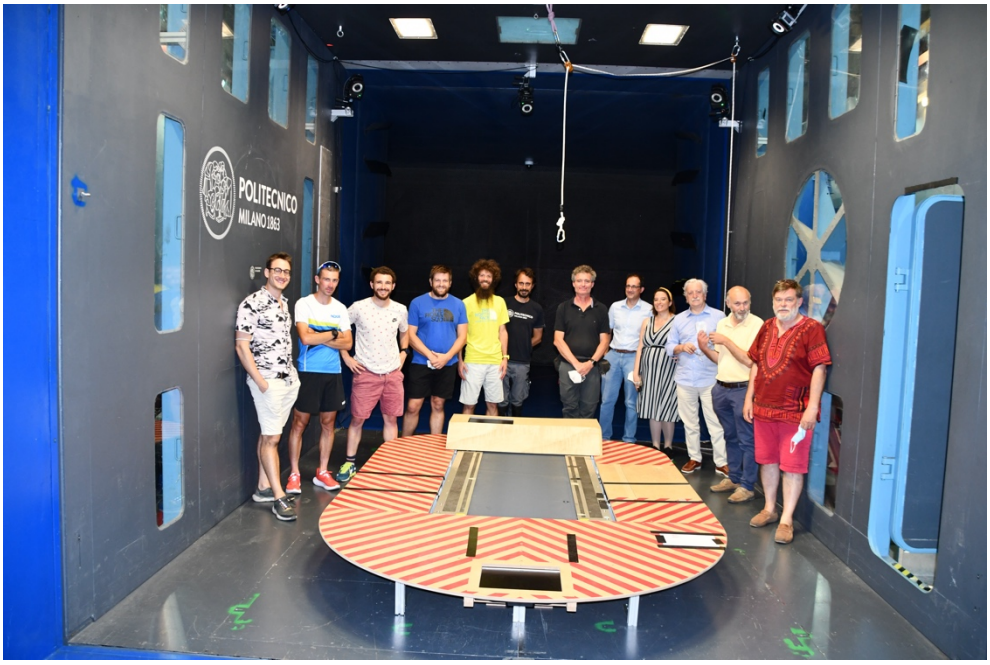

Experimental team, composed of three research groups, for the wind tunnel experiments. From left to right: Francesco Luciano, subject of the day, Raphael Mesquita, Arthur Dewolf, Gaspare Pavei, Donato Grassi, Mario Legramandi, Matteo Pecchiari, Giovanna Catavitello (and daughter), Alberto Minetti, Giuseppe Gibertini & Patrick Willems.

Chapter 4. General discussion

Locomotion enables organisms to move through a surrounding that typically resists movement: bacteria move through extracellular fluid, fish swim in water, birds fly in air, *etc*. (Tucker 1975). On land, animals must use mechanical energy to support their weight, move, and perform work against the environment. Movement also demands the intricate coordination of muscular, neurological, and other physiological systems. To explain movement, scientists have studied the detailed physiology of muscles, ligaments, and joints (Hill 1913), but also conducted key experiments in animals to explore the role of the CNS locomotor regions in the brain and spinal cord (Noga and Whelan 2022). While locomotion can be described as a cascade sequence—brain activates muscle, muscle moves skeleton, skeleton acts on the environment—such an approach overlooks the dynamic feedback that occurs between and within each level. The challenge in studying the underlying mechanisms lies in understanding how each component of the locomotor system functions on its own while also discovering how they collectively operate as an integrated system (Dickinson et al. 2000).

Through comparative modelling of locomotion, physiologists, such as G.A Cavagna and colleagues have provided a clearer understanding of its mechanisms. The study of the mechanical energy fluctuations of the CoM during walking and running has revolutionised the field of biomechanics. Walking can be modelled as a pendulum-like system where the CoM's potential and kinetic energy levels are transferred from one to the other. Whereas running can be compared to a bouncing mechanism, where the energy due to the vertical and fore-aft movement of the CoM decreases and increases in phase, mimicking a storage-release system of elastic energy (Cavagna et al. 1963, 1964).

In addition to enabling the characterisation of running biomechanics, it has been hypothesised that the CoM trajectory serves as a target for motor control in legged locomotion (Alexander 1984; Lee and Farley 1998; Ivanenko et al. 2008). It has also been suggested to provide feed-back signals for task-oriented control in posture (Lockhart and Ting 2007; Welch and Ting 2008). Furthermore, CoM displacement depends on the combined movements and coordination of the limb segments, thus, to fully grasp how an integrated system 'codes' for movement, one must also understand the dynamics of the limb segments and their joints.

Considering this, the goal of this thesis was two-fold: 1) to challenge the locomotor system to better understand the modifications or deviations of the CoM mechanical model and 2) gain insight in the interaction between neural commands

and mechanical output of the system. Exaggerating performance, through specific gait modifications, makes structure-function relationships more evident (Dickinson et al. 2000).

Therefore, we firstly investigated gait modifications where no additional work was done against the environment (step frequency, chapter 2.1 and curved running, chapter 2.2 & 2.3). Then, building on the work conducted in our laboratory on slope locomotion (Dewolf et al. 2016, 2018), and P.E di Prampero's work on sprint energetics (di Prampero et al. 2005), we investigated how comparable external forces affected the CoM mechanics (tractive running, 3.1 and wind locomotion, 3.2). While running with tractive forces could be an effective training method, it is somewhat artificial, as humans rarely need to pull loads proportional to a percentage of their body weight in everyday life. Our collaboration with aerodynamic experts from *Politecnico di Milano* and biomechanists from *Università degli Studi di Milano*, formed the first team since the early 1980s to conduct large scale experimental studies on human locomotion in a wind tunnel.

The following sections aim to summarise the findings described in the chapters above and propose situations to explain how either system adapts and or struggles to do so when gait is challenged, further elucidating the relevance of our work.

Mechanical work

To best isolate non-environmental bouncing mechanics modifications, we used an experimental condition which is rather infrequent in nature: the subject runs on level ground, at constant speed, with the foot not skidding on the ground and air resistance being negligible. In such situations, the work against the environment is nil and the external work, W_{ext}, is only due to the work done to maintain the movements of the CoM (*i.e.* $W_{ext} = W_{com}$). From this, the total mechanical work done by the body can be computed as $W_{tot} = W_{ext} + W_{int}$, where W_{int} is the work done to move the limb segments relative to the CoM.

Altering a subject's step frequency (SF) has been shown to vary the amount of external and internal contribution of W_{tot} (Cavagna et al. 1991). We confirmed previous observations that a given speed, running at high SFs results in smaller steps, decreasing the work done to move the CoM (*i.e.* lesser W_{com}), but resulting in faster movements to reset the lower limbs for the following step which increases, W_{int}. Oppositely, running at low SFs results in an increased W_{com} done to increase the lower limb impulse which aids in aerial propulsion but a progressively decreasing W_{int} done to reset the limb at each step.

In curved running, we proposed an adapted method to understand the CoM trajectory and quantify the work done to maintain the CoM movements in the transverse plane. W_{com} increased as the radius of curvature decreased since the CoM was required to do more work to sustain the inward motion. At the smallest radius, we observed a difference in the role that the inner and outer limb play when turning: the inner limb did more work than the outer limb to deviate the CoM laterally whereas the outer limb did more work to accelerate the CoM "forwards", (*i.e.* along the tangent of the curve). Consequently, albeit increased compared to straight-line running, the work necessary to move the CoM in the transverse plane was approximately the same in the inner and outer limb.

In situations where the environmental conditions are no longer negligible, W_{ext} is done both to sustain body motion, W_{com}, but also do work against the environment, W_{env} ($W_{ext} = W_{com} + W_{env}$). In the frame of this work, we have studied two different situations: locomotion against tractive forces and locomotion in the wind. When the additional external force hinders progression, an imbalance exists between the positive and negative work done to sustain CoM motion, respectively W_{ext}^{+} and W_{ext}^{-}, tipping towards W_{ext}^{+}. The contrary is observed when running with an external force aiding progression. In the latter, the imbalance tips towards W_{ext}^{-}.

Throughout chapter 3, we explain how the metabolic similarity observed when moving against tractive forces or against wind forces on the level (Davies 1980; Lloyd and Zacks 1972), and on slope locomotion may be explained by the similar mechanical work done in both situations. This may seem peculiar since when running against a horizontal hindering force, the MTUs are doing work each step to overcome a rather small force (~10% of BW) over a long distance, whereas when moving on slopes, the MTUs are doing work each step against an important force (BW) over a shorter distance. Here we showed that the direction in which the force was exerted does not influence the amount of external work done, leading to similar metabolic energy consumption, mechanical work and gait coordination patterns.

A practical application: the evaluation of mechanical workload using a GPS-tracking device[1]

Based on the mechanical and metabolic similarities between slope running and accelerative sprinting explained above (di Prampero et al. 2005), we were able to extrapolate the notion of "equivalent slope" explained in the beginning of chapter 3 to observe the mechanical variations of speed on level ground (Fig. 3.0.1).

Indeed, while di Prampero's method provides useful information on the metabolic cost, it does not reflect the mechanical workload performed, a variable more closely related to muscle damage (Simmons et al. 2021) which could provide key performance data for managing sports practice. The metabolic cost of an eccentric muscle contraction is approximately four times lower than that of a concentric muscle contraction (Abbott et al. 1952). Although these deceleration phases are not metabolically demanding, they do generate greater muscle damage, increased delayed onset muscle soreness and have a higher injury rate (Stožer et al. 2020).

From the documented biomechanical similarities, we developed an algorithm estimating the instantaneous mechanical workload based on the fore-aft speed variations of an athlete's movements. From the accelerative/decelerative phases during their activity, we estimated the positive and negative mechanical work of the CoM based on the published data of slope running (Dewolf et al. 2016).

The study was designed in two parts. Firstly, the positive and negative increments and net difference of the work done to move the CoM over one metre normalised by body mass (W_{com}^{+}, W_{com}^{-} in J kg^{-1} m^{-1}) were calculated for each subject in Dewolf et al. (2016). When running uphill/downhill, the length normalised net work done ($W_{\mathrm{net}} = |W_{\mathrm{com}}^{+}| - |W_{\mathrm{com}}^{-}|$) corresponds to the minimum vertical work necessary to overcome the slope over a horizontal distance of 1 m. W_{net} is only dependent on the inclination (α) of the terrain (di Prampero et al. 2005). From these calculations, an exponential regression was applied to both measured W_{com}^{+} and W_{com}^{-}

[1] Modified from a conference paper published as: Evaluation of mechanical workload using a GPS-tracking device, R.M. Mesquita and A.H. Dewolf (2022) *Computer Methods in Biomechanics and Biomedical Engineering*

variables to calculate theoretical values of each work increment done at higher/lower slopes than the ones analysed in the study, *i.e.* in slopes outside of a positive and negative 3° - 9° range. Both the regressions had a $r \geq 0.97$ and allowed us to estimate values for all slopes which went beyond those recorded experimentally. Secondly, using the equivalent slope (α) calculations of di Prampero et al. (2005), the positive/negative and net mechanical work as well as the instantaneous positive and negative mechanical power were approximated on subjects running on level ground with a varying speed (Fig. 4.1).

Although the tracking of different data during training sessions and matches is not novel, the extrapolation of this data to obtain instantaneous work and power values is. Such information is useful as it gives insight into the power required to accelerate and brake the movements of the CoM. Such data can shed light on high intensity phases done positively (concentrically) and negatively (eccentrically) during a session, which in turn could be indicative of the kind stress the subject is performing (Fig. 4.1). The estimation of work, power, and workload is not only useful for a better follow-up in training sessions and in-game but also as a potential comeback from injury marker, as eccentric contractions generate more muscle damage than concentric contractions. Relating these findings to muscular fatigue variables such as creatine kinase values and muscular fatigue in other team sports could be interesting.

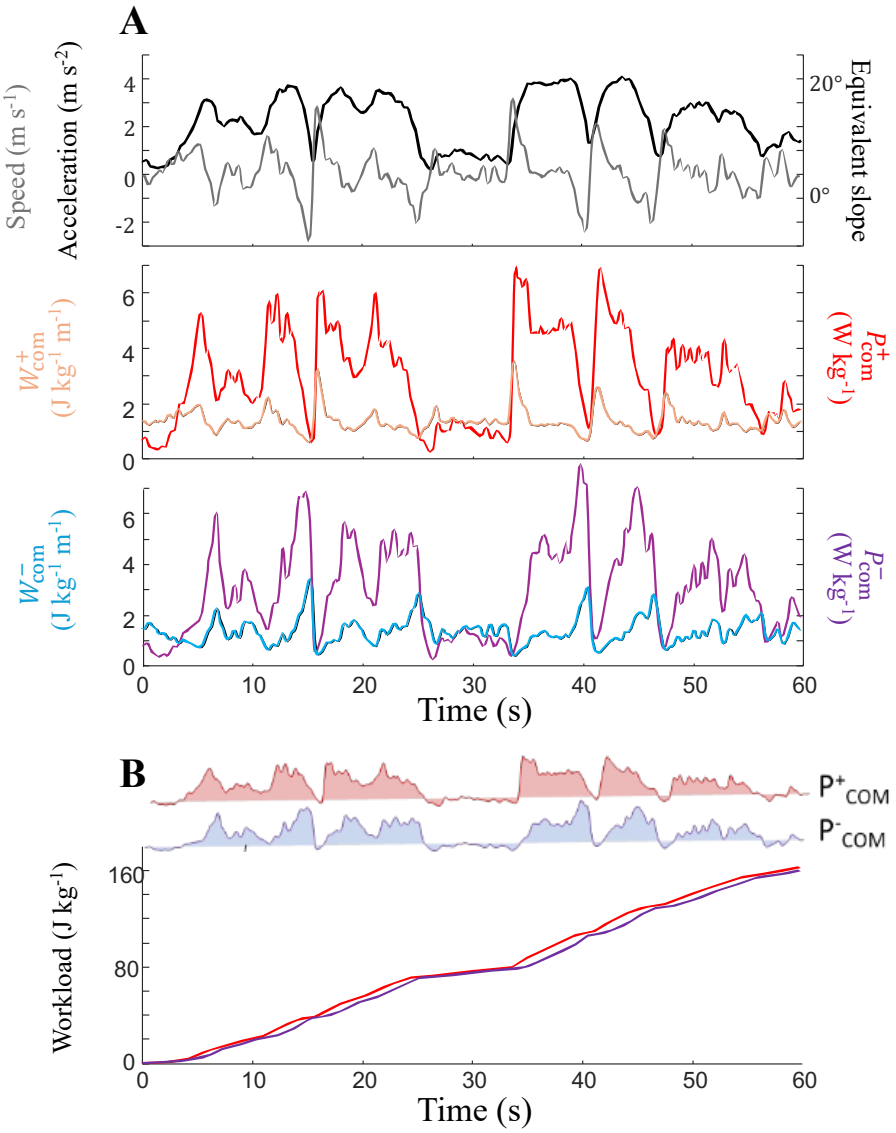

Fig. 4.1 A) *60s window of a football player's training session. From top to bottom:* ***A-*** *the speed (grey) and acceleration (black); the extrapolation of the* W^{+}_{com} *and* P^{+}_{com}*; the extrapolation of the* W^{-}_{com} *and* P^{-}_{com}*.* ***B)*** *total positive (red) and negative (blue) workload over the running session.*

Using the bouncing mechanism as a performance indicator

In its athletic role, running performance has been a key focus since Ancient Greece, *circa* 776 BCE, where the winner of the '*stade-race*' (short-foot race) had the Olympiad named in his honour (Swaddling 2015). From a competitive perspective,

running performance is typically evaluated based on speed: faster athletes outperform the slower ones (Emig and Peltonen 2020). Therefore, understanding running performance in relation to the bouncing mechanism should emphasise the changes that occur with increasing speed. As speed increases, lower-limb spring stiffness also increases allowing the system to operate more efficiently (Cavagna et al. 1988; Cavagna 2010). Greater stiffness in the muscles enhances muscular activation resulting in larger force production (Morgan 1977; Kyröläinen et al. 2005).

In chapter 2.1 we showed that increasing SF at a fixed speed also increases k_{vert}. Athletes that are better trained (*i.e.* that have higher average $VO_{2,max}$) showed increased SFs, and thus increased lower limb stiffness at similar speeds. These athletes had a smaller t_{ce} and larger t_{ae} as compared to lesser trained athletes, leading to a greater $t_{ce} - t_{ae}$ asymmetry and a more effective force application on the ground (da Rosa et al. 2019). Similarly, athletes who are habitually confronted with both eccentric and concentric contractions (such as football players), similarly show larger $t_{ce} - t_{ae}$ asymmetry and greater k_{vert}, as compared to athletes which are habitually only using concentric contractions (such as swimmers) (Nuñez Lisboa et al. 2021).

A second mechanism describing the spring characteristics is the landing-takeoff asymmetry described by Cavagna (2006) (used in chapters 2.1, 3.1, and 3.2). When increasing speeds, muscles switch from having more compliant concentric contractions at lower speeds to *quasi*-isometric contractions at higher speeds (Cavagna 2006). Indeed, running at slow constant speeds requires less force production and muscles are content in deviating from an elastic rebound by increasing the propulsion time ($t_{push} > t_{brake}$) to conserve momentum. Higher speed running requires greater force generation, therefore by relying more on the stretch-shortening of the elastic tendon and less the muscle's concentric capabilities to restore work, the MTU hysteresis is reduced leading to a more efficient spring (Cavagna 2006, 2009). Although da Rosa et al. (2019) do not observe significant differences between higher and lesser trained runners. Athletes who do not run nor perform regular stretch-shortening cycle contractions, have a larger landing-takeoff asymmetry than those who regularly run (Nuñez Lisboa et al. 2021). Furthermore, we have shown that characterising the t_{push} and t_{brake} is an effective manner to explain the general parameters of the spring both in situations with and without work done against the environment applied to the system (chapters 2.1 & 3.1).

Thus, describing the bouncing gait performance by the landing-takeoff asymmetry is a useful variable when observing large differences, like those of swimmers *vs.* footballers, however they are perhaps not sensitive enough to

distinguish smaller differences in habituated runners. A more fine-tuned approach to characterising the bounce-mechanics seems to be its spring stiffness properties.

When the bouncing mechanism fails to capture the entire picture

The model described by Cavagna (1988) and Blickhan (1989) almost at the same time, despite its vast usefulness in characterising running mechanics, is not infallible. The spring-mass system supposes that the lower limb works as a (almost) perfect linear symmetrical spring over a step cycle (Cavagna 2006; Cavagna et al. 2008b). However, the model tends to lose its efficiency and fail mechanically when energy needs to be added to or dissipated by the system, as in running on a slope (Dewolf et al. 2016). To solve for this, an actuator/damper must be added to the model to account for these energy changes. Here, we show that the optimisation of the spring is also modified over steady state conditions, such as that of constant average speed over ground running with a change in SF.

At higher SF, the elastic bounce of running is accentuated (acting more like a linear spring, with little force-length hysteresis) as the MTU becomes stiffer and runners naturally adopted a more symmetrical rebound pattern ($t_{ce} \approx t_{ae}$). In this situation the duration of the downward and upward phases of vertical oscillation are nearly equal, reducing the hysteresis of the spring leg.

On the contrary, running at low SF reduces the efficiency (increased hysteresis) of elastic rebound, regardless of speed. In situations such as low SF, where no clear addition or dissipation of energy is required in the system, one cannot theoretically justify including an actuator to the model to compensate for the loss in efficiency. Indeed, the subject maintains a constant speed and does not gain or lose height over the step, they should therefore maintain a *quasi*-linear relationship over the stance phase. Yet, we see a greater hysteresis, particularly at faster speeds (Fig. 2.1.3A).

The spring-mass model and the CoM mechanics are not able to account for soft tissue energy dissipations, which have been shown to increase with speed (Riddick and Kuo 2016, 2022). Soft tissue energy dissipation occurs in non-contractile elements of the body (heel pad and foot arch compressions, visceral sway, cartilage and intervertebral disc compressions, *etc.*) and affects the work production during locomotion (Riddick and Kuo 2016, 2022). We hypothesised that, at low SF, the runner increased the amount of energy dissipated by their soft tissues as the impact with the ground is increased. Thus, to maintain constant speed, the muscles must actively reset the energy lost and increase the amount of positive mechanical work to counter this dissipation. As a result of this, the lower limb muscles no longer act as

perfect linear springs capable of balancing braking as propulsive movements of the CoM equally and the model would fail to account for this scenario (Dewolf et al. 2024).

In Dewolf et al. (2024), we proposed an adaption to the spring-mass force-displacement curve from a method adapted by Gill et al. (2020) and Dewolf et al. (2016). We suggested using the force vector (rather than only F_v) projected along the leg ($F_{projected}$) and the displacement of the leg, measured as the distance between the trochanter and $V^{th.}$ metatarsal (L_{leg}) (Fig. 4.2). The compression of the leg starts at touch down until the minimum of L_{leg}, followed by the leg decompression (Fig. 4.2). In this revised model, the spring-mass, accompanied by a damper, accounted for the lower limb motion working proportionally to its velocity.

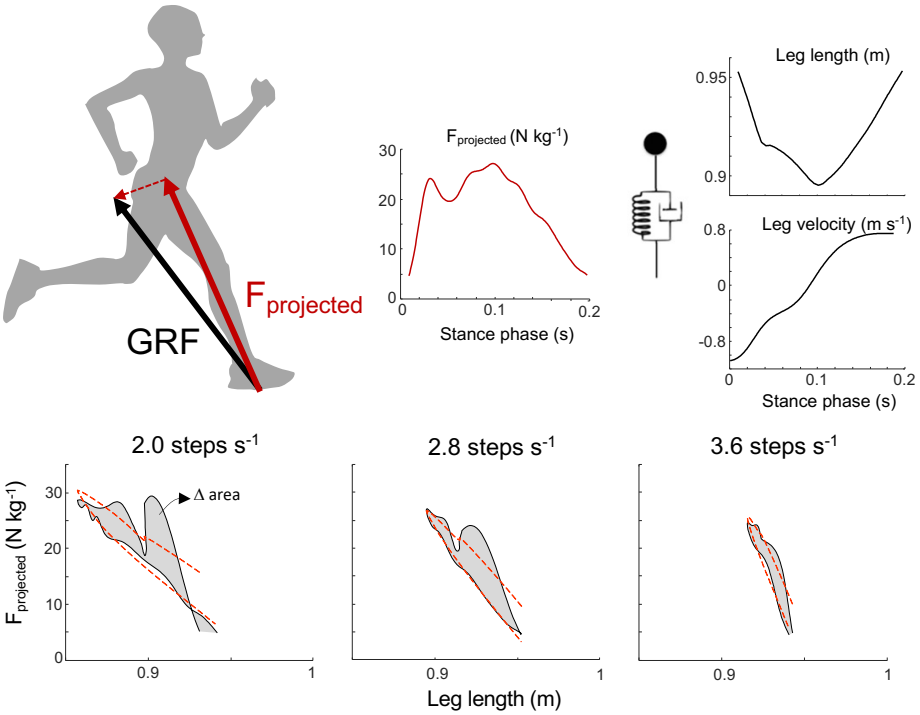

Fig. 4.2 Schematic representation of the method used to computed leg stiffness. *On the right, one typical trace of the force projected on the leg, the leg length and leg velocity during a typical step. Below are typical traces of the projected force during the contact period plotted as a function of leg length during running at 2, 2.8 and 3.6 steps s^{-1} at 14 km h^{-1}. The red dashed lines correspond to the predicted value of $F_{projected}$ computed using the values of the adapted model. The hysteresis (grey area) in the F-L curves shows the amount of energy dissipation within in the step which must be reset. Modified from Dewolf et al. 2024.*

As running speed increases, particularly at lower frequencies, the area (hysteresis) between the compressive and decompressive phases of the adapted force-length curve increases (Fig. 4.2), suggesting a deviation from a linear elastic behaviour. This deviation from the simple spring-mass model demonstrates that part of the work must always be actively performed by the muscle. At higher step frequencies, together with the already documented increase in lower-limb stiffness, a reduction of the hysteresis supports the optimisation of the elastic mechanism documented in chapter 2.1 (Mesquita et al. 2024a).

Interestingly, this compression-decompression area was positively associated with the total soft tissue work dissipation, indicating that the deviation from an elastic spring can be partly related to the energy fluctuation of the soft tissues (Fig. 4.3). Note, this energy fluctuation can also be partly due to other factors, such as treadmill compliance and ground vibrations and resonance.

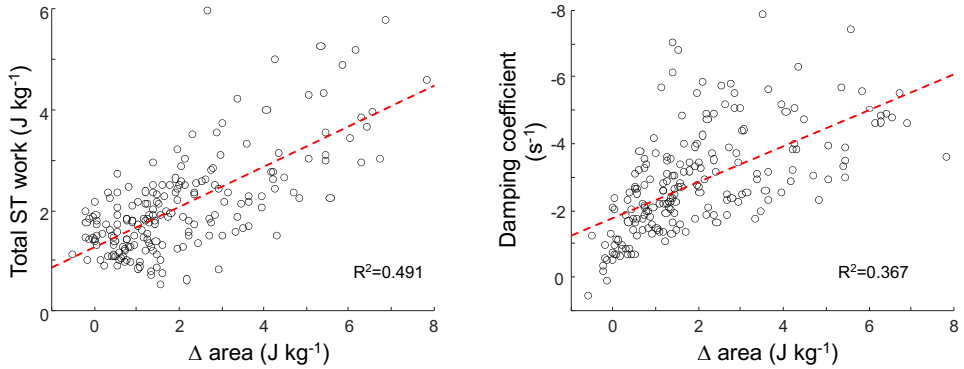

Fig. 4.3 *Correlations between the area between the compression and decompression phase of the force-displacement curve (normalised by body weight) and other gait parameters. Each point represents the stride-averaged value for one subject. Linear regression lines are also plotted. Left - Relationships between the area and the total soft tissue work (positive + negative). Right - Relationships between the area and the damping coefficient of the damped spring-mass model. The R^2 values are indicated on each graph. From Dewolf et al. (2024).*

The use of this updated method for evaluating the bouncing mechanism by quantitatively assessing the stiffness and damping coefficient may open new areas of investigation of muscle physiology during running. For example, in situations where the spring model does not fill all its initial assumptions (Cavagna 2009), *e.g.* the accentuation of the asymmetry between energy storage and release in the MTUs as in tractive running or against wind forces, this adapted technique could provide a more reasonable measure of the spring-mass stiffness and its modification.

Curved running poses other problems regarding its modelling. In chapter 2.3 we allude to a difference in lower limb stiffnesses between the outer and inner leg by explaining that the respective limbs showed a difference in joint compliance. We did not however measure the stiffness of the inner or outer limb directly. On a curve, the leg bends both in the sagittal, frontal, and in the transverse plane over the stance. Thus, confining a model to one vertical axis, k_{vert}, or even a sweeping spring 2D-model, k_{leg}, famously described by (McMahon and Cheng 1990) or *via* the method explained above could miss several key parameters regarding the motion being done. To appropriately model curved running's lower limb spring, at least initially, one should consider the motion in all three axes, considering the spring bend over the step cycle.

Kinematic coordination of gait

From a kinematic point of view, the lower limb intersegmental coordination was expected to contribute to the modification of stiffness observed above. Although largely valid in different types of gait conditions and across animal species (Ivanenko et al. 2008; Catavitello et al. 2018), few studies had used this analysis in running prior to our work (Ivanenko et al. 2007; Oshima et al. 2019), and none had altered running conditions to understand how the intersegmental coordination adapted during a bouncing gait.

Running at lower SF increased the ROM of the lower limb segment elevation angles and increased the phase-lag between the shank and foot segments. This led to a larger and less characteristic 3D-loop. Due to the phase changes, the third eigenvector, u_3t, decreased due to plane rotation, which is evidence of an adapted kinematic strategy (plane rotation). At high SF, the ROM was reduced and the elevation angles were more in-phase, which is translated by small loops and counter-rotation of the plane. Moreover, u_3t had been previously correlated with the mechanical energy expenditure during walking (Borghese et al. 1996; Grasso et al. 2000), which could imply that the reason u_3t is furthest from 0 at the slowest SF (and closest to zero at higher SF) is because the mechanical power developed to move the CoM forward and upward increases at low SFs.

In curved running, when comparing the outer and inner limb segmental coordination, differences in the movement programming patterns emerged. The coordination loops revealed that the outer limb's motion followed the long axis more closely, which is better explained by the first eigenvector (increased PV1), whereas the inner limb aligned more with the wide axis, better explained by the second

eigenvector (increased PV2). This suggests that the outer limb's movement is primarily governed by variations in limb orientation, while the inner limb's motion is more influenced by telescopic length changes (Ivanenko et al. 2008), indicating distinct strategies for managing the curved running motion.

Gait modifiers with additional work done against the environment had been previously investigated in relation to the kinematic coordination in different walking conditions, *e.g.* slope walking (Dewolf et al. 2018), or walking on slippery surfaces (Cappellini et al. 2010). In running, Fig. 4.4 shows the 3D-plots of the segmental relationship between segments and the best fitting plane against the strongest head and tailwind. At large headwinds, the plane rotated around u_3t, shown above to be related to a more in-phase shank - foot motion and an increase in SF. Moreover, as wind speeds progressively counter the motion of the body, the kinematic coordination was less explained by PV1 and more by PV2. Again, this suggests that the limb motion against the wind was better explained by its length rather than its orientation changes which is consistent with the lower limb being more retracted (flexed) as it touches the ground, decreasing its projected area to the wind and braking motion, then stretching to increase the push time.

Oppositely, with increasing tailwinds, we did not observe a decreased SF, most likely since the highest tailwind condition was only equal to a hindering force of ~8%*BW* which was approximately half the magnitude of the highest negative slope and aiding tractive conditions measured. Thus, the plane did not oppositely rotate and u_3t was not different from running with no wind. Despite this lack of plane rotation, the body is more upright against heavy tailwinds to project a larger frontal area to the external force, seen by an increased PV1, suggesting that limb orientation was more prevalent than its length.

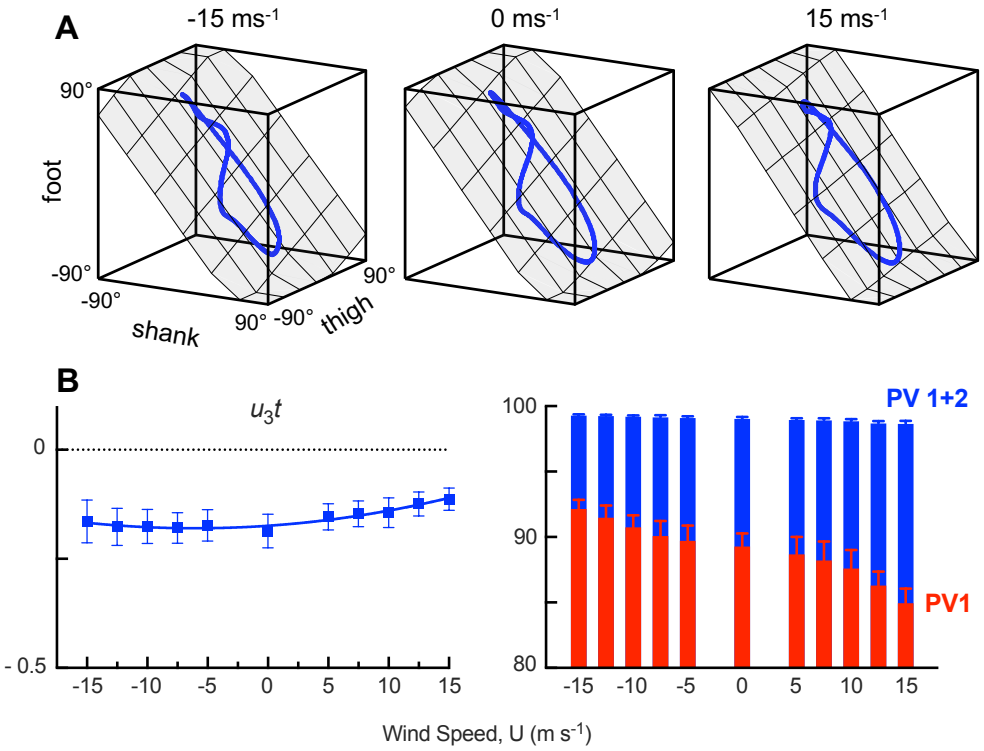

Fig. 4.4 A) *3D-plots of thigh, shank foot elevation angles, along with the best-fitting planes in wind running at the highest head (+15 m s^{-1}) and tail (-15 m s^{-1}) winds.* ***B)*** *Left: the averages and standard deviations of the direction cosine for the thigh axis of the third eigenvector, u_3t, as a function of wind speed. Right: percentage of variance average and standard deviations explained by the first eigenvector (PV1) and percentage of variance explained by the first and second eigenvector (PV1+2). (Unpublished data).*

The role of kinematic coordination in the running gait

Full and Koditschek (1999) explain that legged locomotion in living beings has a hierarchal modelling structure which is consistently alternating between often simple "templates" which are used for controlling gait and more complex "anchors" which are more representative of mechanisms occurring within limbs, joints and muscles. Templates are generally simple models, which strip back all information occurring peripherally to explain a general gait design. In running, this template design can be described as the bouncing motion of the CoM over the step whereas its anchors habitually consider the motion of the lower limb segments and joints to characterise gait representatively with greater complexity and capacity of reducing the degrees of freedom which are implemented as feedback to the template design (Fig. 4.5).

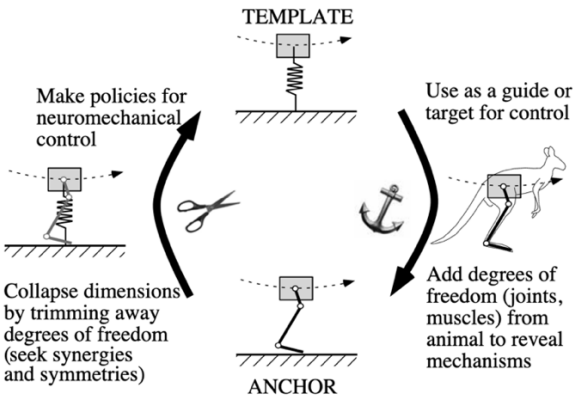

Fig. 4.5 *Relationship between a template and anchor model as described by Full and Koditschek (1999). Templates are simple models which are used as targets of gait, such as the bouncing mechanism of running. Anchors are more complex mechanisms which describe gait. Their use encompass the role of individual joints, segment positions and muscle lengths to explain motion with the goal of reducing the degrees of freedom which can be fed-back as neuromechanical control to the template model (Full and Koditschek 1999).*

In 1999, the authors note the lack of comparative biology anchors which describe movement. Since then, and as evidenced by the analyses used in chapter 2.3, models such as the planar covariance law and proximal-distal control of joint segments largely corroborate such hierarchal design. In regards to both models, the anchor coordinates the many redundant degrees of freedom and possible movements the body proposes and restricts itself to a low-dimensional subset (Bernstein 1967; Full and Koditschek 1999). From these same principles, the planar covariance law has been shown to reduce the large positioning possibilities of the lower limb into its length and orientation changes over a cycle (Borghese et al. 1996; Ivanenko et al. 2008).

As expected, running maintains its characteristic kinematic coordination pattern which adapts to the environment as observed in walking gaits (Cappellini et al. 2010; Dewolf et al. 2018). The fact that the planar covariance law is maintained at multiple speeds and within gait modifications emphasises the robustness of the planar covariance law in the sagittal plane segment angular motion (Ivanenko et al. 2008; Lacquaniti et al. 2012).

Shortcomings

This thesis represents the culmination of seven years (officially six) of research. While it has provided me with significant personal growth and knowledge, it has also allowed me to recognise both small and sometimes more substantial limitations within the work. Although each section addressed its specific limitations, this upcoming section provided a view of limitations across the entire thesis rather than focusing on any one particular study.

The first limitation to this thesis was the *"size of the elephant"*. Indeed, the goal of this thesis was to challenge the locomotor system to better understand CoM mechanics and the interaction between neural commands and mechanical output. Each chapter aimed to characterise running mechanics with specific gait modifications and integrate a kinematic coordination approach within each section. Although the mechanical analyses for each section are complete, some chapters still lack a full kinematic analysis, which has only been addressed in the discussion above.

Additionally, a more in-depth analysis of the neural control mechanisms would further increase the impact of this thesis. By examining movement from the periphery inward, we aim to understand how motion is centrally regulated. However, many unanswered questions remain regarding the interaction between the mechanical system and central control strategies. For instance, kinematic coordination patterns are influenced by step frequency but not by running speed, as seen in chapter 2.1 — so why do muscular coordination patterns change as running speed increases (*e.g.* increased number of synergies (Yokoyama et al. 2016), less complex coordination patterns and more robust temporal modules (Santuz et al. 2020))? Possibly, these changes observed in muscle coordination could be related to the change in the spontaneous step frequency chosen at different speeds. For example, when speeds increase beyond those studied in this paper (>7 m s^{-1}) the plantar flexor muscles lose their ability to generate force, making subjects rely on their hip flexor muscles to increase step frequency rather than privileging increased contact time to increase speeds (Dorn et al. 2012). Furthermore, in terms of muscular coordination, at the speeds mostly covered in this thesis ~ 2.5 to 4.7 m s^{-1} motor complexity does not appear to significantly decrease, however as speeds increase beyond this point, modules appear less complex and more robust while SF are increasing (Santuz et al. 2020).

In this thesis we showed specific situations where joint functions vary significantly, *e.g.* between straight-line and curved running, indicating distinct adaptations in motor coordination. Such analyses of muscular coordination could paint a broader picture of how the locomotor system is adapting. In some instances, this muscular activity data has not been fully analysed or other cases, not recorded from our experiments. Furthermore, techniques such as transcranial magnetic stimulation (TMS) transcutaneous spinal stimulation (TSS) could help in explaining differences between cortical and spinal control in locomotion (Quartarone et al. 2005; Carroll et al. 2006; Steele et al. 2022; Stefanovic et al. 2023) ; while electroencephalography (EEG) offers a window into cortical activation patterns during movement (Gwin et al. 2010; Gwin 2012; Gorjan et al. 2022; Zandvoort et al.

2022). Despite their methodological challenges, these approaches could help bridge gaps in the understanding of mechanical function and neural adaptation to a task. Fortunately, while this thesis does not fully resolve the intricacies of the neuromechanical interactions, it contributes to the understanding between the mechanical and nervous system and sets a foundation for future studies to explore the neural signatures to locomotor adaption in running.

Secondly, all studies were conducted in controlled laboratory settings. It is important for those, such as coaches or elite athletes, who may wish to apply these findings practically to recognise that controlled experimental conditions may not directly reflect real-world scenarios. In more natural settings, athletes often adjust their behaviours: runners, for example, tend to increase speed when they voluntarily increase step frequency (Gidley 2023) adjust rather than maintain constant speed in search for stability when turning (Churchill et al. 2015), and may choose walking over running when facing challenging wind or traction conditions, as on slopes (Ortiz et al. 2017). Thus, while laboratory findings offer valuable insights, they should be applied with caution, as real-world variability in running conditions can lead to different outcomes than those observed in controlled settings.

Finally, among the more than sixty subjects analysed across the studies conducted over recent years, only two were female. This imbalance is concerning. Women are consistently underrepresented in clinical research, and studies that disclose participant sex often face lower publication impact than those that don't (Geller et al. 2018; Sugimoto et al. 2019). In much of the present research, we opted for homogeneity to control for variability, rather than considering sex as a potential factor. However, this choice is neither justifiable nor should it set a standard for future researchers. Such imbalances risk skewing findings when generalising across genders (Jones et al. 2023). As scientists, we must prioritise larger, more representative sample sizes to ensure the inclusivity and validity of our conclusions. Among researchers, gender disparity remains significant in biomechanics, with men making up 73% of STEM-skilled roles and 70% of professional biomechanics society members (Van Schooten et al. 2023).

Future perspectives - Understanding performance

This thesis presents the utility of a neuromechanical rather than a purely biomechanical analysis. Below is one of many potential, practical applications of such analysis. Running performance is somewhat vague and multifaceted which can lead to different interpretations. At a competitive level, running performance is rather

straight forward: faster athletes perform better than slower ones (Emig and Peltonen 2020). However, this criterion for performance is not necessarily all encompassing. For example, such high performing fast athletes could have a running gait which is largely prone to injury. Moreover, as recently commented in Nature (Bates et al. 2024; Conroy 2024), skeletal evidence suggests that endurance running contributed to human evolution over 2 million years ago (Lieberman and Bramble 2007). Australopithecus may have not cared about their 10 km personal best; however, a tibial stress fracture could be life threatening.

Thus, considering performance should perhaps not only focus on speed but also track running experience and injury. By understanding if and how running coordination correlates with speed but also with the runner's experience provides insight both into athletic ability and injury prevention. One can suppose that limb coordination will adapt differently depending on the runner's experience and athletic performance; for example, a change in step frequency or change in elevation affects the bouncing mechanics differently depending on athletic level (da Rosa et al. 2019; Padulo et al. 2012). Furthermore, segment coordination in sprinting is crucial in influencing technique and athletic performance (Donaldson et al. 2022). However, whether the limb coordination is primarily influenced by running speed, running experience or anatomical constraints is not well understood.

Such a project would aim in explaining how the neuromechanics of running, *i.e.* bounce biomechanics, limb coordination and motor control are correlated with the following 1) physiological and race-related performance indicators over a specific running distance and 2) the number of years of running and a subject's running related injury background. Note that this analysis should most likely be distance dependant and have different results if we focus on different distances. Sprinters should not have the same performance indicators as long distance runners nor ultramarathoners (Costill et al. 1976; Maruo et al. 2018).

First, a sufficiently large sample of runners should be included to be able to separate subjects into classes *via* cluster analysis and/or through artificial neural network analysis based on their neuromechanical variables. The former is a characterisation similar to the methods applied in Chollet et al. (2023), where the authors separate runners based on 7 variables, adapted from the runner profile characterisations of van Oeveren et al. (2021). The latter has been in work such as that of Van Hooren et al. (2024), where the authors are able to classify runners as more or less economical based on their running technique through machine learning.

This could be accompanied by analyses like dynamical simulation modelling, *e.g.* OpenSim, of high and low performers' gait characteristics to understand if and how MTU morphology plays a role in determining performance and injury. Such modelling, effectively estimates muscle forces and segment loading, showing reliable results in muscle-tendon force loading with gait modifications (Aftabi et al. 2021; Swinnen et al. 2022).

Ultimately, by combining such analyses this project seeks to provide a comprehensive understanding of how coordination, performance, and injury risk interrelate in runners. Such research aims lays the groundwork for personalised, data-driven approaches to run training and return from injury, impacting both elite athletes and recreational runners alike by promoting personal athletic performance analysis and avoiding injury.

Conclusion

This thesis explored the neuromechanics of running by examining specific gait modifications with and without work needing to be done against the environment. It extended from a biomechanical analysis to include the coordination of body segments, aiming to integrate both perspectives to gain insights into the central modulation of running gait. By bridging two key fields of human movement sciences —biomechanics and motor control, which have progressively diverged over recent decades (Juras and Wit 2016) —this work provides a deeper understanding of how dynamic feedback at each level contributes to the locomotor system's independent function. Additionally, it reveals how these levels are collectively managed as part of an integrated system.

By using biomechanics as a lens to explore neuromuscular regulation, we showed how movement mechanics guides motor control. Much work remains to be done to fully explain how not only running, but locomotion in general regulates the interactions between the nervous and musculoskeletal systems during movement. Given their interdependence and common goals, biomechanics and motor control should converge at all levels. As scientists, we should not content ourselves with only observing phenomena but also explaining the mechanisms behind it. This thesis represents a step towards this integration.

References

Abbott BC, Bigland B, Ritchie JM (1952) The physiological cost of negative work. *Journal of Physiology* 117:380–390

Abu-Faraj ZO, Harris GF, Smith PA, Hassani S (2015) Human gait and Clinical Movement Analysis. In: Webster JG (ed) *Wiley Encyclopedia of Electrical and Electronics Engineering*, 1st edn. Wiley, pp 1–34

Aftabi H, Nasiri R, Ahmadabadi MN (2021) Simulation-based biomechanical assessment of unpowered exoskeletons for running. *Scientific Reports* 11:11846. https://doi.org/10.1038/s41598-021-89640-3

Ahn AN, Brayton C, Bhatia T, Martin P (2014) Muscle activity and kinematics of forefoot and rearfoot strike runners. *Journal of Sport and Health Science* 3:102–112. https://doi.org/10.1016/j.jshs.2014.03.007

Alexander RM (2002) Stability and Manoeuvrability of Terrestrial Vertebrates. *Integrative and Comparative Biology* 42:158–164. https://doi.org/10.1093/icb/42.1.158

Alexander RM (1984) The Gaits of Bipedal and Quadrupedal Animals. The International *Journal of Robotics Research* 3:49–59. https://doi.org/10.1177/027836498400300205

Almeida MO, Davis IS, Lopes AD (2015) Biomechanical Differences of Foot-Strike Patterns During Running: A Systematic Review With Meta-analysis. *Journal of Orthopaedic & Sports Physical Therapy* 45:738–755. https://doi.org/10.2519/jospt.2015.6019

Alt T, Heinrich K, Funken J, Potthast W (2015) Lower extremity kinematics of athletics curve sprinting. *Journal of Sports Sciences* 33:552–560. https://doi.org/10.1080/02640414.2014.960881

Anderson BD (2008) The physics of sailing. *Physics Today* 61:38–43. https://doi.org/10.1063/1.2883908

Aoi S, Tsuchiya K (2006) Bifurcation and chaos of a simple walking model driven by a rhythmic signal. *International Journal of Non-Linear Mechanics* 41:438–446. https://doi.org/10.1016/j.ijnonlinmec.2005.09.001

Asmussen E, Bonde-Petersen F (1974) Apparent Efficiency and Storage of Elastic Energy in Human Muscles during Exercise. *Acta Physiologica Scandinavica* 92:537–545. https://doi.org/10.1111/j.1748-1716.1974.tb05776.x

Ayres TR, Gottlieb MS (2006) Occurrence of right vs. left side injury location in elite sprinters who train on an oval 400m track. *New Studies in Athletics* 21:51–56

Barliya A, Omlor L, Giese MA, Flash T (2009) An analytical formulation of the law of intersegmental coordination during human locomotion. *Experimental Brain Research* 193:371–385. https://doi.org/10.1007/s00221-008-1633-0

Bates KT, McCormack S, Donald E, et al (2024) Running performance in Australopithecus afarensis. *Current Biology* S0960982224015665. https://doi.org/10.1016/j.cub.2024.11.025

Baur H, Hirschmüller A, Cassel M, et al (2010) Gender-specific neuromuscular activity of the M. peroneus longus in healthy runners — A descriptive laboratory study. *Clinical Biomechanics* 25:938–943. https://doi.org/10.1016/j.clinbiomech.2010.06.009

Beaumont F, Legrand F, Bogard F, et al (2021) Aerodynamic interaction between in-line runners: new insights on the drafting strategy in running. *Sports Biomechanics* 1–16. https://doi.org/10.1080/14763141.2021.2006295

Bernstein N (1967) The Co-ordination and Regulation of movements, 1st edn. *Pergamon Press*

Bezodis IN, Kerwin DG, Salo AIT (2008) Lower-Limb Mechanics during the Support Phase of Maximum-Velocity Sprint Running. *Medicine & Science in Sports & Exercise* 40:707–715. https://doi.org/10.1249/MSS.0b013e318162d162

Bianchi L, Angelini D, Orani GP, Lacquaniti F (1998) Kinematic Coordination in Human Gait: Relation to Mechanical Energy Cost. *Journal of Neurophysiology* 79:2155–2170. https://doi.org/10.1152/jn.1998.79.4.2155

Biewener AA, Daley MA (2007) Unsteady locomotion: integrating muscle function with whole body dynamics and neuromuscular control. *Journal of Experimental Biology* 210:2949–2960. https://doi.org/10.1242/jeb.005801

Blickhan R (1989) The spring-mass model for running and hopping. *Journal of Biomechanics* 22:1817–1227

Borghese NA, Bianchi L, Lacquaniti F (1996) Kinematic determinants of human locomotion. *The Journal of Physiology* 494:863–879. https://doi.org/10.1113/jphysiol.1996.sp021539

Bramah C, Preece SJ, Gill N, Herrington L (2018) Is There a Pathological Gait Associated With Common Soft Tissue Running Injuries? *American Journal of Sports Medicine* 46:3023–3031. https://doi.org/10.1177/0363546518793657

Brody F, Vámos T (eds) (1995) *The Neumann Compendium*. World Scientific Publisher

Burden AM, Trew M, Baltzopoulos V (2003) Normalisation of gait EMGs: a re-examination. *Journal of Electromyography and Kinesiology* 13:519–532. https://doi.org/10.1016/S1050-6411(03)00082-8

Burns GT, Zendler JM, Zernicke RF (2019) Step frequency patterns of elite ultramarathon runners during a 100-km road race. *Journal of Applied Physiology* 126:462–468

Cappellini G, Ivanenko YP, Dominici N, et al (2010) Motor Patterns During Walking on a Slippery Walkway. *Journal of Neurophysiology* 103:746–760. https://doi.org/10.1152/jn.00499.2009

Cappellini G, Ivanenko YP, Poppele RE, Lacquaniti F (2006) Motor Patterns in Human Walking and Running. *Journal of Neurophysiology* 95:3426–3437. https://doi.org/10.1152/jn.00081.2006

Carlet G (1872) Essai expérimental sur la locomotion humaine. Etude de la marche. Université de Paris

Carroll TJ, Baldwin ERL, Collins DF, Zehr EP (2006) Corticospinal Excitability Is Lower During Rhythmic Arm Movement Than During Tonic Contraction. *Journal of Neurophysiology* 95:914–921. https://doi.org/10.1152/jn.00684.2005

Catavitello G, Ivanenko YP, Lacquaniti F (2018) A kinematic synergy for terrestrial locomotion shared by mammals and birds. *eLife* 7:e38190. https://doi.org/10.7554/eLife.38190

Catavitello G, Ivanenko YP, Lacquaniti F (2015) Planar Covariation of Hindlimb and Forelimb Elevation Angles during Terrestrial and Aquatic Locomotion of Dogs. *PLoS ONE* 10:e0133936. https://doi.org/10.1371/journal.pone.0133936

Cavagna GA (1975) Force platforms as ergometers. *Journal of Applied Physiology* 39:174–179. https://doi.org/10.1152/jappl.1975.39.1.174

Cavagna GA (2005) Effect of an increase in gravity on the power output and the rebound of the body in human running. *Journal of Experimental Biology* 208:2333–2346. https://doi.org/10.1242/jeb.01661

Cavagna GA (2006) The landing-take-off asymmetry in human running. *Journal of Experimental Biology* 209:4051–4060. https://doi.org/10.1242/jeb.02344

Cavagna GA (2009) The two asymmetries of the bouncing step. *European Journal of Applied Physiology* 107:739–742. https://doi.org/10.1007/s00421-009-1179-2

Cavagna GA (2010) Symmetry and Asymmetry in Bouncing Gaits. *Symmetry* 2:1270–1321. https://doi.org/10.3390/sym2031270

Cavagna GA, Franzetti P, Heglund NC, Willems P (1988) The determinants of the step frequency in running, trotting and hopping in man and other vertebrates. *The Journal of Physiology* 399:81–92. https://doi.org/10.1113/jphysiol.1988.sp017069

Cavagna GA, Heglund NC, Taylor CR (1977) Mechanical work in terrestrial locomotion: two basic mechanisms for minimizing energy expenditure. *American Journal of Physiology-Regulatory, Integrative and Comparative Physiology* 233:R243–R261. https://doi.org/10.1152/ajpregu.1977.233.5.R243

Cavagna GA, Legramandi MA, Peyré-Tartaruga LA (2008a) Old men running: mechanical work and elastic bounce. *Proceedings of the Royal Society B: Biological Sciences* 275:411–418. https://doi.org/10.1098/rspb.2007.1288

Cavagna GA, Legramandi MA, Peyre-Tartaruga LA (2008b) The landing-take-off asymmetry of human running is enhanced in old age. *Journal of Experimental Biology* 211:1571–1578. https://doi.org/10.1242/jeb.013805

Cavagna GA, Mantovani M, Willems PA, Musch G (1997) The resonant step frequency in human running. *Pflügers Archives* 434:678–684. https://doi.org/10.1007/s004240050451

Cavagna GA, Saibene FP, Margaria R (1963) External work in walking. *Journal of Applied Physiology* 18:1–9. https://doi.org/10.1152/jappl.1963.18.1.1

Cavagna GA, Saibene FP, Margaria R (1964) Mechanical work in running. *Journal of Applied Physiology* 19:249–256. https://doi.org/10.1152/jappl.1964.19.2.249

Cavagna GA, Thys H, Zamboni A (1976) The sources of external work in level walking and running. *The Journal of Physiology* 262:639–657. https://doi.org/10.1113/jphysiol.1976.sp011613

Cavagna GA, Willems PA, Franzetti P, Detrembleur C (1991) The two power limits conditioning step frequency in human running. *The Journal of Physiology* 437:95–108. https://doi.org/10.1113/jphysiol.1991.sp018586

Cavagna GA, Willems PA, Heglund NC (1998) Walking on Mars. *Nature*

Cavagna GA, Willems PA, Legramandi MA, Heglund NC (2002) Within-step energy transduction. *Journal of Experimental Biology* 205:3413–3422

Chang Y-H, Hamerski CM, Kram R (2001) Applied horizontal force increases impact loading in reduced-gravity running. *Journal of Biomechanics* 34:679–685. https://doi.org/10.1016/S0021-9290(00)00196-2

Chang Y-H, Kram R (2007) Limitations to maximum running speed on flat curves. *Journal of Experimental Biology* 210:971–982. https://doi.org/10.1242/jeb.02728

Chang Y-H, Kram R (1999) Metabolic cost of generating horizontal forces during human running. *Journal of Applied Physiology* 86:1657–1662. https://doi.org/10.1152/jappl.1999.86.5.1657

Chollet M, Michelet S, Horvais N, et al (2023) Individual physiological responses to changes in shoe bending stiffness: a cluster analysis study on 96 runners. *European Journal of Applied Physiology* 123:169–177. https://doi.org/10.1007/s00421-022-05060-9

Churchill SM, Salo AIT, Trewartha G (2011) The effect of the bend on technique and performance during maximal speed sprinting. *Portuguese Journal of Sport Sciences* 11:471–474

Churchill SM, Trewartha G, Bezodis IN, Salo AIT (2016) Force production during maximal effort bend sprinting: Theory vs reality: Force production during bend sprinting. *Scandinavian Journal of Medicine & Science in Sports* 26:1171–1179. https://doi.org/10.1111/sms.12559

Churchill SM, Trewartha G, Salo AIT (2019) Bend sprinting performance: new insights into the effect of running lane. *Sports Biomechanics* 18:437–447. https://doi.org/10.1080/14763141.2018.1427279

Clarke TE, Cooper LB, Hamill CL, Clark DE (1985) The effect of varied stride rate upon shank deceleration in running. *Journal of Sports Sciences* 3:41–49. https://doi.org/10.1080/02640418508729731

Conroy G Humans evolved for distance running – but ancestor 'Lucy' didn't go far or fast. https://www.nature.com/articles/d41586-024-04194-4. Accessed 29 Dec 2024

Costill DL, Daniels J, Evans W, et al (1976) Skeletal muscle enzymes and fiber composition in male and female track athletes. *Journal of Applied Physiology* 40:149–154. https://doi.org/10.1152/jappl.1976.40.2.149

Courtine G, Roy RR, Hodgson J, et al (2005) Kinematic and EMG Determinants in Quadrupedal Locomotion of a Non-Human Primate (Rhesus). *Journal of Neurophysiology* 93:3127–3145. https://doi.org/10.1152/jn.01073.2004

Courtine G, Schieppati M (2003) Human walking along a curved path. II. Gait features and EMG patterns. *European Journal of Neuroscience* 18:191–205. https://doi.org/10.1046/j.1460-9568.2003.02737.x

Crouch TN, Burton D, Thompson MC, et al (2016) Dynamic leg-motion and its effect on the aerodynamic performance of cyclists. *Journal of Fluids and Structures* 65:121–137. https://doi.org/10.1016/j.jfluidstructs.2016.05.007

da Rosa RG, Oliveira HB, Gomeñuka NA, et al (2019) Landing-Takeoff Asymmetries Applied to Running Mechanics: A New Perspective for Performance. *Frontiers in Physiology* 10:415. https://doi.org/10.3389/fphys.2019.00415

Da Silva ES, Kram R, Hoogkamer W (2022) The metabolic cost of emulated aerodynamic drag forces in marathon running. *Journal of Applied Physiology* 133:766–776. https://doi.org/10.1152/japplphysiol.00086.2022

Daffertshofer A, Lamoth CJC, Meijer OG, Beek PJ (2004) PCA in studying coordination and variability: a tutorial. *Clinical Biomechanics* 19:415–428. https://doi.org/10.1016/j.clinbiomech.2004.01.005

Daley M (2013) Tendons: Energy Managers During Movement. *Exercise and Sport Sciences Reviews* 41:185. https://doi.org/10.1097/JES.0b013e3182a4e707

Daley MA, Felix G, Biewener AA (2007) Running stability is enhanced by a proximo-distal gradient in joint neuromechanical control. *Journal of Experimental Biology*

Daley MA, Usherwood JR (2010) Two explanations for the compliant running paradox: reduced work of bouncing viscera and increased stability in uneven terrain. *Biology Letters* 6:418–421. https://doi.org/10.1098/rsbl.2010.0175

Davies CT (1980) Effects of wind assistance and resistance on the forward motion of a runner. *Journal of Applied Physiology* 48:702–709. https://doi.org/10.1152/jappl.1980.48.4.702

Dempster WT, Gaughran GRL (1967) Properties of body segments based on size and weight. *American Journal of Anatomy* 120:33–54. https://doi.org/10.1002/aja.1001200104

Dewolf AH, Ivanenko YP, Zelik KE, et al (2018) Kinematic patterns while walking on a slope at different speeds. *Journal of Applied Physiology* 125:642–653. https://doi.org/10.1152/japplphysiol.01020.2017

Dewolf AH, Ivanenko YP, Lacquaniti F, Willems PA (2017b) Pendular energy transduction within the step during human walking on slopes at different speeds. *PLoS ONE* 12:1–25. https://doi.org/10.1371/journal.pone.0186963

Dewolf AH, Ivanenko YP, Mesquita RM, et al (2020b) Neuromechanical adjustments when walking with an aiding or hindering horizontal force. *European Journal of Applied Physiology* 120:91–106. https://doi.org/10.1007/s00421-019-04251-1

Dewolf AH, Ivanenko YP, Zelik KE, et al (2019a) Differential activation of lumbar and sacral motor pools during walking at different speeds and slopes. *Journal of Neurophysiology* 122:872–887. https://doi.org/10.1152/jn.00167.2019

Dewolf AH, Ivaniski-Mello A, Peyré-Tartaruga LA, Mesquita RM (2024) Relation between soft tissue energy dissipation and leg stiffness in running at different step frequencies. *Royal Society Open Science* 11:231736. https://doi.org/10.1098/rsos.231736

Dewolf AH, Lejeune T, Willems PA (2019c) The on-off ground asymmetry during running on sand. *Computer Methods in Biomechanics and Biomedical Engineering* 22:S291–S293. https://doi.org/10.1080/10255842.2020.1714917

Dewolf AH, Mesquita RM, De Jaeger D (2022) The effects of an increased step frequency on running economy and injury risk factors during downhill running. *Science & Sports* 37:446–453. https://doi.org/10.1016/j.scispo.2021.07.010

Dewolf AH, Mesquita RM, Willems PA (2020c) Intra-limb and muscular coordination during walking on slopes. *European Journal of Applied Physiology* 120:1841–1854. https://doi.org/10.1007/s00421-020-04415-4

Dewolf AH, Peñailillo LE, Willems PA (2016) The rebound of the body during uphill and downhill running at different speeds. *Journal of Experimental Biology* 219:2276–2288. https://doi.org/10.1242/jeb.142976

Dewolf AH, Sylos-Labini F, Cappellini G, et al (2020a) Emergence of Different Gaits in Infancy: Relationship Between Developing Neural Circuitries and Changing Biomechanics. *Frontiers in Bioengineering and Biotechnology* 8:473. https://doi.org/10.3389/fbioe.2020.00473

Dewolf AH, Willems PA (2017a) A collision-based analysis of the landing-takeoff asymmetry during running. *Computer Methods in Biomechanics and Biomedical Engineering* 20:65–66. https://doi.org/10.1080/10255842.2017.1382863

Dewolf AH, Willems PA (2017b) A collision-based analysis of the landing-takeoff asymmetry during running. *Computer Methods in Biomechanics and Biomedical Engineering* 20:S65–S66. https://doi.org/10.1080/10255842.2017.1382863

Dewolf AH, Willems PA (2019) Running on a slope: A collision-based analysis to assess the optimal slope. *Journal of Biomechanics* 83:298–304. https://doi.org/10.1016/j.jbiomech.2018.12.024

di Prampero PE (1986) The Energy Cost of Human Locomotion on Land and in Water. *International Journal of Sports Medicine* 07:55–72. https://doi.org/10.1055/s-2008-1025736

di Prampero PE, Fusi S, Sepulcri L, et al (2005) Sprint running: a new energetic approach. *Journal of Experimental Biology* 208:2809–2816. https://doi.org/10.1242/jeb.01700

di Prampero PE, Osgnach C, Morin J-B, et al (2023) Mechanical and Metabolic Power in Accelerated Running–PART I: the 100-m dash. *European Journal of Applied Physiology* 123:2473–2481. https://doi.org/10.1007/s00421-023-05236-x

Dickinson MH, Farley CT, Full RJ, et al (2000) How Animals Move: An Integrative View. *Science* 288:100–106. https://doi.org/10.1126/science.288.5463.100

Dierick F, Penta M, Renaut D, Detrembleur C (2004) A force measuring treadmill in clinical gait analysis. *Gait & Posture* 20:299–303. https://doi.org/10.1016/j.gaitpost.2003.11.001

Donaldson BJ, Bezodis NE, Bayne H (2022) Inter- and intra-limb coordination during initial sprint acceleration. *Biology Open* 11:bio059501. https://doi.org/10.1242/bio.059501

Donelan JM, Kram R, Kuo AD (2001) Mechanical and metabolic determinants of the preferred step width in human walking. *Proceedings of the Royal Society London B* 268:1985–1992. https://doi.org/10.1098/rspb.2001.1761

Donelan JM, Kram R, Kuo AD (2002) Step-to-step transition costs. *Journal of Experimental Biology*

Dorn TW, Schache AG, Pandy MG (2012) Muscular strategy shift in human running: dependence of running speed on hip and ankle muscle performance. *Journal of Experimental Biology* 215:2347–2347. https://doi.org/10.1242/jeb.075051

Dos'Santos T, McBurnie A, Thomas C, et al (2019) Biomechanical Comparison of Cutting Techniques: A Review and Practical Applications. *Strength & Conditioning Journal* 41:40–54. https://doi.org/10.1519/SSC.0000000000000461

Edouard P, Navarro L, Branco P, et al (2020) Injury frequency and characteristics (location, type, cause and severity) differed significantly among athletics ('track and field') disciplines during 14 international championships (2007–2018): implications for medical service planning. *Brazilian Journal of Sports Medicine* 54:159–167. https://doi.org/10.1136/bjsports-2019-100717

Elftman H (1934) A cinematic study of the distribution of pressure in the human foot. *Anatomical Record* 59:481–491. https://doi.org/10.1002/ar.1090590409

Emig T, Peltonen J (2020) Human running performance from real-world big data. *Nature Communications* 11:4936. https://doi.org/10.1038/s41467-020-18737-6

Exell TA, Gittoes MJR, Irwin G, Kerwin DG (2012) Gait asymmetry: Composite scores for mechanical analyses of sprint running. *Journal of Biomechanics* 45:1108–1111. https://doi.org/10.1016/j.jbiomech.2012.01.007

Farley CT, González O (1996) Leg stiffness and stride frequency in human running. *Journal of Biomechanics* 29:181–186. https://doi.org/10.1016/0021-9290(95)00029-1

Farris DJ, Sawicki GS (2012) Human medial gastrocnemius force–velocity behavior shifts with locomotion speed and gait. *Proceedings of the National Academy of Science USA* 109:977–982. https://doi.org/10.1073/pnas.1107972109

Faul F, Erdfelder E, Lang A-G, Buchner A (2007) G*Power 3: A flexible statistical power analysis program for the social, behavioral, and biomedical sciences. *Behavior Research Methods* 39:175–191. https://doi.org/10.3758/BF03193146

Fenn WO (1930) Work against gravity and work due to velocity changes in running. *American Journal of Physiology-Legacy Content* 93:433–462. https://doi.org/10.1152/ajplegacy.1930.93.2.433

Fernandes G, Gandur NL, Santos D, Maldonado V (2025) The sub 2-hour official marathon is possible: developing a drafting strategy for a historic breakthrough in sports. *Sports Medicine - Open*

Ferris DP, Farley CT (1997) Interaction of leg stiffness and surface stiffness during human hopping. *Journal of Applied Physiology* 82:15–22. https://doi.org/10.1152/jappl.1997.82.1.15

Ferris DP, Louie M, Farley CT (1998) Running in the real world: adjusting leg stiffness for different surfaces. *Proceedings of the Royal Society London B* 265:989–994. https://doi.org/10.1098/rspb.1998.0388

Fílter A, Olivares-Jabalera J, Santalla A, et al (2020) Curve Sprinting in Soccer: Kinematic and Neuromuscular Analysis. *International Journal of Sports Medicine* a-1144-3175. https://doi.org/10.1055/a-1144-3175

Folland JP, Allen SJ, Black MI, et al (2017) Running Technique is an Important Component of Running Economy and Performance. *Medicine & Science in Sports & Exercise* 49:1412–1423. https://doi.org/10.1249/MSS.0000000000001245

Forte P, Sousa N, Teixeira JE, et al (2022) Aerodynamic analysis of human walking, running and sprinting by numerical simulations. *Acta of Bioengineering and Biomechanics* 24:. https://doi.org/10.37190/ABB-02019-2022-06

Franz JR, Paylo KW, Dicharry J, et al (2009) Changes in the coordination of hip and pelvis kinematics with mode of locomotion. *Gait & Posture* 29:494–498. https://doi.org/10.1016/j.gaitpost.2008.11.011

Full RJ, Koditschek DE (1999) Templates and anchors: neuromechanical hypotheses of legged locomotion on land. *Journal of Experimental Biology* 202:3325–3332. https://doi.org/10.1242/jeb.202.23.3325

Gabaldón AM, Nelson FE, Roberts TJ (2004) Mechanical function of two ankle extensors in wild turkeys: shifts from energy production to energy absorption during incline *versus* decline running. *Journal of Experimental Biology* 207:2277–2288. https://doi.org/10.1242/jeb.01006

Gabbett TJ, Kelly JN, Sheppard JM (2008) Speed, Change of Direction Speed, and Reactive Agility of Rugby League Players. *Journal of Strength and Conditioning Research* 22:174–181. https://doi.org/10.1519/JSC.0b013e31815ef700

Gambelli CN, Theisen D, Willems PA, Schepens B (2016) Motor control of landing from a countermovement jump in simulated microgravity. *Journal of Applied Physiology* 120:1230–1240. https://doi.org/10.1152/japplphysiol.00993.2015

Geller SE, Koch AR, Roesch P, et al (2018) The More Things Change, the More They Stay the Same: A Study to Evaluate Compliance With Inclusion and Assessment of Women and Minorities in Randomized Controlled Trials. *Academic Medicine* 93:630–635. https://doi.org/10.1097/ACM.0000000000002027

Genin JJ, Willems PA, Cavagna GA, et al (2010) Biomechanics of locomotion in Asian elephants. *Journal of Experimental Biology* 213:694–706. https://doi.org/10.1242/jeb.035436

Gidley A (2023) Mechanical modifications to increased step frequency while running freely outside. *Journal of Sports Medicine and Physical Fitness* 63:536–42. https://doi.org/10.23736/S0022-4707.22.14365-3

Gill N, Preece SJ, Baker R (2020) Using the spring-mass model for running: Force-length curves and foot-strike patterns. *Gait & Posture* 80:318–323. https://doi.org/10.1016/j.gaitpost.2020.06.023

Gollhofer A, Kyröläinen H (1991) Neuromuscular Control of the Human Leg Extensor Muscles in Jump Exercises Under Various Stretch-Load Conditions. *International Journal of Sports Medicine* 12:34–40. https://doi.org/10.1055/s-2007-1024652

Gorjan D, Gramann K, De Pauw K, Marusic U (2022) Removal of movement-induced EEG artifacts: current state of the art and guidelines. *Journal of Neural Engineering* 19:011004. https://doi.org/10.1088/1741-2552/ac542c

Gosseye TP, Willems PA, Heglund NC (2010) Biomechanical analysis of running in weightlessness on a treadmill equipped with a subject loading system. *European Journal of Applied Physiology* 110:709–728. https://doi.org/10.1007/s00421-010-1549-9

Gottschall JS, Kram R (2005) Ground reaction forces during downhill and uphill running. *Journal of Biomechanics* 38:445–452. https://doi.org/10.1016/j.jbiomech.2004.04.023

Grasso R, Zago M, Lacquaniti F (2000) Interactions Between Posture and Locomotion: Motor Patterns in Humans Walking With Bent Posture Versus Erect Posture. *Journal of Neurophysiology* 83:288–300. https://doi.org/10.1152/jn.2000.83.1.288

Greene PR (1985) Running on Flat Turns: Experiments, Theory, and Applications. *Journal of Biomechanical Engineering* 107:96–103. https://doi.org/10.1115/1.3138542

Greene PR (1987) Sprinting with banked turns. *Journal of Biomechanics* 20:667–680. https://doi.org/10.1016/0021-9290(87)90033-9

Günther M, Blickhan R (2002) Joint stiffness of the ankle and knee in running. *Journal of Biomechanics* 35:1459–1474

Gwin JT (2012) Noninvasive Electrical Neuroimaging of the Human Brain during Mobile Tasks including Walking and Running. University of Michigan

Gwin JT, Gramann K, Makeig S, Ferris DP (2010) Removal of Movement Artifact From High-Density EEG Recorded During Walking and Running. *Journal of Neurophysiology* 103:3526–3534. https://doi.org/10.1152/jn.00105.2010

Hamill J, Murphy M, Sussman D (1987) The Effects of Track Turns on Lower Extremity Function. *International Journal of Sport Biomechanics* 3:276–286

Hardin EC, Van Den Bogert AJ, Hamill J (2004) Kinematic Adaptations during Running: Effects of Footwear, Surface, and Duration. *Medicine & Science in Sports & Exercise* 838–844. https://doi.org/10.1249/01.MSS.0000126605.65966.40

Hase K, Stein RB (1999) Turning Strategies During Human Walking. *Journal of Neurophysiology* 81:2914–2922. https://doi.org/10.1152/jn.1999.81.6.2914

Hatsopoulos NG (1996) Coupling the Neural and Physical Dynamics in Rhythmic Movements. *Neural Computation* 8:567–581. https://doi.org/10.1162/neco.1996.8.3.567

He JP, Kram R, McMahon TA (1991) Mechanics of running under simulated low gravity. *Journal of Applied Physiology* 71:863–870. https://doi.org/10.1152/jappl.1991.71.3.863

Heinrich K, Alt T, Funken J, et al (2015) Contribution of the lower extremity joints to mechanical energy in athletics curve sprinting. *In: lSBS - Conference Proceedings Archive. Poitiers, France*

Hill AV (1913) The absolute mechanical efficiency of the contraction of an isolated muscle. *The Journal of Physiology* 46:435–469. https://doi.org/10.1113/jphysiol.1913.sp001600

Hill AV (1928) The air-resistance to a runner. *Proceedings of the Royal Society of London 6*

Hoerner S (1965) Fluid Dynamic Drag. Wiley

Hoogkamer W, Kipp S, Frank JH, et al (2018) A Comparison of the Energetic Cost of Running in Marathon Racing Shoes. *Sports Medicine* 48:1009–1019. https://doi.org/10.1007/s40279-017-0811-2

Hoogkamer W, Kram R, Arellano CJ (2017) How Biomechanical Improvements in Running Economy Could Break the 2-hour Marathon Barrier. *Sports Medicine* 47:1739–1750. https://doi.org/10.1007/s40279-017-0708-0

Hopkins WG, Marshall SW, Batterham AM, Hanin J (2009) Progressive Statistics for Studies in Sports Medicine and Exercise Science. *Medicine & Science in Sports & Exercise* 41:3–12. https://doi.org/10.1249/MSS.0b013e31818cb278

Inman VT, Ralston HJ, Todd F (1981) Human Walking. Williams & Wilkins, London, UK

Inoue T, Takafumi O, Takahiro T, et al (2016) Wind-tunnel experiment on aerodynamic characteristics of a runner using a moving-belt system. *Cogent Engineering* 3:. https://doi.org/10.1080/23311916.2016.1231389

Ishimura K, Sakurai S (2015) Asymmetric contribution of support leg to curved running velocity. *In: ISBS - Conference Proceedings Archive. Poitiers, France*

Ivanenko YP (2004) Development of pendulum mechanism and kinematic coordination from the first unsupported steps in toddlers. *Journal of Experimental Biology* 207:3797–3810. https://doi.org/10.1242/jeb.01214

Ivanenko YP, Cappellini G, Dominici N, et al (2007) Modular Control of Limb Movements during Human Locomotion. *Journal of Neuroscience* 27:11149–11161. https://doi.org/10.1523/JNEUROSCI.2644-07.2007

Ivanenko YP, d'Avella A, Poppele RE, Lacquaniti F (2008) On the Origin of Planar Covariation of Elevation Angles During Human Locomotion. *Journal of Neurophysiology* 99:1890–1898. https://doi.org/10.1152/jn.01308.2007

Ivanenko YP, Grasso R, Macellari V, Lacquaniti F (2002) Two-thirds power law in human locomotion: role of ground contact forces. *Neuroreport* 13:1171–1174. https://doi.org/10.1097/00001756-200207020-00020

Ivanenko YP, Poppele RE, Lacquaniti F (2006) Motor Control Programs and Walking. *Neuroscientist* 12:339–348. https://doi.org/10.1177/1073858406287987

Jain PC (1980) On a Discrepancy in Track Races. *Research Quarterly for Exercise and Sport* 51:432–436. https://doi.org/10.1080/02701367.1980.10605212

Jones AM, Doust JH (1996) A 1% treadmill grade most accurately reflects the energetic cost of outdoor running. *Journal of Sports Sciences* 14:321–327. https://doi.org/10.1080/02640419608727717

Jones CF, Ploeg H-L, Sparrey CJ, Tanner KE (2023) Women in impact biomechanics research. *Proceedings of the Institution of Mechanical Engineering Part H* 237:1119–1121. https://doi.org/10.1177/09544119231210104

Judson LJ, Churchill SM, Barnes A, et al (2020a) Joint moments and power in the acceleration phase of bend sprinting. *Journal of Biomechanics* 101:

Judson LJ, Churchill SM, Barnes A, et al (2020b) Measurement of bend sprinting kinematics with three-dimensional motion capture: a test–retest reliability study. *Sports Biomechanics* 19:761–777. https://doi.org/10.1080/14763141.2018.1515979

Judson LJ, Churchill SM, Barnes A, et al (2019) Horizontal force production and multi-segment foot kinematics during the acceleration phase of bend sprinting. *Scandinavian Journal of Medicine & Science in Sports* 29:1563–1571. https://doi.org/10.1111/sms.13486

Juras G, Wit A (2016) Bridging motor control and biomechanics. *Journal of Human Kinetics* 52:5–6. https://doi.org/10.1515/hukin-2015-0189

Kendall FP, McCreary E, Provenance P, et al (2005) Muscle testing and function with posture and pain, 5th edn. Lippincott Williams & Wilkins, Philadelphia.

Kerdok AE, Biewener AA, McMahon TA, et al (2002) Energetics and mechanics of human running on surfaces of different stiffnesses. *Journal of Applied Physiology* 92:469–478. https://doi.org/10.1152/japplphysiol.01164.2000

Kreidler SM, Muller KE, Grunwald GK, et al (2013) **GLIMMPSE**: Online Power Computation for Linear Models with and without a Baseline Covariate. *Journal of Statistical Software* 54:. https://doi.org/10.18637/jss.v054.i10

Kyle CR, Caiozzo VJ (1986) The effect of athletic clothing aerodynamics upon running speed. *Medicing and Science in Sports and Exercise* 18:509–515

Kyröläinen H, Avela J, Komi PV (2005) Changes in muscle activity with increasing running speed. *Journal of Sports Sciences* 23:1101–1109. https://doi.org/10.1080/02640410400021575

La Scaleia V, Ivanenko YP, Zelik KE, Lacquaniti F (2014) Spinal motor outputs during step-to-step transitions of diverse human gaits. *Frontiers in Human Neuroscience* 8:. https://doi.org/10.3389/fnhum.2014.00305

Lacquaniti F, Grasso R, Zago M (1999) Motor Patterns in Walking. *Physiology* 14:168–174. https://doi.org/10.1152/physiologyonline.1999.14.4.168

Lacquaniti F, Ivanenko YP, Zago M (2012) Patterned control of human locomotion: Control of human locomotion. *Journal of Physiology* 590:2189–2199. https://doi.org/10.1113/jphysiol.2011.215137

Lee CR, Farley CT (1998) Determinants of the center of mass trajectory in human walking and running. *Journal of Experimental Biology* 201:2935–2944

Lejeune TM, Willems PA, Heglund NC (1998) Mechanics and energetics of human locomotion on sand. *Journal of Experimental Biology* 201:2071–2080

Lieberman DE, Bramble DM (2007) The Evolution of Marathon Running: Capabilities in Humans. *Sports Medicine* 37:288–290. https://doi.org/10.2165/00007256-200737040-00004

Lieberman DE, Warrener AG, Wang J, Castillo ER (2015) Effects of stride frequency and foot position at landing on braking force, hip torque, impact peak force and the metabolic cost of running in humans. *Journal of Experimental Biology* 218:3406–3414. https://doi.org/10.1242/jeb.125500

Linssen WHJP, Stegeman DF, Joosten EMG, et al (1993) Variability and interrelationships of surface EMG parameters during local muscle fatigue. *Muscle and Nerve* 16:849–856. https://doi.org/10.1002/mus.880160808

Lloyd BB, Zacks RM (1972a) The mechanical efficiency of treadmill running against a horizontal impeding force. *Journal of Physiology* 223:355–363. https://doi.org/10.1113/jphysiol.1972.sp009851

Lloyd BB, Zacks RM (1972b) The mechanical efficiency of treadmill running against a horizontal impeding force. *Journal of Physiology* 223:355–363. https://doi.org/10.1113/jphysiol.1972.sp009851

Lockhart DB, Ting LH (2007) Optimal sensorimotor transformations for balance. *Nature Neuroscience* 10:1329–1336. https://doi.org/10.1038/nn1986

Luo G, Stefanyshyn D (2012) Limb force and non-sagittal plane joint moments during maximum-effort curve sprint running in humans. *Journal of Experimental Biology* 215:4314–4321. https://doi.org/10.1242/jeb.073833

Marey E (1873) La Machine Animale. Paris, G. Baillie

Margaria R (1968) Positive and negative work performances and their efficiencies in human locomotion. *International Zeitschrift für Angewandte Physiologie Einschleisslich Arbeitsphysiologie* 25:339–351. https://doi.org/10.1007/BF00699624

Marro M, Leckert J, Rollier E, et al (2023) Wind tunnel evaluation of novel drafting formations for an elite marathon runner. *Proceedings of the Royal Society A* 479:20220836. https://doi.org/10.1098/rspa.2022.0836

Martino G, Ivanenko YP, Serrao M, et al (2014) Locomotor patterns in cerebellar ataxia. *Journal of Neurophysiology* 112:2810–2821. https://doi.org/10.1152/jn.00275.2014

Maruo Y, Murphy TI, Masaki H (2018) Long-Distance Runners and Sprinters Show Different Performance Monitoring – An Event-Related Potential Study. *Frontiers in Psychology* 9:653. https://doi.org/10.3389/fpsyg.2018.00653

Mauroy G, Schepens B, Willems PA (2014) Leg stiffness and joint stiffness while running to and jumping over an obstacle. *Journal of Biomechanics* 47:526–535. https://doi.org/10.1016/j.jbiomech.2013.10.039

Maykranz D, Seyfarth A (2014) Compliant ankle function results in landing-take off asymmetry in legged locomotion. *Journal of Theoretical Biology 6*

McGowan CP, Baudinette RV, Biewener AA (2005) Joint work and power associated with acceleration and deceleration in tammar wallabies (*Macropus eugenii*). *Journal of Experimental Biology* 208:41–53. https://doi.org/10.1242/jeb.01305

McMahon TA, Cheng GC (1990) The mechanics of running: How does stiffness couple with speed? *Journal of Biomechanics* 23:65–78. https://doi.org/10.1016/0021-9290(90)90042-2

Mendiguchia J, Gonzalez De La Flor A, Mendez-Villanueva A, et al (2021) Training-induced changes in anterior pelvic tilt: potential implications for hamstring strain injuries management. *Journal of Sports Sciences* 39:760–767. https://doi.org/10.1080/02640414.2020.1845439

Mesquita RM, Dewolf AD (2022) Evaluation of mechanical workload using a GPS-tracking device. *Computer Methods in Biomechanics and Biomedical Engineering*

Mesquita RM, Dewolf AH, Catavitello G, et al (2020) The bouncing mechanism of running against hindering, or with aiding traction forces: a comparison with running on a slope. *European Journal of Applied Physiology* 120:1575–1589. https://doi.org/10.1007/s00421-020-04379-5

Mesquita RM, Dewolf AH, Catavitello G, Willems PA (2019) Energy exchange during running with an aiding and hindering force. *Computer Methods in Biomechanics and Biomedical Engineering* 22:S283–S285. https://doi.org/10.1080/10255842.2020.1714914

Mesquita RM, Dewolf AH, Desimpelaere F, et al (2021) The bouncing mechanism of running when changing step frequency at a given speed. *Computer Methods in Biomechanics and Biomedical Engineering* 24:21–23. https://doi.org/10.1080/10255842.2021.1978758

Mesquita RM, Morin J-B, Dewolf AH (2024c) The Effect of Step Frequency and Running Speed on the Coordination of the Pelvis and Thigh Segments During Running. *Journal of Applied Biomechanics* 1–10. https://doi.org/10.1123/jab.2024-0016

Mesquita RM, Willems PA, Catavitello G, Dewolf AH (2024a) Kinematics and mechanical changes with step frequency at different running speeds. *European Journal of Applied Physiology*

Mesquita RM, Willems PA, Dewolf AH, Catavitello G (2024b) Kinetics and mechanical work done to move the body centre of mass along a curve. *PLoS ONE* 19:21

Meurisse GM, Bastien GJ (2014) Determination of vertical ground reaction forces under each foot during walking. *Computer Methods in Biomechanics and Biomedical Engineering* 17:110–111. https://doi.org/10.1080/10255842.2014.931483

Meyer M (1972) Zeno: His Fictions and His Problems. *SubStance* 1:121. https://doi.org/10.2307/3684173

Miller JR, Van Hooren B, Bishop C, et al (2019) A Systematic Review and Meta-Analysis of Crossover Studies Comparing Physiological, Perceptual and Performance Measures Between Treadmill and Overground Running. *Sports Medicine* 49:763–782. https://doi.org/10.1007/s40279-019-01087-9

Minetti AE, Ardigò LP, Saibene F (1994) Mechanical determinants of the minimum energy cost of gradient running in humans. *Journal of Experimental Biology* 15. https://doi.org/10.1242/jeb.195.1.211

Minetti AE, Ardigò LP, Saibene F (1993) Mechanical determinants of gradient walking energetics in man. *Journal of Physiology* 472:725–735. https://doi.org/10.1113/jphysiol.1993.sp019969

Minetti AE, Cazzola D, Seminati E, et al (2011) Skyscraper running: physiological and biomechanical profile of a novel sport activity. *Scandinavian Journal of Medicine & Science in Sports* 21:293–301. https://doi.org/10.1111/j.1600-0838.2009.01043.x

Monte A, Maganaris C, Baltzopoulos V, Zamparo P (2020) The influence of Achilles tendon mechanical behaviour on "apparent" efficiency during running at different speeds. *European Journal of Applied Physiology* 120:2495–2505. https://doi.org/10.1007/s00421-020-04472-9

Monte A, Nardello F, Magris R, et al (2021) The influence of *in vivo* mechanical behaviour of the Achilles tendon on the mechanics, energetics and apparent efficiency of bouncing gaits. *Journal of Experimental Biology* 224:jeb242453. https://doi.org/10.1242/jeb.242453

Moore IS (2016) Is There an Economical Running Technique? A Review of Modifiable Biomechanical Factors Affecting Running Economy. *Sports Medicine* 46:793–807. https://doi.org/10.1007/s40279-016-0474-4

Morgan DL (1977) Separation of active and passive components of short-range stiffness of muscle. *American Journal of Physiology-Cell Physiology* 232:45–49. https://doi.org/10.1152/ajpcell.1977.232.1.C45

Nagahara R, Matsubayashi T, Matsuo A, Zushi K (2018) Kinematics of the thorax and pelvis during accelerated sprinting. *Journal of Sports Medicine and Physical Fitness* 58:. https://doi.org/10.23736/S0022-4707.17.07137-7

Nishikawa K, Biewener AA, Aerts P, et al (2007) Neuromechanics: an integrative approach for understanding motor control. *Integrative and Comparative Biology* 47:16–54. https://doi.org/10.1093/icb/icm024

Noga BR, Whelan PJ (2022) The Mesencephalic Locomotor Region: Beyond Locomotor Control. *Frontiers in Neural Circuits* 16:884785. https://doi.org/10.3389/fncir.2022.884785

Novacheck TF (1998) The biomechanics of running. *Gait & Posture* 19

Nuñez Lisboa M, Peñailillo LE, Cancino J, Dewolf AH (2021) Influence of sports background on the bouncing mechanism of running. *Sports Biomechanics* 1–12

Ogihara N, Oku T, Andrada E, et al (2014) Planar covariation of limb elevation angles during bipedal locomotion in common quails (Coturnix coturnix). *The Journal of Experimental Biology*

Orendurff MS, Kobayashi T, Tulchin-Francis K, et al (2018) A little bit faster: Lower extremity joint kinematics and kinetics as recreational runners achieve faster speeds. *Journal of Biomechanics* 71:167–175. https://doi.org/10.1016/j.jbiomech.2018.02.010

Ortega C, Simpson JD, Donovan L, et al (2024) Gait Training Interventions for Individuals with Chronic Ankle Instability: A Systematic Review & Meta-Analysis. *Journal of Athletic Training*. https://doi.org/10.4085/1062-6050-0499.23

Ortiz ALR, Giovanelli N, Kram R (2017) The metabolic costs of walking and running up a 30-degree incline: implications for vertical kilometer foot races. *European Journal of Applied Physiology* 117:1869–1876. https://doi.org/10.1007/s00421-017-3677-y

Osgnach C, Poser S, Bernardini R, et al (2010) Energy Cost and Metabolic Power in Elite Soccer: A New Match Analysis Approach. *Medicine & Science in Sports & Exercise* 42:170–178. https://doi.org/10.1249/MSS.0b013e3181ae5cfd

Oshima H, Aoi S, Funato T, et al (2019) Variant and Invariant Spatiotemporal Structures in Kinematic Coordination to Regulate Speed During Walking and Running. *Frontiers in Computational Neuroscience* 13:63. https://doi.org/10.3389/fncom.2019.00063

Padulo J, Buglione A, Larion A, et al (2023) Energy cost differences between marathon runners and soccer players: Constant versus shuttle running. *Frontiers in Physiology* 14:1159228. https://doi.org/10.3389/fphys.2023.1159228

Padulo J, Chamari K, Ardigò LP (2014) Walking and running on treadmill: the standard criteria for kinematics studies. *Muscles, Ligaments, Tendons Journal* 4:159–162

Pavei G, Seminati E, Cazzola D, Minetti AE (2017) On the Estimation Accuracy of the 3D Body Center of Mass Trajectory during Human Locomotion: Inverse vs. Forward Dynamics. *Frontiers in Physiology* 8:. https://doi.org/10.3389/fphys.2017.00129

Pecchiari MM, Legramandi MA, Gibertini G, Cavagna GA (2023) Still air resistance during walking and running. *Proceedings of the Royal Society London B* 290:20231763. https://doi.org/10.1098/rspb.2023.1763

Peyré-Tartaruga LA, Coertjens M (2018) Locomotion as a Powerful Model to Study Integrative Physiology: Efficiency, Economy, and Power Relationship. *Frontiers in Physiology* 9:1789. https://doi.org/10.3389/fphys.2018.01789

Peyré-Tartaruga LA, Dewolf AH, Di Prampero PE, et al (2021) Mechanical work as a (key) determinant of energy cost in human locomotion: recent findings and future directions. *Experimental Physiology* 106:1897–1908. https://doi.org/10.1113/EP089313

Pietraszewski P, Gołaś A, Krzysztofik M (2021) Comparison of Muscle Activity During 200 m Indoor Curve and Straight Sprinting in Elite Female Sprinters. *Journal of Human Kinetics* 80:309–316. https://doi.org/10.2478/hukin-2021-0111

Polidori G, Legrand F, Bogard F, et al (2020) Numerical investigation of the impact of Kenenisa Bekele's cooperative drafting strategy on its running power during the 2019 Berlin marathon. *Journal of Biomechanics* 107:109854. https://doi.org/10.1016/j.jbiomech.2020.109854

Poppele RE, Bosco G, Rankin AM (2002) Independent Representations of Limb Axis Length and Orientation in Spinocerebellar Response Components. *Journal of Neurophysiology* 87:409–422. https://doi.org/10.1152/jn.00022.2001

Pugh LGCE (1970) Oxygen intake in track and treadmill running with observations on the effect of air resistance. *Journal of Physiology* 207:823–835. https://doi.org/10.1113/jphysiol.1970.sp009097

Pugh LGCE (1971) The influence of wind resistance in running and walking and the mechanical efficiency of work against horizontal or vertical forces. *Journal of Physiology* 213:255–276. https://doi.org/10.1113/jphysiol.1971.sp009381

Qiao M, Abbas JJ, Jindrich DL (2017) A model for differential leg joint function during human running. Bioinspir Biomim 12:016015. https://doi.org/10.1088/1748-3190/aa50b0

Qiao M, Brown B, Jindrich DL (2014) Compensations for increased rotational inertia during human cutting turns. *Journal of Experimental Biology* 217:432–443. https://doi.org/10.1242/jeb.087569

Qiao M, Jindrich DL (2014) Compensations during Unsteady Locomotion. Integrative and Comparative Biology 54:1109–1121. https://doi.org/10.1093/icb/icu058

Quartarone A, Bagnato S, Rizzo V, et al (2005) Distinct changes in cortical and spinal excitability following high-frequency repetitive TMS to the human motor cortex. *Experimental Brain Research* 161:114–124. https://doi.org/10.1007/s00221-004-2052-5

Quinn MD (2009) The effect of track geometry on 200- and 400-m sprint running performance. *Journal of Sports Sciences* 27:19–25. https://doi.org/10.1080/02640410802392707

Rand MK, Ohtsuki T (2000) EMG analysis of lower limb muscles in humans during quick change in running directions. *Gait & Posture* 12:169–183. https://doi.org/10.1016/S0966-6362(00)00073-4

Riddick RC, Kuo AD (2022) Mechanical work accounts for most of the energetic cost in human running. *Scientific Reports* 12:645. https://doi.org/10.1038/s41598-021-04215-6

Riddick RC, Kuo AD (2016) Soft tissues store and return mechanical energy in human running. *Journal of Biomechanics* 49:436–441. https://doi.org/10.1016/j.jbiomech.2016.01.001

Roberts TJ, Azizi E (2011) Flexible mechanisms: the diverse roles of biological springs in vertebrate movement. *Journal of Experimental Biology* 214:353–361. https://doi.org/10.1242/jeb.038588

Ruina A, Bertram JEA, Srinivasan M (2005) A collisional model of the energetic cost of support work qualitatively explains leg sequencing in walking and galloping, pseudo-elastic leg behavior in running and the walk-to-run transition. *Journal of Theoretical Biology* 237:170–192. https://doi.org/10.1016/j.jtbi.2005.04.004

Santuz A, Ekizos A, Eckardt N, et al (2018) Challenging human locomotion: stability and modular organisation in unsteady conditions. *Scientific Reports* 8:2740. https://doi.org/10.1038/s41598-018-21018-4

Santuz A, Ekizos A, Kunimasa Y, et al (2020) Lower complexity of motor primitives ensures robust control of high-speed human locomotion. *Heliyon* 6:e05377. https://doi.org/10.1016/j.heliyon.2020.e05377

Saunders JB dec. M, Inman VT, Eberhart HD (1953) The Major determinant in normal and pathological gait. *Journal of Bone & Joint Surgery* 35:

Schepens B, Bastien GJ, Heglund NC, Willems PA (2004) Mechanical work and muscular efficiency in walking children. *Journal of Experimental Biology* 207:587–596. https://doi.org/10.1242/jeb.00793

Schepens B, Willems PA, Cavagna GA (1998) The mechanics of running in children. *Journal of Physiology* 509:927–940. https://doi.org/10.1111/j.1469-7793.1998.927bm.x

Schickhofer L, Hanson H (2021) Aerodynamic effects and performance improvements of running in drafting formations. *Journal of Biomechanics* 122:110457. https://doi.org/10.1016/j.jbiomech.2021.110457

Segal AD, Orendurff MS, Czerniecki JM, et al (2008) Local dynamic stability in turning and straight-line gait. *Journal of Biomechanics* 41:1486–1493. https://doi.org/10.1016/j.jbiomech.2008.02.012

Seyfarth A, Zhao G, Jörntell H (2022) Whole Body Coordination for Self-Assistance in Locomotion. *Frontiers in Neurorobotics* 16:

Simmons R, Doma K, Sinclair W, et al (2021) Acute Effects of Training Loads on Muscle Damage Markers and Performance in Semi-elite and Elite Athletes: A Systematic Review and Meta-analysis. *Sports Medicine* 51:2181–2207. https://doi.org/10.1007/s40279-021-01486-x

Slawinski JS, Billat VL (2004) Difference in Mechanical and Energy Cost between Highly, Well, and Nontrained Runners. *Medicine & Science in Sports & Exercise* 36:1440–1446. https://doi.org/10.1249/01.MSS.0000135785.68760.96

Steele AG, Manson GA, Horner PJ, et al (2022) Effects of transcutaneous spinal stimulation on spatiotemporal cortical activation patterns: a proof-of-concept EEG study. *Journal of Neural Engineering* 19:046001. https://doi.org/10.1088/1741-2552/ac7b4b

Stefanovic F, Martinez JA, Saleem GT, et al (2023) A blended neurostimulation protocol to delineate cortico-muscular and spino-muscular dynamics following neuroplastic adaptation. *Frontiers in Neurology* 14:1114860. https://doi.org/10.3389/fneur.2023.1114860

Stožer A, Vodopivc P, Križančić Bombek L (2020) Pathophysiology of exercise-induced muscle damage and its structural, functional, metabolic, and clinical consequences. *Physiology Research* 565–598. https://doi.org/10.33549/physiolres.934371

Sugimoto CR, Ahn Y-Y, Smith E, et al (2019) Factors affecting sex-related reporting in medical research: a cross-disciplinary bibliometric analysis. *The Lancet* 393:550–559. https://doi.org/10.1016/S0140-6736(18)32995-7

Sutherland DH (2001) The evolution of clinical gait analysis part l: kinesiological EMG. *Gait & Posture* 14:61–70. https://doi.org/10.1016/S0966-6362(01)00100-X

Sutherland DH (2005) The evolution of clinical gait analysis part III – kinetics and energy assessment. *Gait & Posture* 21:447–461. https://doi.org/10.1016/j.gaitpost.2004.07.008

Swaddling J (2015) The Ancient Olympic Games. University of Texas Press

Swinnen W, Mylle I, Hoogkamer W, et al (2022) Triceps surae muscle force potential and force demand shift with altering stride frequency in running. *Scandinavian Medicine & Science in Sports* 32:1444–1455. https://doi.org/10.1111/sms.14209

Taga G (1995) A model of the neuro-musculo-skeletal system for human locomotion. *Biological Cybernetics* 73:113–121

Taylor JB, Wright AA, Dischiavi SL, et al (2017) Activity Demands During Multi-Directional Team Sports: A Systematic Review. *Sports Medicine* 47:2533–2551. https://doi.org/10.1007/s40279-017-0772-5

Taylor MJ, Beneke R (2012) Spring Mass Characteristics of the Fastest Men on Earth. *International Journal of Sports Medicine* 33:667–670. https://doi.org/10.1055/s-0032-1306283

Torricelli D, Barroso FO, Coscia M, et al (2016) Muscle Synergies in Clinical Practice: Theoretical and Practical Implications. In: Emerging Therapies in Neurorehabilitation II. Springer International Publishing, Cham

Toussaint TD, Schepens B (2024) Biomechanical behavior of the lower limbs and of the joints when landing from different heights. *Journal of Biomechanics* 165:112014. https://doi.org/10.1016/j.jbiomech.2024.112014

Tucker VA (1975) The Energetic Cost of Moving About: Walking and running are extremely inefficient forms of locomotion. Much greater efficiency is achieved by birds, fish—and bicyclists. *American Scientist*

Usherwood JR, Wilson AM (2006) Accounting for elite indoor 200 m sprint results. *Biology Letters* 2:47–50. https://doi.org/10.1098/rsbl.2005.0399

Valsecchi V, Gibertini G, Morelli A (2022) Wind Tunnel Test of Drafting at Endurance Run Velocity. *Mathematical Modelling of Engineering Problems* 9:27–35. https://doi.org/10.18280/mmep.090104

Van Caekenberghe I, Segers V, Willems P, et al (2013) Mechanics of overground accelerated running vs. running on an accelerated treadmill. *Gait & Posture* 38:125–131. https://doi.org/10.1016/j.gaitpost.2012.10.022

Van Hooren B, Fuller JT, Buckley JD, et al (2020) Is Motorized Treadmill Running Biomechanically Comparable to Overground Running? A Systematic Review and Meta-Analysis of Cross-Over Studies. *Sports Medicine* 50:785–813. https://doi.org/10.1007/s40279-019-01237-z

van Leeuwen AM, van Dieën JH, Daffertshofer A, Bruijn SM (2021) Ankle muscles drive mediolateral center of pressure control to ensure stable steady state gait. *Scientific Reports* 11

van Oeveren BT, de Ruiter CJ, Beek PJ, van Dieën JH (2021) The biomechanics of running and running styles: a synthesis. *Sports Biomechanics* 1–39. https://doi.org/10.1080/14763141.2021.1873411

Van Schooten KS, David S, Diamond LE (2023) Editorial: Women in Biomechanics and Control of Human Movement: 2022–2023. *Frontiers in Sports and Active Living* 5:1337636. https://doi.org/10.3389/fspor.2023.1337636

Van Wingerden JP, Vleeming A, Snijders CJ, Stoeckart R (1993) A functional-anatomical approach to the spine-pelvis mechanism: interaction between the biceps femoris muscle and the sacrotuberous ligament. *European Spine Journal* 2:140–144. https://doi.org/10.1007/BF00301411

Van Hooren B, Lennartz R, Cox M, et al (2024) Differences in running technique between runners with better and poorer running economy and lower and higher milage: An artificial neural network approach. *Scandinavian Journal of Medicine & Science in Sports* 34:e14605. https://doi.org/10.1111/sms.14605

Viellehner J, Heinrich K, Funken J, et al (2016) Lower extremity joint moments in athletics curve sprinting. *In: lSBS - Conference Proceedings Archive. Tsukuba, Japan*, p 4

Vogel S (1994) Life in moving fluids: the physical biology of flow, 2nd ed., rev.expanded. Princeton University Press, Princeton, N.J

Warrener A, Tamai R, Lieberman DE (2021) The effect of trunk flexion angle on lower limb mechanics during running. *Human Movement Science* 78:102817. https://doi.org/10.1016/j.humov.2021.102817

Welch TDJ, Ting LH (2008) A Feedback Model Reproduces Muscle Activity During Human Postural Responses to Support-Surface Translations. *Journal of Neurophysiology* 99:1032–1038. https://doi.org/10.1152/jn.01110.2007

Willems PA, Cavagna GA, Heglund NC (1995) External, internal and total work in human locomotion. III. Energy Changes of the centre of mass as a function of speed and body size in birds and mammals. *Journal of Experimental Biology* 198:379–393

Willems PA, Gosseye TP (2013) Does an instrumented treadmill correctly measure the ground reaction forces? *Biology Open* 2:1421–1424. https://doi.org/10.1242/bio.20136379

Williams KR, Cavanagh PR (1987) Relationship between distance running mechanics, running economy, and performance. *Journal of Applied Physiology* 63:1236–1245. https://doi.org/10.1152/jappl.1987.63.3.1236

Wilson JW, Mills MGL, Wilson RP, et al (2013a) Cheetahs, *Acinonyx jubatus* , balance turn capacity with pace when chasing prey. *Biology Letters* 9:20130620. https://doi.org/10.1098/rsbl.2013.0620

Wilson RP, Griffiths IW, Legg PA, et al (2013b) Turn costs change the value of animal search paths. *Ecology Letters* 16:1145–1150. https://doi.org/10.1111/ele.12149

Winter DA (2009) Biomechanics and motor control of human movement, 4th ed. Wiley, Hoboken, N.J

World Athletics (2019) Track and Field Facilities Manual

World Athletics (2023) World Record Progression of Marathon

World Athletics (2024) Competition Rules: Book C

Yakovenko S, Mushahwar V, VanderHorst V, et al (2002) Spatiotemporal Activation of Lumbosacral Motoneurons in the Locomotor Step Cycle. *Journal of Neurophysiology* 87:1542–1553. https://doi.org/10.1152/jn.00479.2001

Yokoyama H, Ogawa T, Kawashima N, et al (2016) Distinct sets of locomotor modules control the speed and modes of human locomotion. *Scientific Reports* 6:36275. https://doi.org/10.1038/srep36275

Zagatto AM, González JAM, De Poli RAB, et al (2023) Mechanical energy on anaerobic capacity during a supramaximal treadmill running in men: Is there influence between runners and active individuals? *Physiological Reports* 11:e15564. https://doi.org/10.14814/phy2.15564

Zamparo P, Pavei G, Monte A, et al (2019) Mechanical work in shuttle running as a function of speed and distance: Implications for power and efficiency. *Human Movement Science* 66:487–496. https://doi.org/10.1016/j.humov.2019.06.005

Zamparo P, Pavei G, Nardello F, et al (2016) Mechanical work and efficiency of 5 + 5 m shuttle running. *European Journal of Applied Physiology* 116:1911–1919. https://doi.org/10.1007/s00421-016-3443-6

Zandvoort CS, Daffertshofer A, Dominici N (2022) Cortical contributions to locomotor primitives in toddlers and adults. *iScience* 25:105229. https://doi.org/10.1016/j.isci.2022.105229